

**SEISMIC RESPONSE OF RC FRAME BUILDINGS
WITH NON REINFORCED EXTERIOR BEAM
COLUMN JOINTS**

by

Norberto José Rojas Mercedes

A dissertation submitted in partial fulfillment of the requirements for the degree of

DOCTOR OF PHILOSOPHY
in
CIVIL ENGINEERING

UNIVERSITY OF PUERTO RICO
MAYAGÜEZ CAMPUS
2011

Approved by:

Luis E. Suárez Colche, Ph.D.
Member, Graduate Committee

Date

José A. Martínez Cruzado, Ph.D.
Member, Graduate Committee

Date

Genock Portela Gautier, Ph.D.
Member, Graduate Committee

Date

Ricardo R. López Rodríguez, Ph.D.
President, Graduate Committee

Date

Gustavo Gutiérrez, Ph.D.
Representative of Graduate Studies

Date

Ismael Pagán Trinidad, MSCE
Chairperson of the Department

Date

ABSTRACT

Recent earthquakes have demonstrated the risk that reinforced concrete structures constructed before 1970 represent for society since these structures were designed with design codes in which the seismic provisions were not as strict as they are nowadays. This makes such structures vulnerable to strong earthquakes. Generally these codes did not have special provisions for the design of beam-column connections and therefore it was common that these elements were not confined with transverse reinforcement. Past earthquakes also have demonstrated that exterior connections without reinforcement are more prone to fail than the interior ones in some cases initiating the collapse of structures. This investigation is focused in the development of a model of exterior connections without reinforcement that can be used in the study of the seismic vulnerability of reinforced concrete frames designed before 1970. This model consisted of an envelope curve that identifies three important points of the behavior of such connections: the point of cracking, the point of maximum resistance and the residual strength point. The model was corroborated with 19 experimental tests of the literature. The results of the predictions compare favorably with the experimental results. The model was implemented in the Opensees program for the static and dynamic analysis of structures designed with the Puerto Rico building code of 1968, whose main system of lateral resistance was the moment resisting frames. For each structure two models were created. In one the connections were modeled as rigid and in the other they were modeled as flexible with the proposed model. From the static analysis one concluded that the frames modeled with flexible joints experienced a decrease in the lateral load capacity ranging from 16 to 32% with respect to the frames modeled with rigid joints. From the dynamic analysis it was observed that the maximum drifts increased between 10 and 78% with respect to the drifts obtained from the analysis with rigid connections. This increase was related directly with the damage of the exterior joints in the analysis.

RESUMEN

Terremotos recientes han evidenciado el riesgo que representan para la sociedad las estructuras de hormigón armado construidas antes de 1970, ya que las mismas fueron diseñadas con códigos en los cuales las disposiciones sísmicas no eran tan estrictas como lo son actualmente. Esto hace a estas estructuras vulnerables a terremotos fuertes. Generalmente estos códigos no tenían disposiciones especiales para el diseño de conexiones viga-columna y por tanto era común que estos elementos no se confinaran con refuerzo transversal. Pasados terremotos también han evidenciado que las conexiones exteriores sin refuerzo son más propensas a fallar que las interiores, en algunos casos llegando a iniciar el colapso de estructuras. Esta investigación está enfocada en el desarrollo de un modelo de juntas exteriores sin refuerzo que pueda utilizarse en el estudio de la vulnerabilidad sísmica de pórticos diseñados antes de 1970. Este modelo consistió en una envolvente que identifica tres puntos importantes del comportamiento de dichas juntas: el punto de agrietamiento, el punto de máxima resistencia y el punto de resistencia residual. El modelo fue corroborado con 19 pruebas experimentales de la literatura. Los resultados de las predicciones comparan favorablemente con los resultados experimentales. El modelo se implementó en el programa Opensees para el análisis estático y dinámico de estructuras diseñadas con el código de Puerto Rico de 1968 cuyo sistema de resistencia lateral eran los pórticos resistentes a momento. Para cada estructura se crearon dos modelos. En uno las conexiones se modelaron rígidas y en el otro se modelaron como flexibles con el modelo propuesto. Del análisis estático se concluyó que los pórticos modelados con juntas flexibles experimentaron una disminución en la carga lateral de entre 16 a 32% respecto a los pórticos modelados con junta rígida. Del análisis dinámico se observó que las derivas máximas aumentaron entre un 10 y un 78% respecto a las derivas obtenidas del análisis con conexión rígida. Este aumento estuvo directamente relacionado al daño que alcanzaron las juntas exteriores en el análisis.

To God and for all the people that supported me during this adventure and always encourage me to keep going: My wife Gina, my sons Eduardo and Diego, my parents Norberto and Geralda, my sisters Noelia and Gloria, my brother Norberto Luis, and my mother-in-law María.

ACKNOWLEDGEMENTS

I would like to express my gratitude to God, for giving me the life and the courage to continue at the most difficult moments of all this process. Thanks Lord for demonstrating me that you are an alive God and that always listens when I request your favor.

I wish to express my sincere gratitude to Dr. Ricardo López, my advisor, for his guidance and his support during this research work. I also appreciate the valuable suggestions and contributions of my graduate committee members, Dr. José A. Martínez Cruzado, Dr. Luis Suárez, and Dr. Genock Portela.

I would like to acknowledge to the National Science Foundation (NSF) who sponsored this project under grant number 0618804.

I would like to thank all the personnel from the Civil Engineering and Surveying Department of the University of Puerto Rico at Mayagüez for their collaboration.

I also want to express my gratitude to my friends John, Amilcar, and Ulises for all their friendship. Specially, I want to acknowledge Jairo and his wife, Erika, for supporting me during the most difficult moments of my research work.

I would like to thank, very specially, Dr. Augusto Poitevín, who always motivated and supported me when I needed most and for being more than a friend, my brother.

I would like to express my gratitude to Ms. Alicia Torres and her family and Víctor Mesa and his wife, Glenda, for their support and their affection.

I would like to express all my love and my gratitude to my wife Gina and my sons Eduardo and Diego for being my inspiration and motivation to keep me going in the middle of the adversities. To my parents, Norberto Rojas and Geralda Mercedes, for always being there when I needed most. Thanks Mom for giving me all that I am. To my sister Gloria and her husband Israel, my sister Noelia and her husband Rommel, and my brother Norberto Luis for their support. To my mother-in-law María for always encouraging me at the difficult moments.

Table of Contents

ABSTRACT.....	II
RESUMEN	III
ACKNOWLEDGEMENTS.....	V
TABLE OF CONTENTS	VII
TABLE LIST.....	X
FIGURE LIST	XI
1 INTRODUCTION.....	16
1.1 MOTIVATION	16
1.2 OBJECTIVES	4
1.3 SCOPE	5
1.4 SUMMARY OF THE CHAPTERS	5
2 LITERATURE REVIEW	7
2.1 INTRODUCTION.....	7
2.2 EXPERIMENTAL TEST BACKGROUND.....	8
2.3 EXPERIMENTAL TESTS OF INTERIOR AND ISOLATED EXTERIOR JOINTS	16
2.4 EXPERIMENTAL TESTS IN CORNER JOINTS	28
2.5 PARAMETERS AFFECTING THE SEISMIC PERFORMANCE OF CONCRETE JOINTS.....	31
2.6 RESISTING MECHANISM OF EXTERIOR JOINTS	36
2.7 MODE OF FAILURE IN BEAM-COLUMN JOINTS.....	38
2.8 MODELS FOR THE PREDICTION OF JOINT SHEAR STRENGTH	41
2.9 JOINT ELEMENT MODELS OF EXTERIOR OR INTERIOR JOINTS	41
2.9.1 <i>ZERO LENGTH ELEMENT</i>	42
2.9.2 <i>MULTI SPRING ELEMENT</i>	44
2.10 ENVELOPE BACKBONE CURVE FOR SUBSTANDARD RC ISOLATED JOINTS SUSTAINING J AND BJ FAILURE	46
2.11 RIGID JOINT ASSUMPTION	49
2.12 RELATIONSHIP BETWEEN JOINT SHEAR STRENGTH AND THE BEAM SHEAR	53
3 DEVELOPMENT OF THE ANALYTICAL MODEL	57
3.1 INTRODUCTION.....	57
3.2 DETAILS OF THE METHODOLOGY	58
3.2.1 <i>DATABASE CONSTRUCTION</i>	58
3.2.2 <i>ENVELOPE CURVE DEFINITION</i>	63
3.2.2.1 ORDINATE OF THE CRACKING POINT	65
3.2.2.2 ORDINATE OF THE PEAK STRENGTH POINT	66
3.2.2.2.1 ACI 318 SOFTENED STRUT AND TIE MODEL.....	66
3.2.2.2.2 MODEL FOR THE PREDICTION OF BJ FAILURE	69
3.2.2.2.3 VALIDATION OF THE JOINT SHEAR METHODOLOGY	72
3.2.2.3 ORDINATE OF THE RESIDUAL POINT	75
3.2.2.4 ABSCISSA OF THE PEAK STRENGTH POINT	75

3.2.2.4.1	ELASTIC ROTATIONS	76
3.2.2.4.2	JOINT SHEAR DISTORTION	79
3.2.2.4.3	ROTATION DUE TO BOND SLIP	81
3.2.2.5	ABSCISSA OF THE CRACKING POINT	83
3.2.2.5.1	ELASTIC ROTATIONS AT CRACKING	83
3.2.2.5.2	JOINT SHEAR DISTORTION AT CRACKING	84
3.2.2.5.3	ROTATION DUE TO BOND SLIP AT CRACKING	85
3.2.2.6	ABSCISSA OF THE RESIDUAL MOMENT POINT	85
3.2.2.7	APLICACION EXAMPLE	88
4	NUMERICAL MODEL	96
4.1	INTRODUCTION	96
4.2	MODEL OF THE SUBASSEMBLY	96
4.2.1	<i>UNIAXIAL MATERIALS</i>	97
4.2.1.1	CONCRETE 01 MATERIAL	97
4.2.1.2	STEEL01 MATERIAL	99
4.2.1.3	PINCHING4 MATERIAL	101
4.2.1.4	SECTIONS	105
4.2.1.5	ELEMENTS	106
4.2.1.5.1	BEAM WITH HINGE ELEMENT	106
4.2.1.5.2	ZERO LENGTH ELEMENT	107
4.3	MODEL CALIBRATION	107
5	MODEL VALIDATION	110
5.1	INTRODUCTION	110
5.2	COMPARISON OF MODEL SIMULATION WITH EXPERIMENTAL RESPONSE	110
5.2.1	<i>WONG TEST</i>	110
5.2.2	<i>PANTELIDES TEST</i>	114
5.2.3	<i>CLYDE TEST</i>	117
5.2.4	<i>ANTONOPOULOS & TRIANTAFILLOU TEST</i>	119
5.3	CONCLUSION	120
6	GROUND MOTION RECORDS FOR DYNAMIC ANALYSIS	122
6.1	INTRODUCTION	122
6.2	SELECTED EARTHQUAKE GROUND RECORDS	122
6.2.1	<i>MAYAGUEZ SYNTHETIC ACCELERATION RECORD</i>	122
6.2.2	<i>EL CENTRO ACCELERATION RECORD</i>	124
6.2.3	<i>MEXICO ACCELERATION RECORD</i>	126
7	ANALYSIS OF SCHOOL BUILDINGS	129
7.1	INTRODUCTION	129
7.2	DESCRIPTION OF THE FRAMES	130
7.3	MODEL OF THE FRAME	131
7.4	STATIC PUSHOVER ANALYSIS	133
7.4.1	<i>RESULTS FOR THE TWO STORY FRAME</i>	134
7.4.2	<i>DISCUSSION OF RESULTS</i>	137
7.4.3	<i>RESULTS FOR THE THREE STORY FRAME</i>	139
7.4.4	<i>DISCUSSION OF RESULTS</i>	143
7.5	DYNAMIC ANALYSIS	145
7.5.1	<i>RESULTS FOR THE TWO STORY FRAME</i>	145

7.5.1.1	RESULTS FOR THE EL CENTRO EARTHQUAKE.....	145
7.5.1.2	RESULTS FOR THE MAYAGÜEZ EARTHQUAKE.....	149
7.5.1.2.1	DISCUSSION OF THE RESULTS.....	149
7.5.2	<i>RESULTS FOR THE THREE STORY BUILDING</i>	<i>153</i>
7.5.2.1	RESULTS FOR THE EL CENTRO EARTHQUAKE.....	153
7.5.2.1.1	DISCUSSION OF RESULTS.....	154
7.5.2.2	RESULTS FOR THE MAYAGÜEZ EARTHQUAKE.....	157
7.5.2.2.1	DISCUSSION OF RESULTS.....	159
7.6	COMPARISON OF THE RESPONSE FROM THE STATIC AND DYNAMIC ANALYSIS	162
7.7	CONCLUSIONS.....	165
8	ANALYSIS OF MULTISTORY BUILDINGS.....	167
8.1	INTRODUCTION.....	167
8.2	DESCRIPTION OF THE FRAMES	167
8.3	MODEL OF THE FRAMES.....	173
8.4	STATIC PUSHOVER ANALYSIS.....	174
8.4.1	<i>RESULTS FOR THE FIVE STORY FRAME</i>	<i>174</i>
8.4.2	<i>RESULTS FOR THE TEN STORY FRAME</i>	<i>178</i>
8.4.3	<i>RESULTS FOR THE 15 STORY FRAME</i>	<i>183</i>
8.5	DYNAMIC ANALYSIS.....	188
8.5.1	<i>RESULTS FOR THE FIVE STORY FRAME</i>	<i>189</i>
8.5.1.1	RESULTS FOR EL CENTRO EARTHQUAKE.....	189
8.5.1.2	RESULTS FOR THE MAYAGÜEZ EARTHQUAKE.....	192
8.5.1.3	RESULTS FOR THE MEXICO EARTHQUAKE.....	195
8.5.2	<i>RESULTS FOR THE TEN STORY FRAME</i>	<i>199</i>
8.5.2.1	RESULTS FOR EL CENTRO EARTHQUAKE.....	199
8.5.2.2	RESULTS FOR THE MAYAGÜEZ EARTHQUAKE.....	202
8.5.2.3	RESULTS FOR THE MEXICO EARTHQUAKE.....	205
8.5.3	<i>RESULTS FOR THE 15 STORY FRAME</i>	<i>208</i>
8.5.3.1	RESULTS FOR EL CENTRO EARTHQUAKE.....	208
8.5.3.2	RESULTS FOR THE MAYAGÜEZ EARTHQUAKE.....	211
8.5.3.3	RESULTS FOR THE MEXICO EARTHQUAKE.....	215
8.6	COMPARISON OF THE RESPONSE FROM THE STATIC AND DYNAMIC ANALYSES	218
8.7	CONCLUSIONS.....	222
9	CONCLUSIONS AND FUTURE WORK	224
9.1	SUMMARY	224
9.2	CONCLUSIONS.....	225
9.3	RECOMENDATIONS FOR FUTURE WORK.....	227
	REFERENCES.....	229

Table List

Table	Page
Table 2-1 Summary of some findings of the literature review	34
Table 3-1 Database of unreinforced concrete joints tests from the literature	61
Table 3-2 Type of failure validation	74
Table 3-3 Experimental measured joint shear strain.....	80
Table 3-4 Summary of Envelope Point for the Application Example	95
Table 4-1 Computation of the Experimental factor for Peak Moment Point.....	109
Table 7-1 Natural Period of the School Buildings Frames	133
Table 7-2 Summary of maximum response from the dynamic analyses	162
Table 8-1 Distributed weight along members used in the analysis	169
Table 8-2 Natural period of the multistory frames	173
Table 8-3 Summary of maximum response from the dynamic analysis.....	218

Figure List

Figure	Page
Figure 1-1 Olive View Hospital, San Fernando, California, after the 1971 San Fernando Earthquake. [Adapted from www.cartage.org]	3
Figure 1-2 Collapse due to beam-column joint failure [Adapted from Pantelides et al. 2002].	4
Figure 2-1 Geometric description of joints as per ACI-ASCE 352 Committee	7
Figure 2-2 Nomenclature of exterior joints	8
Figure 2-3 Deformed shape of a typical reinforced concrete frame	9
Figure 2-4 Isolated beam-column subassembly: (a) Real situation (b) Testing configuration.	9
Figure 2-5 Example of testing beam-column subassembly in vertical position	10
Figure 2-6 Example of testing beam-column subassembly in horizontal position	10
Figure 2-7 Example of cyclic lateral loading and displacement history	11
Figure 2-8 Example of lateral displacement history based on inter-story drift ratio	12
Figure 2-9 Instrumented Beam-Column joint subassembly (adapted from Pantelides et al. 2002)	13
Figure 2-10 Example of Lateral Load vs Drift ratio graph (adapted from Pantelides et al. 2002)	14
Figure 2-11 Example of a normalized joint shear stress versus joint shear strain graph (adapted from Pantelides et al. 2002)	15
Figure 2-12 Effective joint area (adapted from ACI-352)	16
Figure 2-13 Exterior beam-column joint subjected to seismic actions. (adapted from R. Park 2002)	37
Figure 2-14 Mechanisms of shear transfer at exterior joint: (a) diagonal strut mechanism; and (b) truss mechanism. (adapted from Park and Paulay 1975)	37
Figure 2-15 Load – Drift curve showing J failure	38
Figure 2-16 Load – Drift curve showing BJ failure	39
Figure 2-17 Exterior beam-column joint presenting anchorage failure (adapted from Jirsa 1981)	40
Figure 2-18 Existing joint element models for beam-column simulation (adapted from Celik and Elingwood 2008): (a) Scissor Model (Alath and Kunnath (1995), (b) Biddah and Ghobarah (1999), (c) Youssef and Ghobarah (2001), (d) Lowes and Altoontash (2003), (e) Shin and LaFave (2004)	44
Figure 2-19 Envelope backbone curve for J failure mode	48
Figure 2-20 Envelope backbone curve for BJ failure mode	48
Figure 2-21 Example of a well detailed beam-column connection (adapted from Paulay and Scarpas (1981)) All units in millimeters (mm)	50
Figure 2-22 Load-displacement response of unit 1 (Paulay and Scarpas 1981)	51

Figure 2-23 Specimen conditions at the end of the test (adapted from Paulay and Scarpas 1981).....	51
Figure 2-24 Example of an unreinforced beam-column joint Specimen BSL (adapted from Wong 2005. All units in millimeters (mm)).....	52
Figure 2-25 Lateral load-drift hysteresis loop of Specimen BSL (adapted from Wong 2005).....	52
Figure 2-26 Crack pattern of specimen BSL (adapted from Wong 2005).....	53
Figure 2-27 External and internal forces on a beam column joint.....	55
Figure 3-1 Simple rotational spring for the proposed model.....	57
Figure 3-2 Anchorage details for selected specimens.....	59
Figure 3-3 Variables definition for the database.....	60
Figure 3-4 Proposed envelope curve for the joint.....	64
Figure 3-6 Definitions used for the ACI-318 Softened Strut and Tie Model.....	69
Figure 3-7 External and internal forces on a beam-column joint.....	70
Figure 3-8 Predictions of the $\bar{\tau}_{Peak}$ obtained with the proposed methodology.....	72
Figure 3-9 Predictions of the $\bar{\tau}_{Peak}$ obtained with Analytical model from Park and Mosalam (2009).....	73
Figure 3-10 Contribution of the joint rotation (adapted from Hanson and Connor 1967).....	75
Figure 3-11 Joint subassembly idealization: a) Model b) Free body diagram.....	77
Figure 3-12 Joint shear distortion.....	79
Figure 3-13 Experimental measured of γ_{xy} versus $\bar{\tau}$ from Clyde et al (2000) and Pantelides et al (2002).....	80
Figure 3-14 Rotation due to Bond Slip.....	81
Figure 3-15 Bond and bar stress distribution for a reinforcing bar anchored in a joint (adapted from Park and Mosalam 2009).....	82
Figure 3-16 Proposed moment rotation for the rotational spring.....	85
Figure 3-18 Slope – Axial Load Graph from test of the database with available Load-Drift graph.....	87
Figure 3-19 Dimension of Specimen BSL (Wong 2005).....	89
Figure 3-20 Moment-Rotation Envelope for Specimen BSL (Wong 2005).....	95
Figure 4-1 Concrete 01 Material Parameters (adapted from Mazzoni et al (2007)).....	98
Figure 4-2 Definition of Confined and Unconfined region (adapted from Mazzoni et al (2007)).....	98
Figure 4-3 Hysteretic Stress-Strain Response of Concrete 01 (adapted from Mazzoni et al (2007)).....	99
Figure 4-4 Steel 01 Material Parameters (adapted from Mazzoni et al (2007)).....	100
Figure 4-5 Hysteretic Stress-Strain response of Steel 01 Material without Isotropic Hardening (adapted from Mazzoni et al (2007)).....	100
Figure 4-6 Pinching4 Material Model (adapted from Mazzoni et al (2007)).....	102
Figure 4-7 Figure 3-3 Proposed envelope curve for the joint.....	104
Figure 4-8 Fiber element approach.....	105
Figure 4-9 Beam with hinge element (adapted from Mazzoni et al (2007)).....	106

Figure 4-10 The Opensees model of the subassembly.....	108
Figure 4-11 Comparison of results of Test 3 from Pantelides <i>et al</i> (2000)	108
Figure 5-1 Details of specimens tested by Wong (2005) (All units in mm).....	111
Figure 5-2 Comparison of response for test of Wong (2005): a) specimen BSU, b) specimen BSL, c) specimen BSLLS and d) specimen BSLV2T10	112
Figure 5-3 Comparison of response for test of Wong (2005): a) specimen BSLV4T10, b) specimen JANN03, c) specimen JANN15 and d) specimen BSL300	113
Figure 5-4 Details of specimens tested by Pantelides <i>et al</i> (2002) (All units in inches)	115
Figure 5-5 Comparison of response for test of Pantelides <i>et al.</i> (2002): a) Test 3, b) Test 4, c) Test 5 and d) Test 6.....	116
Figure 5-6 Details of specimen tested by Clyde <i>et al</i> (2000) (All units in inches).....	117
Figure 5-7 Comparison of response for test of Clyde <i>et al.</i> (2000): a) Test 2, b) Test 5, c) Test 4 and d) Test 6.....	118
Figure 5-8 Details of specimen tested by Antonopoulos & Triantafillou (2003).....	119
Figure 5-9 Comparison of response for test Antonopoulos & Triantafillou (2003): a) specimen C1, b) specimen C2 and c) specimen T-C	120
Figure 6-1 Synthetic Ground Record for Mayagüez and Ponce cities (Irizarry 1999) with base line correction by Montejo (2004)	123
Figure 6-2 Fourier spectrum for the Mayagüez and Ponce Synthetic	123
Figure 6-3 Response Acceleration Spectra for 5% of damping for Mayagüez and Ponce cities Synthetic Record.....	124
Figure 6-4 NS Ground Record from the 1940 El Centro earthquake at Imperial Valley. Station 117 El Centro Array #9117	125
Figure 6-5 Fourier Spectrum for El Centro earthquake.....	125
Figure 6-6 Response Acceleration Spectra for 5% of damping from El Centro Earthquake	126
Figure 6-7 Ground record for the Mexico earthquake (1985)	127
Figure 6-8 Fourier Spectrum for the Mexico earthquake (1985).....	127
Figure 6-9 Response Acceleration Spectrum for 5% of damping for the Mexico 1985 earthquake.....	128
Figure 7-1 Typical two story school building in Puerto Rico; a) Front view and b) Lateral view.....	129
Figure 7-2 Details of the two and three level school frame building.....	130
Figure 7-3 Two story frame model.....	132
Figure 7-4 Pushover analysis results for the two story frame.....	135
Figure 7-5 Sequence of plastic hinges events for the two story frame	136
Figure 7-6 Local behavior of the joints for the two story frame pushover analysis.	137
Figure 7-7 Pushover analysis results for the three story frame.....	140
Figure 7-8 Sequence of plastic hinges events for the three story frame	142
Figure 7-9 Local behavior of the joints for the three story frame pushover analysis	143
Figure 7-10 Top Story Drift versus time for the El Centro earthquake for the two story frame	146

Figure 7-11 Sequence of plastic hinges for the two story frame for the El Centro earthquake (values in parentheses are in seconds)	146
Figure 7-12 Local behavior of the joints for the two story frame for the El Centro earthquake	147
Figure 7-13 Maximum story displacement for the El Centro earthquake	148
Figure 7-14 Top Story Drift versus time for the Mayagüez earthquake for the two story frame	150
Figure 7-15 Sequence of plastic hinges for the two story frame for the Mayagüez earthquake (values in parentheses are in seconds)	151
Figure 7-16 Local behavior of the joints for the two story frame for the Mayagüez earthquake	151
Figure 7-17 Maximum story displacement for the Mayaguez earthquake	152
Figure 7-18 Top Story Drift versus time for the El Centro earthquake for the three story frame	155
Figure 7-19 Sequence of plastic hinges for the El Centro earthquake for the three story frame	155
Figure 7-20 Local behavior of joints for the El Centro earthquake for the three story frame	156
Figure 7-21 Maximum story displacement for the El Centro earthquake for the three story frame	157
Figure 7-22 Top Story Drift versus time for the Mayagüez earthquake for the three story frame	158
Figure 7-23 Sequence of plastic hinges for the Mayagüez earthquake	159
Figure 7-24 Local behavior of joints for the Mayagüez earthquake for the three story frame	160
Figure 7-25 Maximum story displacement for the Mayagüez earthquake for the three story frame	161
Figure 7-26 Static versus dynamic response for the two story building with rigid joints	163
Figure 7-27 Static versus dynamic response for the two story building with flexible joints	163
Figure 7-28 Static versus dynamic response for the three story building with rigid joints ..	164
Figure 7-29 Static versus dynamic response for the three story building with flexible joints	164
Figure 8-1 Layout of 5, 10 and 15 Story Building Frame (Daza Duarte 1996).....	168
Figure 8-2 Cross sectional sizes and reinforcement details at member ends of the 5 Story frame (Daza Duarte 1996)	170
Figure 8-3 Cross sectional sizes and reinforcement details at member ends of the 10 Story frame (Daza Duarte 1996)	171
Figure 8-4 Cross sectional sizes and reinforcement details at member ends of the 15 Story frame (Daza Duarte 1996)	172
Figure 8-5 Pushover analysis results for the five story frame	174
Figure 8-6 Sequence of plastic hinges events for the five story frame	176
Figure 8-7 Pushover analysis results for the ten story frame.....	178

Figure 8-8 Sequence of plastic hinges events at 1% drift for the ten story frame	179
Figure 8-9 Sequence of plastic hinges events at 2% drift for the ten story frame	180
Figure 8-10 Sequence of plastic hinges events at 5% drift for the ten story frame	181
Figure 8-11 Pushover analysis results for the 15 story frame.....	183
Figure 8-12 Sequence of plastic hinges events at 1% drift for the 15 story frame	184
Figure 8-13 Sequence of plastic hinges events at 2% drift for the 15 story frame	185
Figure 8-14 Sequence of plastic hinges events at 5% drift for the 15 story frame	186
Figure 8-15 Top Story Drift versus time for El Centro earthquake for the five story frame	189
Figure 8-16 Sequence of plastic hinges for the five story frame for El Centro earthquake .	190
Figure 8-17 Maximum story drift for El Centro earthquake.....	190
Figure 8-18 Local behavior of first story joints for El Centro earthquake	191
Figure 8-19 Top Story Drift versus time for the Mayagüez earthquake for the five story frame	193
.....	193
Figure 8-20 Sequence of plastic hinges for the five story frame for the Mayagüez earthquake	193
.....	194
Figure 8-21 Maximum story drift for the Mayagüez earthquake	194
Figure 8-22 Local behavior of first story joints for the Mayagüez earthquake	194
Figure 8-23 Top Story Drift versus time for the Mexico earthquake for the five story frame	196
.....	196
Figure 8-24 Sequence of plastic hinges for the five story frame for the Mexico earthquake	197
Figure 8-25 Maximum story drift for the Mexico earthquake.....	197
Figure 8-26 Local behavior of first story joints for the Mexico earthquake.....	198
Figure 8-27 Top Story Drift versus time for El Centro earthquake for the ten story frame .	199
Figure 8-28 Sequence of plastic hinges for the ten story frame for El Centro earthquake...	200
Figure 8-29 Maximum story drift for El Centro earthquake.....	201
Figure 8-30 Top Story Drift versus time for the Mayagüez earthquake for the ten story frame	202
.....	202
Figure 8-31 Sequence of plastic hinges for the ten story frame for the Mayagüez earthquake	203
.....	204
Figure 8-32 Maximum story drift for the Mayagüez earthquake	204
Figure 8-33 Top Story Drift versus time for the Mexico earthquake for the ten story frame	205
.....	205
Figure 8-34 Sequence of plastic hinges for the ten story frame for the Mexico earthquake	206
Figure 8-35 Maximum story drift for the Mexico earthquake.....	207
Figure 8-36 Top Story Drift versus time for El Centro earthquake for the 15 story frame ..	208
Figure 8-37 Sequence of plastic hinges for the 15 story frame for El Centro earthquake....	209
Figure 8-38 Maximum story drift for the El Centro earthquake.....	210
Figure 8-39 Top Story Drift versus time for the Mayagüez earthquake for the 15 story frame	212
.....	212
Figure 8-40 Sequence of plastic hinges for the 15 story frame for the Mayagüez earthquake	213
.....	213
Figure 8-41 Maximum story drift for the Mayagüez earthquake	214

Figure 8-42 Top Story Drift versus time for the Mexico earthquake for the 15 story frame 215

Figure 8-43 Sequence of plastic hinges for the 15 story frame for the Mexico earthquake. 216

Figure 8-44 Maximum story drift for the Mexico earthquake 217

Figure 8-45 Static versus dynamic response for the five story building with rigid joints 219

Figure 8-46 Static versus dynamic response for the five story building with flexible joints 219

Figure 8-47 Static versus dynamic response for the ten story building with rigid joints 220

Figure 8-48 Static versus dynamic response for the ten story building with flexible joints. 220

Figure 8-49 Static versus dynamic response for the fifteen story building with rigid joints 221

Figure 8-50 Static versus dynamic response for the fifteen story building with flexible joints
..... 221

1 INTRODUCTION

1.1 MOTIVATION

The deficient seismic behavior of reinforced concrete frame buildings built prior to the 1970's has been evident in recent earthquakes such as Northridge (1994), Chi Chi, Taiwan (1999) and Izmit Turkey (1999). Damages observed during these earthquakes is a clear indication of the serious structural deficiencies that some of these type of buildings may have. This performance can be attributed to the fact that seismic design requirements and construction practices at that time were not as strict as they are nowadays, resulting in vulnerable structures.

The first really practical test of United States earthquake codes in or close to an epicentral region occurred during the San Fernando Earthquake in 1971. Structures that were located in the region of strong shaking and designed according to the earthquake requirements of the building code were seriously damaged (National Academy of Science 1971). The Olive View Hospital, shown in Figure 1-1 is a showcase of this behavior. The damage observed is attributed to drastic changes of stiffness and strength along the height of the structure.



Figure 1-1 Olive View Hospital, San Fernando, California, after the 1971 San Fernando Earthquake. [Adapted from www.cartage.org]

The poor performance of these structures during this earthquake demonstrated that the existing building codes were not providing adequate damage-control features and forced the design codes to be revised (National Academy of Science 1971). The problem lies in that many existing buildings were constructed before 1971, not only in the US but worldwide. These buildings pose a danger of partial or complete collapse (Moehle 2007, Pantelides *et al.* 2002) and due to their vulnerability they are the principal seismic safety concern in the world (Moehle 2007).

Even though there is no inventory of these types of buildings, some estimates exist [Moehle 2007, Anderson 2008]. For example, the Los Angeles County Assessor point out that about 14,000 of them exist in LA County alone; the California Seismic Safety Commission believe that there are 40,000 such buildings in California. These numbers imply that the problem is very serious not only in the US but globally, where non-ductile concrete buildings are more

common than in California. Development of models for this type of building is necessary for their seismic evaluation.

One of the most important part in an reinforced concrete frame are the joints, because they transfer the moments and internal forces among adjacent beams and columns, and may experience high shear stresses. Their main role is to provide the connecting beams the capacity to dissipate energy through inelastic deformation [Uzumeri 1977]. As mentioned before the reinforcing details of buildings built prior to the 1970's do no lead to a ductile response, implying that a premature failure of the joints can results in brittle failure of the structures as shown in Figure 1-2, taken during the Izmit Earthquake in 1999. Moreover, the high demand and the inadequate reinforcing increase their vulnerability [Anderson 2008]. Thus the understanding of the performance of connections in old structures is essential.



Figure 1-2 Collapse due to beam-column joint failure [Adapted from Pantelides et al. 2002].

1.2 OBJECTIVES

The main objective of this research is to develop, implement and verify an analytical model of a corner joint that can serve as basis for the seismic evaluation of frame structures designed before 1970. This model should be able to account for the loss of stiffness and the maximum capacity of the joint.

The specific objectives established in order to accomplish the principal goal proposed in this work are:

1. Identify the main characteristics of the behavior of unreinforced joints.
2. Develop equations for each one of the points that characterize the local behavior of unreinforced concrete exterior joints.
3. Implement the model in a structural analysis program.
4. Validate the model with experiments of unreinforced concrete exterior joints.
5. Include the model in the analysis of concrete frames and evaluate the results.

1.3 SCOPE

This research is restricted to the study of two dimensional unreinforced exterior joints; thus the tridimensional exterior joints are not addressed in this study. These are addressed in a companion study which is being conducted now at the University of California at Berkeley.

1.4 SUMMARY OF THE CHAPTERS

This research is divided in nine chapters. Chapter 1 introduces the theme of this thesis. The motivation, objectives and scope are also presented here. Chapter 2 presents a literature review and the most important concepts that will be used throughout this research. The general methodology used to develop the proposed model is present in Chapter 3. The main characteristics of the structural program used to implement the model are present in Chapter 4. The validation of the proposed model is presented in Chapter 5. The description of the earthquakes ground motion records selected to perform the dynamic analyses of frames are briefly summarized in Chapter 6. The analysis of a two and three story frame typical of school buildings in Puerto Rico is carry out in Chapter 7. The analysis of three multistory frame buildings is presented in Chapter 8. Finally the general conclusions from this research are presented in Chapter 9.

2 LITERATURE REVIEW

2.1 INTRODUCTION

ACI – ASCE Committee 352 [Pinkham et al. 1997] classifies joints according to their geometry or the degree of confinements provided by the beams framing into the joint (Figure 2-1). An interior joint has beams framing into all sides of the joint. An exterior joint has at least two beams framing into opposite sides of the joint. A corner joint has two beams framing in adjacent sides or only one beam.

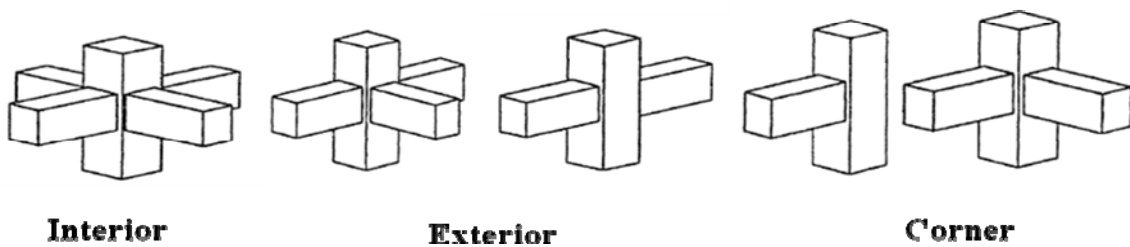


Figure 2-1 Geometric description of joints as per ACI-ASCE 352 Committee

Commonly, exterior joints are subdivided as follows (Figure 2-2): a) edge joints (two beams framing in opposite sides or three beams framing into the joint); b) isolated joints (one beam framing into the joint); c) knee joints (one beam framing into the joint in a roof) and d) corner joints (two beams framing in adjacent sides). In the literature it is common to find isolated joints called exterior joints.

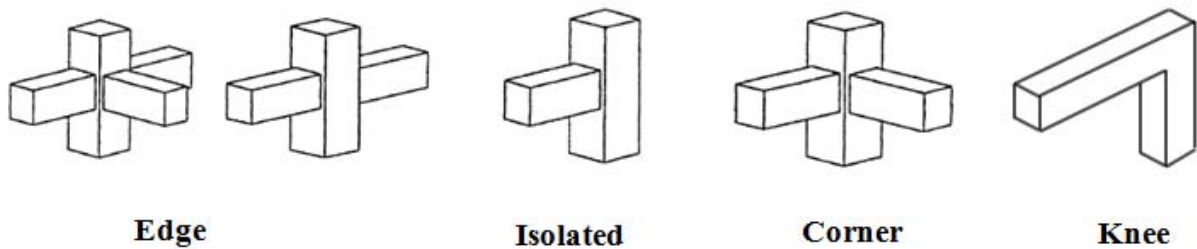


Figure 2-2 Nomenclature of exterior joints

A considerable amount of research on the seismic behavior of RC building beam column joints has been accomplished in the last forty years. Most of it has been focused in experimental studies of the behavior of interior and exterior joints in terms of the variables affecting their seismic performance. A small group has been concentrated in the analytical part. The following sections present a brief background on experimental test as well as a chronological review of some of the most important experimental investigations with respect to the performance of RC joint in moment resisting frames.

2.2 EXPERIMENTAL TEST BACKGROUND

During an earthquake, a reinforced concrete frame is subjected to the action of inertial forces that deforms it as shown in the two dimensions Figure 2-3. Figure 2-4 (a) represents the left corner joint that has been isolated along with its free body diagram. It can be appreciated that this configuration is very difficult to achieve in the laboratory and for that reason the subassembly is rotated as shown in Figure 2-4 (b). This configuration is the adopted one by

the majority of the researchers in beam-column joints. Depending on the laboratory facilities, this configuration can be either vertical (Figure 2-5) or horizontal (Figure 2-6).

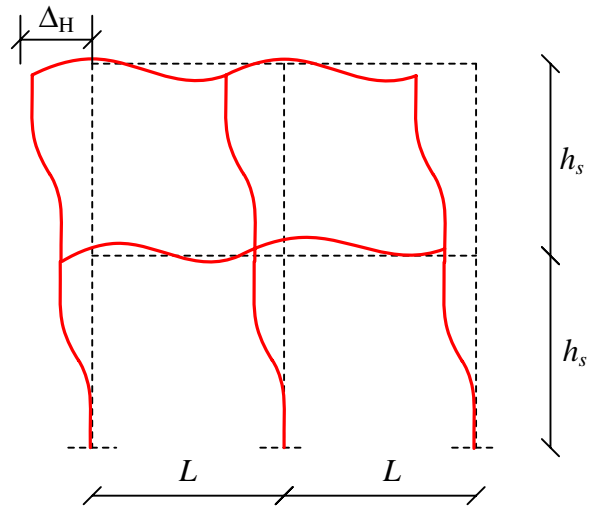


Figure 2-3 Deformed shape of a typical reinforced concrete frame

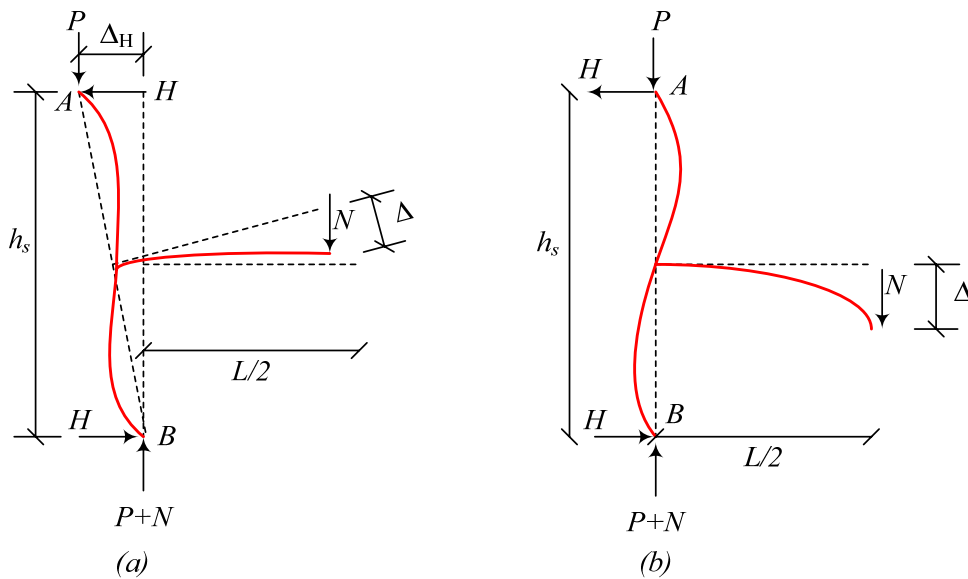


Figure 2-4 Isolated beam-column subassembly: (a) Real situation (b) Testing configuration

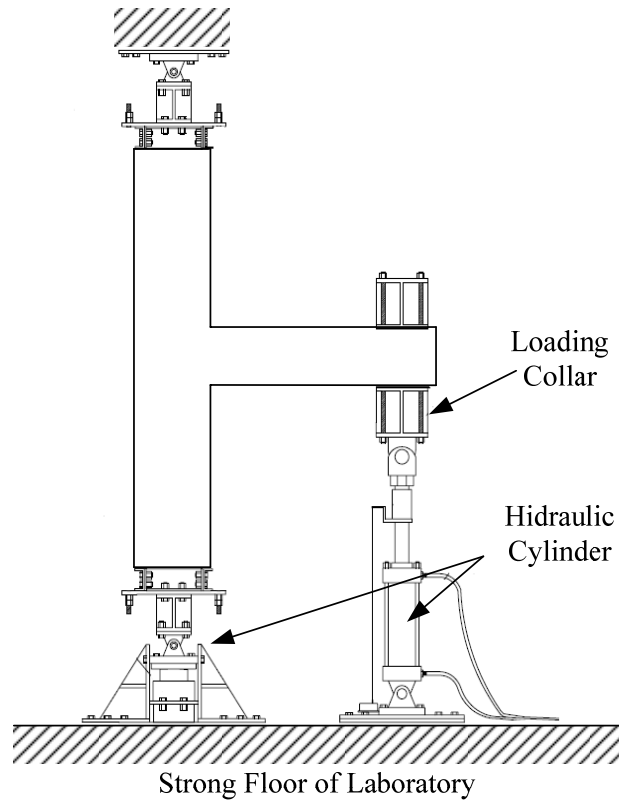


Figure 2-5 Example of testing beam-column subassembly in vertical position

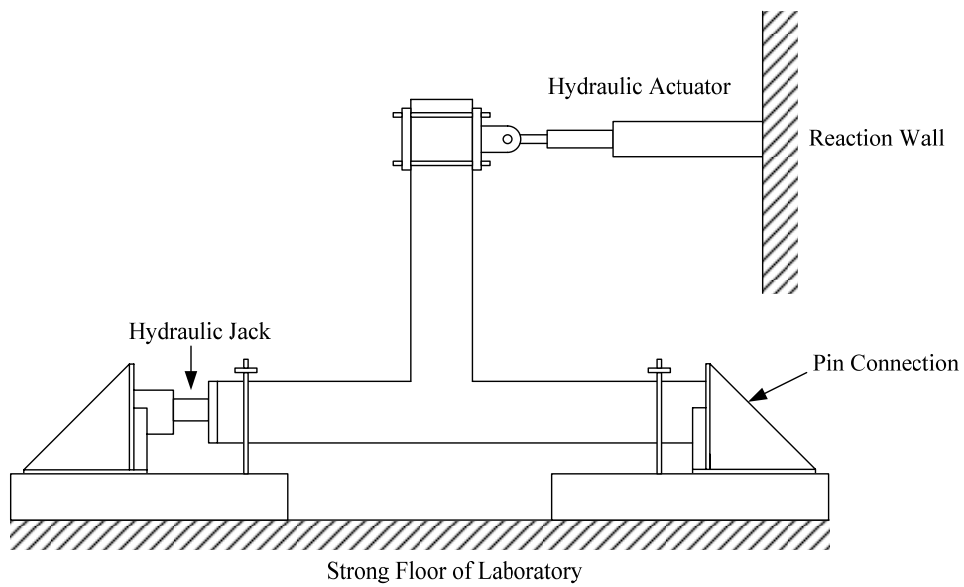


Figure 2-6 Example of testing beam-column subassembly in horizontal position

In the subassembly, the column length is the distance between upper and lower column inflection points. The beam length is taken as half of the beam span. With regard to the boundary condition, the point in which the axial load is applied is simulated with a roller, while the support at the other part of the column is simulated with a support that restrains both vertical and horizontal displacement but allows the rotation. This configuration simulates the real situation of the beam column joint as if it were part of a frame structure. The earthquake loading is simulated through hydraulic actuators. The testing procedure can be briefly explained as follows: the column axial load is applied first and kept nearly constant during the test; the lateral load is applied, controlling the load until certain level of load is reached and then continuing controlling the displacements (Figure 2-7) or controlling the displacement from the beginning to the end of the test (Figure 2-8).

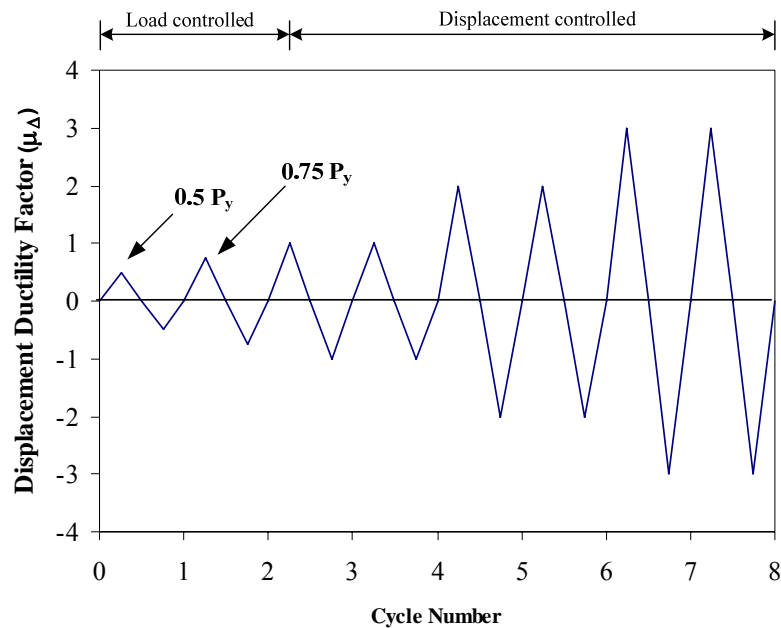


Figure 2-7 Example of cyclic lateral loading and displacement history

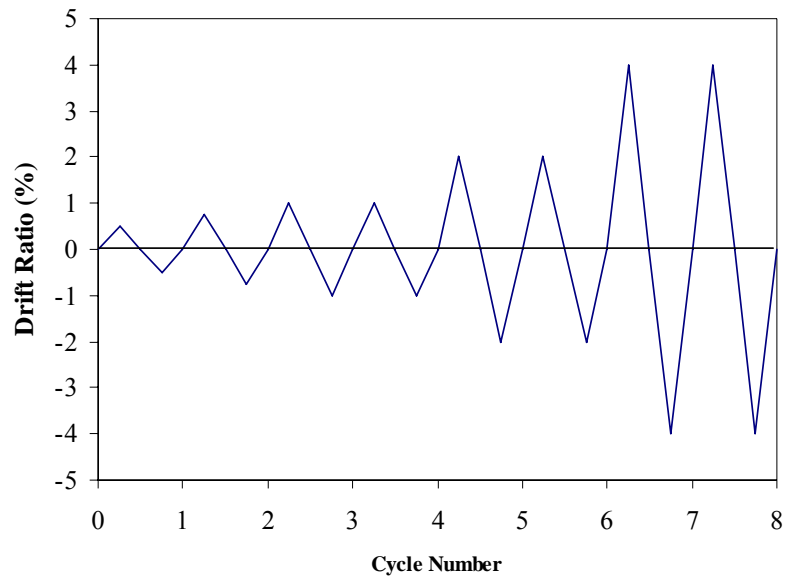


Figure 2-8 Example of lateral displacement history based on inter-story drift ratio

In order to monitor the displacement of the beam tip, distortion of the joint, rotations, etc, devices called Linear Voltage Displacement Transducer (LVDTs) are used. Load magnitude at beam and columns are monitored by load cells. Figure 2-9 shows an example of the instrumentation implemented in a beam –column joint subassembly.

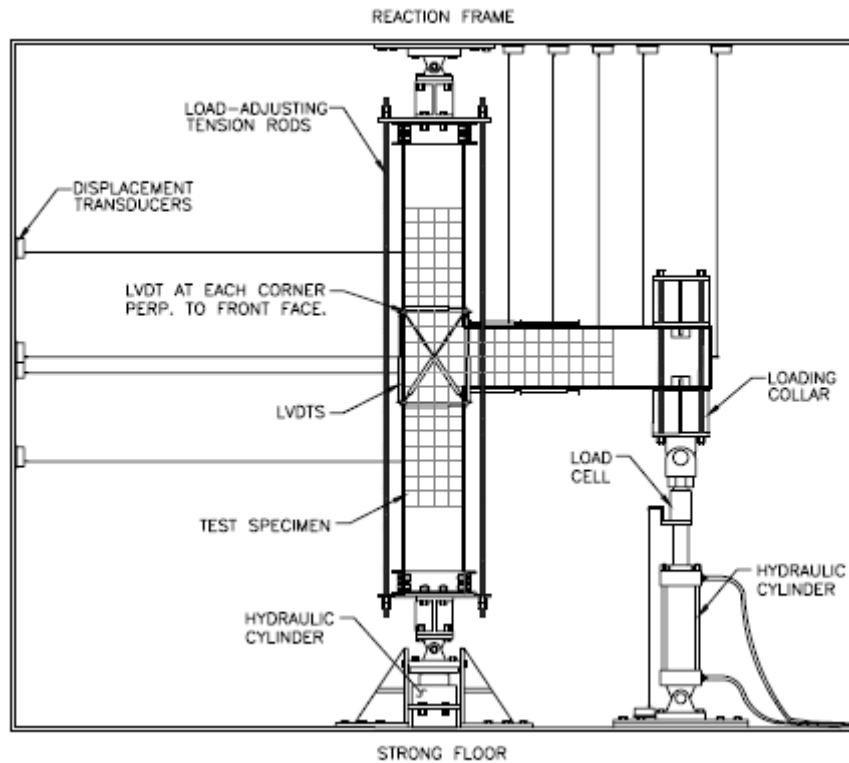


Figure 2-9 Instrumented Beam-Column joint subassembly (adapted from Pantelides et al. 2002)

The results of experimental test are displayed by means of a plot of the beam load versus the vertical displacement at the beam tip of the subassembly. This plot represents the global behavior of the test specimen. An example of this plot is presented in Figure 2-10, in which the drift ratio is the displacement divided by the length of the beam, measured from the center of the column.

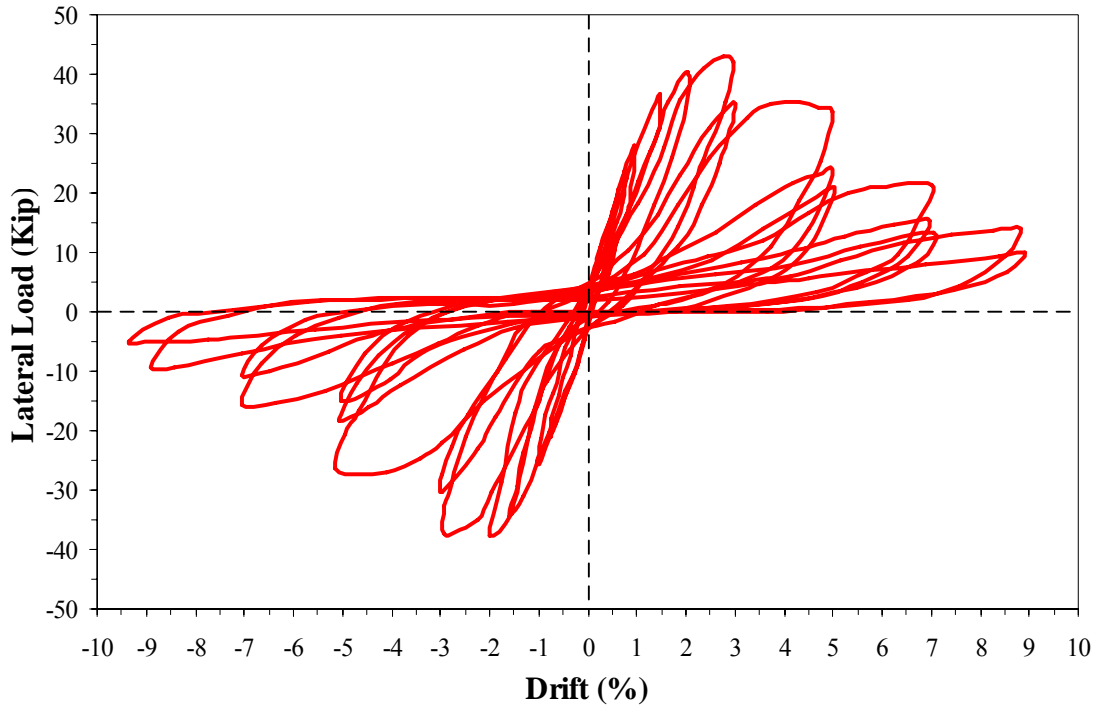


Figure 2-10 Example of Lateral Load vs Drift ratio graph (adapted from Pantelides et al. 2002)

In the same way, the local behavior of the joint is also presented by means of a plot of the normalized joint shear stress versus the shear strain obtained from the lecture of the LVDTs (Figure 2-11). The normalized joint shear stress is defined as:

$$\bar{\tau}_{jh} = \frac{V_{jh}}{b_j h_c \sqrt{f'_c}}$$

2.1

Where V_{jh} is the joint shear force which is a function of the lateral applied force; h_c is the height of the column in the direction of loading and b_j is the effective joint width, which is defined by the ACI 352 as the average between column and beam width (Figure 2-12), but not to exceed: a) the column width and b) the beam width plus half the column depth on each side of the beam. In the literature is common to use the letter γ to identify the joint shear stress. Since this letter is commonly used to define the shear strain, in this research the letter τ will be used to define the joint shear stress and thus avoid confusing with the joint shear strain.

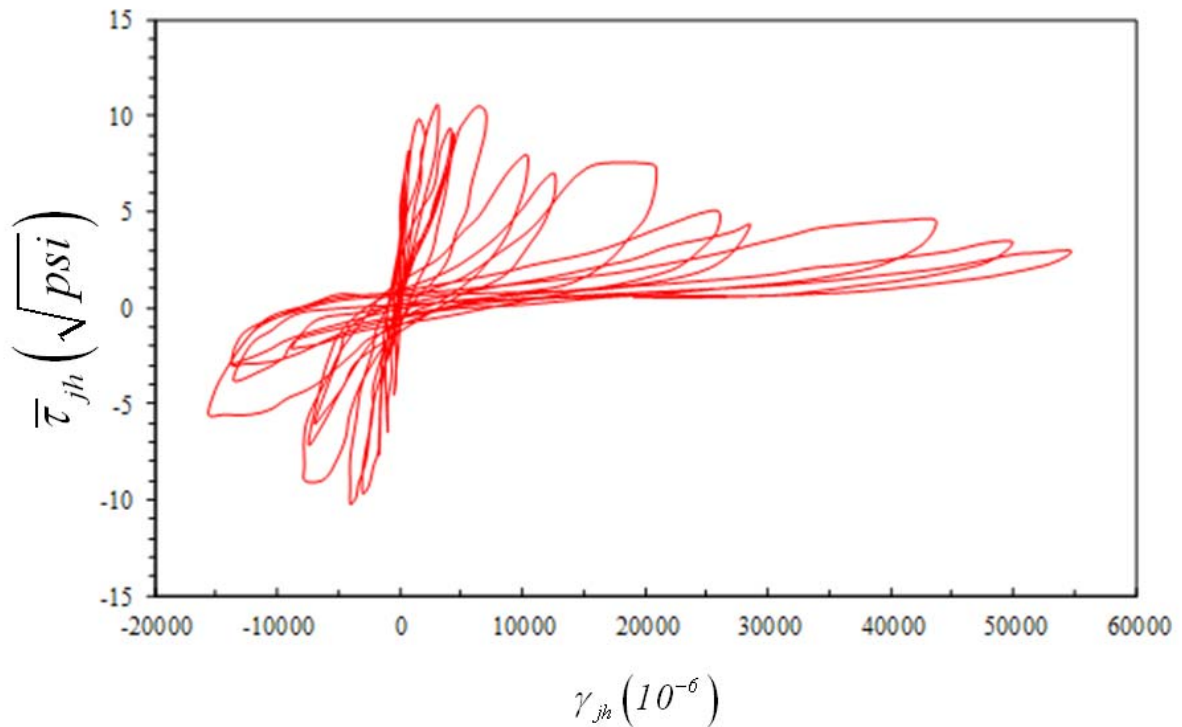


Figure 2-11 Example of a normalized joint shear stress versus joint shear strain graph (adapted from Pantelides *et al.* 2002)

The normalized joint shear stress is an important parameter since the design codes (i.e. ACI-318) limits the shear design of joints not to exceed an established value, which was based from experimental evidence. Such value will depend on the type confinement provided from the beams that frames into the joint. For the evaluation of existing structures, FEMA 273 establishes that for an unconfined exterior joint the normalized joint shear strength shall be taken as 6.

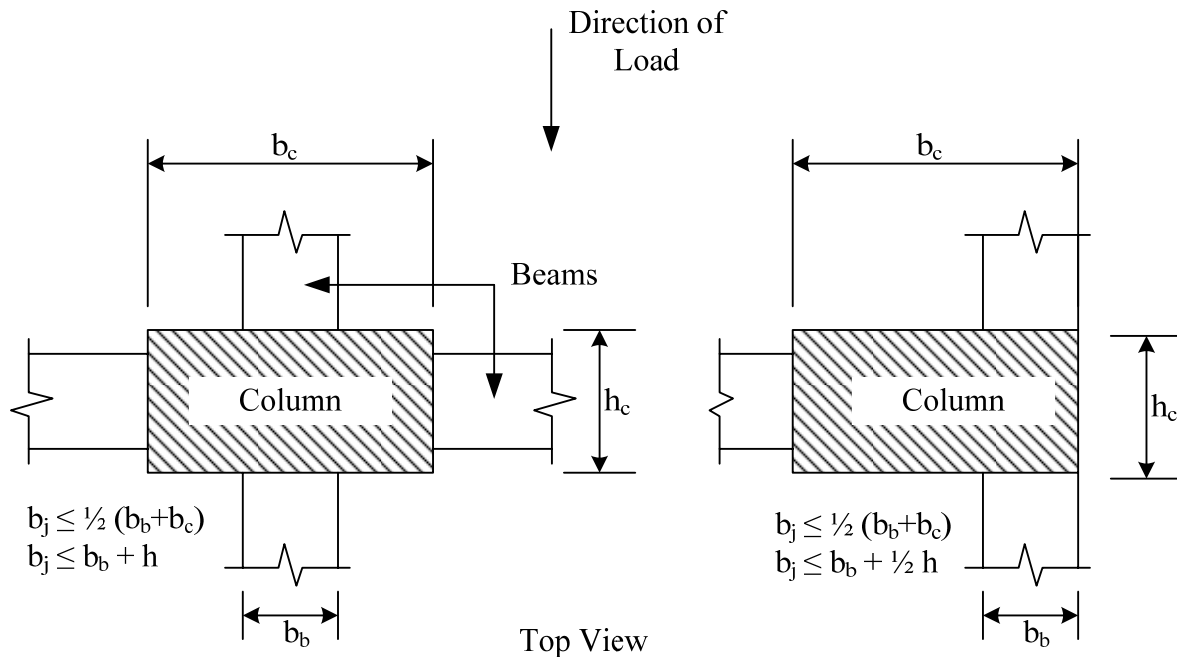


Figure 2-12 Effective joint area (adapted from ACI-352)

2.3 EXPERIMENTAL TESTS OF INTERIOR AND ISOLATED EXTERIOR JOINTS

One of the first experimental research projects was made by Hanson and Connor (1967), who studied the requirements for maintaining the ultimate capacity for cast-in-place beams and

column joints subjected to multiple reversals of loading. Seven full size specimens were tested: five representing an exterior joint at a low level of a tall building and two representing an exterior joint of the upper stories of a building. The main variables studied were column size, column axial load, the degree of confinement of concrete in the joint and the effect of the presence of spandrel beams at both sides of the column face. The beams and columns were designed with the ACI-318-1963 code. The results demonstrated that properly designed and detailed cast-in-place reinforced concrete frames can resist moderate earthquake without damage and severe earthquake without loss of strength. From the test results, the following observations can be drawn: a) specimens with adequate detailing in the joints perform very well and were capable of sustaining an axial load of 1,000 kip ($0.78 f'_c A_g$); b) specimens without transverse reinforcement in the joint perform poorly with the combined shear and bursting forces in the joint causing rapid deterioration; c) hoop reinforcement is necessary to avoid the buckling of the column reinforcement inside the joint and resisting the tendency of the joint to expand under multiple reversals of beam loading; d) the presence of the spandrel beam in three faces of the column was beneficial since the behavior of the joint without any hoops was clearly improved due to the confinement effects of such beams and, e) hoops are necessary for corner joints (confined on only two column faces) and isolated joints (unconfined).

Uzumeri (1977) conducted an experimental study of the behavior of cast-in-place RC beam-column joints subjected to slow load reversals simulating seismic loading. Four corner joints

and four isolated joint full size specimens were tested under a constant axial compressive force of 520 kip ($0.41 f'_c A_g$). The variables investigated were the amount and size of joint reinforcement, and stress – strain characteristics of the joint steel. The experimental results showed that: a) the behavior of the joints was greatly influenced by the amount of transverse reinforcement, since the confinement provided to the joints by transverse joint steel increased the ductility of the subassembly several times over the unreinforced joints; b) the ACI equations predict the cracking shear force well but the 45° truss analogy does not predict the behavior of reinforced joints; c) no significant effect of the stub beam (in corners joints) was observed, although the stub beam appeared to be providing marginal restraint to the joint; and d) the presence of the high axial compressive force ($0.41 f'_c A_g$) seemed to help at the early stages of loading; however when the joint deterioration started and the concrete in the core acted as a series of struts, this large force may be detrimental rather than helpful.

Seckin and Uzumeri (1980) studied the performance of nine full size beam-column exterior connections. Among the parameters studied were the column axial load and the amount of transverse reinforcement into the joint. The columns of all the specimens were subjected to variations of axial load from $0.09 P_o$ to $0.79 P_o$. Some of the conclusions presented by the authors are: a) in seismic risk areas, the presence of stirrups at the joint are essential since they provide confinement, shear resistance and increase the ability of the joint to provide continued anchorage to the beam steel; b) the ductility of the joint is undesirable, thus the yielding of the joint transverse steel should be avoided; c) the effect of the anchorage of the

beam steel provided by the joint was significant on the energy dissipation of the beams; and d) the magnitude of column axial load had little effect on the performance of a well designed exterior joint.

Ehsani and Wight (1985) studied the behavior of external reinforced concrete beam-to-column connections subjected to earthquake-type-loading (cyclic). Six specimens were tested, in which five of them were subjected to a constant axial load of approximately $0.07 f'_c A_g$ and the other one was subjected to a constant axial load of $0.13 f'_c A_g$. The scale of the specimens is not specified in the article. The effect of the following parameters was investigated: a) flexural strength ratio MR, defined as the sum of the flexural capacities of the columns to that of the beam; b) amount of transverse reinforcement used within the joint; and c) shear stress in the joint. From the test results, the following conclusions were drawn: a) flexural strength ratio MR greater than 1.4 avoid the formation of plastic hinges in the joints; b) to reduce excessive joint damage, column bar slippage and beam bar pullout, the maximum joint shear stress in exterior connections should be limited to $12\sqrt{f'_c}$ psi ($1.0\sqrt{f'_c}$ MPa); c) additional transverse reinforcement, when combined with conclusions 1 and 2, does enhance the behavior of the subassemblage; d) the amount of joint transverse reinforcement could be reduced if the flexural strength ratio, the joint shear stress or the anchorage requirements are significantly more conservative than the limits of the design

recommendations limits; and e) the confinement effect of the stirrups were observed even though the concrete in the joint was cracked, it was not crushed in all specimens.

Fuji and Morita (1991) studied the factors that influence the basic shear strength of beam-column joints without transverse beams and slabs. Eight one-third scale specimens, consisting of four interior and four exterior beam-column subassemblages in one-way frames were tested. Test variables were beam bar strength, column axial load and amount of joint hoops. The test results showed that: a) the magnitude of column axial load had no influence on the ultimate shear strength of the interior joints, however for exterior joints the magnitude of the axial load increases the shear strength; b) when the shear strength of the exterior joints was evaluated on the basis of projected length of hooked beam bars instead of total column depth, nearly the same strength was obtained for both types of joint; c) the increase of joint shear reinforcement ratio from 0.41 to 1.1% did not have notable effect on the behavior of the both types of joint; and d) once joint shear strain reached 0.5%, degradation of shear rigidity was accelerated under subsequent load reversals.

Kaku and Asakusa (1991) conducted tests of eighteen one-third scale specimens of RC exterior beam-column subassemblages under reversed cyclic loading. Test variables were column axial force, amount of joint hoop reinforcement, existence of intermediate bars and moment resisting capacity of columns. Test results showed that: a) the ductility of the subassemblages was increased due to the presence of the column axial compressive force, the

amount of the joint hoop reinforcement and the existence of the intermediate column bars. However, the presence of tensile axial force reduced the ductility dramatically and b) increase in the magnitude of the column compressive axial force increased the ultimate shear strength of the subassemblages.

Beres et al. (1996) studied the seismic behavior of exterior and interior RC joints designed for gravity loads only, that are characterized by non-ductile reinforcing details. Thirty four full scale specimens were tested. The parameters considered included: the amount of joint reinforcement, column bar arrangement, size of the embedded reinforcement, column axial force level (0.11 and $0.39 f'_c A_g$), concrete strength of the joint and the presence of a transverse beam stubs projecting from the sides of the joints to simulate the presence of beams framing in from out of plane. From the results of the test, the following conclusions are drawn: a) for interior joints, the presence of higher axial force ($0.39 f'_c A_g$) resulted in higher shear strength of the joints, but also the specimens show more rapid strength degradation; b) there was little difference in the joint strength based on other factors, like the presence of the transverse beam or the amount of reinforcement; c) for the exterior joints, the higher axial force, or the presence of 2 # 3 ties, resulted in a increase of the shear strength in the joint and a more gradual strength degradation; d) the presence of transverse beams resulted in slower strength degradation, but no increase in capacity and e) the joint shear strength factor obtained from the test was 30-40% below the limiting values specified by the ACI-ASCE 352 Recommendations.

Clyde et al. (2000) studied the performance under cyclic loading of RC joints with non ductile details, typical of buildings that were built in the 1960's. Four half-scale RC exterior joints were tested. Among the criteria of performance investigated are: effect of the axial compression load in the column on the joint performance at high levels of drift, lateral load capacity, drift, ductility and others. Two levels of axial compression load ($0.10 f'_c A_g$ and $0.25 f'_c A_g$) in the columns were studied. From the results of the test the following findings can be drawn: a) the joint shear coefficient γ changes with the variation of the axial compressive load, being 12.4 (psi) for joint with $0.1 f'_c A_g$ and 13.4 (psi) for joint with $0.25 f'_c A_g$; b) specimens with lower axial load were over 1.5 times more ductile than specimens with higher axial load; c) specimens with the higher axial load dissipated 20% less energy than the specimens with the smaller level of axial load; and d) the maximum nominal joint shear stress occurred at a joint shear strain between 0.0035 and 0.0045 for the specimens with $0.1 f'_c A_g$ and in a range of 0.0030 and 0.0035 for the specimens with $0.25 f'_c A_g$.

Hacuto et al. (2000) studied experimentally the seismic performance of poorly detailed RC interior and exterior beam-column joints, typical of pre-1970's designed moment-resisting frames in New Zealand. A total of eight full size specimens without axial load were tested. The parameters investigated were the amount of transverse reinforcement in the joint, the anchorage of the longitudinal bars passing through the joint and the effect of the bent of the

beams longitudinal reinforcement into the joint. Among the findings of the results are: a) if the nominal shear stress in the joint core exceeds approximately $0.17 f'_c$ the behavior of the interior joints would be poor in a severe earthquake; and b) the direction of the beam bar hooks in the joint core significantly influence the seismic performance of the exterior joints. This behavior was considerably improved when the ends of the hooks of the top and bottom longitudinal beam bars were bent into the joint core, as in current practice.

Pampanin *et al.* (2002) studied the behavior of RC joints designed for gravity only, under seismic loads. They performed an experimental test on six two third scale beam-column subassemblies, consisting of four exterior joints (Two "Knee" joints and two "tee" joints) and two interior joints, with structural deficiencies typical of Italian construction before the introduction of seismic code provisions in the middle of 70's. Among these deficiencies can be mentioned the use of smooth bars; inadequate detailing of the reinforcement (lack of transverse reinforcement into the joint; insufficient amount of column longitudinal reinforcement, etc.); inadequate anchorage detailing, etc. During the test, the column axial load was varied as a function of the lateral load, trying to better simulate the actual state of stress of the beam-column joint, with a constant values of axial force due to the gravity load of 100 kN ($0.10 f'_c A_g$) for exterior joints and 120 kN ($0.12 f'_c A_g$) for interior joints. The article does not explain in detail the way of the axial load was changed. The results showed that the combined use of smooth reinforcing bars with end-hook anchorage is a critical

source of significantly brittle damage mechanisms. They also introduced the concept of “shear hinge” that is characterized by severe strength degradation.

Park (2002) presents a summary of the results of several experimental seismic load tests on reinforced concrete full scale interior and exterior joints with substandard reinforcing details typical of building constructed in New Zealand before the 1970's. The more relevant effects that were investigated in the tests were: a) use of deformed and plain round longitudinal reinforcement; b) amount of transverse reinforcement in the joint core; c) poor anchorage of the longitudinal reinforcement passing through the joint; d) effect of the bend of the hook inside and outside the joint core; e) effect of the axial load and f) use of splices of the beam longitudinal reinforcement bars near the columns face (potential plastic hinge regions). From the results of the tests, the principal conclusions are: a) due to the presence of diagonal tension cracking in the joint core and the bond slip, the performance of typical interior joints designed before 1970's without transverse reinforcement in the joint core would be poor in a severe earthquake; b) the direction in which the ends of the beam bars hooks in the joint core were bending influenced the seismic performance of the exterior joints, being the behavior significantly improved when the beams bars were bent into the joint core; c) the specimens that use deformed bars instead of plain round longitudinal bars showed better performance in all the tests and it was found that the use of plain round longitudinal reinforcement enhance premature concrete tension cracking failure along the beam bar hooks; d) the presence of the compressive axial column load of about $0.25 f'_c A_g$ showed to be helpful, since it was

associated to a large increase of the stiffness and the strength of the joints and the compressive axial column load delayed premature tension cracking initiated by the beam bar hooks.

Pantelides et al. (2002) studied the seismic performance of beam-column joints designed before the mid-1970s. A total of six full scale reinforced concrete exterior joints were tested. All the specimens were constructed with the following characteristics: Absence of transverse reinforcement within the joint core; inadequate embedment of the longitudinal reinforcement of the beam into the joint, and poor confining reinforcement detail. Likewise, three of the specimens were subjected to a constant axial load of $0.10 f'_c A_g$ and the other three to a constant axial load of $0.25 f'_c A_g$. From the test results the following findings stand out: a) two failure modes related with the substandard details were primarily identified: a bond-slip failure and joint shear failure; b) the joint strength coefficient changes with the variation of the column compressive axial load, this change being of the order of 15 to 35%; c) the presence of the higher axial load was beneficial in terms of the joint strength coefficient, but was detrimental for displacement ductility and energy dissipation.

Hwang et al. (2005) studied the effect of joint hoops on the shear strength of exterior reinforced concrete beam-column joints. Nine specimens were tested under reverse cyclic loading. The scale is not specified in the article. All test specimens were designed to have adequate shear strength of joints. The main parameters investigated were the amount and

detail of joint hoops. The following conclusions were drawn from the tests: a) joint hoops have three major function: 1) carry shear as a tension tie; 2) constrain the width of crack and 3) retard the strength deterioration of concrete and not to enhance the strength of concrete; b) no evidence of the beneficial effect of confinement by transverse reinforcement was found; c) a lesser amount of hoop reinforcement with a wider spacing up to 300 mm, could be used without significantly affecting the behavior of joints and d) test data also demonstrated that a beam-column joint without hoop bars can show satisfactory seismic behavior, as long as the joint is provided with adequate shear strength.

Wong (2005) studied the shear strength and seismic behavior of non-seismically designed beam-column exterior joints. He tested under reversed cyclic loading, a total of seventeen large scale specimens divided into two groups: a) BS series that were eleven in total in which the parameters investigated were the beam to column depth ratio, the transverse reinforcement ratio, longitudinal reinforcement ratio and the type of beam reinforcement anchorage. All the BS series, were tested under a constant axial load of $0.15 f'_c A_g$ considering the practical range of axial load in real frame building and b) J series, that were six in total, in which the parameters investigated were the effect of the joint span-to-depth ratio, amount of transverse reinforcement and the column axial load level ($0.03 f'_c A_g$ and $0.15 f'_c A_g$). Based on the results of the test, the following conclusions are drawn: a) the type of beam reinforcement anchorage has significant effect on the load-displacement hysteretic behavior and shear resistance of the exterior beam-column joints; b) laps in column

reinforcement located at the column end zones seem not to affect the shear strength of beam-column joints under reversed cyclic loading; c) beam-column depth ratio was shown to be an important factor to affecting the shear strengths and ductility of beam-column joints; d) transverse reinforcement can increase the shear strength and enhance the ductility of joints even though moderate amount of transverse reinforcement is incorporated; d) the axial load do not show to have influence on the behavior of joints with and without transverse reinforcement since it is demonstrated that similar ductility and maximum shear strength can be obtained for specimens having different axial load levels and e) the shear strength predicted by the ACI 318-02 and AIJ, for non-seismically detailed exterior beam-column joint, was significantly overestimated with values higher than 50% of the experimental results.

Moacyr *et al.* (2007) studied experimentally the influence of the joint transverse reinforcement rate and concrete compressive strength (f'_c) on the RC beam-column connection behavior, under cyclic loading. A total of four (4) specimens were tested (the scale is not specified by the author) in which the amount of joint shear reinforcement and concrete compressive strength were the studied variables. To reproduce the effects of gravity loads, a constant axial load equivalent to $0.15 f'_c A_g$ was applied to the column. Cyclic loads were applied to the end of the beam to simulate cyclic lateral actions on reinforced concrete building frame. From test results some observations can be drawn: a) the number of stirrups affects the global response of exterior joints since the shear capacity of the joints was

improved when the amount of stirrups was increased and specimens with less rate of shear reinforcement showed longer and more opened cracks pattern; b) the concrete compressive strength f'_c has great influence on the joint performance since it increase the shear capacity and the global behavior of the joint and c) the shear capacity of the joint is affected more by the concrete compressive strength than by the number of stirrups.

2.4 EXPERIMENTAL TESTS IN CORNER JOINTS

Priestley and Hart (1994), based on the damaged observed in the Royal Palm Resort Hotel during the August 1993 Guam earthquake, conducted an experimental study of two 2/3 scale exterior joints that represented a second floor corner joint of the hotel, that failed during the ground motion, causing a partial pancaking of the second story. A post earthquake research suggests that the main reason of such failure was the lack of the transverse reinforcement into the joint core that was omitted during the construction stage in many locations of the building. One of the specimens was constructed based on the design drawings ("as-designed"), while the second, which omitted the horizontal joint shear reinforcement, represented the actual or "as-built" condition. Both specimens included the presence of a drop panel below the beams. The principal parameter studied was the amount of transverse reinforcement inside the joint. Trying to simulate the seismic response of the ten stories above the second level, they used a sophisticated form of axial load control (as a function of the beam load) consisting in a constant axial load, representing the algebraic sum of the dead load of the columns and the vertical loads resulting from the beam shears. The two specimens were subjected to the same

pattern of load, being the first five stages load controlling, while the last seven stages were displacement controlled, by specified forces and displacements applied to the beam ends, uniaxial (longitudinal beam was loaded first, thereafter the transverse beam) and biaxial (both beams simultaneously). This research is the first registered in applying biaxial load, and thus the first to study the behavior of corner joints. From the experimental test it was observed that the behavior of the "as designed" unit was very good. The axial load recorded at the first stage of the test was $0.18 f'_c A_g$ and was gradually increased up to $0.39 f'_c A_g$. Even though the presence of several cracking in the joint region and the degradation of shear strength was observed, it was able to maintain its structural integrity and the condition of the joint region at the end of the testing was such that repairing the cracks and putting back the concrete cover, it would expect to give back the full structural capacity of the joint. By contrast, the performance of the "as-built" unit was very poor. The axial load recorded at the first stage of the test was $0.18 f'_c A_g$ (like the "as designed" unit). At larger displacements, load capacity decreased (the axial load recorded decreased from approximately $0.38 f'_c A_g$ at one stage before the last to $0.23 f'_c A_g$ at the last stage) and physical degradation became severe. At maximum displacement, joint degradation involving spalling of concrete, straightening of beam rebar hooks and crushing of joint concrete occurred. This resulted in loss of capacity to carry, first the seismic axial load, and finally the gravity load, resulting in a gravity load collapse situation. It is concluded that the omission of joint shear reinforcement had a very significant and detrimental effect on the seismic capacity of the

corner columns, and would appear to be a significant contributor to the failure of the structure.

Pampanin *et al.* (2007) studied experimentally the 3-D behavior of a corner joint with typical details of the 1970s, subjected to bi directional cycling loading. These details include the use of plain rounds bars with end hooks and the presence of a minimum amount of transverse reinforcement. They compared the performance of the 3-D corner with an exterior 2-D joint. To provide a more realistic simulation of what would occur on a beam-column joint during an earthquake, the axial load was varied as a function of the lateral force. The results of the test, corroborated the higher vulnerability of exterior 3D corner joints, when compared with the performance of 2D joint subjected to uni-directional loading protocol. The 3D specimen shows a more complex three-dimensional concrete wedge mechanism as compared with the 2D wedge mechanism. Finally the 3D arrangement and bi-directional loading resulted into a reduction of the overall lateral load capacity of 33% and 15% in the positive and negative direction, respectively (corresponding to decreasing and increasing of the axial load) when compared with the 2-D specimen.

2.5 PARAMETERS AFFECTING THE SEISMIC PERFORMANCE OF CONCRETE JOINTS

After reviewing the results of the experimental investigation made in the past four decades, findings of the effects of some of the principal parameters that affect the seismic performance of the concrete joints can be summarized as follow:

a) Presence of Transverse Beams:

- The presence of the spandrel beam in three faces of column was beneficial due to the confinement effects provided by such beams (Hanson and Connor 1967). For the case of corner joints confined only by two beams in adjacent direction Uzumeri 1977, found that they provide marginal restraint to the joint and Beres et al. 1996, found that the presence of transverse beams resulted in slower strength degradation, but no increase in capacity of the joint. These authors have in common that their tests use stubs beams with no load or have a very small load applied in these beams (a constant load of 5 kips for Uzumeri 1977) and joints without transverse reinforcing.

b) Transverse reinforcement:

- It has been demonstrated that the presence of hooks inside the joint core is important since: a) it prevent the buckling of the column reinforcement (Hanson and Connor 1967); b) It provide confinement to the concrete core in the joint (Uzumeri 1977, Ehsani and Wight 1985); c) increase the shear capacity of the joint and help to show more gradual strength

degradation (Seckin and Uzumeri 1980, Beres et al. 1996, Wong 1995, Moacyr et al. 2007); and d) provide continued anchorage to beam steel (Seckin and Uzumeri 1980).

c) Column Axial Load:

- The results have shown that the increase in axial load increased the stiffness of the subassemblage (Uzumeri 1977, Park 2002). In terms of shear capacity, results found in the literature are divided, because some researchers have found that when they use high axial loads in their test, they observed an improvement in the shear strength of exterior joints (Fuji and Morita, 1991; Kaku and Asakusa 1991; Beres et al. 1996; Clyde et al. 2000; Pantelides et al. 2002; Park 2002) and interior joints (Beres et al. 1996). However, others have found little or no effects in the shear strength of exterior joints (Meinheit and Jirsa 1977, Seckin and Uzumeri 1980, Wong, 2005) and interior joints (Fuji and Morita 1991). The discrepancies also exist in terms of behavior, in which some researchers found that high axial loads was detrimental in terms of displacement ductility, energy dissipation and strength degradation (Uzumeri 1977, Beres et al. 1996, Clyde et al. 2000, Pantelides et al. 2000) but the test performed by Wong 2005, shows that specimens having different axial load levels behaved similar in terms of ductility.

d) Anchorage of the beam bars into joint:

- The direction of the beam bar hooks into the joint core significantly influences the seismic performance of the exterior joints. This behavior was considerably improved when the ends of the hooks of the top and bottom longitudinal beam bars were bent inside the joint core (Seckin and Uzumeri 1980; Hacuto et al. 2000; R. Park 2002; Wong 2005).

e) Concrete compressive strength:

- From the results of their research Moacyr *et al.* 2007, concluded that the concrete compressive strength f_c' has great influence on the joint performance since it increases the shear capacity and the global behavior of the joint and the shear capacity of the joint is affected more by the concrete compressive strength than by the number of stirrups.

A summary containing the major findings of some of the research of the literature review is present in Table 2-1.

Table 2-1 Summary of some findings of the literature review

Author	Type of joint	Major Findings
Hanson and Connor (1967)	Exterior	Specimens with adequate detailing in the joints, performs very well. Specimens without transverse reinforcements performs very poor. Sprandel beams improve the behavior of the joints due to confinement effects.
Megget (1974)	Exterior	The presence of transverse beam, greatly contribute to the confinement of joint core.
Uzumeri (1977)	Exterior	Transverse reinforcing in joints increase the ductility. Flexural strength ratio less than 1.57 produce hinge of columns. Stub beam have no significant effect, although it appear to provide marginal restrain to joint. High axial force helps at early stage of loading, but is detrimental once the joint core is cracked.
Meinheit and Jirsa (1977)	Exterior	Dimension of cross section greatly influence the strength of the joint. No evidence of the influence of axial load in the shear capacity of the joint. High axial load increased the size of the cracking once it's appearing.
Seckin and Uzumeri (1980)	Exterior	Stirrups at joint core provide confinement, shear resistance and continuing anchorage to beam steel. The magnitude of column axial load had little effect on the performance of well designed exterior joint.
Ehsani and Wight (1985)	Exterior	Flexural strength ratio greater than 1.4 avoid formation of plastic hinges in the joints. Shear stress below $12\sqrt{f'_c}$ psi reduce excessive joint damage in exterior joints.
Fuji and Morita (1991)	Interior Exterior	Increase of the column axial load: a) Did not influenced the shear strength of interior joints. b) Improved the shear strength of exterior joints.
Kaku and H. Asakusa (1991)	Exterior	Column axial force and amount of joint hoop influence the ductility of subassemblage. Intermediate column bars increase the ductility of the subassemblage.
Priestley and Hart (1994)	Corner	Specimen with adequate detailing in the joint, performs very well. Specimen without transverse reinforcements performs very poor, with loss of axial capacity.
Beres <i>et al.</i> (1996) (non ductile)	Interior Exterior	Higher axial force increases the shear strength in interior joints and accelerates the strength degradation. Transverse beams and amount of reinforcement has little influence in the joint strength of interior joints. The presences of 2 # 3 ties increased the shear strength in the joint and help to show more gradual strength degradation. Higher axial force increases the shear strength in exterior joints and help to show more gradual strength degradation. Transverse beams resulted in slower strength degradation, but no increase in capacity.

Table 2-1 Summary of some findings of the literature review (Cont.)

Author	Type of joint	Major Findings
Clyde <i>et al.</i> (2000) (non ductile)	Exterior	Joint strength coefficient change with the variation of the column axial load. The increase in axial load is translated in terms of less energy dissipation.
Hakuto <i>et al.</i> (2000) (non ductile)	Interior Exterior	Direction of the beam bars hooks into the joint core significantly influences the seismic performance of exterior joints. Bars ends hooks bent into the joint core considerable improve the behavior of exterior joints. Shear stress greater than $12\sqrt{f'_c}$ psi will produce excessive joint damage in interior joints designed before 1970's.
Pampanin <i>et al.</i> (2002) (non ductile)	Interior Knee	Combination of smooth reinforcing bars, with end hook anchorage is a critical source of brittle damage mechanisms. Direction of the beam bars hooks into the joint core significantly influence the seismic performance of both joints. Bar slip phenomena resulted in marked cyclic stiffness degradation ("pinching" effect).
Park (2002) (non ductile)	Interior Exterior	Joint without transverse reinforcement will performance poorly due to bond slip and presence of diagonal tension cracking. Bars ends hooks bent into the joint core considerable improve the behavior of exterior joints. Use of plain round longitudinal bars enhances premature concrete tension cracking failure along the beam bar hooks. Axial load about $0.25 f'_c A_g$, showed to be helpful since it increase the stiffness and strength of the joints, delaying premature tension cracking initiated by the beams bar hooks.
Pantelides <i>et al.</i> (2002) (non ductile)	Exterior	Substandard details lead to two type of failure: bond slip and joint shear failure. Joint strength coefficient change with the variation of the column axial load (15 to 35 %). Axial load of about $0.25 f'_c A_g$ was beneficial in terms of join strength. Axial load of about $0.25 f'_c A_g$ was detrimental for displacement ductility and energy dissipation.
Hwang <i>et al.</i> (2005)	Exterior	The function of the joint hoops is to carry shear as tension tie and constrain the width of crack. A spacing of the hoops of 12 in (300 mm) could be used without significantly affecting the behavior of the joints. Joints without hoops bar can show satisfactory seismic behavior if the joint is provided with adequate shear strength.
Wong (2005) (non ductile)	Exterior	Anchorage of the beam reinforcement significantly affects the hysteretic behavior and the shear resistance. Laps in column reinforcement located at the column end zone no affect the shear strength of the joints. Transverse reinforcement increases the shear strengths. The ductility of the joint was enhanced even only moderate amount of transverse reinforcement is incorporated. The axial load does not show to have influence on the behavior of joints with and without transverse reinforcement.
Moarcy <i>et al.</i> (2007) (non ductile)	Exterior	Compression strength is the major factor that governs the joint shear capacity. Joint transverse reinforcement rate influence the global response of joints; It become more relevant for high-level forces, such as the ones close to the capacity of the connection. Increasing the number of stirrups in the joint also increases its shear capacity.

2.6 RESISTING MECHANISM OF EXTERIOR JOINTS

The internal forces acting on an exterior beam column joint during seismic actions, when a plastic hinge forms in the beam is shown in Figure 2-13(a). Tension and compression forces produced in the steel in the beam and columns faces are labeled as T and C_s , respectively. C_c represents the compression forces produced in the concrete. V and V_c are the beam and column shear respectively. By equilibrium in the upper part of the joint, the horizontal shear force in the joint core is expressed as follows:

$$V_{jh} = T - V_c \quad 2.2$$

According to Park and Paulay (1975) this shear force is resisted by two kinds of mechanisms called the diagonal strut mechanism and the truss mechanism (Figure 2-14). In the diagonal strut mechanism, all the shear force is resisted by a concrete strut. In the truss mechanism it is assumed that part of the joint shear force is resisted by the joint steel. For an exterior joint without transverse reinforcement, only the diagonal strut mechanism will be present.

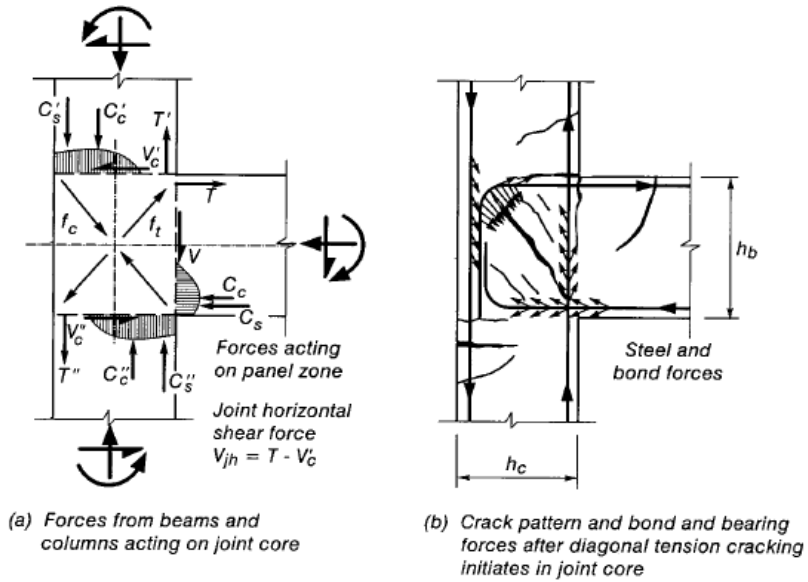


Figure 2-13 Exterior beam-column joint subjected to seismic actions. (adapted from R. Park 2002)

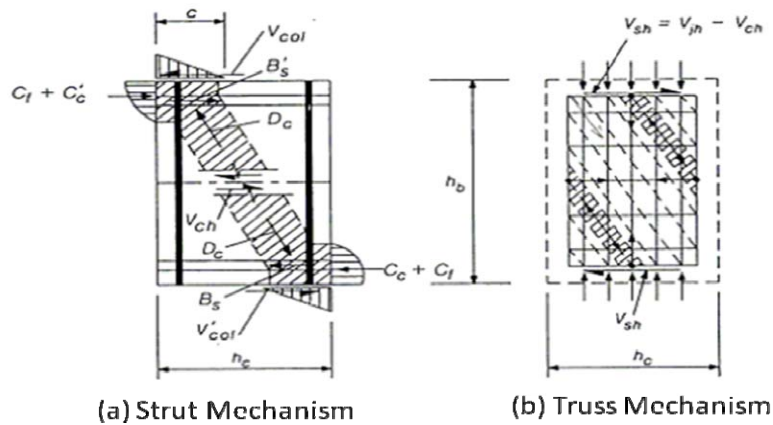


Figure 2-14 Mechanisms of shear transfer at exterior joint: (a) diagonal strut mechanism; and (b) truss mechanism. (adapted from Park and Paulay 1975)

2.7 MODE OF FAILURE IN BEAM-COLUMN JOINTS

Jirsa (1981) have classified the modes of failure in beam to column joints into the following types:

- 1. Joint shear failure:** Can occur either without yielding of the beam reinforcement (so called J Failure) (Figure 2-15) or with the beam reinforcement yielding (BJ Failure) (Figure 2-16). In the case of BJ failure, once the beam attains its yielding stress, as a result of successive cycling loads, a decrease in the capacity occurs and finally the failure is controlled by shear capacity. Both J and BJ failure are more prone to take place in unreinforced concrete joints.

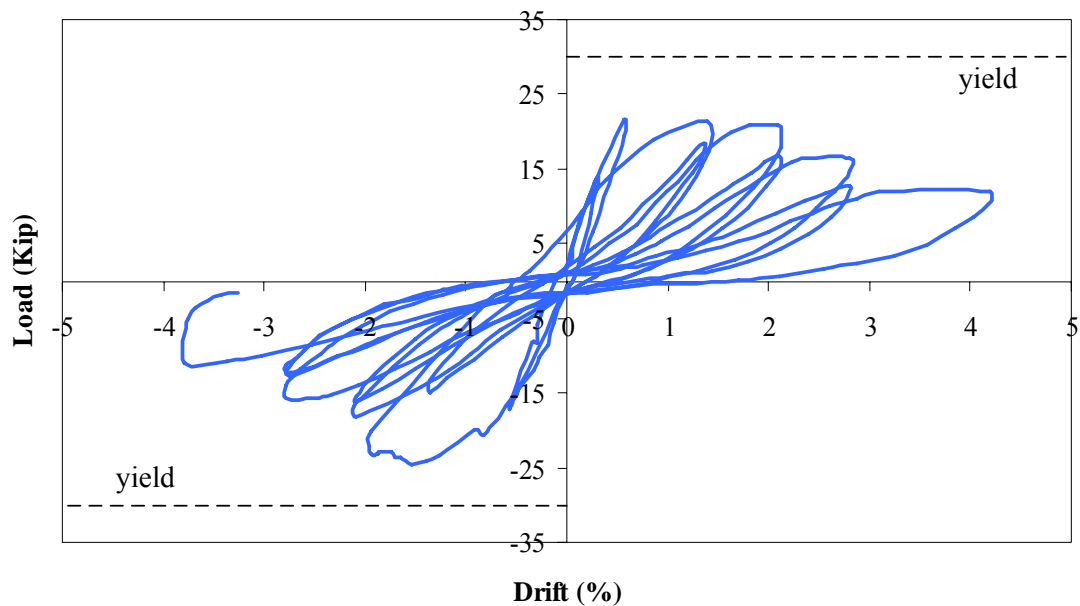


Figure 2-15 Load – Drift curve showing J failure

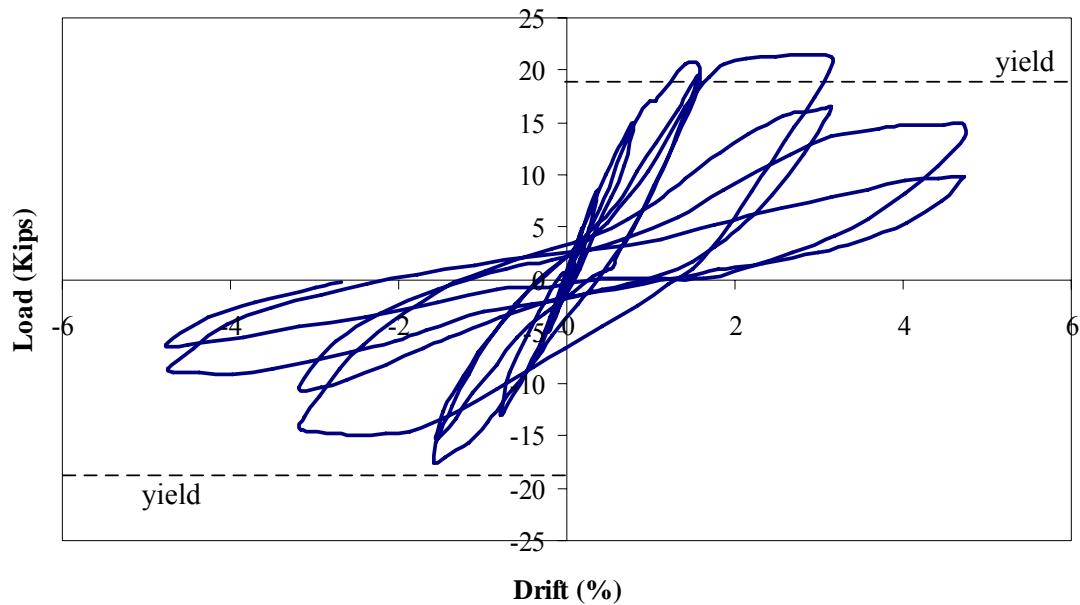


Figure 2-16 Load – Drift curve showing BJ failure

2. **Anchorage Failure:** This type of failure can happen because two main reasons: a) Once the beam reinforcement yields, under successive cycle of loading, the yielding penetrates into the joint and dilate the surrounding concrete or b) Due to large bond stresses product of excessive bar diameter passing through the joint. The load versus displacement curve from anchorage failure are similar to the shear failure, hence is not easy to distinguish both type of failure and thus only the crack pattern can give a suggestion of the mode (Jirsa 1981). Figure 2-17 shows an exterior joint presenting anchorage failure.

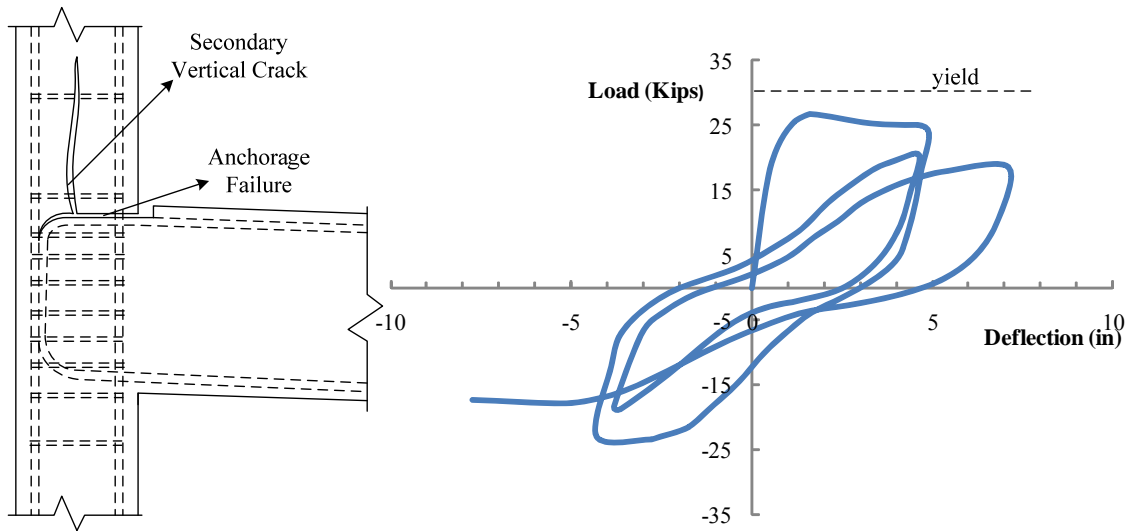


Figure 2-17 Exterior beam-column joint presenting anchorage failure (adapted from Jirsa 1981)

3. **Beam or column hinging:** In this type of failure, the inelastic deformation occurs in the beam or column framing into the joint.

4. **Compressive failure:** Compressive failure is prone to occur in exterior or corner joints due to the lack of total confinement of the joint in all sides. This type of failure is not typically reproduced in laboratories.

2.8 MODELS FOR THE PREDICTION OF JOINT SHEAR STRENGTH

Several models for the prediction of the joint shear strength for reinforced and unreinforced joints have been proposed in the literature. There are based in different resisting mechanism or basic concepts for their development. Some models have been based in the Strut and Tie concept (Hwang and Lee (1999, 2000), Ortiz (1993), Vollum (1998), Hassam et al (2010)). Others have adopted a single strut mechanism (i.e. Zhang and Jirsa (1982)). Another group (i.e. Pantazopoulou and Bonacci (1992), Wong (2005), Tsonos (2007)) have use the average plane stress-strain approach to develop their model. Other researchers have proposed empirical models (i.e. Sarsam and Phipps (1985), Taylor (1974), Scott et al. (1994), among others).

In a recent study Park and Mosalam (2009) used a large database composed by test of unreinforced exterior joint from the literature and proposed two joint shear models, one semi empirical and another analytical, in which the shear force is resisted by a mechanism composed by two parallel concrete struts.

2.9 JOINT ELEMENT MODELS OF EXTERIOR OR INTERIOR JOINTS

The simulation of the seismic response of beam-column joints have been largely studied for the past 25 years. Researchers have been focused in modeling the behavior observed in laboratory test with elements that take into account the main variables that affect such behavior. As result, several models that ranges from a simple rotational spring element to

as sophisticated as multi spring element have been proposed and implemented in structural analysis programs. Some of these models are summarized in the following subsection.

2.9.1 ZERO LENGTH ELEMENT

El-Metwally and Chen (1988) applied the thermodynamics field theory to develop a moment-rotation relationship of a RC joint modeled as a concentrated rotational spring. This model was limited to connections properly designed and having adequate shear strength. The spring stiffness is a function of the initial rotational stiffness of the connection, the ultimate moment capacity of the connection M_u , and of an internal variable that depends of the energy dissipation in the joint.

Alath and Kunnath (1995) used a zero length element along with rigid links to model the joint panel geometry (Figure 2-18(a)). This rigid links controls the relative rotation between the beam and column, like a scissor. The property of the rotational spring was determined from empirical shear-strain relations and the hysteretic rules were assigned experimentally.

Ghobarah and Biddah (1999) developed a macro-model that represents the joint by two rotational springs in series, one representing the joint shear deformation and the other the reinforcing bars bond-slip that are only influenced by the relative rotational displacements between the nodes, as illustrated in Figure 2-18 (b). The softening truss

model theory was used to satisfy equilibrium of stress resultants and compatibility of deformation within the joint, taking into account the constitutive laws of concrete and reinforcement. Hysteretic models for the spring bond slip and the concrete joint shear spring were used. The model was implemented into the nonlinear dynamic analysis program SARCF to analyze two buildings designed on early 1960s with nonductile details assuming flexible joints and comparing the results with rigid joints assumption.

Pampanin et al. (2003) proposed a simplified analytical model which consists of a rotational spring that considers the nonlinear behavior of joints with substandard details. The moment-rotation characteristics of the spring were based on equilibrium considerations of the principal tensile stress-shear deformation curve. The cyclic performance of the joint was considered by means of suitable hysteresis rules with pinching behavior. Based on the shear distortion of the spring, limit states for exterior tee joints also were proposed.

Based on the scissor model of Alath and Kunnath (1995), Celik and Ellingwood (2008) developed a joint model whose envelope backbone curve was based in available test data. The shear stress-strain relationship was transformed into a moment-rotation relationship from equation resulting from the joint dimension and the equilibrium of the joint. The hysteretic and pinching behavior was calibrated with experimental data.

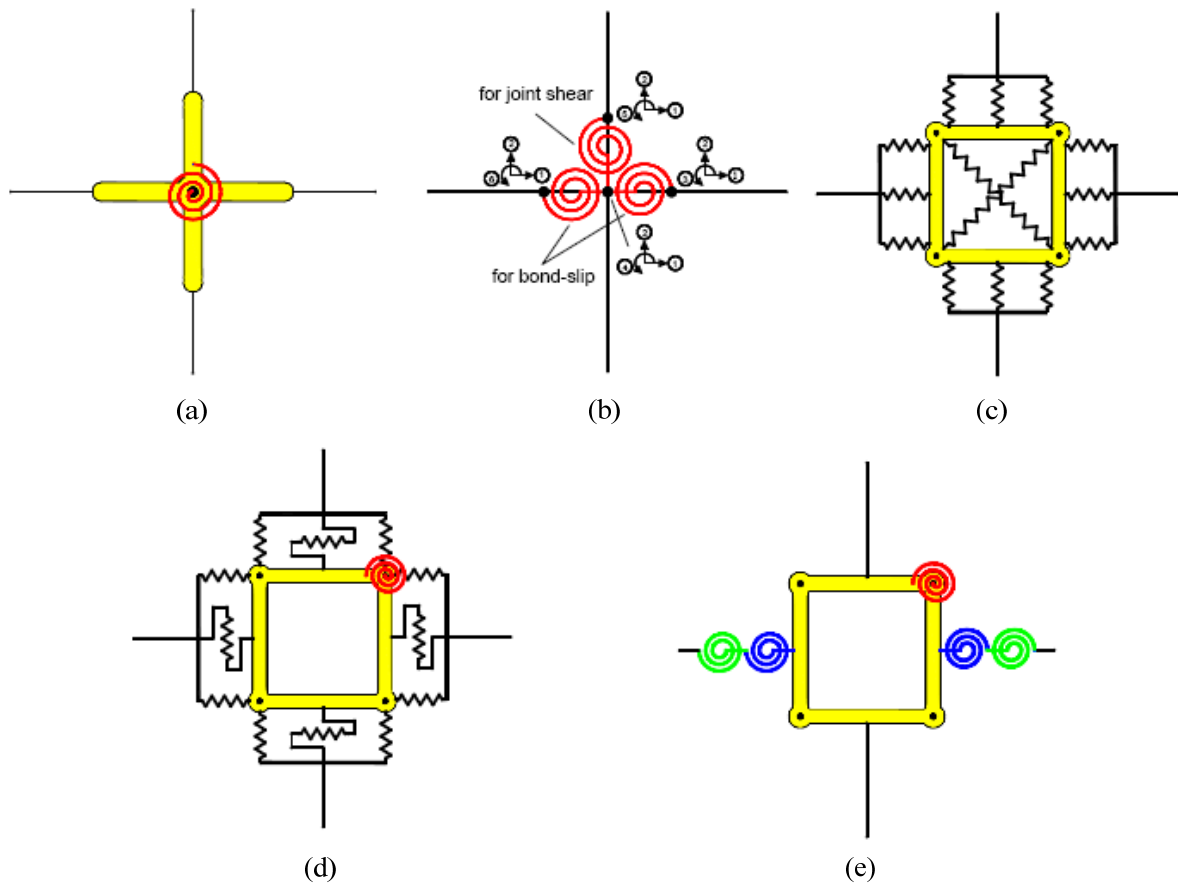


Figure 2-18 Existing joint element models for beam-column simulation (adapted from Celik and Elingwood 2008): (a) Scissor Model (Alath and Kunnath (1995), (b) Biddah and Ghobarah (1999), (c) Youssef and Ghobarah (2001), (d) Lowes and Altoontash (2003), (e) Shin and LaFave (2004)

2.9.2 MULTI SPRING ELEMENT

Youssef and Ghobarah (2001) presented a model for the joint that takes into account the shear deformations and the bond-slip deformations as well as flexural deformations in the plastic hinge regions. The model is shown in Figure 2-18(c). The bond slip and concrete crushing is represented using three concrete springs and three steel springs respectively, while the shear deformations are represented by two shear springs. Each of these springs

has associated hysteretic behavior models developed by the authors in a previous work (Ghobarah and Youssef 1999). The proposed model was incorporated in the structural analysis program PC-ANSR (Maison, 1992). The model was validated with experimental data (assuming rigid joint and flexible joint).

Lowes and Altoontash (2003) proposed a macro-element model of the entire joint that simulate the inelastic joint response due to anchorage failure, failure of the joint core under shear loading and failure of interface-shear transfer mechanisms. The model is shown in Figure 2-18(d). A constitutive model to represent load-deformation history of the bond-slip springs that simulates inelastic anchorage failure was developed. The inelastic response of the joint core is simulated by a shear-panel component in which its constitutive model employed the modified compression field theory to define the envelope of the shear stress-strain history of the joint core. The load deformation behavior of the shear panel and the bar slip are functions of the material properties, joint geometry and joint reinforcement arrangement.

Shin and LaFave (2004) proposed a macro model composed by four rigid link elements that represent the joint panel zone, one rotational spring in one of the joint panel and two rotational springs in series located between the beam and the joint (Figure 2-18 (e)). The envelope of the shear response of the interior beam-column joint and the hysteretic parameters were calibrated using available test data.

Mitra and Lowes (2007) developed a model to simulate the response of RC interior joints that was evaluated with a wide range of experimental data, which include a wide variety of design parameters, but excluding joints with plain round bars. The model is a modification of the previous model presented by Lowes and Altoontash (2003). These modifications consisted in relocate bar-slip springs, at the centroid of beam and column flexural tension and compression zones and includes a new model for calibration of the joint-panel component, which assumes a diagonal compression strut mechanisms for load transfer within the joint, rather than a uniform shear stress field as in the previous model; and the inclusion of a new bar-slip response model. The model was implemented in the OpenSees analysis program.

It can be appreciated that the multi spring element models are not easy to use for the analysis of an entire building and for that reason the simple element joint are more attractive for this purpose.

2.10 ENVELOPE BACKBONE CURVE FOR SUBSTANDARD RC ISOLATED JOINTS SUSTAINING J AND BJ FAILURE

The behavior of a structure subjected to cyclic loading can be studied by means of an envelope backbone curve of its load versus displacement graph. A backbone curve is defined generally through of a series of points that mark where a change of the stiffness takes place. The backbones are the basis of models for the prediction of cyclic behavior

of concrete frames. Figure 2-19 and Figure 2-20 shows the load versus displacement graph of a specimen corresponding to the setup shown in Figure 2-5 experimenting J and BJ failure, respectively along with its envelope backbone curve. The explanation of each point is as follows:

- **J failure:** The first important change in the stiffness occurs at point A which represents the cracking of the joint. The second change of stiffness occurs at point B which represents the point in which the specimens attains its maximum strength. After reaching point B, the subassembly presents stiffness degradation until it fails or until the test is finished at point C. Point C, often represents the point of residual strength of the specimen.
- **BJ failure:** Point A, as in J failure, represents the cracking of the joint. Point B represents the point in which the beam reinforcement reaches its yield stress. Point C represents the point in which the specimens reach its maximum strength. After this point a degradation of the strength and stiffness appears, until reaching the point D which represents the end of the test or the point of residual strength.

For modeling purposes, instead of having a four segment envelope curve, for the case of BJ failure, a simplified envelope backbone could be a three linear path represented by 0-A-B'-D segment.

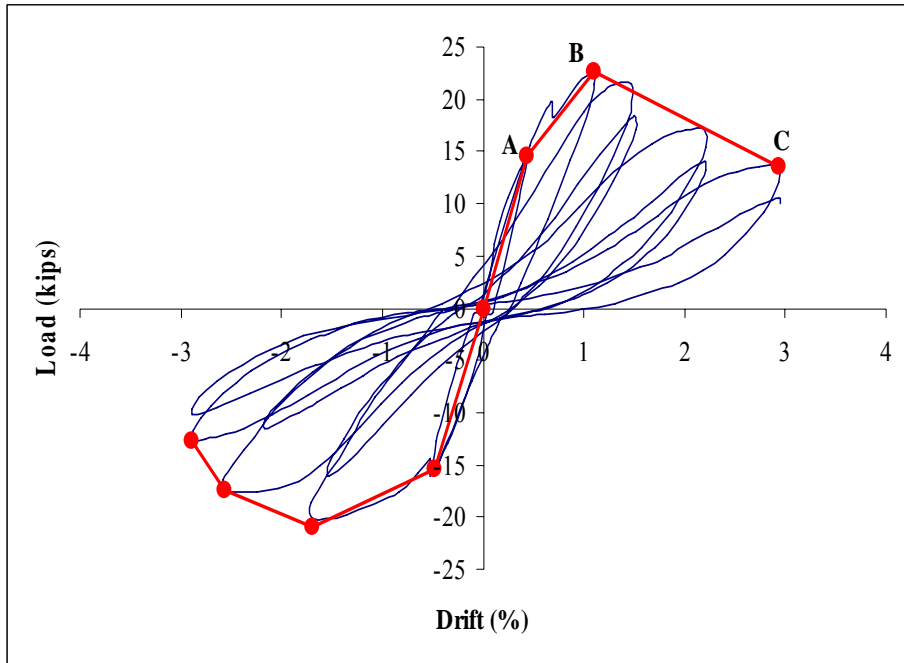


Figure 2-19 Envelope backbone curve for J failure mode

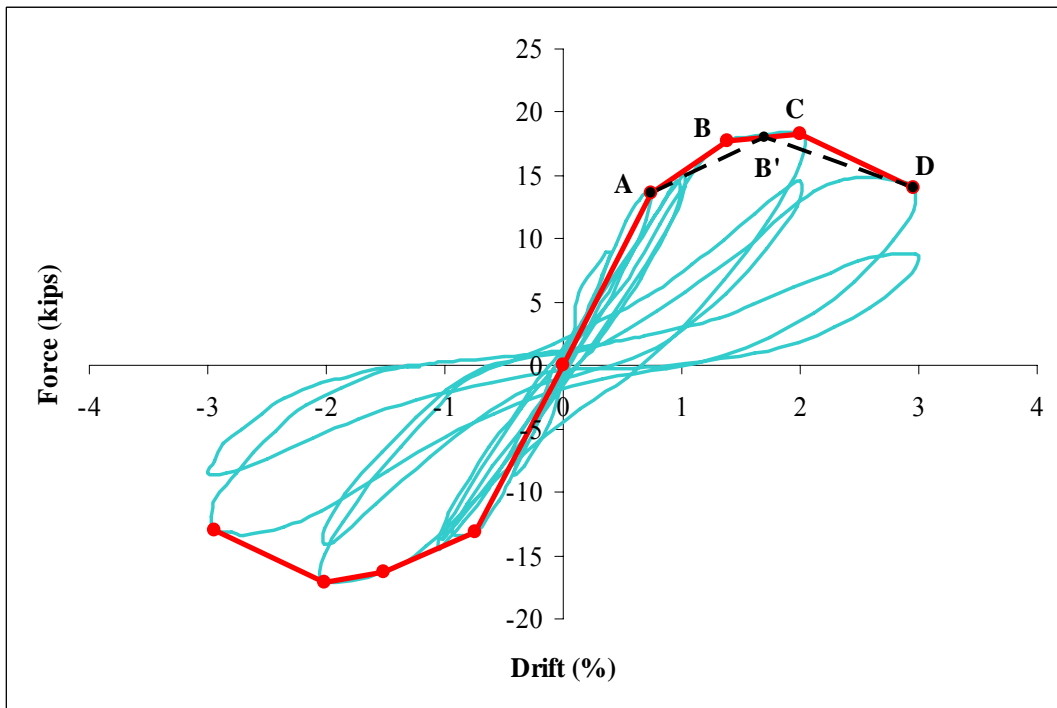


Figure 2-20 Envelope backbone curve for BJ failure mode

2.11 RIGID JOINT ASSUMPTION

A common practice in modeling a reinforced concrete frame is to assume that joints are rigid. With this assumption it is implied that joints are going to transfer forces without suffering significant damage, that is, damage is assumed to occur in the adjacent beam and columns that connect the joint. Accordingly, the joint is designed with a proper amount of stirrups, to ensure the confinement of the concrete inside the joint and thus avoiding a shear failure of the connection. This promotes that the adjacent frame members develop their flexural capacities and that the frame structure behaves in a ductile manner which is desirable in the earthquake design philosophy.

An example of a nearly rigid joint is provided in Figure 2-21 which is a specimen designed and detailed according to the New Zealand code of 1980, tested by Paulay and Scarpas (1981). The response of the specimen as shown in Figure 2-22 was excellent, since it exhibits good energy dissipation, no loss of strength either stiffness degradation, as desired in a ductile behavior. At the end of the test, all the damage was located in the beam. The joint was only slightly cracked, as shown in Figure 2-23.

The details of a test specimen of an unreinforced joint in a concrete frame, typical of the construction in the 70's, tested by Wong (2005) is shown in Figure 2-24. The response of the specimen is shown in Figure 2-25. As expected the behavior was very poor, with little energy dissipation. After attaining its maximum strength, shows gradual strength and stiffness degradation. The response presents a pinching effect which is directly related to

the bond slip phenomenon as well as the shear failure. This behavior is unacceptable in a modern reinforced concrete frame, but can be expected in older construction.

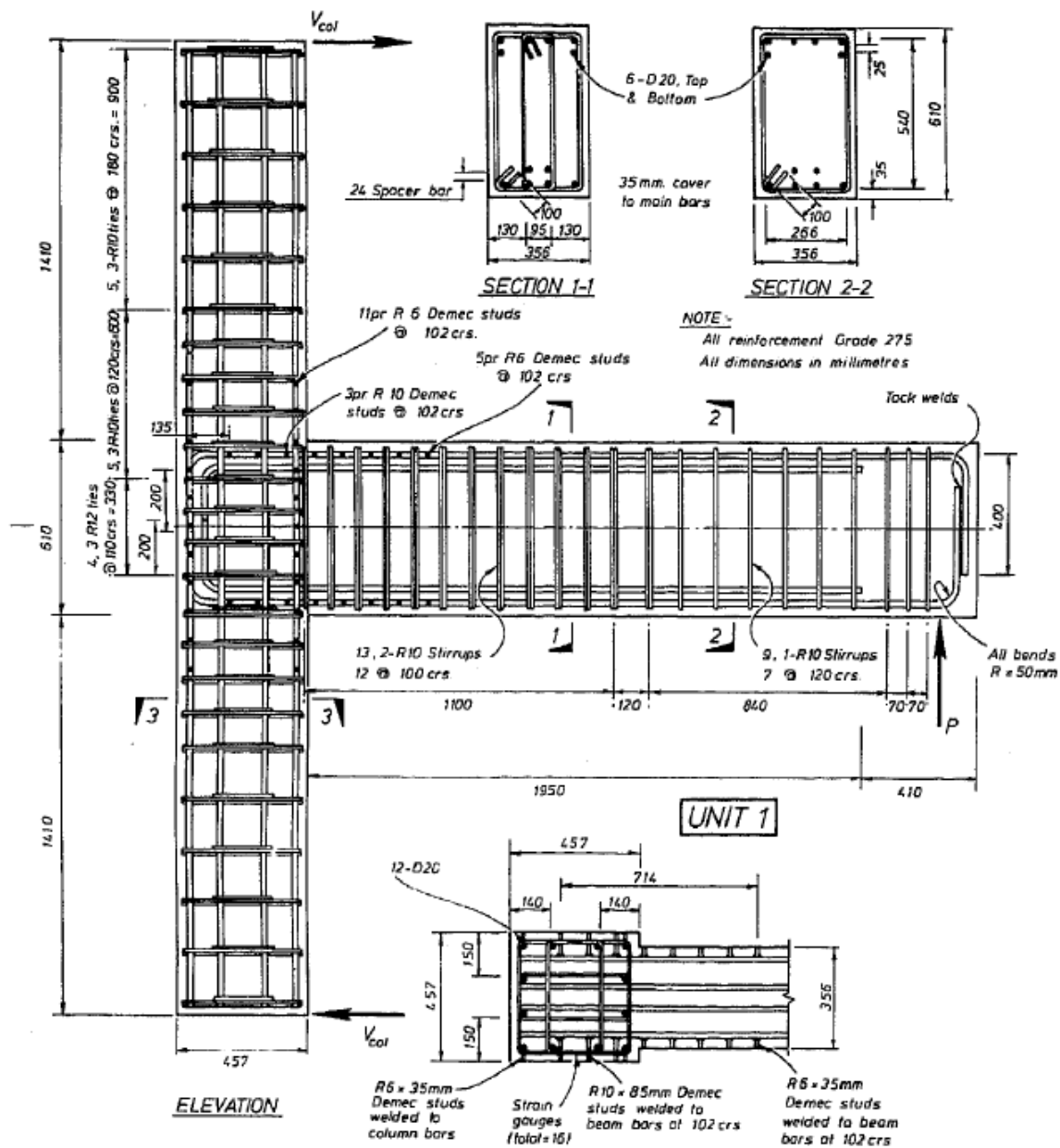


Figure 2-21 Example of a well detailed beam-column connection (adapted from Paulay and Scarpas (1981)) All units in millimeters (mm)

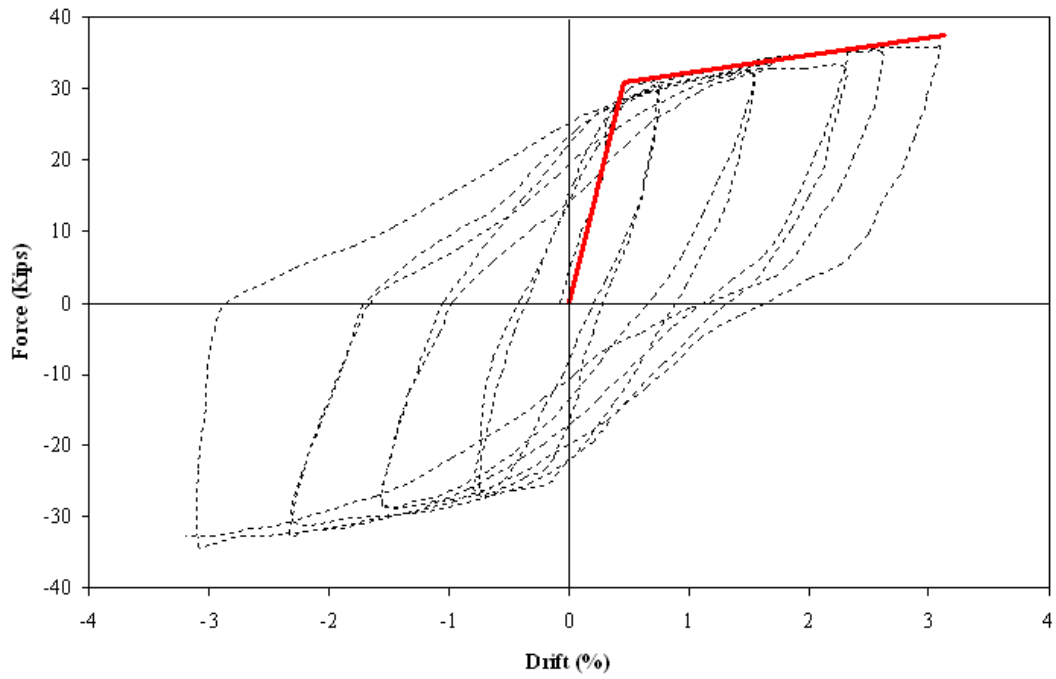


Figure 2-22 Load-displacement response of unit 1 (Paulay and Scarpas 1981)

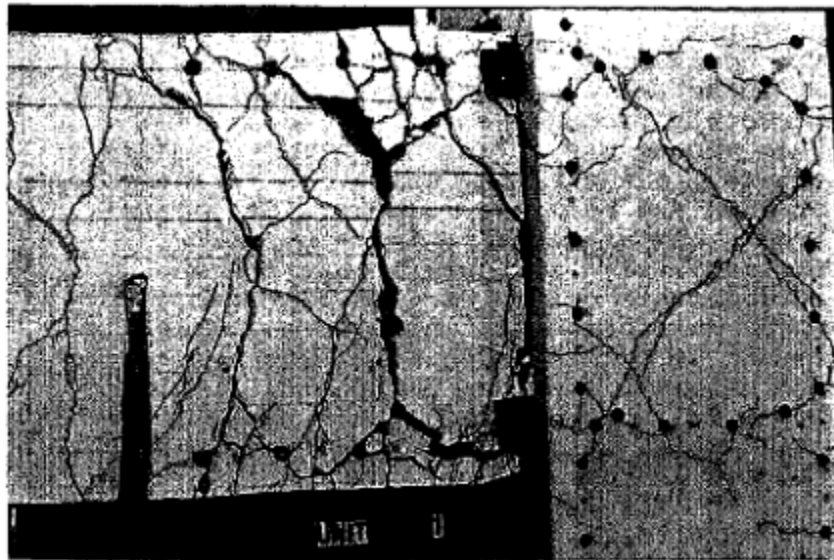


Figure 2-23 Specimen conditions at the end of the test (adapted from Paulay and Scarpas 1981)

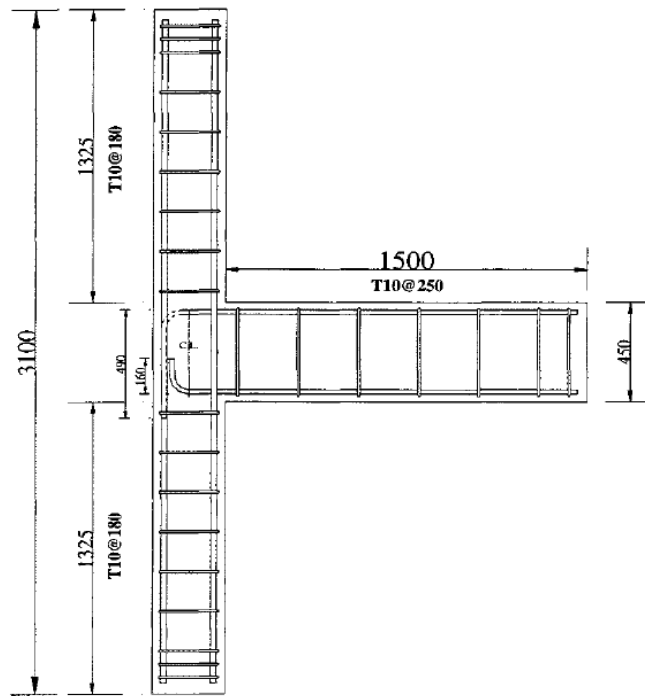


Figure 2-24 Example of an unreinforced beam-column joint Specimen BSL (adapted from Wong 2005. All units in millimeters (mm))

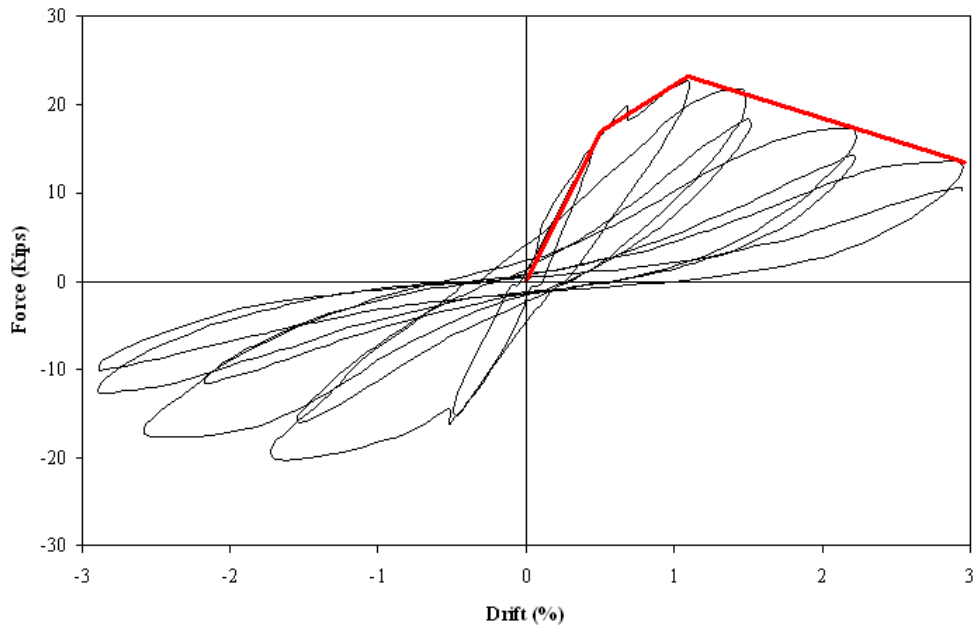


Figure 2-25 Lateral load-drift hysteresis loop of Specimen BSL (adapted from Wong 2005)

The specimen condition at the end of the test is shown in Figure 2-26. The specimens experimented joint failure. It can be appreciated that all the damage was focused in the joint region with large cracks. The beam and columns were practically undamaged. This later example justify why the rigid joint assumption is not valid for unreinforced concrete joints.



Figure 2-26 Crack pattern of specimen BSL (adapted from Wong 2005)

2.12 RELATIONSHIP BETWEEN JOINT SHEAR STRENGTH AND THE BEAM SHEAR

The external forces acting in a beam-column subassembly as well as the internal forces at the beam-column joint are shown in Figure 2-27. From equilibrium at the middle of the joint, the joint shear force is given by:

$$V_{jh} = T_b - V_{col} \quad 2.3$$

where T_b is the tension force of the beam reinforcement and V_{col} is the shear force at column inflection point.

The resisting moment of the beam is:

$$M = T_b jd \quad 2.4$$

where jd is the distance between the centroid of compression and tension steel bars.

The moment at the beam face is:

$$M_{beam} = V_b L_b \quad 2.5$$

From Equations (2.4) and (2.5):

$$T_b = \frac{V_b L_b}{jd} \quad 2.6$$

From global equilibrium:

$$V_{col} = \frac{V_b L}{L_c} \quad 2.7$$

Substituting Equations (2.6) and (2.7) in Equation (2.3), yields:

$$V_{jh} = V_b \left(\frac{L_b}{jd} - \frac{L}{L_c} \right)$$

2.8

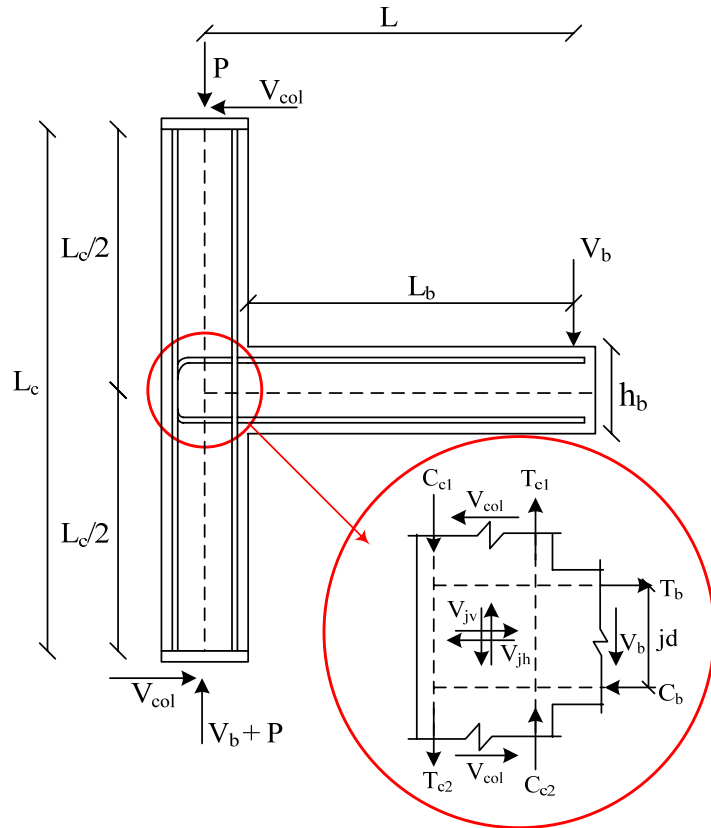


Figure 2-27 External and internal forces on a beam column joint

Equation 2.8 represents the relationship that exist between the beam shear V_b and the joint shear force. Dividing Equation 2.8 by the joint area and by the $\sqrt{f'_c}$ the normalized joint shear stress is obtained:

$$\bar{\tau}_{jh} = \frac{V_{jh}}{b_j h_c \sqrt{f'_c}} = \frac{V_b}{b_j h_c \sqrt{f'_c}} \left(\frac{L_b}{jd} - \frac{L}{L_c} \right) \quad 2.9$$

The moment transferred from the beam to the center of the joint panel is:

$$M_j = V_b L \quad 2.10$$

Solving V_b from Equation 2.9 and substituting in Equation 2.10 yields:

$$M_j = \frac{\bar{\tau}_{jh} b_j h_c \sqrt{f'_c}}{\left(\frac{L_b}{jd} - \frac{L}{L_c} \right)} L \quad 2.11$$

Equation 2.11 transforms the joint shear stress into an equivalent moment at the center of the joint panel. This moment, can be used to model the behavior of unreinforced concrete joints.

3 DEVELOPMENT OF THE ANALYTICAL MODEL

3.1 INTRODUCTION

As shown in the previous chapter several models for modeling the behavior of unreinforced concrete joint have been proposed. These models range from a simple rotational spring element to sophisticated multi spring elements. In this research, a simple rotational spring element, as shown in Figure 3-1 is adopted. This chapter summarizes the methodology adopted to develop the moment versus rotation envelope that will serve as basis for the rotational spring that will control the behavior of unreinforced concrete exterior joints. The procedures followed are briefly described. The most important tasks can be listed as:

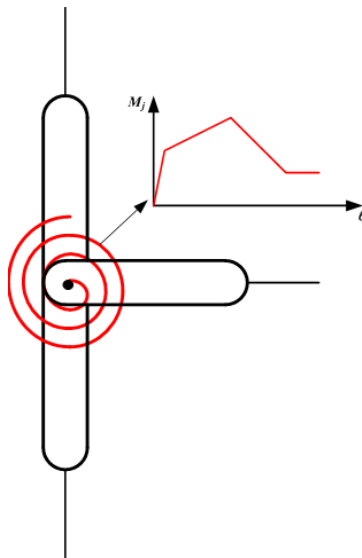


Figure 3-1 Simple rotational spring for the proposed model

1. Construction of a database containing tests of beam-column exterior joints without transverse reinforcement (Section 3.2.1).
2. Definition of the ordinates (Moments) and abscissas (Rotations) at each point of the envelope of the rotational spring (Section 3.2.2).
3. Modeling the subassembly of the test from the constructed database, including the rotational spring that simulates the joint (Section 4.2).
4. Modeling the hysteretic behavior (Chapter 4).
5. Calibration of the rotational spring properties (Chapter 4).

A more detailed explanation of each one of the aforementioned tasks is presented in the following sections

3.2 DETAILS OF THE METHODOLOGY

3.2.1 DATABASE CONSTRUCTION

In order to validate the proposed methodology a database with tests of exterior beam-column joints without transverse reinforcement was compiled. Only tests having joint shear failure without beam reinforcement yielding (J) or with the beam reinforcement yielding (BJ) were selected. Since Jirsa (1981) states that the anchorage failure is not easy to distinguish from the J or BJ failures and that the compressive failures are not easily reproduced in laboratories, these types of failures were not considered in the database. Only tests subjected to cyclic loading having available its force versus displacement graph and with the anchorage details shown in Figure 3-2 were selected. It is important to mention that tests with intermediate longitudinal reinforcement in the columns also were considered.

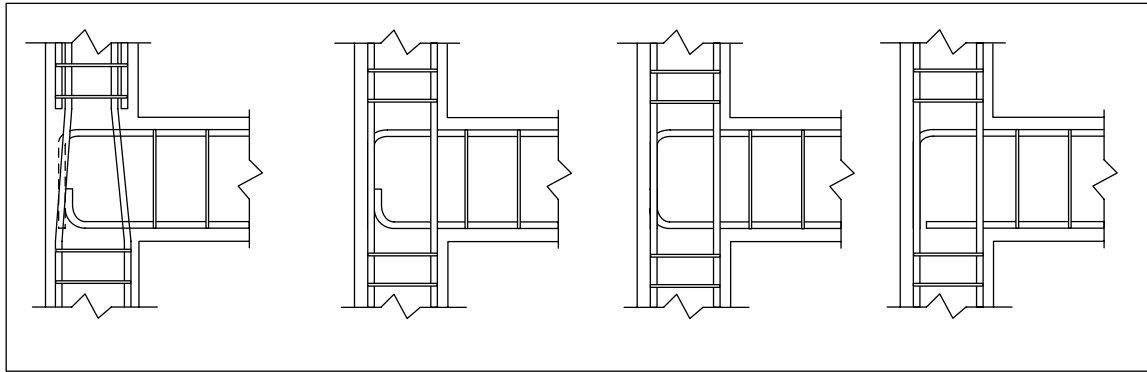


Figure 3-2 Anchorage details for selected specimens

Table 3-1 summarizes the database with the selected experimental tests based on the criteria of selection. In the table b_c is the column width; A_g is the column gross area; P is the column axial load; d_b is the beam effective depth; A_s is the beam tension reinforcement; b_j is the joint width (see Figure 3-3); L_b is the distance from the point of the vertical or lateral load application (depending if the test configuration is horizontal or vertical, as explained in Chapter 2) to the face of the column; L is the distance from the point of the lateral load application to the center of the joint and L_c is the distance between the inflection points of the column. Regarding the value of the normalized shear strength $\bar{\tau}_{jh}$; it was taken directly from the publication for the cases of Pantelides et al (2002) and Clyde et al (2000). For the cases of Wong (2005) and Hwang (2005) tests, it was computed using Equation 2.9 (assuming the internal moment arm jd constant and equal to $\frac{7}{8}d_b$) but using the values of the V_{jh} provided by the authors. For the cases of Ghobarah & Said (2001), Karayannis (2008), Antonopoulos & Triantafyllou (2003), and Parker & Bullman (1997), since in these tests the only data presented by these authors was the beam shear force (V_b), it was computed using Equations 2.8 and 2.9. Finally, for

the Scott & Hamil (1998) test, it was necessary to modify Equation 2.9, subtracting a constant value of 2.25 kip (10 kN) due to test configuration.

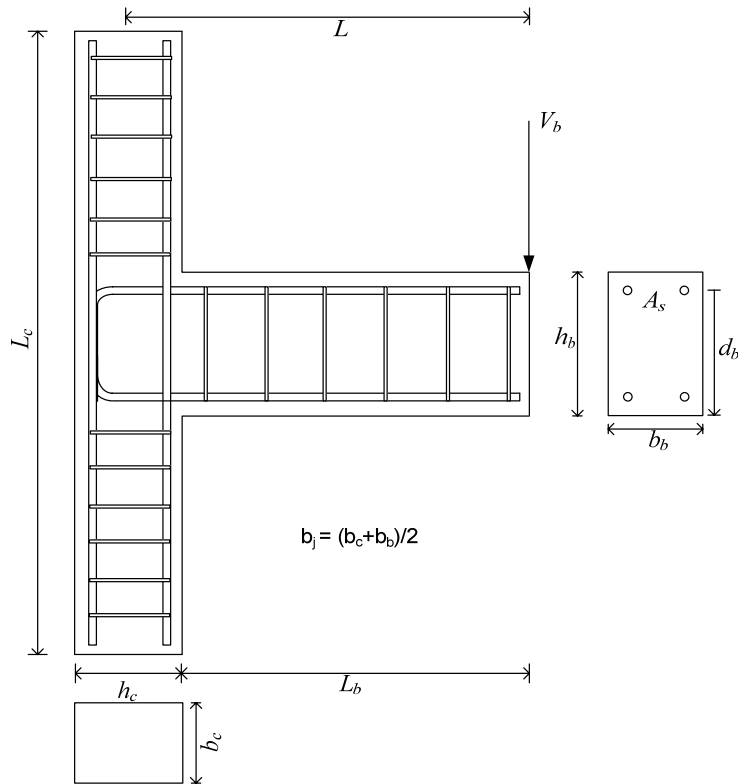


Figure 3-3 Variables definition for the database

Regarding the failure type, for the cases of the test reported by Pantelides et al.(2002) and Clyde et al.(2000) in which failure type for all specimens appears to be a J failure, there is experimental evidence that indicates that in which in both cases beam reinforcement attained the yield stress and thus were corrected as BJ failure. Finally, in the cases where the mode of failure was not provided, it was calculated by comparing the beam internal moment (M_{beam}) with the moment at the center of the joint (M_j) as obtained from Equation 2.12. If M_{beam} is less than M_j , the failure was considered as BJ. Otherwise, the failure was consider as J.

Table 3-1 Database of unreinforced concrete joints tests from the literature

Author	Specimen	f'_c (ksi)	f_y (Ksi)	$\frac{P}{A_g f'_c}$	b_c (in)	A_g (in ²)	P (Kips)	d_b (in)	A_s (in ²)	b_j (in)	L_b (in)	L(in)	L_c (in)	$\bar{\tau}_{jh}$ (psi ^{1/2})	Type of Failure
Wong (2005)	BSL	4.5	75.4	0.15	11.8	139.5	93.7	15.6	1.46	11.0	51.2	57.1	122.1	8.1	J
	BSU	4.5	75.4	0.15	11.8	139.5	94.1	15.6	1.46	11.0	51.2	57.1	122.1	8.8	J
	BSLLS	4.6	75.4	0.15	11.8	139.5	95.8	15.6	1.46	11.0	51.2	57.1	122.1	8.8	J
	BSLV2T10	4.7	75.4	0.15	11.8	139.5	99.0	15.6	1.46	11.0	51.2	57.1	122.1	10.0	J
	BSLV4T10	4.1	75.4	0.15	11.8	139.5	85.8	15.6	1.46	11.0	51.2	57.1	122.1	10.9	J
	BSL600	5.3	75.4	0.15	11.8	139.5	110.5	21.5	1.46	11.0	51.2	57.1	122.1	6.7	J
	BSL300	5.0	75.4	0.15	11.8	139.5	103.6	9.6	1.46	11.0	51.2	57.1	122.1	12.4	BJ
	JA-NN03	6.5	75.4	0.03	11.8	139.5	27.2	13.5	0.97	11.0	51.2	57.1	122.1	6.5	BJ
	JA-NN15	6.7	75.4	0.15	11.8	139.5	139.6	13.5	0.97	11.0	51.2	57.1	122.1	6.9	BJ
Pantelides et al (2002)	3	4.9	66.5	0.10	16.0	256.0	126.2	13.6	4.00	16.0	58.5	66.5	126.0	10.4	BJ
	4	4.9	66.5	0.25	16.0	256.0	315.5	13.6	4.00	16.0	58.5	66.5	126.0	11.7	BJ
	5	4.6	66.5	0.10	16.0	256.0	117.8	13.6	4.00	16.0	58.5	66.5	126.0	11.1	BJ
	6	4.6	66.5	0.25	16.0	256.0	294.4	13.6	4.00	16.0	58.5	66.5	126.0	11.3	BJ
Clyde et al (2000)	2	6.7	65.9	0.10	12.0	216.0	144.7	13.6	4.00	12.0	50.0	59.0	112.0	12.1	BJ
	4	5.9	65.9	0.25	12.0	216.0	320.8	13.6	4.00	12.0	50.0	59.0	112.0	13.4	BJ
	5	5.4	65.9	0.25	12.0	216.0	290.0	13.6	4.00	12.0	50.0	59.0	112.0	13.4	BJ
	6	5.8	65.9	0.10	12.0	216.0	125.8	13.6	4.00	12.0	50.0	59.0	112.0	12.7	BJ
Hwang (2005)	ST0	9.8	62.4	0.02	16.5	273.6	44.1	15.5	3.16	14.5	74.8	83.1	118.1	9.4	BJ
Ghobarah & Said (2001)	T-1	4.5	61.6	0.20	9.8	155.0	138.6	14.0	1.95	9.8	65.8	73.6	118.1	11.9	BJ
Karayannis (2008)	A0	4.6	84.1	0.05	7.9	92.9	21.3	9.8	0.24	7.9	39.4	45.3	70.9	3.44	BJ
	B0	4.6	84.1	0.05	7.9	92.9	21.3	9.8	0.73	7.9	39.4	45.3	70.9	8.3	BJ
	C0	4.6	84.1	0.05	7.9	92.9	21.3	9.8	0.70	7.9	39.4	45.3	70.9	9.2	BJ
Antonopoulos & Triantafillou (2003)	C1	2.8	84.9	0.06	7.9	61.9	10.5	10.4	0.72	7.9	39.4	43.3	51.2	7.4	J
	C2	3.4	84.9	0.05	7.9	61.9	10.7	10.4	0.72	7.9	39.4	43.3	51.2	6.7	J
	T-C	3.6	84.9	0.05	7.9	61.9	10.4	10.4	0.72	7.9	39.4	43.3	51.2	7.6	J

Table 3-1 Database of unreinforced concrete joints tests from the literature

Author	Specimen	f'_c (ksi)	f_y (Ksi)	$\frac{P}{A_g f'_c}$	b_c (in)	A_g (in ²)	P (Kips)	d_b (in)	A_s (in ²)	b_j (in)	L_b (in)	L(in)	L_c (in)	$\bar{\tau}_{jh}$ (psi ^{1/2})	Type of Failure
Ortiz (1993)	BCJ1	4.93	104.35	0.00	7.87	92.94	0.00	14.13	1.25	7.87	41.34	47.24	94.5	11.5	J
	BCJ3	4.78	104.35	0.00	7.87	92.94	0.00	14.13	1.25	7.87	43.31	49.21	94.5	12.3	J
	BCJ5	5.51	104.35	0.13	7.87	92.94	67.40	14.13	1.25	7.87	43.31	49.21	94.5	11.0	J
	BCJ6	5.07	104.35	0.14	7.87	92.94	67.39	14.13	1.25	7.87	43.31	49.21	94.5	11.5	J
Parker & Bullman (1997)	4b	5.69	82.67	0.09	11.81	139.48	67.46	17.53	1.52	10.83	33.47	39.37	78.7	5.4	J
	4c	5.34	82.67	0.17	11.81	139.48	128.48	17.53	1.52	10.83	33.47	39.37	78.7	6.9	J
	4d	5.69	82.67	0.00	11.81	139.48	0.00	17.53	1.52	10.83	33.47	39.37	78.7	5.9	J
	4e	5.80	82.67	0.08	11.81	139.48	67.95	17.53	1.52	10.83	33.47	39.37	78.7	6.2	J
	4f	5.45	82.67	0.02	11.81	139.48	13.53	17.53	1.52	10.83	33.47	39.37	78.7	7.3	J
Scott & Hamil (1998)	C6LN0	7.43	75.71	0.04	5.91	34.93	9.60	6.74	0.62	5.12	30.50	33.46	67.9	10.0	J
	C6LH0	14.62	75.71	0.04	5.91	34.93	20.43	6.74	0.62	5.12	31.50	34.46	68.9	11.8	J

3.2.2 ENVELOPE CURVE DEFINITION

The proposed envelope curve for modeling unreinforced concrete joints is shown in Figure 3-4. The points that define the envelope are the cracking point; the peak strength point and the residual point. Along with each point, a picture that describes the expected state of damage is included.

Equation 3.1 establishes that the equivalent moment at the joint center M_j is related to the joint shear stress as follows:

$$M_j = \frac{\bar{\tau}_{jh} b_j h_c \sqrt{f'_c}}{\left(\frac{L_b}{jd} - \frac{L}{L_c} \right)} L \quad 3.1$$

Knowing the value of the normalized joint shear stress at the first two points of the envelope one can obtain the ordinate in such points. The ordinate of the residual point will depend of the value of the ordinate of the peak point as will be shown in the next sections.

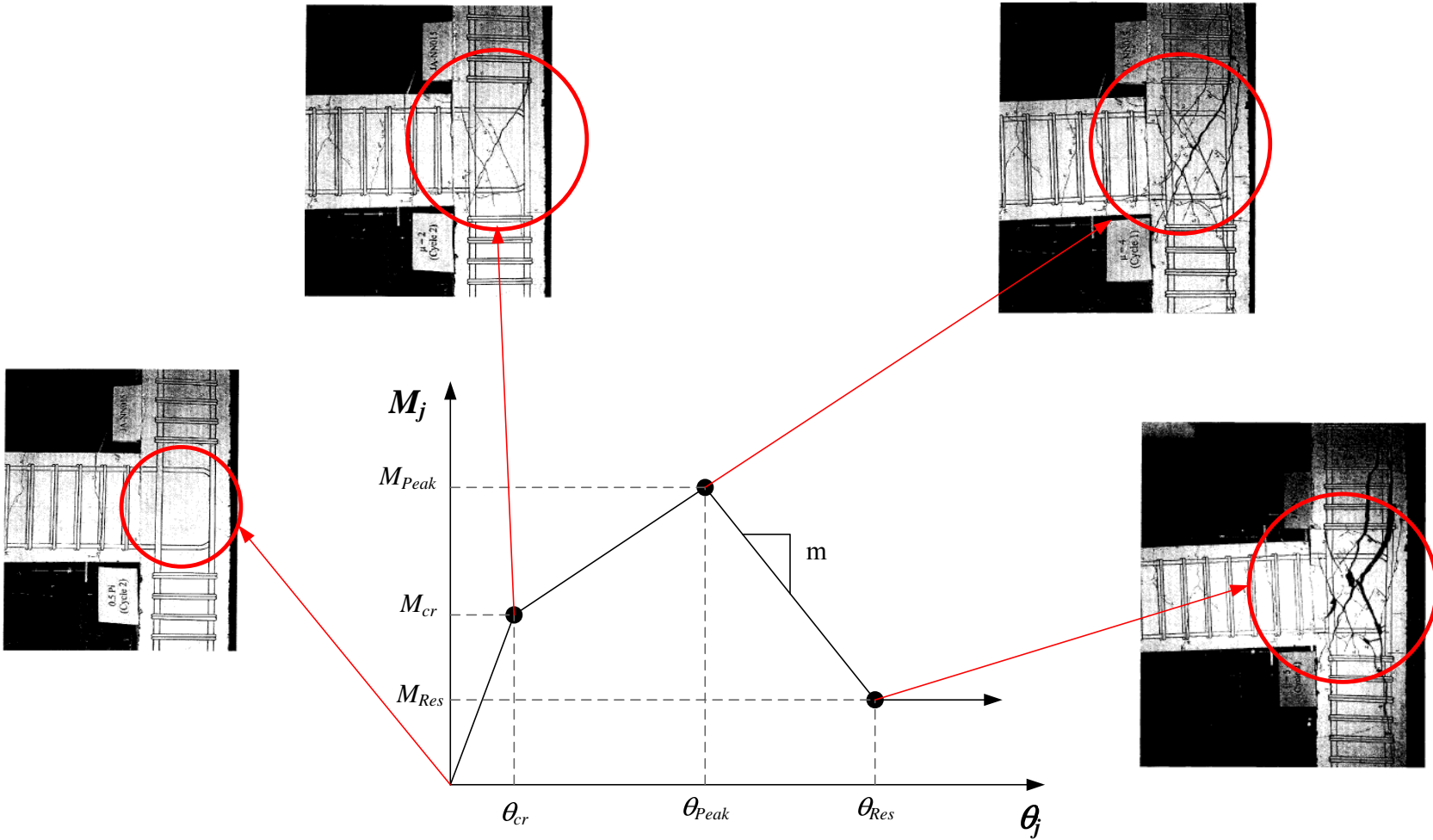


Figure 3-4 Proposed envelope curve for the joint

3.2.2.1 ORDINATE OF THE CRACKING POINT

The joint shear stress at the cracking point can be obtained using Mohr circle. For a plane stress state, the principal tensile stress is:

$$\sigma_T = \frac{\sigma_x + \sigma_y}{2} + \sqrt{\left(\frac{\sigma_x - \sigma_y}{2}\right)^2 + \tau_{Crack}^2} \quad 3.2$$

where σ_x , σ_y , σ_T and τ_{Crack} are, respectively, the beam axial stress, the column axial stress (negative in compression), the principal tensile stress and the joint shear stress. Neglecting the beam axial stress (beam axial loads are very small) and solving for the joint shear stress yields:

$$\tau_{Crack} = \sqrt{\left(\sigma_T - \frac{\sigma_y}{2}\right)^2 - \left(\frac{\sigma_y}{2}\right)^2} \quad 3.3$$

Taking the concrete cracking tensile stress as $4\sqrt{f'_c}$ (Kim and LaFave 2007) and knowing the value of the column axial load, one can obtain the joint shear stress at the cracking point with Equation 3.3. The normalized joint shear strength for the cracking point is therefore:

$$\bar{\tau}_{crack} = \frac{\tau_{crack}}{\sqrt{f'_c}} \leq 0.9\bar{\tau}_{Peak} \quad 3.4$$

The value of Equation 3.4 was limited not to exceed 0.9 the normalized joint shear stress at peak point to ensure that the normalized joint shear strength at crack point is always below the normalized joint shear stress at peak point in the envelope proposed.

Finally substituting Equation 3.4 into Equation 3.1, the ordinate of the cracking point is:

$$M_{crack} = \frac{\bar{\tau}_{crack} b_j h_c \sqrt{f'_c}}{\left(\frac{L_b}{jd} - \frac{L}{L_c} \right)} L \quad 3.5$$

3.2.2.2 ORDINATE OF THE PEAK STRENGTH POINT

As shown in Chapter 2, there are several models for the prediction of the joint shear strength of unreinforced concrete joints available in the literature. For the case of type J failure, the model developed by Hassan *et al.* (2010) is adopted in this research.

3.2.2.2.1 ACI 318 SOFTENED STRUT AND TIE MODEL

Hassan *et al.* (2010) developed a model for the prediction of the strength of exterior joints undergoing J mode of failure based on the strut-and-tie concept. The model was called the ACI 318 Softened Strut and Tie Model. According to this model, the diagonal strut capacity D is defined as:

$$D = f_{cu} A_{str} \quad 3.6$$

where:

f_{cu} is the effective strut compressive strength, defined by the ACI-318-08 as

$$f_{cu} = 0.85 \beta_s f'_c \quad 3.7$$

where:

β_s is the concrete softening coefficient. In accordance with the ACI 318-08 for normal weight concrete and bottle shaped strut without crack control reinforcement $\beta_s = 0.6$

A_{str} is the area of the concrete strut and is defined as $A_{str} = a_s b_j$

b_j is the joint width, defined by the ACI 352-02 as:

$$b_j = \frac{b_c + b_b}{2} \leq b_c \quad 3.8$$

where b_c and b_b are the width of the column and beam respectively (Figure 3-5).

a_s is the equivalent depth of the concrete strut and is defined as:

$$a_s = \sqrt{a_b^2 + a_c^2} \quad 3.9$$

a_b and a_c are the compression zone depths of the beam and column, respectively. The value of a_b is computed as follows:

$$a_b = k d_b \quad 3.10$$

$$k = \sqrt{(\rho + \rho')^2 n^2 + 2 \left(\rho + \rho' \frac{d'_b}{d_b} \right) n - (\rho + \rho') n} \quad 3.11$$

where:

d_b and d'_b are effective depths measured from the extreme compression fiber to the centroid of beam tension and compression longitudinal reinforcement, respectively;

n is the modular ratio and is defined as $n = \frac{E_s}{E_c}$,

E_s is the modulus of elasticity of the reinforcing steel,

E_c is the modulus of elasticity of the concrete and is defined for normal weight concrete

as $E_c = 57000\sqrt{f'_c}$ (f'_c in psi), and

ρ and ρ' are, respectively, the beam tension and compression reinforcement ratios.

The compression zone depth of the column a_c is computed by the following expression:

$$a_c = \left(0.25 + 0.85 \frac{N}{f'_c A_g} \right) h_c \leq 0.4h_c \quad 3.12$$

where N is column axial load in units of pounds, positive in compression

Finally, the joint shear strength is defined as

$$V_{jh} = D \cos \theta \quad 3.13$$

where θ is the angle of inclination of the concrete strut and is defined as:

$$\theta = \tan^{-1} \left(\frac{d_b - d'_b}{d_c - d'_c} \right) \quad 3.14$$

where d_c and d'_c are, respectively, the depths from the extreme compression fiber to the centroid of tension and compression longitudinal reinforcement in the column (see Figure 3-5).

Equation 3.13 gives the joint shear force for unreinforced concrete joint sustaining J failure.

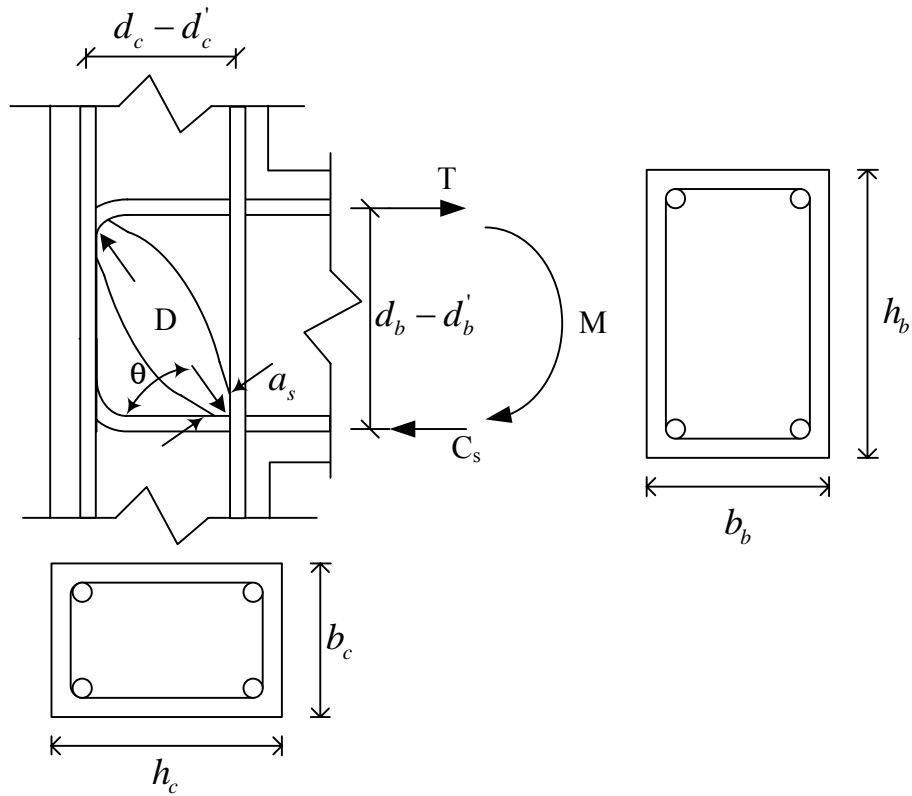


Figure 3-5 Definitions used for the ACI-318 Softened Strut and Tie Model

3.2.2.2.2 MODEL FOR THE PREDICTION OF BJ FAILURE

The joint shear strength for joints sustaining BJ failure can be computed as the joint shear corresponding to the development of the capacity of the beam. Based on Figure 2-27 which is repeated for convenience as Figure 3-6, the free body diagram helps to determine the following equations:

The joint shear is obtained with:

$$V_{jh} = T_b - V_{col} \quad 3.15$$

The internal resisting moment of the beam is:

$$M = T_b j d = A_s f_y j d \quad 3.16$$

The moment at the column face is:

$$M_{beam} = V_b L_b \quad 3.17$$

Equating Equations 3.16 and 3.17 and solving for V_b yields:

$$V_b = \frac{A_s f_y j d}{L_b} \quad 3.18$$

From equilibrium the column shear is:

$$V_{col} = \frac{V_b L}{L_c} \quad 3.19$$

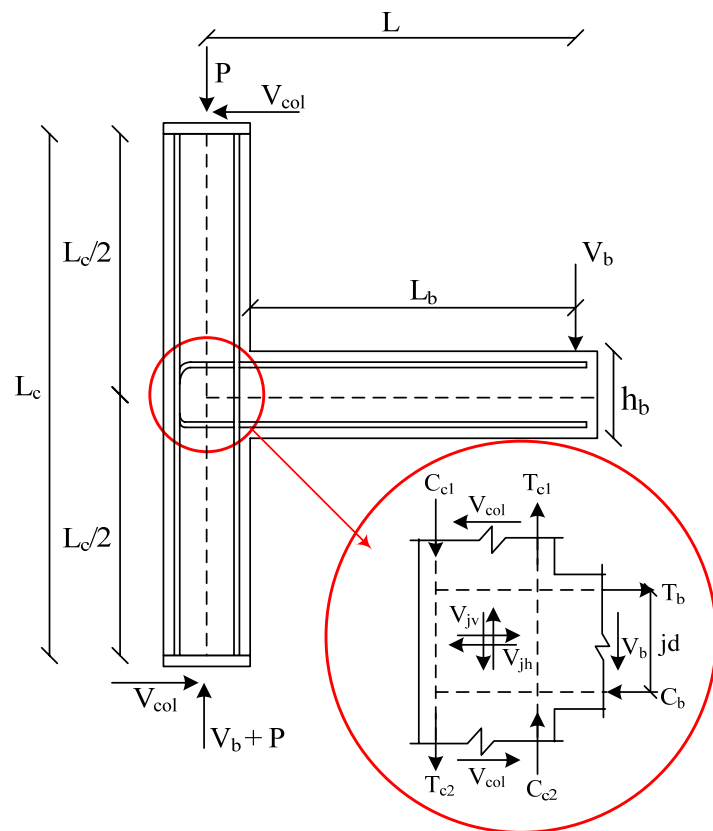


Figure 3-6 External and internal forces on a beam-column joint

Substituting Equation 3.18 in 3.19 yields:

$$V_{col} = \frac{A_s f_y j d}{L_b} \frac{L}{L_c} \quad 3.20$$

Finally, substituting Equation 3.20 into 3.15, with $T_b = A_s f_y$ yields:

$$V_{jh} = A_s f_y \left(1 - \frac{j d}{L_b} \frac{L}{L_c} \right) \quad 3.21$$

Equation 3.21 gives the joint shear force affecting unreinforced concrete joints sustaining BJ failure.

In conclusion, the joint shear force will be the minimum obtained from both types of failure:

$$V_{jh} = \min(V_{jh - J}, V_{jh - BJ}) \quad 3.22$$

The type of failure is also predicted by the assumption that gives the smaller joint shear force at failure. The normalized joint shear strength at peak point is:

$$\bar{\tau}_{Peak} = \frac{V_{jh}}{A_j \sqrt{f'_c}} \quad 3.23$$

Finally substituting Equation 3.23 into Equation 3.1, the ordinate of the peak point is:

$$M_{Peak} = \frac{\bar{\tau}_{Peak} b_j h_c \sqrt{f'_c}}{\left(\frac{L_b}{j d} - \frac{L}{L_c} \right)} L \quad 3.24$$

3.2.2.2.3 VALIDATION OF THE JOINT SHEAR METHODOLOGY

In order to verify the accuracy of the peak joint shear stress computed with the procedure previously described it was applied to the tests of the database of Table 3-1. The results obtained were compared with the predictions of both the normalized joint shear stress and the type of failure from the analytical model of Park and Mosalam (2009). Figures 3-7 and 3-8 shows the evaluation of the results from the proposed methodology and with the analytical model from Park and Mosalam (2009) respectively with the values obtained from the experimental tests. In both figures the mean and the coefficient of variation (COV) refers to the ratio of the normalized joint shear stress from the test to the model.

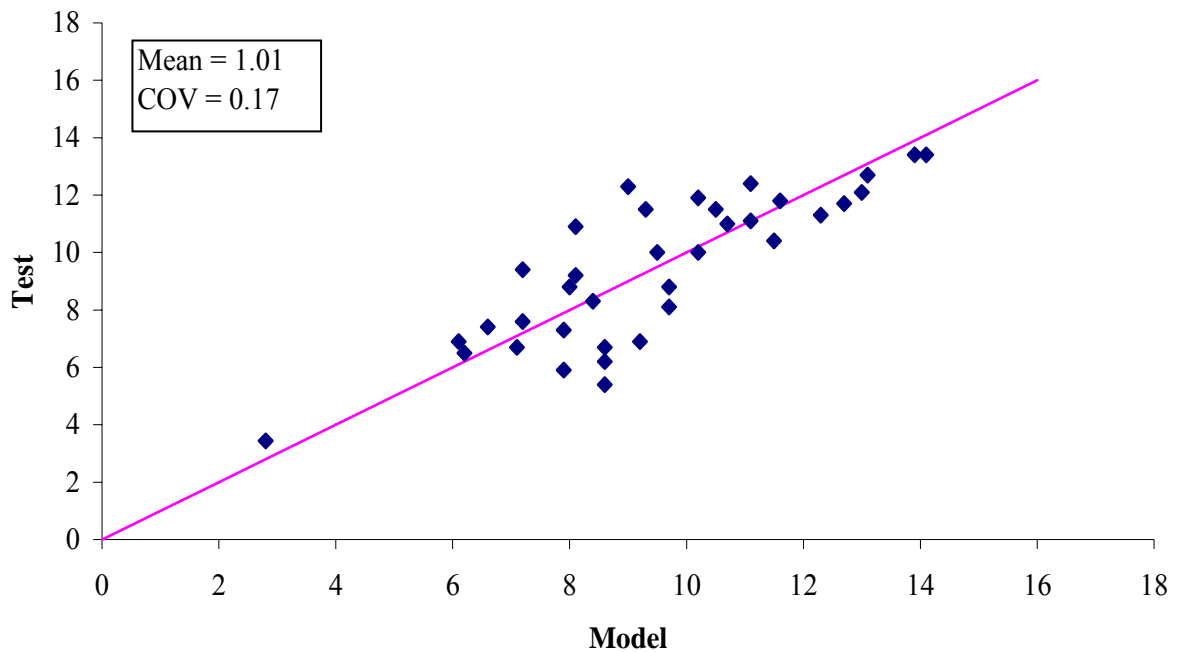


Figure 3-7 Predictions of the $\bar{\tau}_{Peak}$ obtained with the proposed methodology

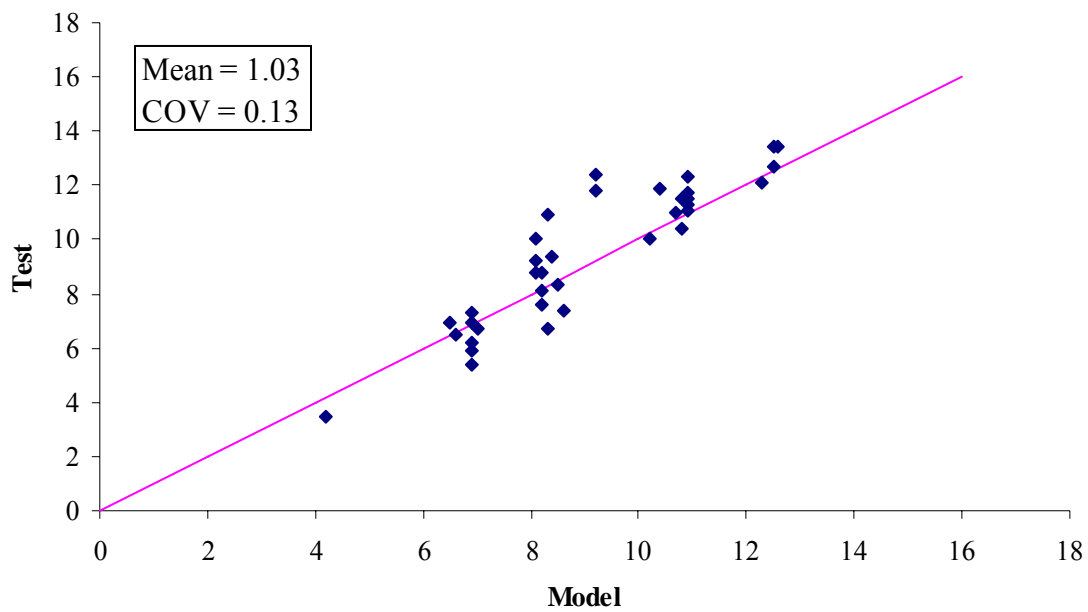


Figure 3-8 Predictions of the $\bar{\tau}_{Peak}$ obtained with Analytical model from Park and Mosalam (2009)

Table 3-2 shows the comparison of the prediction of the type of failure made with the proposed methodology and from Park and Mosalam (2009). It can be appreciated that the results obtained from the proposed procedure compare favorably with the predictions of Park and Mosalam (2009) model. Thus the proposed methodology will be used here for the prediction of the peak joint shear stress of unreinforced concrete joints tested in two dimensions.

Table 3-2 Type of failure validation

Author	Specimen	Experimental Test		Proposed Methodology		Park and Mosalam (2009)	
		$\bar{\tau}_{Peak}$	Type of Failure	$\bar{\tau}_{Peak}$	Type of Failure	$\bar{\tau}_{Peak}$	Type of Failure
Wong (2005)	BSL	8.1	J	9.7	J	8.2	J
	BSU	8.8	J	9.7	J	8.2	J
	BSLLS	8.8	J	8.0	J	8.1	J
	BSLV2T10	10.0	J	9.5	J	8.1	J
	BSLV4T10	10.9	J	8.1	J	8.3	J
	BSL600	6.7	J	8.6	J	7.0	J
	BSL300	12.4	BJ	11.1	BJ	9.2	BJ
	JA-NN03	6.5	BJ	6.2	BJ	6.6	BJ
	JA-NN15	6.9	BJ	6.1	BJ	6.5	BJ
Pantelides (2002)	3	10.4	BJ	11.5	J	10.8	J
	4	11.7	BJ	12.7	J	10.9	J
	5	11.1	BJ	11.1	J	10.9	J
	6	11.3	BJ	12.3	J	10.9	J
Clyde (2000)	2	12.1	BJ	13.0	BJ	12.3	J
	4	13.4	BJ	13.9	BJ	12.5	J
	5	13.4	BJ	14.1	J	12.6	J
	6	12.7	BJ	13.1	J	12.5	J
Hwang (2005)	ST0	9.4	BJ	7.2	BJ	8.4	BJ
Ghobarah & Said (2001)	T-1	11.9	BJ	10.2	BJ	10.4	BJ
Karayannis (2008)	A0	3.44	BJ	2.9	BJ	4.2	BJ
	B0	8.3	BJ	8.4	BJ	8.5	BJ
	C0	9.2	BJ	8.1	BJ	8.1	BJ
Antonopoulos & Triantafillou (2003)	C1	7.4	J	6.6	J	8.6	J
	C2	6.7	J	7.1	J	8.3	J
	T-C	7.6	J	7.2	J	8.2	J
Ortiz (1993)	BCJ1	11.5	J	9.3	J	10.9	J
	BCJ3	12.3	J	9.0	J	10.9	J
	BCJ5	11.0	J	10.7	J	10.7	J
	BCJ6	11.5	J	10.5	J	10.8	J
Parker & Bullman (1997)	4b	5.4	J	8.6	J	6.9	J
	4c	6.9	J	9.2	J	6.9	J
	4d	5.9	J	7.9	J	6.9	J
	4e	6.2	J	8.6	J	6.9	J
	4f	7.3	J	7.9	J	6.9	J
Scott & Hamil (1998)	C6LN0	10.0	J	10.2	J	10.2	J
	C6LH0	11.8	J	11.6	BJ	9.2	J

3.2.2.3 ORDINATE OF THE RESIDUAL POINT

The residual point was selected to be 30% of the value of the peak strength point. That is:

$$M_{res} = 0.3M_{peak} \quad 3.25$$

This approximately value is based on test results.

3.2.2.4 ABSCISSA OF THE PEAK STRENGTH POINT

The rotations at the peak strength point can be computed as the sum of the contribution of the elastic rotations of the beam and column, the distortion of the joint and the rotation due to bond slip in the beam at column face (Figure 3-9):

$$\theta = \theta_{elastic} + \gamma_{joint} + \theta_{Bond\ Slip} \quad 3.26$$

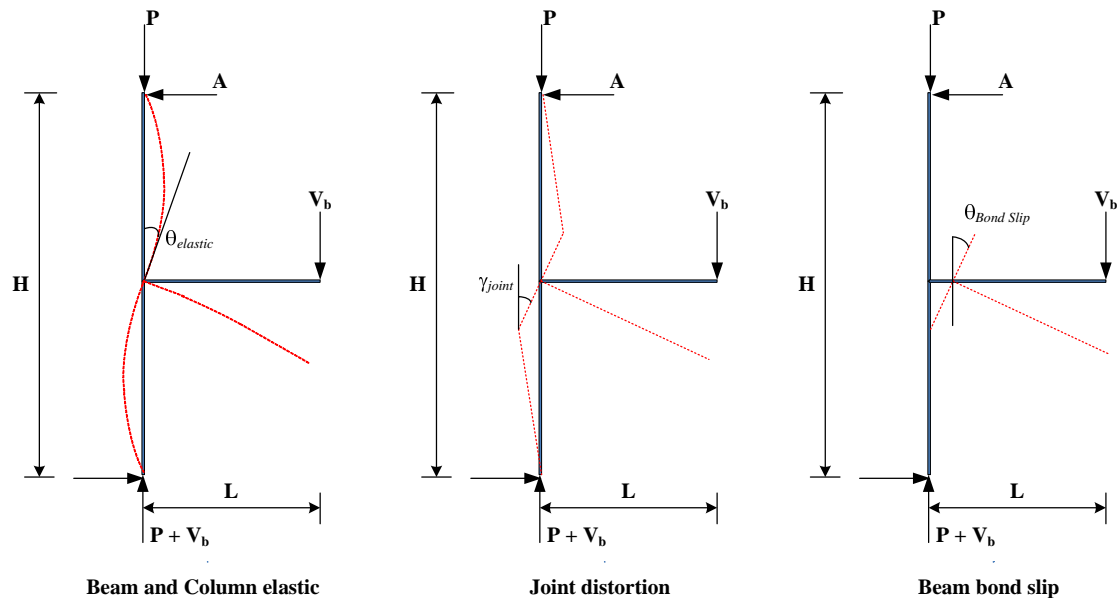


Figure 3-9 Contribution of the joint rotation (adapted from Hanson and Connor 1967)

3.2.2.4.1 ELASTIC ROTATIONS

Once the joint shear strength at peak strength is determined, the corresponding elastic rotations can be computed using the slope-deflection equations. Figure 3-10 (a) shows the model of a typical test specimen of a beam-column joint subassembly. Figure 3-10 (b) shows the internal forces acting in the elements and nodes due to the applied force at the beam end. As only the rotations at the joint center are of interest, the lateral force is substituted by the moment $M = V_b L$. Applying the slope-deflection equations to both column elements at each node yields:

$$M_{12} = 2 \frac{E_{c1} I_{c1}}{\frac{L_{c1}}{2}} (2\theta_1 + \theta_2) \quad 3.27$$

$$M_{21} = 2 \frac{E_{c1} I_{c1}}{\frac{L_{c1}}{2}} (2\theta_2 + \theta_1) \quad 3.28$$

$$M_{23} = 2 \frac{E_{c2} I_{c2}}{\frac{L_{c2}}{2}} (2\theta_2 + \theta_3) \quad 3.29$$

$$M_{32} = 2 \frac{E_{c2} I_{c2}}{\frac{L_{c2}}{2}} (2\theta_3 + \theta_2) \quad 3.30$$

From equilibrium at node 1 and 3 one obtains:

$$M_{12} = M_{32} = 0$$

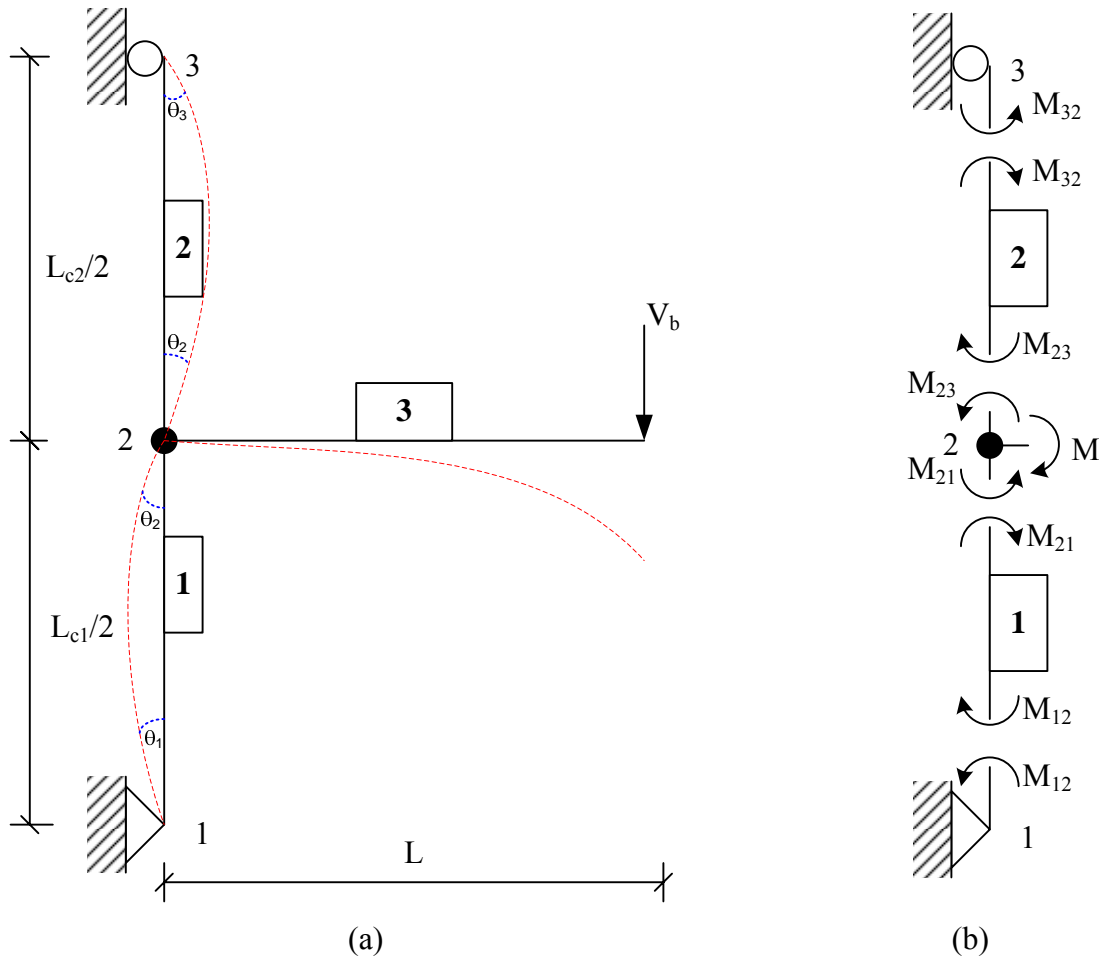


Figure 3-10 Joint subassembly idealization: a) Model b) Free body diagram

$$\theta_1 = -\frac{\theta_2}{2} \tag{3.31}$$

$$\theta_3 = -\frac{\theta_2}{2} \tag{3.32}$$

From equilibrium at node 2:

$$M_{23} + M_{21} = V_b L \tag{3.33}$$

Substituting Equations 3.31 and 3.32 in Equation 3.28 and 3.29 respectively give:

$$M_{23} = 3 \frac{E_{c2} I_{c2}}{\frac{L_{c2}}{2}} \theta_2 \quad 3.34$$

$$M_{21} = 3 \frac{E_{c1} I_{c1}}{\frac{L_{c1}}{2}} \theta_2 \quad 3.35$$

Substituting Equations 3.34 and 3.35 in Equation 3.33 and solving for the rotation, yields:

$$\theta_2 = \frac{V_b L}{\frac{6E_{c1}I_{c1}}{L_{c1}} + \frac{6E_{c2}I_{c2}}{L_{c2}}} \quad 3.36$$

Where E_c is the elasticity modulus of the concrete; L_{ci} is the column length of column i , I_c is the moment of inertia of the column section, L is the distance from the applied beam load to the joint center and indices 1 and 2 refers to the lower and upper column of the joint respectively. If both columns are equal, Equation 3.36 is reduced as follows:

$$\theta_2 = \frac{V_b L}{\frac{12E_c I_c}{L_c}} \quad 3.37$$

The value of the applied beam load is obtained once the joint shear strength is known.

Solving V_b from Equation 2.8 yields:

$$V_b = \frac{\bar{\tau}_{jh} b_j h_c \sqrt{f'_c}}{\left(\frac{L_b}{jd} - \frac{L}{L_c} \right)} \quad 3.38$$

Equation 3.36 along with Equation 3.38 are used to compute the elastic rotation of the joint.

3.2.2.4.2 JOINT SHEAR DISTORTION

The joint shear distortion (Figure 3-11) was computed based on experimental measurements of test from the literature. Only the tests performed by Clyde *et al* (2002) and Pantelides *et al* (2002) had available data concerning the joint shear strains. Table 3-3 shows the values of the joint shear strains related to the maximum joint shear stress of the aforementioned tests.

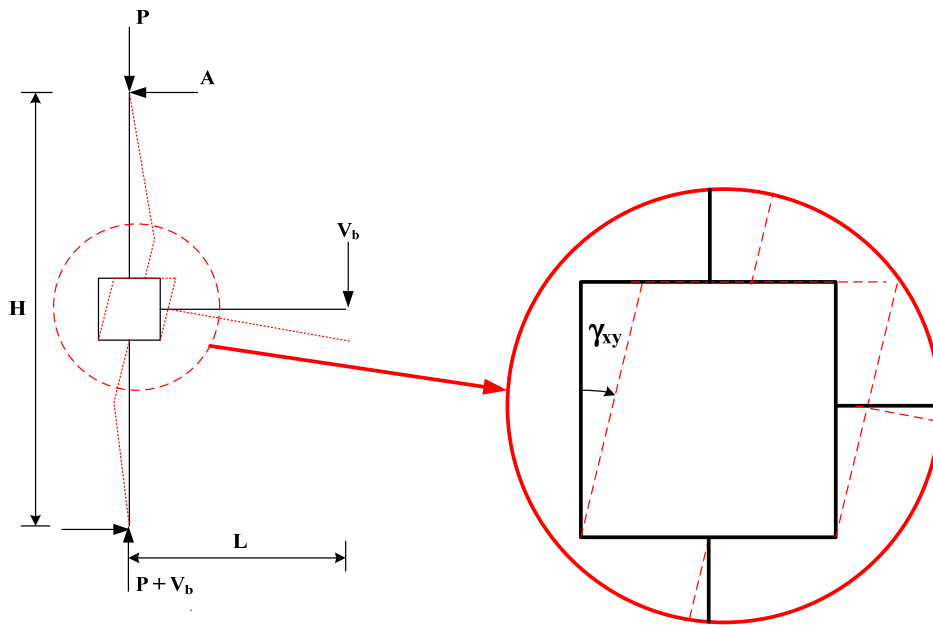


Figure 3-11 Joint shear distortion

Table 3-3 Experimental measured joint shear strain

Author	Test	$\bar{\tau}$ \sqrt{psi}	γ_{xy} (10^{-3})
Clyde et al. (2000)	2	12.1	7.18
	4	13.4	3.44
	5	13.4	4.84
	6	12.7	4.81
Pantelides et al. (2002)	3	10.4	3.28
	4	11.7	2.25
	5	11.1	6.1
	6	11.3	6.54

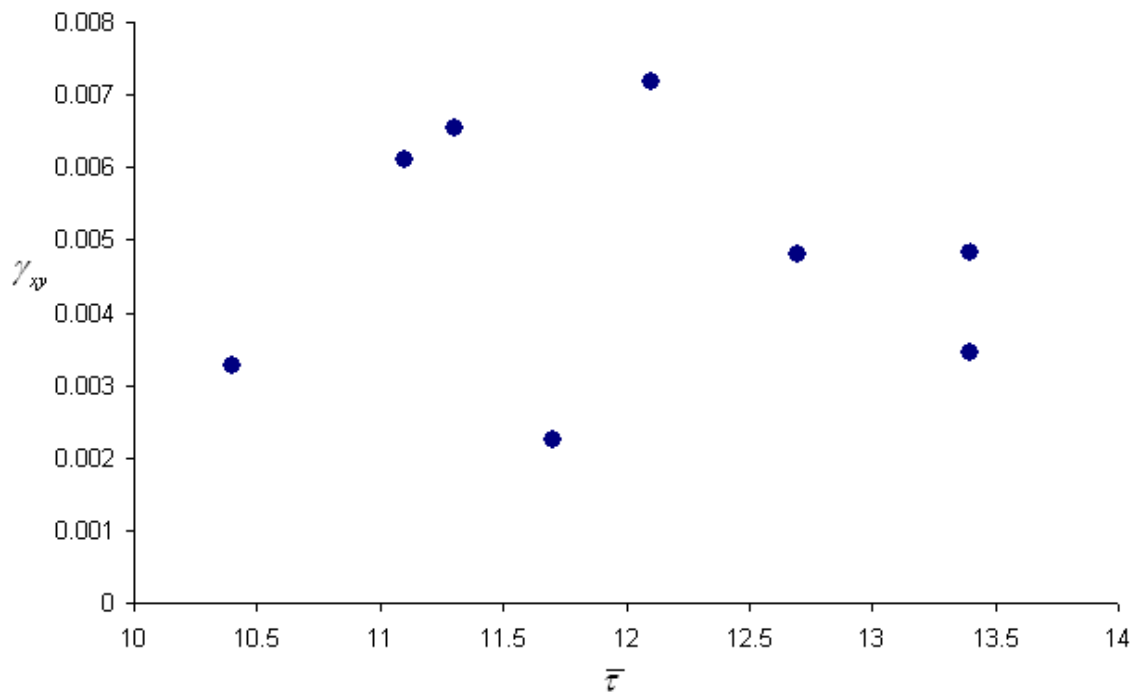


Figure 3-12 Experimental measured of γ_{xy} versus $\bar{\tau}$ from Clyde et al (2000) and Pantelides et al (2002)

The values of the joint shear strain were plotted against the normalized joint shear strength of each test (Figure 3-12). It can be appreciated from this figure that the data is

very scattered and thus a clear trend can not be established. Since there are few data points it was decided to take the joint shear strain as a constant value equals to 0.005.

3.2.2.4.3 ROTATION DUE TO BOND SLIP

Rotations due to bond slip (Figure 3-13) are computed based on the model proposed by Lowes (2003), who assumed the following assumptions: a) bond stress τ_E along the anchored length of a reinforcing bar is assumed to be uniform for reinforcement that remains elastic or piecewise constant for reinforcement loaded beyond yield (Figure 3-14), b) slip is assumed to define the relative movement of the reinforcing bar with respect to the face of the beam-column joint and is a function of the steel strain distribution along the bar and c) the bar exhibits zero slip at the point of zero bar stress. Based in these assumptions, the slip versus bar stress relationship is defined as follows:

$$f_s < f_y \Rightarrow \theta = \left(\frac{\tau_E}{E_s} \frac{2}{\phi_b} l_s^2 \right) \frac{l}{d_b - d_b'} \quad 3.39$$

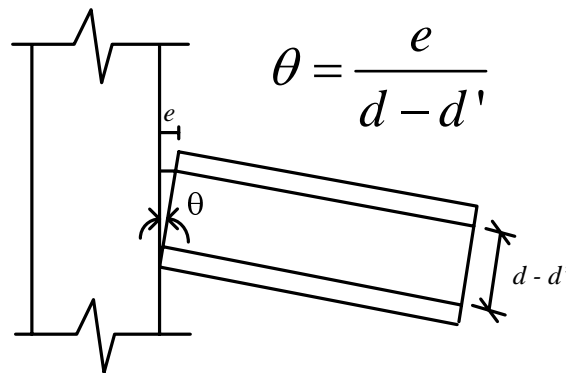


Figure 3-13 Rotation due to Bond Slip

$$f_s \geq f_y \Rightarrow \theta = \left(\frac{\tau_E}{E_s} \frac{2}{\phi_b} l_e^2 + \frac{f_y}{E_s} l_y + \frac{\tau_Y}{E_h} \frac{2}{\phi_b} l_Y^2 \right) \frac{l}{d_b - d_b'} \quad 3.40$$

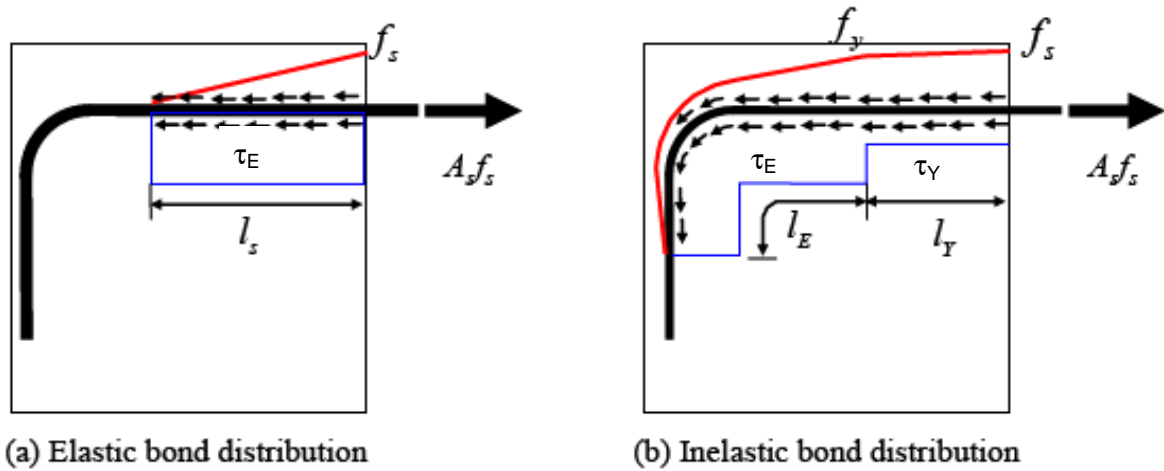


Figure 3-14 Bond and bar stress distribution for a reinforcing bar anchored in a joint (adapted from Park and Mosalam 2009)

$$l_s = \frac{f_s \phi_b}{\tau_E} \frac{1}{4} \quad l_e = \frac{f_y \phi_b}{\tau_E} \frac{1}{4} \quad l_Y = \frac{f_s - f_y \phi_b}{\tau_Y} \frac{1}{4} \quad 3.41$$

where E_s is the steel elasticity modulus, E_h is the steel hardening modulus, ϕ_b is the bar diameter, d_b is the beam effective depth, d_b' is the distance from the compression face in the beam to the centroid of compression steel, τ_E and τ_Y are the bond strength in the elastic and inelastic beam tensile reinforcement respectively. The values for the bond strength were adopted from Lehman and Moehle (2000) as follows:

$$\tau_E = 12\sqrt{f'_c} \text{ (psi)} \quad 3.42$$

$$\tau_Y = 0.5\tau_E = 6\sqrt{f'_c} \text{ (psi)} \quad 3.43$$

In order to be able to compute the rotations due to Bond Slip it is necessary to know the value of the steel stress in the tension bar reinforcement. Equating the internal beam moment with the moment produced by the load V_b (Figure 3-6) in the beam and solving for the steel stress yields:

$$f_s = \frac{V_b L_b}{A_s j d} \quad 3.44$$

The value of V_b is computed with Equation 3.38. For the case in which f_s results equal to f_y . (BJ failure) the value of f_s is corrected and taken as $1.15 f_y$

3.2.2.5 ABSCISSA OF THE CRACKING POINT

3.2.2.5.1 ELASTIC ROTATIONS AT CRACKING

The elastic rotation at cracking point is calculated as follows:

$$\theta_{elas_crack} = \frac{V_{b_crack} L}{\frac{6E_{c1}I_{c1}}{L_{c1}} + \frac{6E_{c2}I_{c2}}{L_{c2}}} \quad 3.45$$

where

$$V_{b_crack} = \frac{\bar{\tau}_{crack} b_j h_c \sqrt{f'_c}}{\left(\frac{L_b}{j d} - \frac{L}{L_c} \right)} \quad 3.46$$

$\bar{\tau}_{crack}$ is obtained from Equation 3.4.

3.2.2.5.2 JOINT SHEAR DISTORTION AT CRACKING

The joint shear strain at cracking point can be obtained using Mohr circle. For a plane strain state, the principal tensile strain is:

$$\varepsilon_T = \frac{\varepsilon_x + \varepsilon_y}{2} + \sqrt{\left(\frac{\varepsilon_x - \varepsilon_y}{2}\right)^2 + \left(\frac{\gamma_{xy}}{2}\right)^2} \quad 3.47$$

where, $\varepsilon_x = \frac{\sigma_x}{E_c}$, $\varepsilon_y = \frac{\sigma_y}{E_c}$ and $\varepsilon_T = \frac{\sigma_T}{E_c}$ are the beam axial strain, the column axial strain (negative in compression) and the principal tensile strain, correspondingly. E_c is concrete elasticity modulus and is taken as $E_c = 57,000\sqrt{f'_c}$ (psi). Neglecting beam axial strain (beam axial load are very small) and solving for the joint shear strain, yields:

$$\gamma_{xy} = 2\sqrt{\left(\varepsilon_T - \frac{\varepsilon_y}{2}\right)^2 - \left(\frac{\varepsilon_y}{2}\right)^2} \quad 3.48$$

Taking the concrete tensile stress as $4\sqrt{f'_c}$ (Kim and LaFave 2007) and knowing the value of the column axial load, one can obtain the joint shear strain at cracking point with Equation 3.48.

3.2.2.5.3 ROTATION DUE TO BOND SLIP AT CRACKING

The rotation due to bond slip at the cracking point is calculated from Equation 3.39, since the stress in the steel will be less than the yield stress at this point.

3.2.2.6 ABSCISSA OF THE RESIDUAL MOMENT POINT

Once the value of the ordinate (Moment) at the residual points as well as the ordinate (moment) and abscissa (rotation) at the peak point are known, the rotation at the residual moment point can be calculated by means of a triangle relationship as shown in Figure 3-3 but repeated here for convenience as Figure 3-15 assuming the slope as follows:

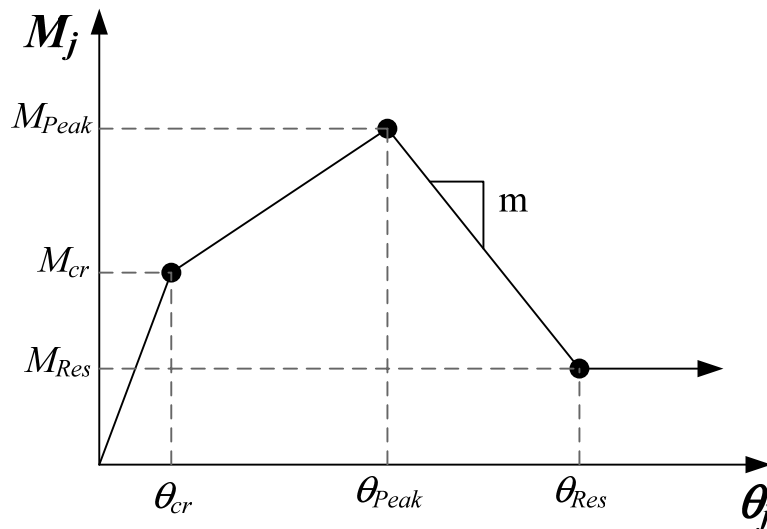


Figure 3-15 Proposed moment rotation for the rotational spring

$$\theta_{Res} = \theta_{Peak} + \frac{M_{Res} - M_{Peak}}{m} \quad 3.49$$

Substituting $M_{Res} = 0.3M_{Peak}$ in Equation 3.50 yields:

$$\theta_{Res} = \theta_{Peak} - \frac{0.7M_{Peak}}{m}$$

3.50

Where m is the slope that represents the strength degradation that unreinforced concrete joints experiments once attains its maximum strength. Since the strength degradation is associated directly with the joint damage, the slope m is obtained from the load versus drift graph of the experiments as shown in Figure 3-16.

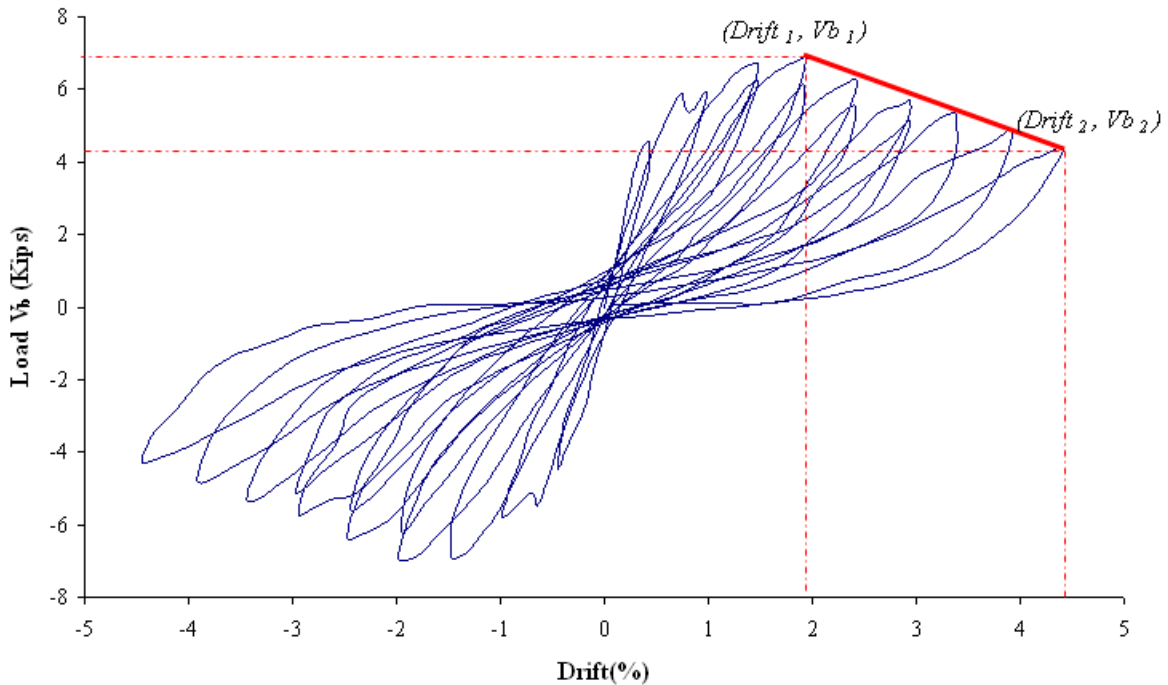


Figure 3-16 Example of a Load-Drift Graph

From Figure 3-16 one can obtain the value of the slope as follows:

$$m = \frac{(V_{b_2} - V_{b_1})}{(Drift_2 - Drift_1)}$$

3.51

In Equation 3.52 the slope m has units of force. As the slope of the proposed model has units of moment/radians Equation 3.51 can be multiplied by the distance from the point of load application to the center of the joint as follows:

$$m = \frac{(V_{b_2} - V_{b_1})L}{(Drift_2 - Drift_1)} \quad 3.52$$

Since the interest is focused in the value of the slope, not in its units, Equation 3.53 has been adopted to compute the slope for the tests of the database and its results were plotted against the column axial load (Figure 3-17).

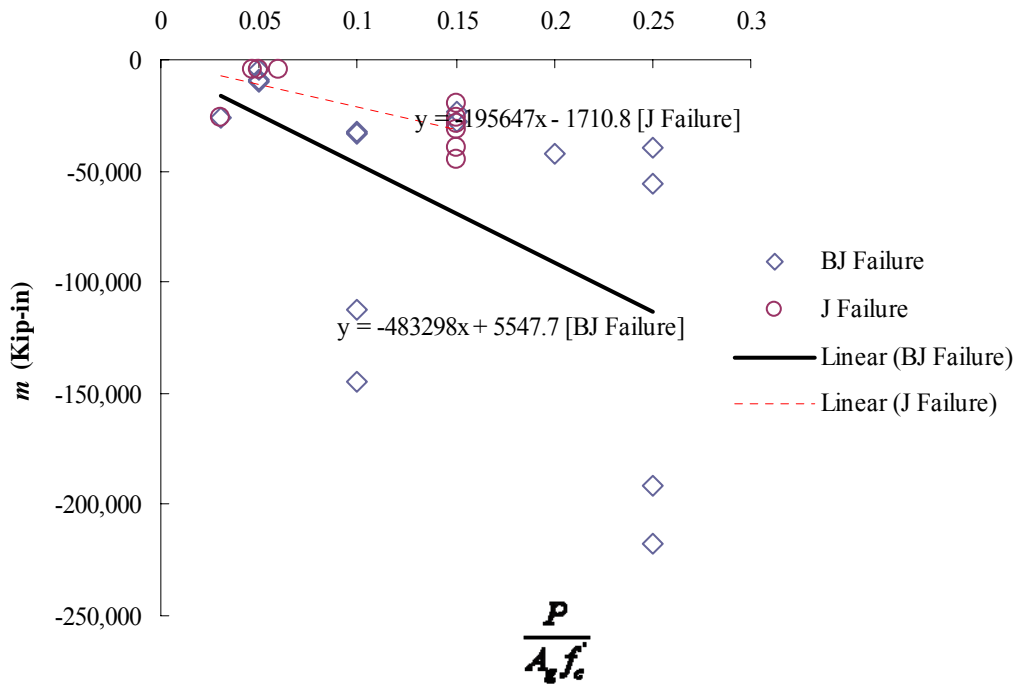


Figure 3-17 Slope – Axial Load Graph from test of the database with available Load-Drift graph

It can be appreciated that even though the data is very scattered, the trend indicates that the slope increases with the axial load for both types of failure. An equation was obtained using linear regression for each type of failure. These were:

$$m = - \left[195.65 \left(\frac{P}{A_g f'_c} \right) + 1.7 \right] 10^3 \quad 3.53$$

$$m = - \left[483.3 \left(\frac{P}{A_g f'_c} \right) - 5.6 \right] 10^3 \quad 3.54$$

Equation 3.53 is the slope for joints with J failure, while Equation 3.54 computes the slope for joints with BJ failure. Finally, substituting Equation 3.53 or 3.54 in Equation 3.50 yields the rotation at the residual strength point.

3.2.2.7 APPLICATION EXAMPLE

In this example, specimen BSL from (Wong 2005) is selected to illustrate the procedure to construct the equivalent Moment-Rotation envelope of the joint. The specimen is shown in Figure 3-18. Since beam top and bottom reinforcement is the same, the positive and negative envelope will be equal. In the case of different beam top and bottom reinforcement, the procedure has to be applied for each case, taking into account that the tension steel depends in whether the beam load is upward (bottom steel in tension) or downward (top steel in tension). The material properties of concrete and steel are $f'_c = 4.5$

ksi and $f_y = 75.4$ ksi respectively. The remaining necessary parameters are: $\frac{P}{A_g f'_c} = 0.15$;

$h_b = 17.72$ in; $b_b = 10.24$ in; $d_b = 15.6$ in; $A_{sb} = A_{st} = 1.46$ in²; $h_c = b_c = 11.81$ in; $L_b = 51.2$ in and $L_c = 122.1$ in.

1. Ordinate of the Cracking Point

$$\sigma_T = 4\sqrt{f'_c} = 4\sqrt{4,500 \text{ psi}} = 268.3 \text{ psi}$$

$$\sigma_y = -\frac{P}{A_g} = -\frac{0.15 f'_c A_g}{A_g} = -0.15(4,500 \text{ psi}) = -675 \text{ psi}$$

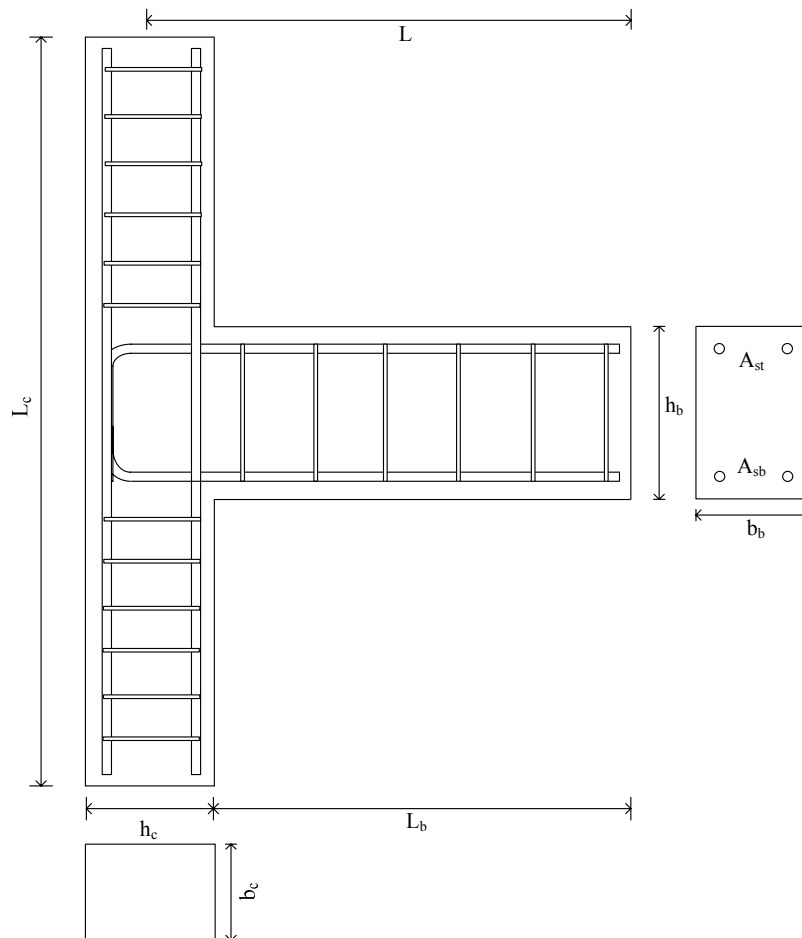


Figure 3-18 Dimension of Specimen BSL (Wong 2005)

From Equation 3.3:

$$\tau_{Crack} = \sqrt{\left(\sigma_T - \frac{\sigma_y}{2}\right)^2 - \left(\frac{\sigma_y}{2}\right)^2} = \sqrt{\left(268.3 - \frac{-675}{2}\right)^2 - \left(\frac{-675}{2}\right)^2} = 503.1 \text{ psi}$$

$$\bar{\tau}_{crack} = \frac{\tau_{crack}}{\sqrt{f'_c}} = \frac{503.1 \text{ psi}}{\sqrt{4,500 \text{ psi}}} = 7.5 \text{ psi} \leq 0.9 \bar{\tau}_{peak}$$

From Equation 3.5:

$$b_j = \frac{b_c + b_b}{2} = \frac{11.81 + 10.24}{2} = 11.03 \text{ in}$$

$$jd = 0.875d_b = 0.875(15.6 \text{ in}) = 13.65 \text{ in}$$

$$L = L_b + \frac{h_c}{2} = 51.2 + \frac{11.81}{2} = 57.1 \text{ in}$$

$$M_{crack} = \frac{\bar{\tau}_{crack} b_j h_c \sqrt{f'_c}}{\left(\frac{L_b}{jd} - \frac{L}{L_c}\right)} L = \frac{7.5 \text{ psi} (11.03 \text{ in}) (11.81 \text{ in}) \sqrt{4,500 \text{ psi}}}{\left(\frac{51.2 \text{ in}}{13.65 \text{ in}} - \frac{57.1 \text{ in}}{122.1 \text{ in}}\right)} (57.1 \text{ in}) = 949.8 \text{ kip-in}$$

2. Ordinate of the Peak Strength Point

According to the ACI-318 Softened Strut and Tie Model, for joint sustaining type of failure J:

$$f_{cu} = 0.85 \beta_s f'_c = 0.85 (0.6) 4,500 \text{ psi} = 2,295 \text{ psi}$$

$$n = \frac{E_s}{E_c} = \frac{29000 \text{ ksi}}{57 \sqrt{4500 \text{ psi}}} = 7.58$$

$$\rho = \rho' = \frac{A_s}{b_b d_b} = \frac{1.46}{(10.24)(15.6)} = 0.0091$$

$$a_c = \left(0.25 + 0.85 \frac{N}{f_c' A_g} \right) h_c = (0.25 + 0.85(0.15)) 11.81 = 4.46 \text{ in}$$

$$0.4h_c = 0.4(11.81) = 4.72 \text{ in}$$

Since 4.46 is less than 4.72:

$$a_c = 4.46 \text{ in}$$

$$k = \sqrt{(\rho + \rho')^2 n^2 + 2 \left(\rho + \rho' \frac{d_b'}{d_b} \right) n} - (\rho + \rho') n$$

$$k = \sqrt{(0.0091 + 0.0091)^2 (7.58)^2 + 2 \left(0.0091 + 0.0091 \frac{2.17}{15.6} \right) 7.58} - (0.0091 + 0.0091) 7.58$$

$$k = 0.28$$

$$a_b = 0.28(15.6) = 4.37 \text{ in}$$

$$a_s = \sqrt{(4.37)^2 + (4.46)^2} = 6.24 \text{ in}$$

$$A_{str} = a_s b_s = 6.24 \text{ in}(11.03 \text{ in}) = 68.8 \text{ in}^2$$

$$D = f_{cu} A_{str} = 2,295 \text{ psi}(68.8 \text{ in}^2) = 158 \text{ ksi}$$

$$\theta = \tan^{-1} \left(\frac{d_b - d_b'}{d_c - d_c'} \right) = \tan^{-1} \left(\frac{15.6 - 2.17}{10.14 - 1.67} \right) = 57.8^\circ$$

$$V_{jh} - J = D \cos \theta = 158(\cos 57.8) = 84.2 \text{ kips}$$

From Equation 3.21, for BJ failure, the joint shear force is:

$$V_{jh-BJ} = A_s f_y \left(1 - \frac{jd}{L_b} \frac{L}{L_c} \right) = 1.46 (75.4) \left(1 - \frac{13.65}{51.2} \frac{57.1}{122.1} \right) = 96.34 \text{ kips}$$

$$V_{jh} = \min(V_{jh-J}, V_{jh-BJ}) = \min(84.2, 96.34) = 84.32 \text{ kips} \therefore J \text{ failure governs}$$

From Equation 3.23, the normalized joint shear strength at peak is:

$$\bar{\tau}_{Peak} = \frac{V_{jh}}{A_j \sqrt{f'_c}} = \frac{84.32 \text{ ksi}}{11.03(11.81)\sqrt{4,500 \text{ psi}}} = 9.65 \text{ psi}$$

Finally, from Equation 3.24, the ordinate of the peak strength point is:

$$M_{Peak} = \frac{\bar{\tau}_{Peak} b_j h_c \sqrt{f'_c}}{\left(\frac{L_b}{jd} - \frac{L}{L_c} \right)} L = \frac{9.65 \text{ psi} (11.03 \text{ in}) (11.81 \text{ in}) \sqrt{4,500 \text{ psi}}}{\left(\frac{51.2 \text{ in}}{13.65 \text{ in}} - \frac{57.1 \text{ in}}{122.1 \text{ in}} \right)} (57.1 \text{ in}) = 1,466.01 \text{ kip-in}$$

3. Ordinate of the Residual Moment Point

$$M_{res} = 0.3 M_{peak} = 0.3 (1,466) = 439.8 \text{ kip-in}$$

4. Abscissa of the Cracking Point

Elastic Rotations at cracking point:

$$V_{b_crack} = \frac{\bar{\tau}_{crack} b_j h_c \sqrt{f'_c}}{\left(\frac{L_b}{jd} - \frac{L}{L_c} \right)} = \frac{7.5 \text{ psi} (11.03 \text{ in}) (11.81 \text{ in}) \sqrt{4,500 \text{ psi}}}{\left(\frac{51.2 \text{ in}}{13.65 \text{ in}} - \frac{57.1 \text{ in}}{122.1 \text{ in}} \right)} = 19.96 \text{ kip}$$

$$\theta_{elas_crack} = \frac{V_{b_crack} L}{\frac{3E_{c1} I_{c1}}{L_{c1}} + \frac{3E_{c2} I_{c2}}{L_{c2}}} = \frac{19.96 \text{ kip} (57.1 \text{ in})}{\frac{6 \left(57 \sqrt{4,500 \text{ psi}} \right) \left(\frac{11.81 \text{ in}^4}{12} \right) \text{ in}^4}{122.1 \text{ in}} \cdot \frac{1}{2}} = 0.0019$$

$$\varepsilon_y = \frac{\sigma_y}{E_c} = \frac{-675 \text{ psi}}{57,000 \sqrt{4,500 \text{ psi}}} = -0.00018$$

$$\varepsilon_T = \frac{\sigma_T}{E_c} = \frac{268.3 \text{ psi}}{57,000 \sqrt{4,500 \text{ psi}}} = 0.00007$$

From Equation 3.49:

$$\gamma_{xy_Crack} = 2 \sqrt{\left(\varepsilon_T - \frac{\varepsilon_y}{2} \right)^2 - \left(\frac{\varepsilon_y}{2} \right)^2} = 2 \sqrt{\left(0.00007 + \frac{0.00018}{2} \right)^2 - \left(\frac{0.00018}{2} \right)^2} = 0.00026$$

Rotations due to bond slip:

$$f_{s_Crack} = \frac{V_{b_Crack} L_b}{A_s j d} = \frac{19.96 \text{ kip} (51.2 \text{ in})}{1.46 \text{ in}^2 (13.65 \text{ in})} = 51.3 \text{ ksi}$$

$$l_s = \frac{f_{s_Crack} \phi_b}{\tau_E} = \frac{51.3 \text{ ksi} \cdot 0.787 \text{ in}}{12 \sqrt{4,500 \text{ psi}} \cdot 4} = 12.54 \text{ in}$$

$$\theta_{BS_Crack} = \left(\frac{\tau_E}{E} \frac{2}{\phi_b} l_s^2 \right) \frac{1}{d_b - d_b'} = \left(\frac{805 \text{ psi}}{29,000 \text{ ksi}} \frac{2}{0.787} (12.54 \text{ in})^2 \right) \frac{1}{15.6 \text{ in} - 2.17 \text{ in}} = 0.00083$$

The total rotation at cracking point is:

$$\theta_{Crack} = \theta_{Elast_Crack} + \gamma_{xy_Crack} + \theta_{BS_Crack}$$

$$\theta_{Crack} = 0.0019 + 0.00026 + 0.00083 = 0.003 \text{ rads}$$

5. Abscissa of the Peak Point

Elastic Rotations at peak point:

$$V_{b_Peak} = \frac{\bar{\tau}_{Peak} b_j h_c \sqrt{f'_c}}{\left(\frac{L_b}{j d} - \frac{L}{L_c} \right)} = \frac{9.65 \text{ psi} (11.03 \text{ in}) (11.81 \text{ in}) \sqrt{4,500 \text{ psi}}}{\left(\frac{51.2 \text{ in}}{13.65 \text{ in}} - \frac{57.1 \text{ in}}{122.1 \text{ in}} \right)} = 25.68 \text{ kip}$$

$$\theta_{elas_peak} = \frac{V_{b_peak} L}{\frac{3E_{c1}I_{c1}}{L_{c1}} + \frac{3E_{c2}I_{c2}}{L_{c2}}} = \frac{25.68 \text{ kip}(57.1 \text{ in})}{\frac{6(57\sqrt{4,500 \text{ psi}})\left(\frac{11.81^4}{12}\right) \text{ in}^4}{\frac{122.1 \text{ in}}{2}}} = 0.0024$$

$$\gamma_{xy} = 0.005$$

Rotations due to bond slip:

$$f_{s_Peak} = \frac{V_{b_Peak} L_b}{A_s j d} = \frac{25.68 \text{ kip}(51.2 \text{ in})}{1.46 \text{ in}^2 (13.65 \text{ in})} = 66 \text{ ksi} < f_y$$

$$l_s = \frac{f_{s_Peak} \phi_b}{\tau_E} = \frac{66 \text{ ksi}}{12\sqrt{4,500 \text{ psi}}} \frac{0.787 \text{ in}}{4} = 16.13 \text{ in}$$

$$\theta_{BS_Peak} = \left(\frac{\tau_E}{E} \frac{2}{\phi_b} l_s^2 \right) \frac{l}{d_b - d_b'} = \left(\frac{805\sqrt{\text{psi}}}{29,000 \text{ ksi}} \frac{2}{0.787 \text{ in}} (16.13 \text{ in})^2 \right) \frac{l}{15.6 \text{ in} - 2.17 \text{ in}} = 0.0014$$

The total rotation at cracking point is:

$$\theta_{Peak} = \theta_{Elas_Peak} + \gamma_{xy_Peak} + \theta_{BS_Peak}$$

$$\theta_{Peak} = 0.0024 + 0.005 + 0.0014 = 0.0088 \text{ rads}$$

6. Abscissa of the Residual Moment Point

Since the predicted mode of failure is J, Equation 3.55 applies for this case.

$$m = - \left[195.65 \left(\frac{P}{A_g f_c'} \right) + 1.7 \right] 10^3 = - [195.65(0.15) + 1.7] 10^3 = -31,047.5 \text{ kip-in}$$

$$\theta_{Res} = \theta_{Peak} - \frac{0.7M_{Peak}}{m} = 0.0088 + \frac{0.7(1,466.01 \text{ kip-in})}{31,047.5 \text{ kip-in}} = 0.0419$$

Table 3-4 shows the summary of the envelope points for the specimen BSL (Wong 2005). The complete envelope is shown in Figure 3-19. The next step is to model the beam-column subassemblies from experimental tests, including the joint. This step is described in details in the following chapters.

Table 3-4 Summary of Envelope Point for the Application Example

Point	Rotation (Rad)	Moment (Kip-in)
Crack	0.0030	1,140
Peak	0.0088	1,466
Residual	0.0419	440

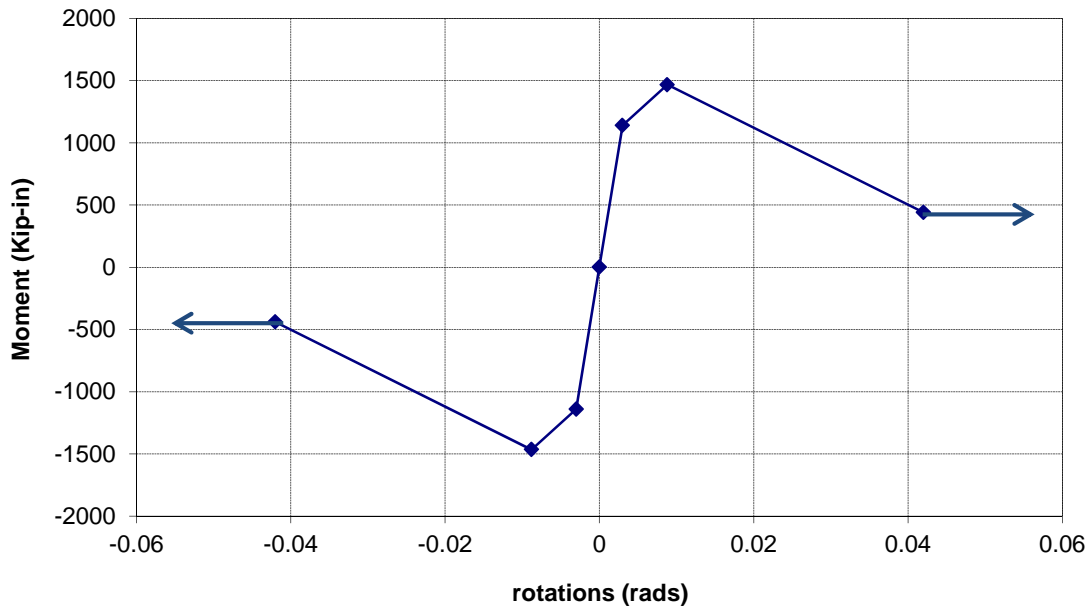


Figure 3-19 Moment-Rotation Envelope for Specimen BSL (Wong 2005)

4 NUMERICAL MODEL

4.1 INTRODUCTION

Once the points that define the envelope of the moment versus rotation that represent the behavior of unreinforced concrete joints were presented, the next step is to model the entire beam-column subassembly that was tested in past laboratory test. The program Opensees (Open System for Earthquake Engineering Simulation) (Mckenna and Fenves 2000) was selected to do this task since it has available a wide range of elements, material and sections models focused in the nonlinear model of structures that made Opensees one of the most powerful nonlinear programs available to researchers. This chapter presents a brief explanation of the commands used to build the model including the material models, sections and elements. For more details concerning the commands of the program, it is recommended to read the User's Manual of Opensees (Mckenna and Fenves 2000).

4.2 MODEL OF THE SUBASSEMBLY

The model of the subassembly was built in Opensees a program based on the finite element analysis used for the simulation of the seismic response of structural and geotechnical systems, initially created at the University of California at Berkeley. The program provides advanced capabilities to model the nonlinear response of systems, using a wide range of material models, elements and solution algorithms that make the program a powerful tool for the numerical modeling of structural and geotechnical

systems. One advantage over other structural analysis software is that it is an open code program that allows the user to create his own material, element or tool of analysis and to integrate them into the program. Therefore the program is being continuously updated.

4.2.1 UNIAXIAL MATERIALS

This command is used to define a material which represents the stress-strain or the force-deformation relationship. Opensees has available different types of uniaxial materials but only those that were used in the model are discussed here.

4.2.1.1 CONCRETE 01 MATERIAL

The concrete was modeled using the Concrete01 Material assuming the concrete does not have tensile strength, as shown in Figure 4-1. The required input parameters for this material are the concrete compressive strength at 28 days, the concrete strain at maximum strength, the concrete crushing strength and the concrete strain at crushing strength. In this research, the value for these parameters were calculated using the equations for confined (for the concrete inside the concrete core) and unconfined concrete (for the concrete outside of the concrete core) of the Modified Kent and Park stress-strain relations (Park et. *al* 1982), as shown in Figure 4-2. The hysteretic Stress-Strain relation of this model has a degraded linear unloading/reloading stiffness according to the work of Karsan and Jirsa (1969). A typical hysteretic Stress-Strain Relation of the model is shown in Figure 4-3.

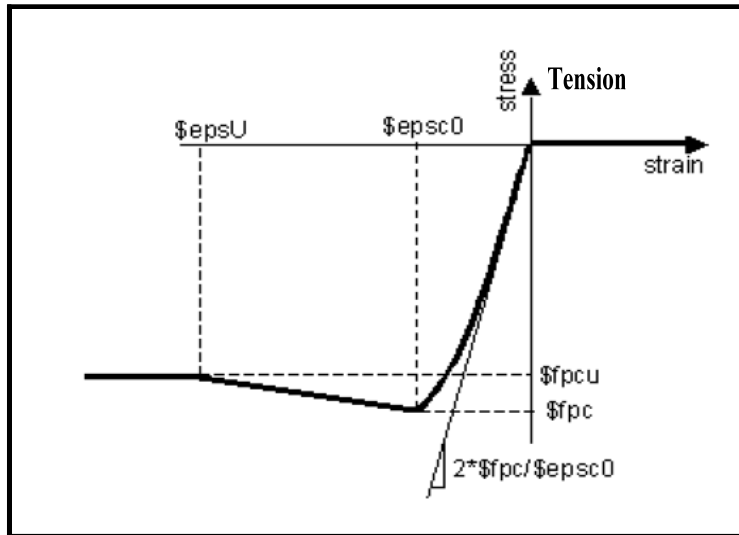


Figure 4-1 Concrete 01 Material Parameters (adapted from Mazzoni *et al* (2007))

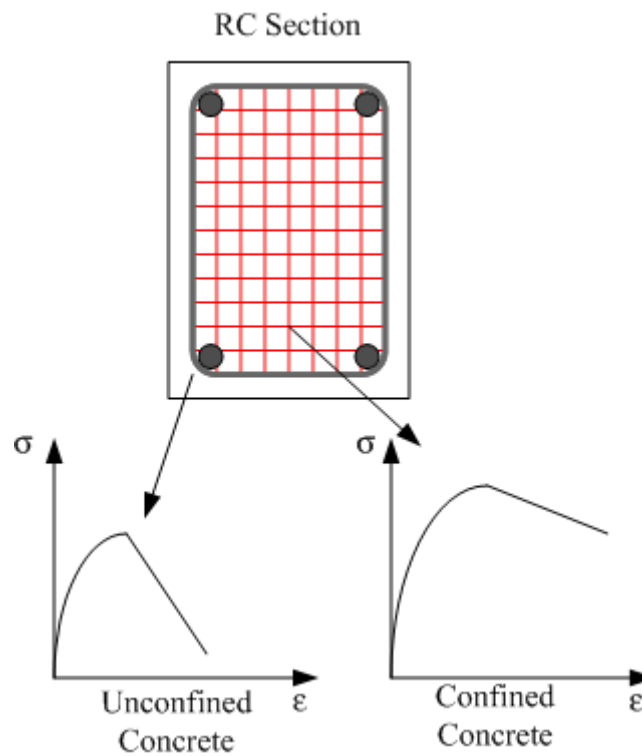


Figure 4-2 Definition of Confined and Unconfined region (adapted from Mazzoni *et al* (2007))

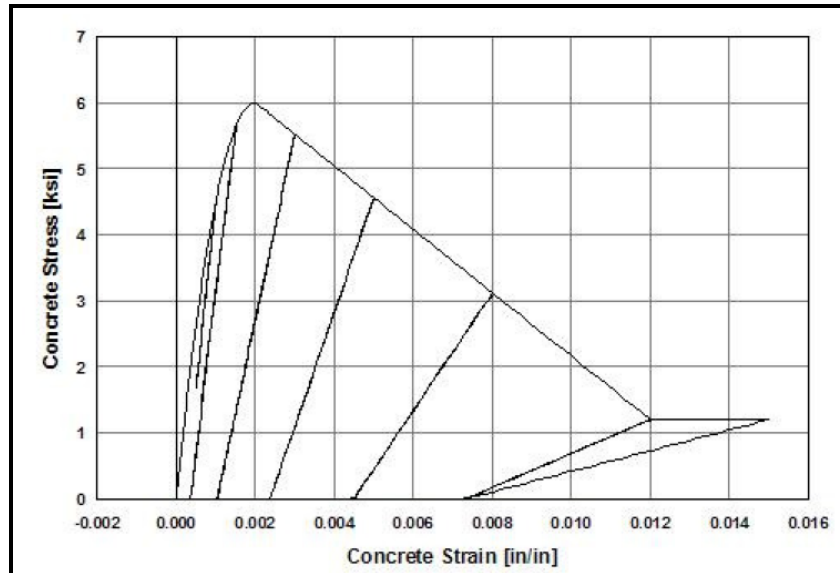


Figure 4-3 Hysteretic Stress-Strain Response of Concrete 01 (adapted from Mazzoni et al (2007))

4.2.1.2 STEEL01 MATERIAL

The steel was modeled using the Steel01 Material as shown in Figure 4-4. The required input parameters for this material are the steel yield strength, the steel elasticity modulus and the strain hardening ratio b which is the ratio between the post-yield tangent and the initial elastic tangent. In this research the value of b was assumed to be 0.01. A typical hysteretic Stress-Strain behavior of the Steel01 model is shown in Figure 4-5. It can be appreciated that the material follows the initial slope for loading, unloading and reloading.

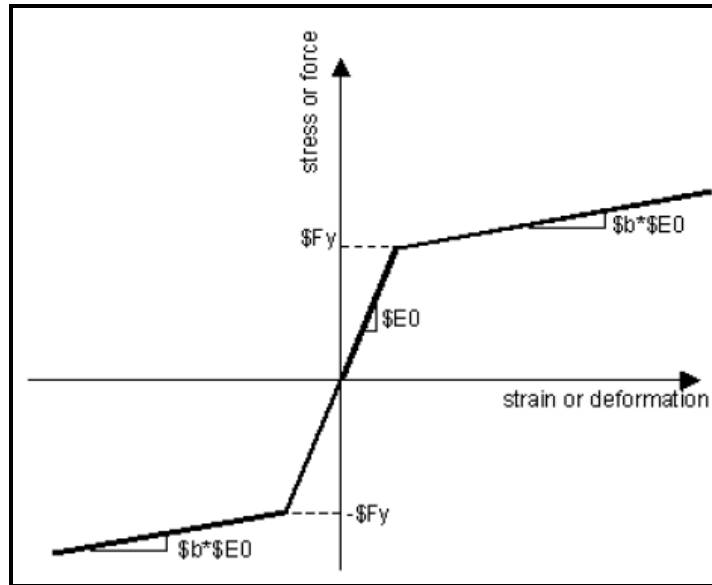


Figure 4-4 Steel 01 Material Parameters (adapted from Mazzoni et al (2007))

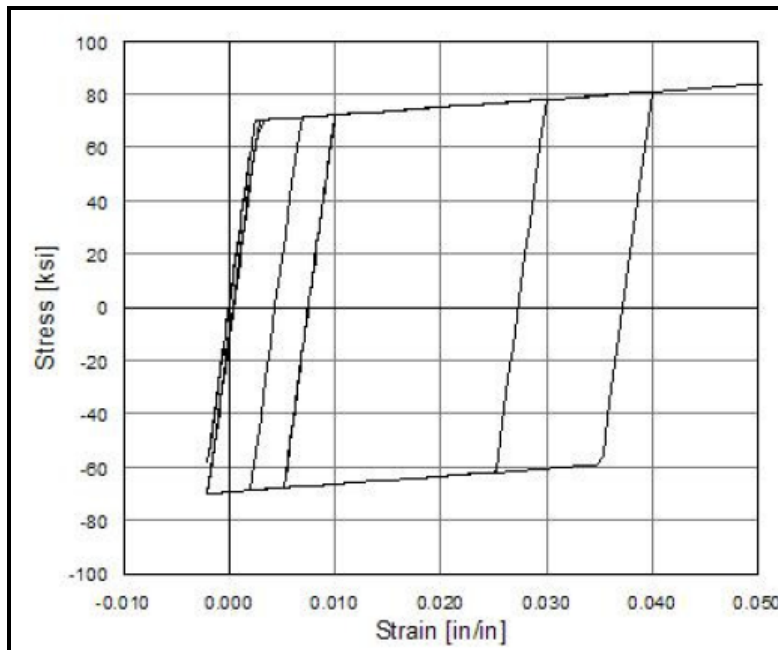


Figure 4-5 Hysteretic Stress-Strain response of Steel 01 Material without Isotropic Hardening (adapted from Mazzoni et al (2007))

4.2.1.3 PINCHING4 MATERIAL

The behavior of the joint was modeled using the Pinching4 Material (Lowe and Altoontash 2004) which can take into account a “pinched” load-deformation response, as well as degradation of strength and stiffness (unloading stiffness degradation, reloading stiffness degradation and strength degradation) under cyclic loading.

Figure 4-6 shows the envelope backbone curve as well as the hysteretic behavior rules for one cycle of the Pinching4 material. The monotonic backbone curve for positive and negative envelope is defined by eight points of stress-strain or force-deformation of the behavior that is being modeled. By default the material is assumed as symmetric. The general hysteretic rules of the material are based on three straight lines that define the unloading-reloading path that can be explained as follows: The material follows the primary backbone curve. Then at the point of unloading (Point A) it is unloaded with the initial slope up to the first pinching point (point B), which is defined as a fraction of the maximum strength in the other direction ($eNf3$). Then continue to point C (second pinching point) that represents the point in which reloading begins, defined as a fraction of the maximum historic deformation in this direction and its corresponding force (Point D).

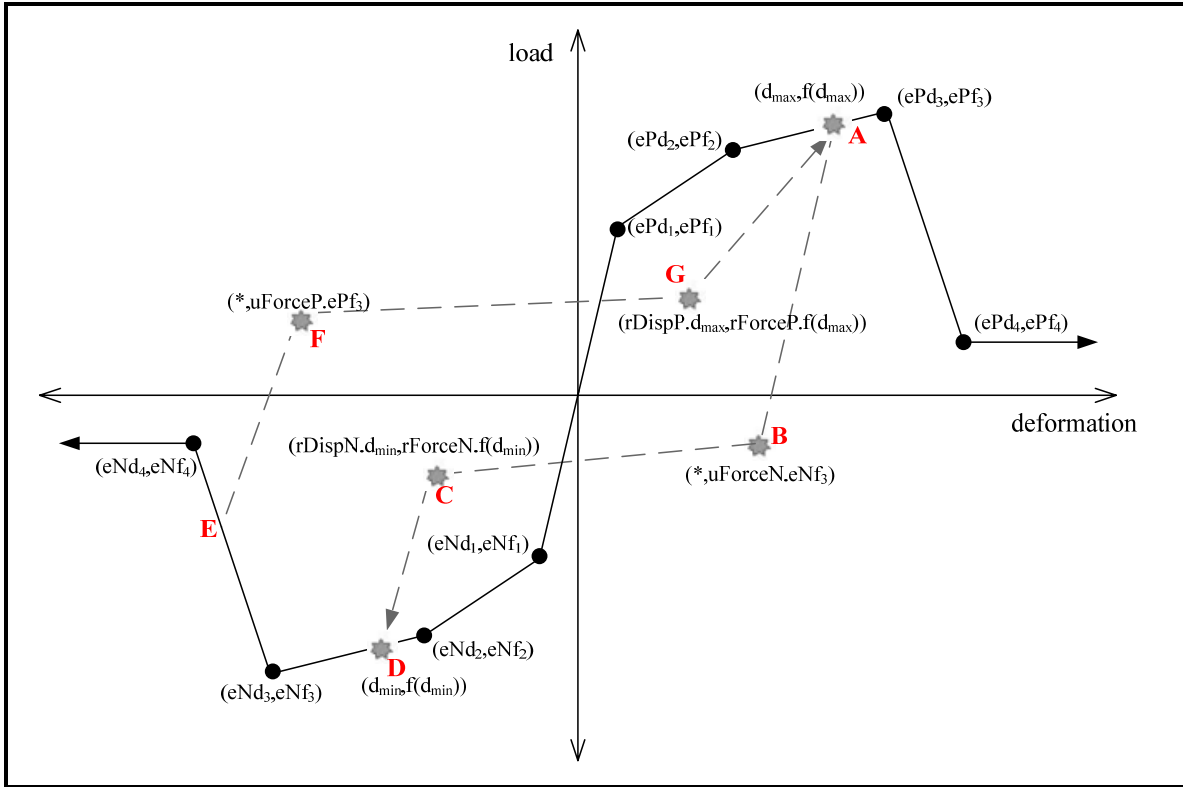


Figure 4-6 Pinching4 Material Model (adapted from Mazzone *et al* (2007))

From point C, it continues to the point D, which is the point in the negative envelope where the minimum historic deformation occurred. From this point, it continues through the envelope curve until unloading again (point E). From this point, it unloads with the initial slope up to the third pinching point (F), which is defined as a fraction of the peak strength (ePf3). Then continues to the fourth pinching point (G) which represents the point in which reloading occurs to the positive envelope curve, defined as a fraction of the maximum historic deformation and its corresponding force (Point A). Finally, from point G continues to point A and continues through the positive envelope curve.

The simulations of the strength and stiffness degradation are based in damage models which depend on whether the damage is function of the displacement history only (cycle) or function of the displacement history and energy accumulation (energy). More explanation of these damage models can be found in Lowes et *al* (2004).

The required input parameters for this material are:

1. The sixteen points defining the envelope in the positive and negative direction. By default the programs assumes that these values are symmetric.
2. The six floating point values that define the pinching behavior.
3. The sixteen floating point values that define the cyclic degradation models.
4. The string that indicates the type of damage (cycle or energy).

The positive envelope curve used to model the joint in this research is shown in Figure 4-7. The values of the ordinates (Moments) and the abscissas (rotations) for the joint were obtained through the methodology explained in the previous chapter. It is assumed that the negative envelope is the same as the positive. However, this can be different, depending of the characteristics of the joint that is being modeled. Although only three points are defined (crack, peak and residual) the first point is duplicated, having the same coordinates in order to fulfill the requirements of the material model.

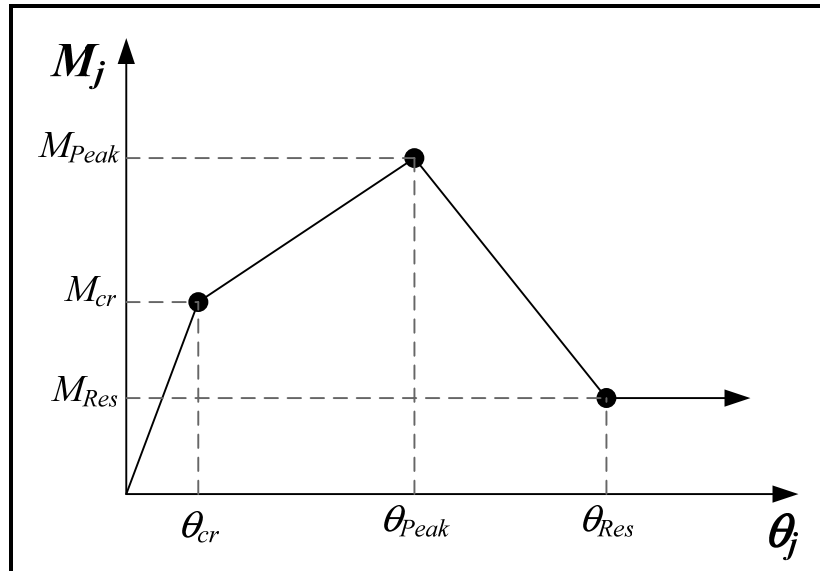


Figure 4-7 Proposed envelope curve for the joint

The values of the floating points were adopted from Celik and Ellingwood (2008) as follows:

$$uForceP = uForceN = -0.10$$

$$rForceP = rDispP = rForceN = rDispN = 0.15$$

Only the unloading stiffness degradation was considered into the model. Thus the values of the parameters that control the cyclic degradation model for the reloading stiffness degradation and strength degradation were set equal to zero. The values of the parameters that take into account the unloading stiffness degradation were:

$$gK1 = 0$$

$$gK2 = gK3 = gK4 = 0.2$$

$g_{KLim} = 0.5$

Finally, the damage model was based on the displacement history and accumulation of energy.

4.2.1.4 SECTIONS

Beam and column sections were modeled using the fiber element approach (Figure 4-8), which consists in dividing the section in several layers in both directions of the section, forming a mesh. To each element of this mesh (fiber) a stress-strain relationship of the material of the section is assigned. The integration of the stress-strain response of the individual fibers of the section allows taking into account the spread of the material nonlinearity across the whole section area.

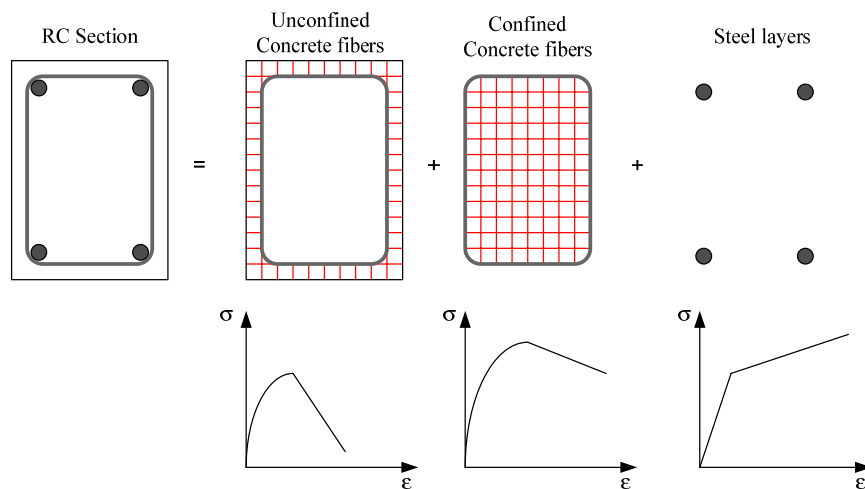


Figure 4-8 Fiber element approach

4.2.1.5 ELEMENTS

In Opensees, like in other structural softwares, beams and columns are modeled as straight lines that connect two points or nodes. Opensees has available a wide variety of elements. Only the ones used in the models are presented and discussed hereinafter.

4.2.1.5.1 BEAM WITH HINGE ELEMENT

The beam and the column of the subassembly were modeled with the beam with hinge element (Figure 4-9). This element concentrates the nonlinearity at the end of the members over a plastic hinge length. To each of the plastic hinge region, a previously defined section is assigned. The rest of the structural member is a linear elastic element.

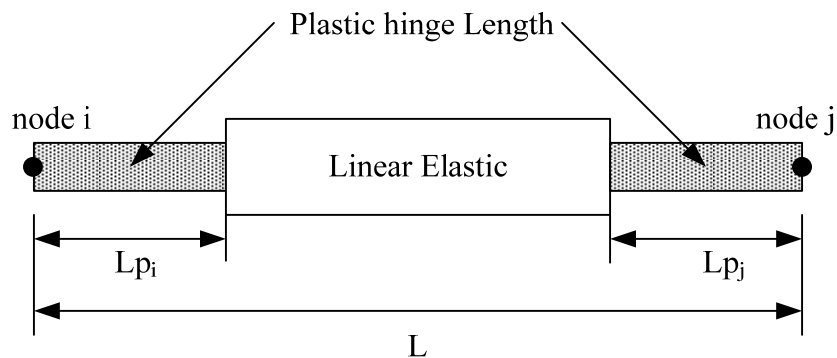


Figure 4-9 Beam with hinge element (adapted from Mazzoni et al (2007))

The required input parameter for this element are plastic hinge length, the modulus of elasticity, the cross sectional area and the moment of inertia of the section. Several models of plastic hinge are available in the literature. In this research the plastic hinge length was defined as half of the beam or column height for beam and columns respectively.

4.2.1.5.2 ZERO LENGTH ELEMENT

The zero length element was used to model the rotational spring that represents the joint. This element connects two points with the same location. To achieve that, a node with the same coordinates that the joint center node was created. The horizontal and vertical degree of freedom of the duplicated node was slaved to the center joint node and only the rotational degree of freedom is left independent. This rotation will activate the spring which has been assigned the Pinching4 material that represent the joint response. Actually, there is available in Opensees a script called rotString2D.tcl that implements the rotational spring. The user only has to specify the retained node and the constrained one.

4.3 MODEL CALIBRATION

In order to verify the accuracy of the numerical model (Figure 4-10) tests with available load versus deflection graph from the data base were modeled, taking the normalized joint shear stress coefficient ($\bar{\tau}$) at each point of the envelope (i.e. cracking point, peak point and residual strength point) directly from the experimental results and replacing its value in Equation 2.11 to find the joint equivalent moment at each point of the envelope. It was noticed that even using experimental values, the model constantly underestimates the value of the peak load. An example of this observation is shown in Figure 4-11, which is the comparison of the model (using the experimental joint shear stress) with the experimental results for test 3 of Pantelides et al (2002). Thus it was necessary to find an experimental value to adjust the joint model, mainly in the peak strength point. This value

was taken as the average of the ratio between the peak load obtained from the experiments and the peak load predicted by the model, as shown in Table 4-1.

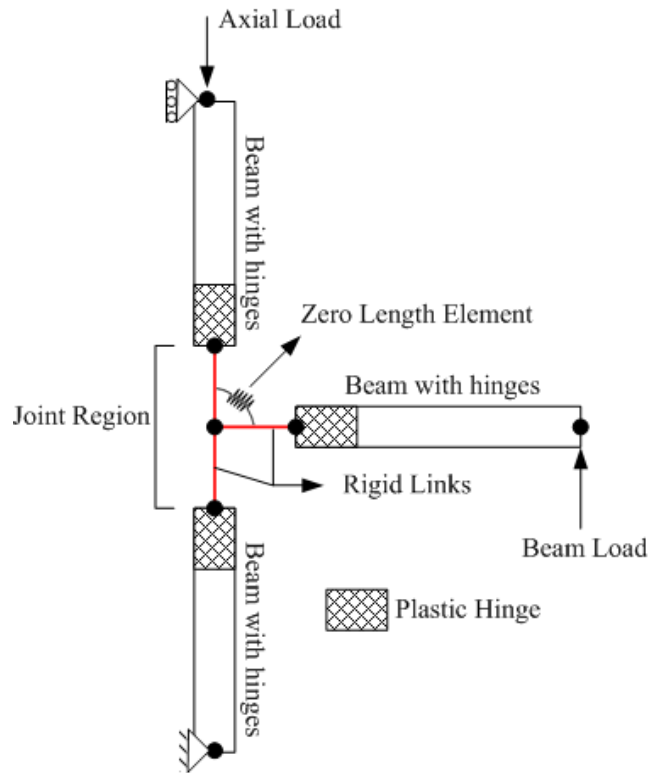


Figure 4-10 The Opensees model of the subassembly

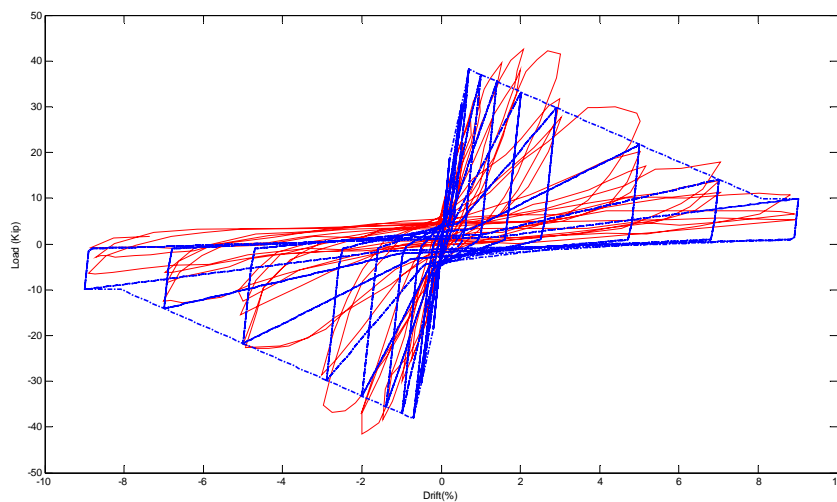


Figure 4-11 Comparison of results of Test 3 from Pantelides et al (2000)

Table 4-1 Computation of the Experimental factor for Peak Moment Point

Author	Specimen	Peak Load		Test / Model
		Test	Model	
Wong (2005)	BSL	22.7	18.8	1.21
	BSU	24.3	20.4	1.19
	BSLLS	24.7	20.6	1.20
	BSLV2T10	28.6	23.7	1.20
	BSLV4T10	29.1	24.1	1.21
	BSL600	30.0	24.8	1.21
	BSL300	21.3	17.8	1.19
	JA-NN03	18.3	13.5	1.35
	JA-NN15	19.9	14.8	1.35
Pantelides et al (2002)	3	42.6	38.2	1.12
	4	47.3	42.7	1.11
	5	43.1	39.3	1.10
	6	44.6	39.8	1.12
Clyde et al (2000)	2	64.5	54.3	1.19
	4	65.5	56.3	1.16
	5	60.2	53.8	1.12
	6	62.8	53.0	1.18
Ghobarah & Said (2001)	T-1	26.0	24.7	1.05
Karayannis (2008)	A0	5.4	3.9	1.38
	B0	13.1	9.7	1.35
	C0	14.6	10.8	1.36
Antonopoulos & Triantafillou (2003)	C1	7.0	6.0	1.16
	C2	6.9	6.0	1.16
	T-C	7.9	6.9	1.15
Mean				1.20
STD				0.09
COV				0.08

Equation 2.12 was modified applying a calibration factor taken as 1.20 for the Peak strength moment as shown in Equation 4.1.

$$M_{Peak} = 1.2 \frac{\bar{\tau}_{jh} b_j h_c \sqrt{f'_c}}{\left(\frac{L_b}{jd} - \frac{L}{L_c} \right)} L \quad 4.1$$

5 MODEL VALIDATION

5.1 INTRODUCTION

The response of the experimental test by means of a force versus displacement graph is compared with the prediction given by the joint model for experiments conducted by Wong (2005), Pantelides *et al.* (2002), Clyde *et al.* (2000) and Antonopoulos and Triantafillou (2003). For each one of these specimens, a model of the tested subassembly (as shown in Figure 4-10) was constructed in Opensees, as presented in the previous chapter in which the material properties, element and section dimensions, were taken directly from the data presented by the authors. The discussions of the predictions for each one of the aforementioned authors are presented in this chapter.

5.2 COMPARISON OF MODEL SIMULATION WITH EXPERIMENTAL RESPONSE

5.2.1 WONG TEST

The details of the selected specimens tested by Wong (2005) are shown in Figure 5-1. The beam and column reinforcement are symmetric in all the cases. The difference between the specimens JANN03 and JANN15 was in the column axial load ($0.03 A_g f'_c$ for the first case and $0.15 A_g f'_c$ for the last one). For all other specimens the column axial load was $0.15 A_g f'_c$. Figure 5-2 and Figure 5-3 show the comparison of the model simulated response with the response of the selected tested specimens.

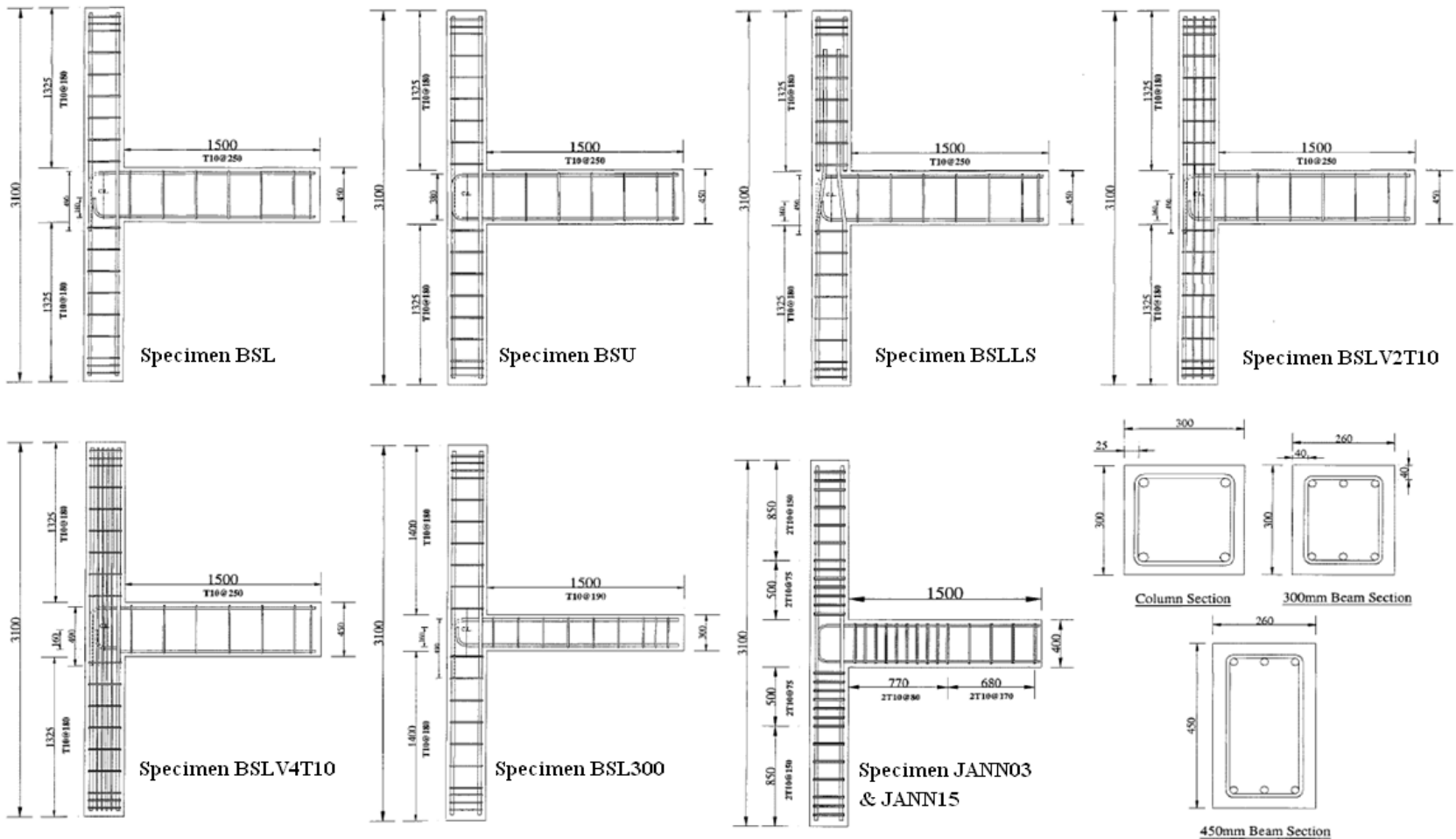


Figure 5-1 Details of specimens tested by Wong (2005) (All units in mm)

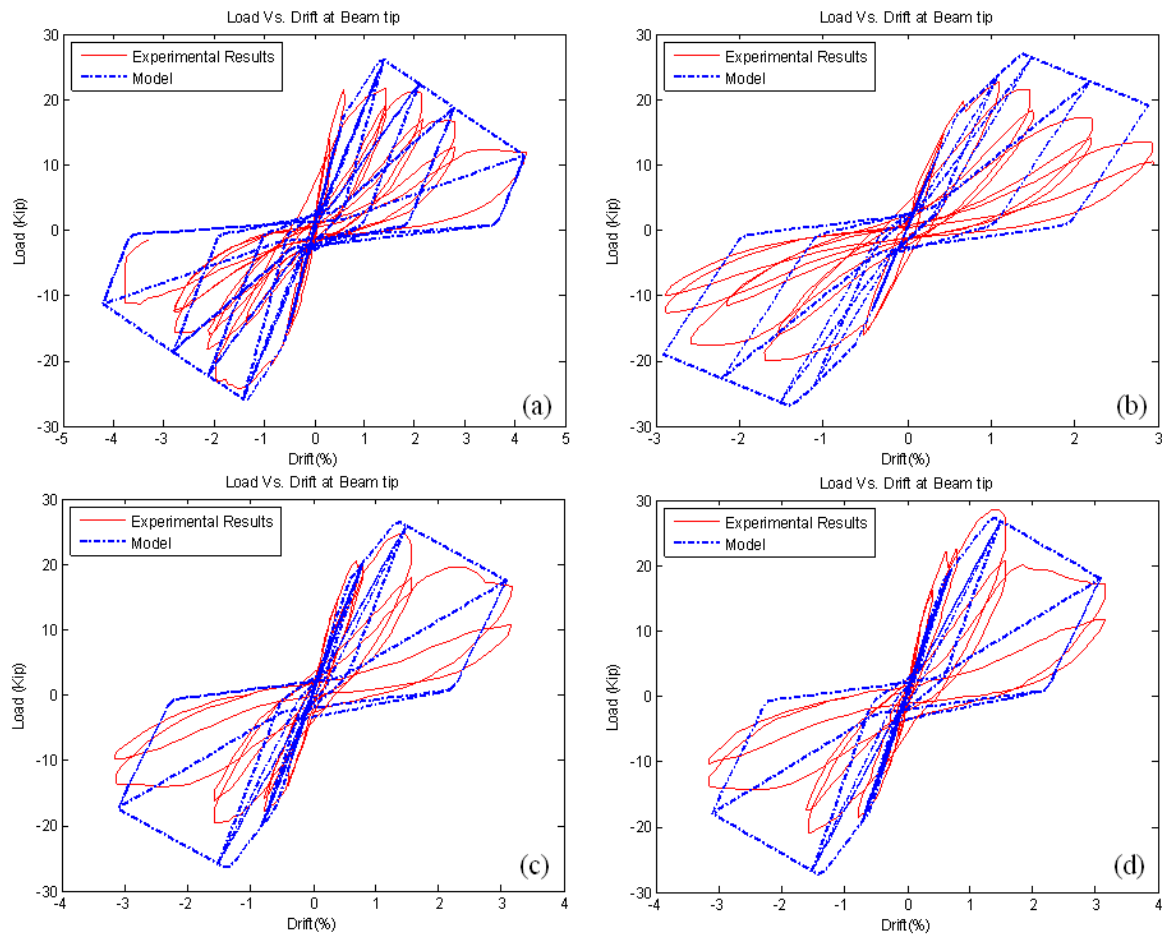


Figure 5-2 Comparison of response for test of Wong (2005): a) specimen BSU, b) specimen BSL, c) specimen BSLLS and d) specimen BSLV2T10

In general the simulated response for the specimen of Figure 5-2 agrees quite well with the test response. The crack load, peak load, ultimate reached load and the pinching effect were captured by the model. The difference observed in the specimens BSL (Figure 5-2 (b)) and BSLV4T10 (Figure 5-3 (a)) in the peak load in both directions is attributed to the predicted peak joint shear strength. The hysteretic behavior looks acceptable showing that the loading and unloading slopes are relatively similar for all the cases. The aforementioned specimens

have in common that they experimented J type of failure and thus the global behavior of the specimens was controlled only by the joint local behavior.

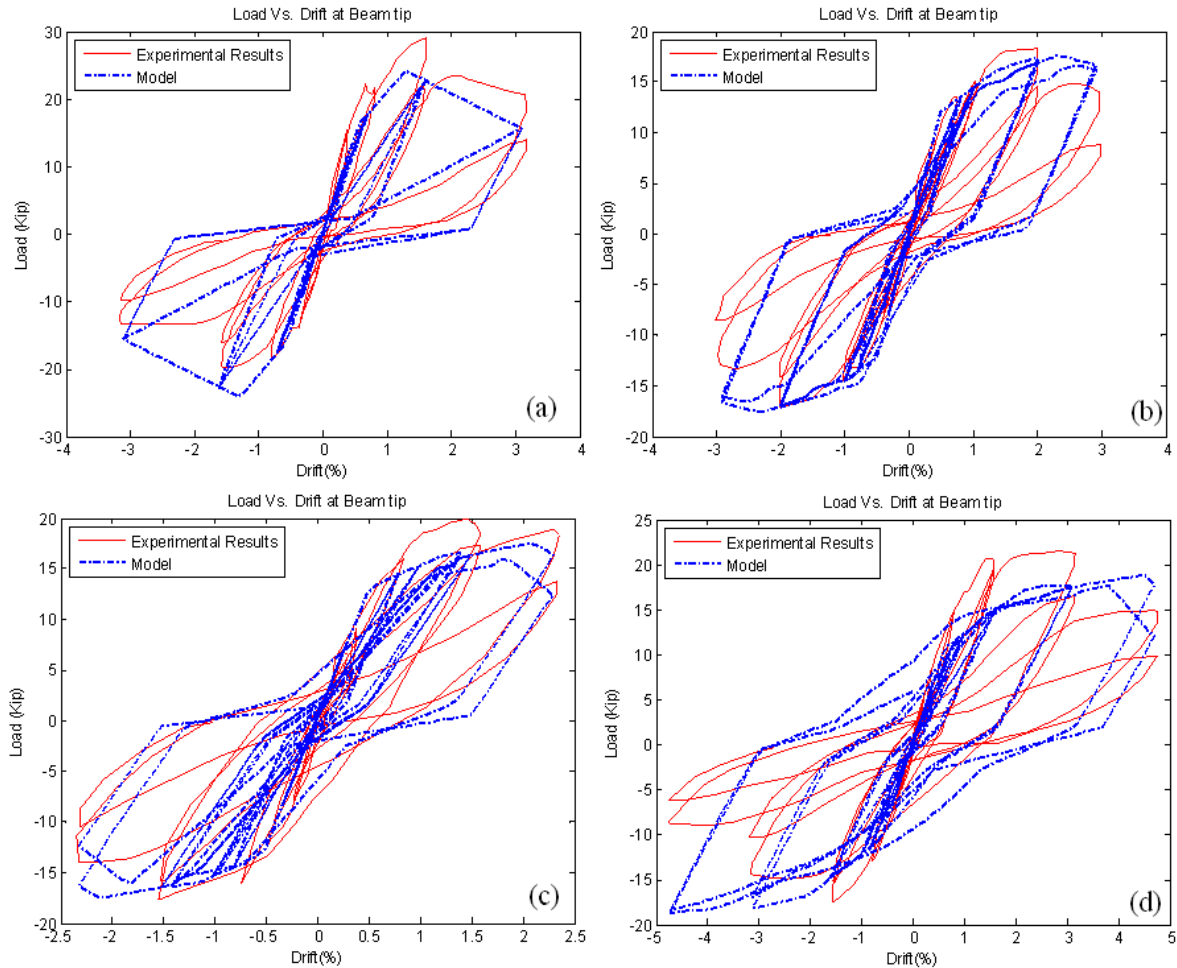


Figure 5-3 Comparison of response for test of Wong (2005): a) specimen BSLV4T10, b) specimen JANN03, c) specimen JANN15 and d) specimen BSL300

Specimens JANN03, JANN15 and BSL300 (Figure 5-3 (b), (c) and (d) respectively) experienced BJ failure and thus the global behavior of these specimens is controlled by the contribution of the beam reinforcement steel and the joint local behavior. The predicted behavior of specimens JANN03 (Figure 5-3 (b)) compares favorably with the experimental tests. Cracking and peak load were captured quite well. The ultimate load is acceptably

reached in both directions. The pinching behavior was predicted well. The cyclic behavior compares favorably since the loading and unloading slope are much similar. The simulated response of specimen JANN15 (Figure 5-3 (c)) also was in good agreement with the experimental test. A slight difference exists in the peak load but in general the model captures the pinching behavior as well as the cyclic behavior with reasonable accuracy. For the case of specimen BSL 300 the prediction of the model was acceptable up to approximately a 3% of drift in both directions. Cyclic behavior as well the pinching effect were captured reasonably well. However, after this point, the behavior is highly influenced by the beam reinforcement. This can be appreciated since the model exhibits higher energy dissipation, characteristics of a ductile behavior.

5.2.2 PANTELIDES TEST

The details of the selected specimens tested by Pantelides *et al* (2002) are shown in Figure 5-4. The beam and column reinforcement are symmetric in all the cases. The difference between the test unit 3 and test unit 4 was in the column axial load ($0.10 A_g f'_c$ for the first case and $0.25 A_g f'_c$ for the last one). This difference also exist for unit test 5 and 6.

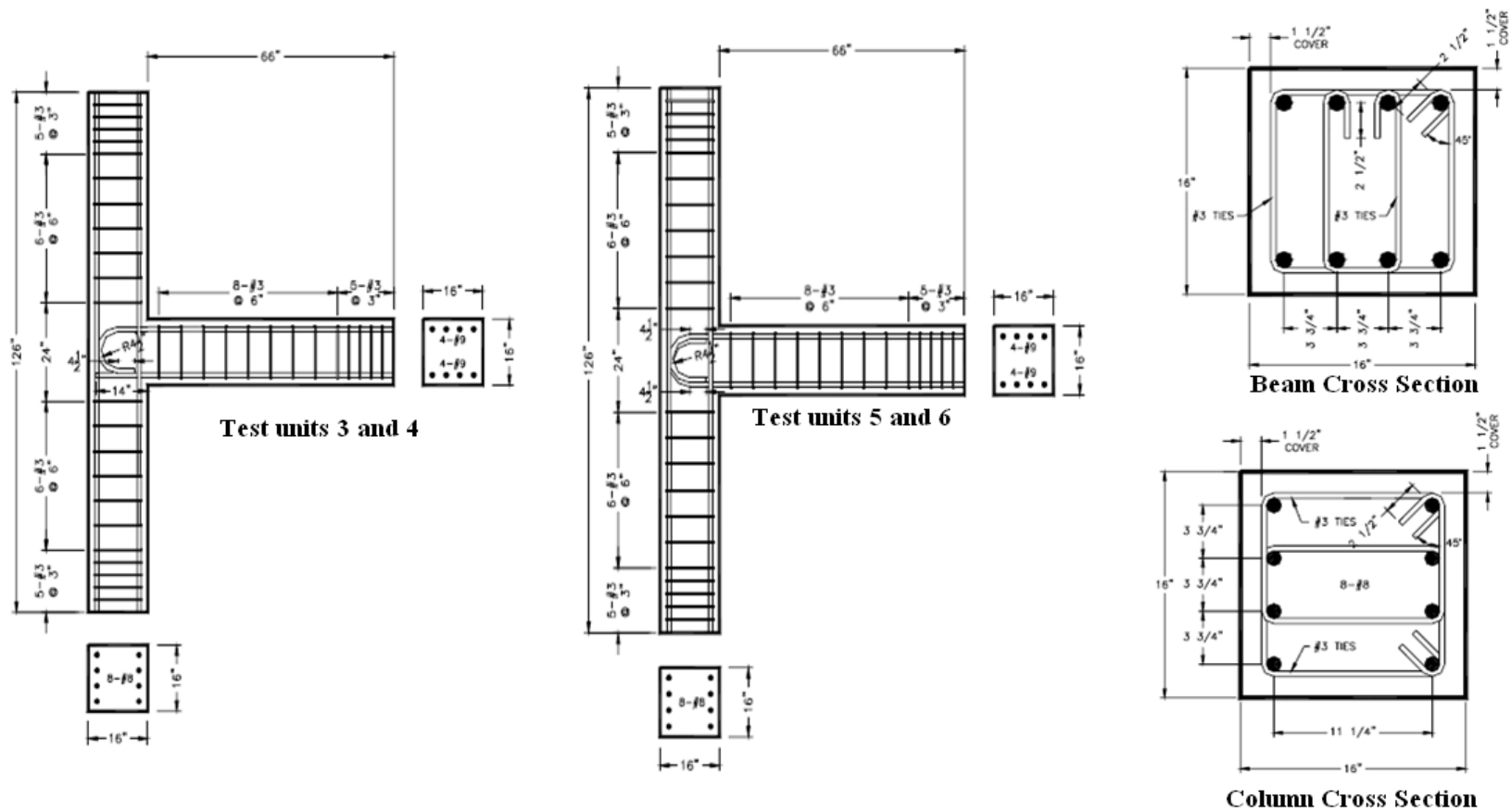


Figure 5-4 Details of specimens tested by Pantelides *et al* (2002) (All units in inches)

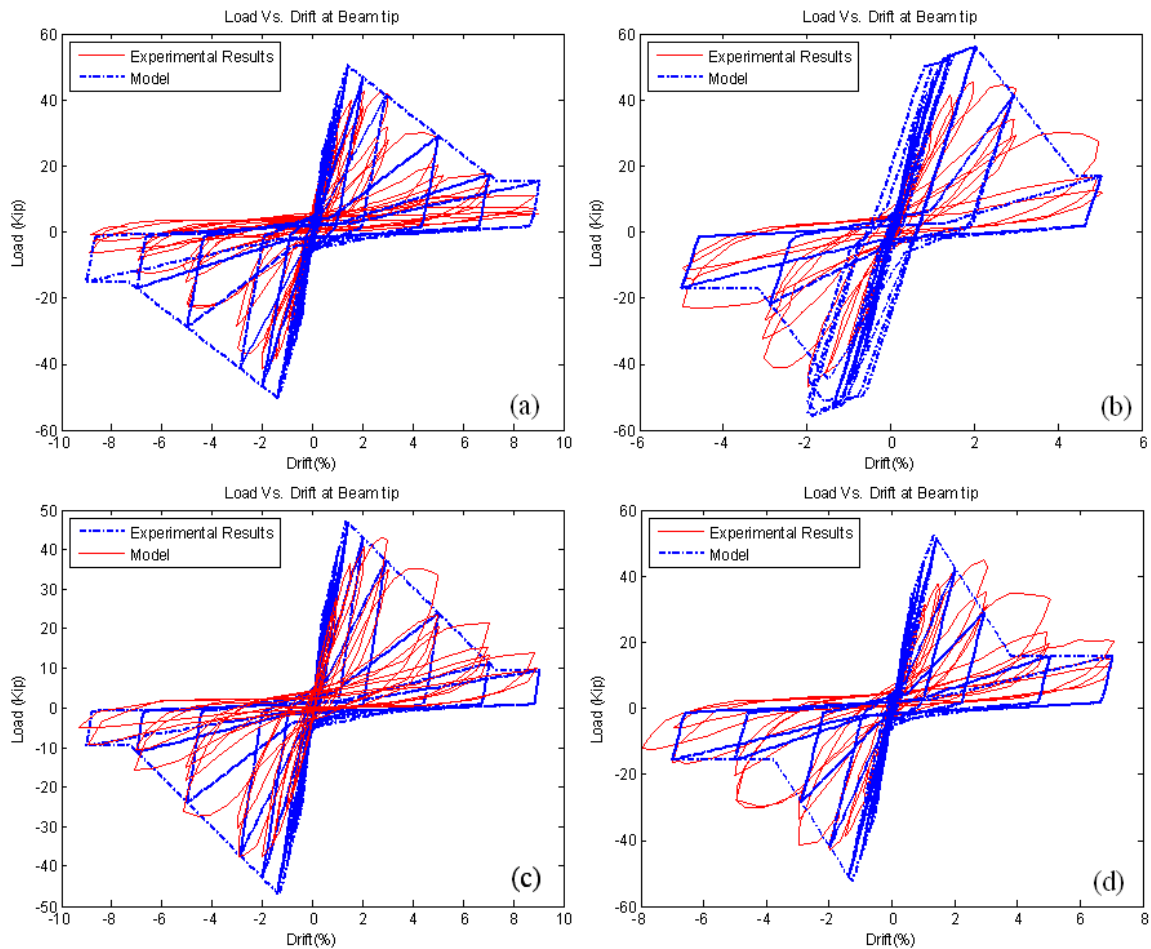


Figure 5-5 Comparison of response for test of Pantelides *et al.* (2002): a) Test 3, b) Test 4, c) Test 5 and d) Test 6

The comparison of the model simulated response with the response of the selected test specimens is shown in Figure 5-5. The predicted response for Test 3, 4 and 5 (Figure 5-5 (a), (b) and (c) respectively) are in agreement with the tests. The envelope of the model captures very well the test results. The initial and the descending slope were well simulated. For the case of Test 6 (Figure 5-5 (d)) even though the descending slope was slightly different, the model captures reasonably the initial slope and the ultimate load. For all cases the pinching behavior and the hysteretic behavior were modeled fairly well.

5.2.3 CLYDE TEST

Figure 5-6 shows the details of the specimens tested by Clyde *et al* (2000). The beam and column reinforcement are symmetric in all the cases. Test units 2 and 6 have a column axial load of $0.10 A_g f'_c$ while in test units 4 and 5 it was of $0.25 A_g f'_c$.

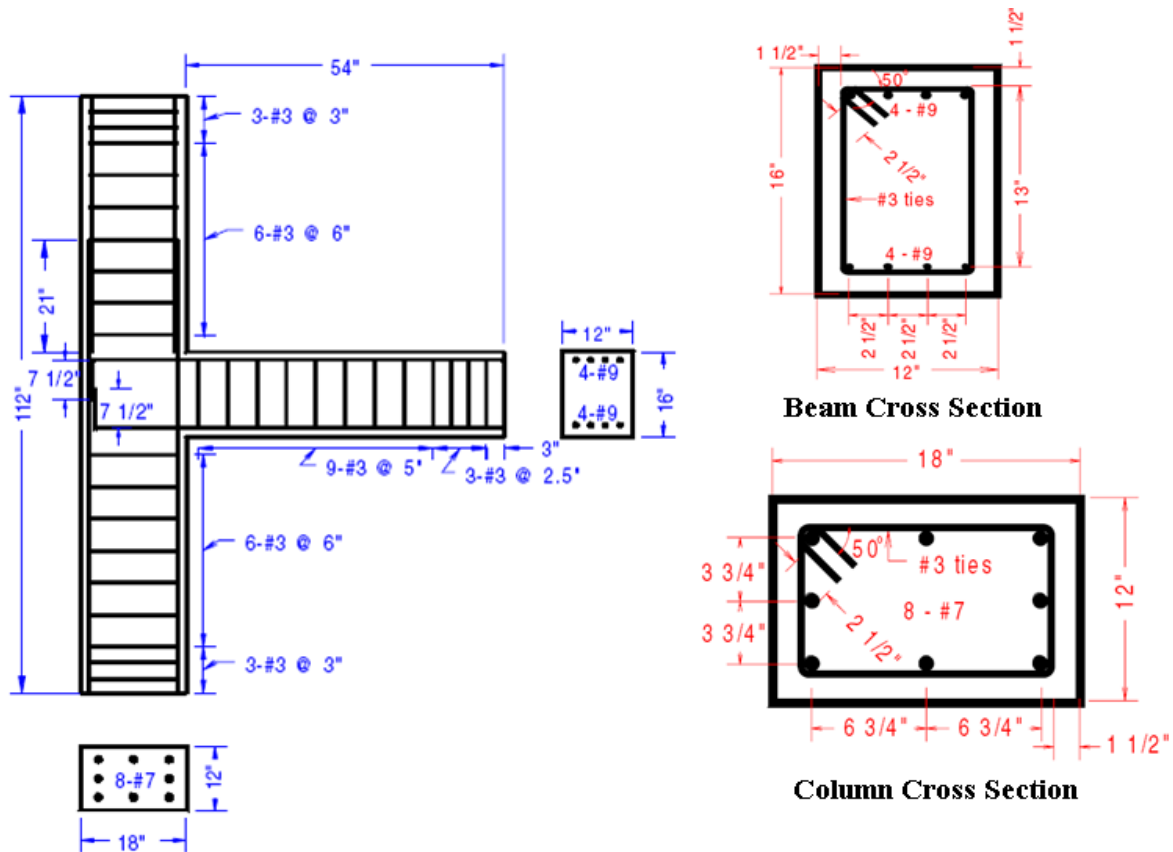


Figure 5-6 Details of specimen tested by Clyde *et al* (2000) (All units in inches)

The comparison of the model simulated response with the response of the test specimens is shown in Figure 5-7. The pinching effect and the hysteretic behavior were captured very well for all the cases. The loading and unloading slopes were simulated with reasonably accuracy. The initial slope of the model envelope agrees quiet well in all cases. For the specific cases of

test units 2, 5 and 6 (Figure 5-7 (a), (b) and (d) respectively) the peak load was modeled adequately. Even though the model presents differences in the ultimate predicted load, for the aforementioned test units the descending slopes are similar to the descending slope of the test unit. The simulated response of test unit 4 (Figure 5-7 (c)) did not reach the descending slope, since the joint model did not reach the peak strength and for that reason, at the end of the simulation the model was still loading.

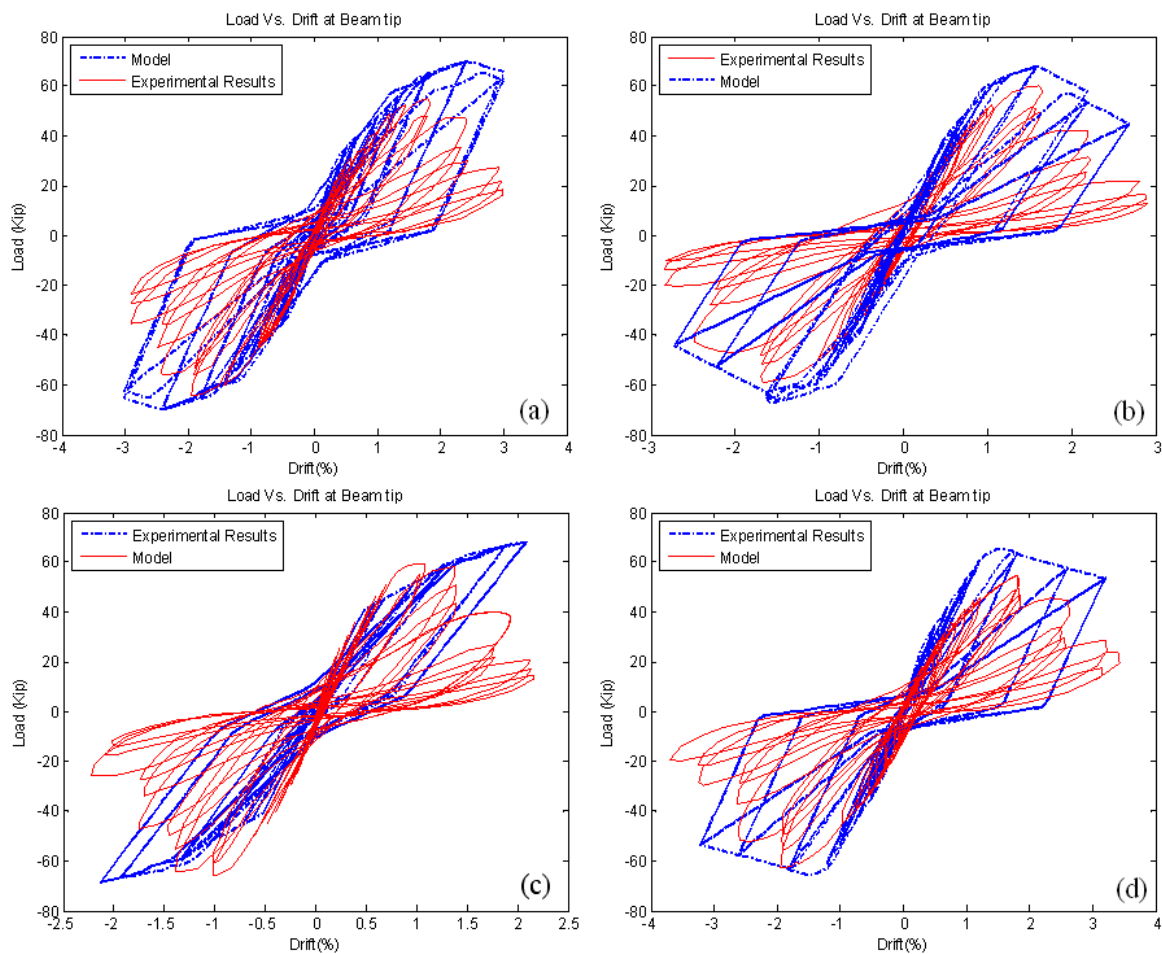


Figure 5-7 Comparison of response for test of Clyde *et al.* (2000): a) Test 2, b) Test 5, c) Test 4 and d) Test 6

5.2.4 ANTONOPOULOS & TRIANTAFILLOU TEST

The details of the selected specimens tested by Antonopoulos & Triantafillou (2003) are shown in Figure 5-8.

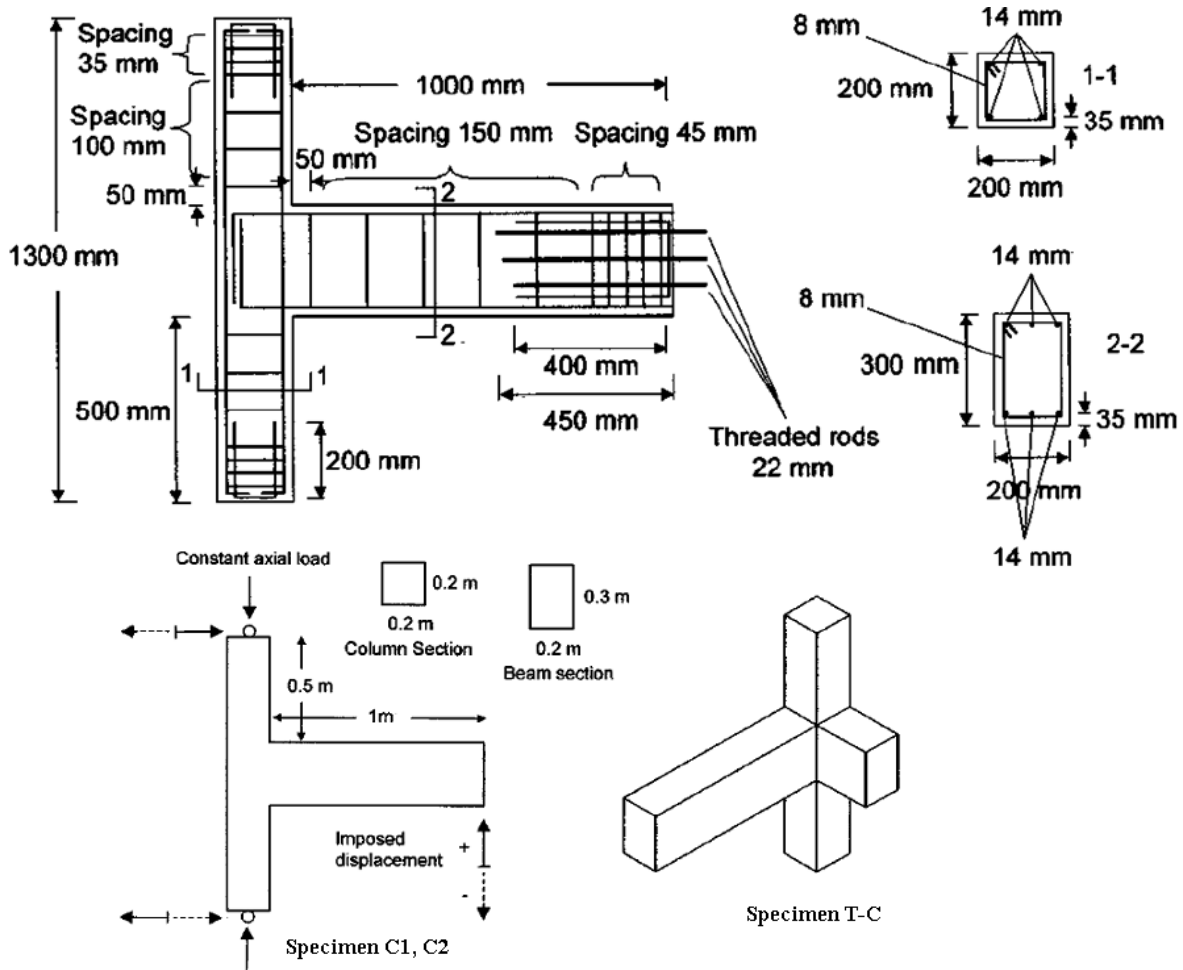


Figure 5-8 Details of specimen tested by Antonopoulos & Triantafillou (2003)

The comparison of the model simulated response with the response of the tested specimens is shown in Figure 5-9. The envelope of the model simulated with relative accuracy the test

results. The pinching behavior was successfully captured for all three cases. The hysteretic behavior seems acceptable. The descending slope was modeled quite well in all cases.

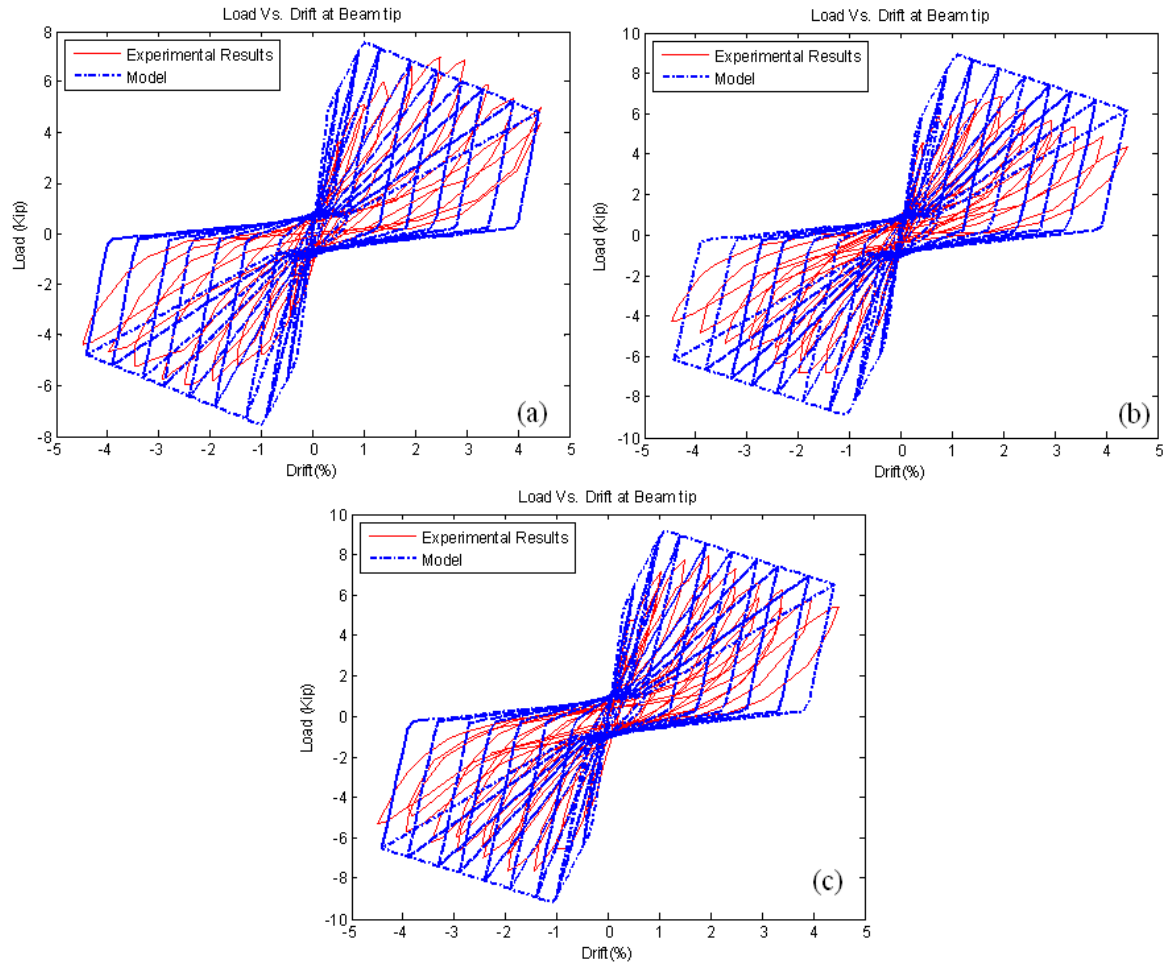


Figure 5-9 Comparison of response for test Antonopoulos & Triantafillou (2003): a) specimen C1, b) specimen C2 and c) specimen T-C

5.3 CONCLUSION

The comparison of the predicted behavior by the proposed model with the experimental test from 19 tests of unreinforced exterior concrete joints from the literature showed that the model is adequate, since it simulates with reasonable accuracy the main characteristics of the response of these types of joint. The best simulation seems to be the specimen BSU from

Wong (2005). The worst simulation was the Test 4 of Clyde et al (2000). The rest of the tests were predicted quite well. It can be concluded that the previous results validates the proposed model and thus the model can be used for the predictions of the behavior of unreinforced concrete exterior joints.

6 GROUND MOTION RECORDS FOR DYNAMIC ANALYSIS

6.1 INTRODUCTION

The model, validated in the previous chapter, is implemented for the static and dynamic analysis of typical frame buildings in Puerto Rico. A two and three story school building frame and five, ten and fifteen story building frames were chosen for evaluating their expected behavior. For the dynamic analysis three earthquake ground records were selected. This chapter summarizes the main characteristics of these ground motions. The next two chapters discussed in detail the description of the selected buildings as well as the analysis results.

6.2 SELECTED EARTHQUAKE GROUND RECORDS

Three acceleration records were selected for the dynamic analysis of two school building and three multistory building. These acceleration records were: the synthetic one created by Irizarry (1999) for Mayagüez and Ponce cities, the NS component of the well known and widely used El Centro 1940 (Imperial Valley, Station 117) earthquake and the EW component from the SCT Station of the 1985 the Mexico earthquake.

6.2.1 MAYAGUEZ SYNTHETIC ACCELERATION RECORD

The acceleration versus time history for the Mayagüez synthetic record is shown in Figure 6-1. The duration of the strong motion (accelerations greater than 0.05 g) was 9.14 seconds.

The peak ground acceleration (PGA) is 0.46 g and it occurred at 3.84 seconds. Figure 6-2 shows the Fourier spectrum for the ground motion. It can be appreciated that this record has several dominant frequencies, the most important ones being 1.37, 1.56 and 1.76 Hertz (period equal to 0.73, 0.64 and 0.57 seconds respectively). The response acceleration spectrum for 5% damping for this ground motion is presented in Figure 6-3.

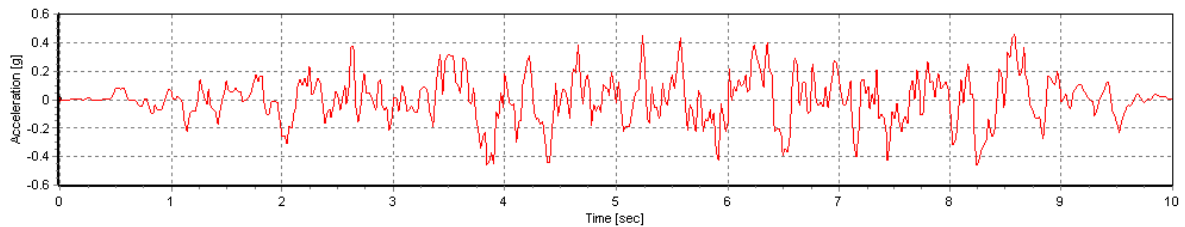


Figure 6-1 Synthetic Ground Record for Mayagüez and Ponce cities (Irizarry 1999) with base line correction by Montejo (2004)

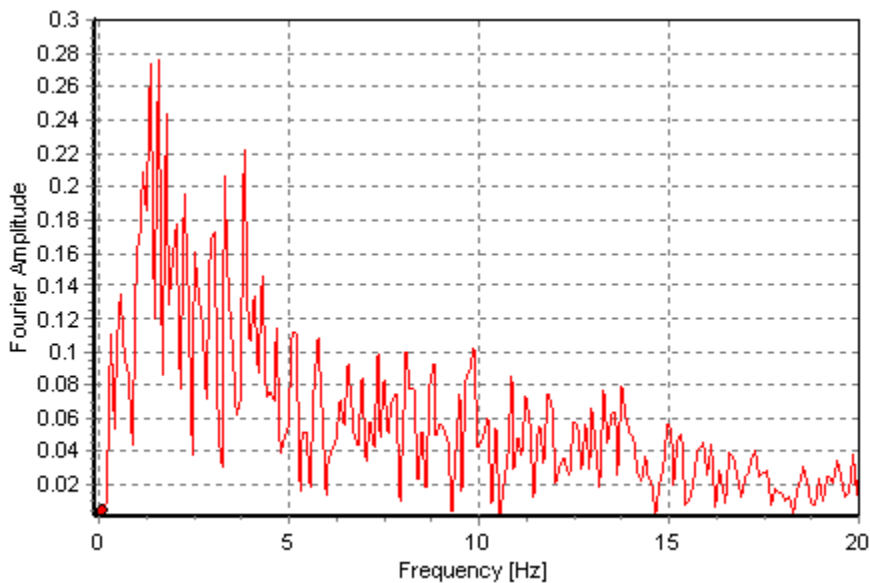


Figure 6-2 Fourier spectrum for the Mayagüez and Ponce Synthetic Record

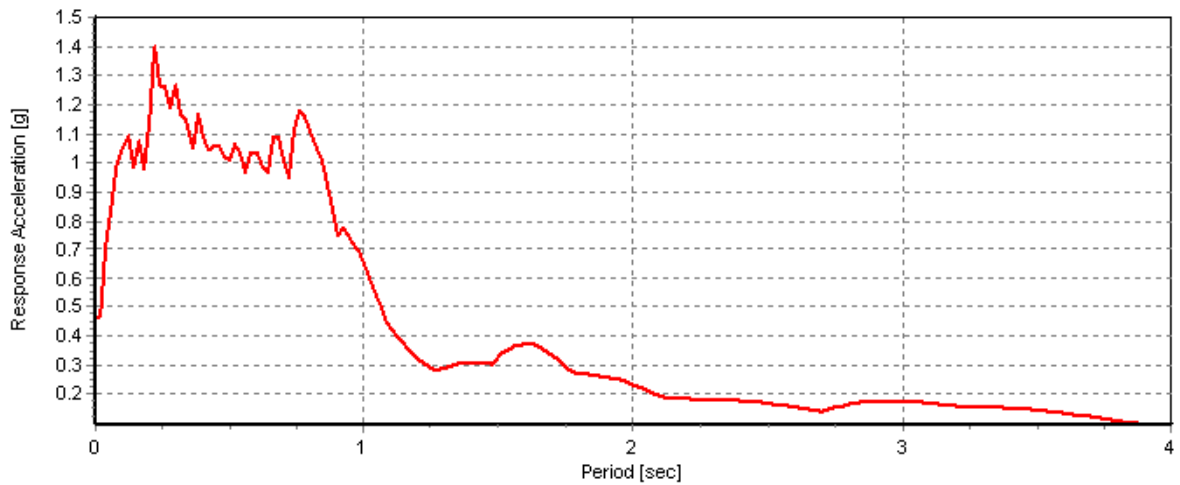


Figure 6-3 Response Acceleration Spectra for 5% of damping for Mayagüez and Ponce cities Synthetic Record

6.2.2 EL CENTRO ACCELERATION RECORD

The NS ground motion record for the El Centro 1940 earthquake is shown in Figure 6-4. The duration of the strong motion was 28.83 seconds. The PGA was of 0.31g and occurred at 2.15 seconds. The Fourier spectrum for this earthquake (Figure 6-5) shows some dominant frequencies, the most important ones being 0.85, 0.68 and 0.46 Hertz (Corresponding to periods equal to 1.17, 1.47 and 2.20 seconds respectively).

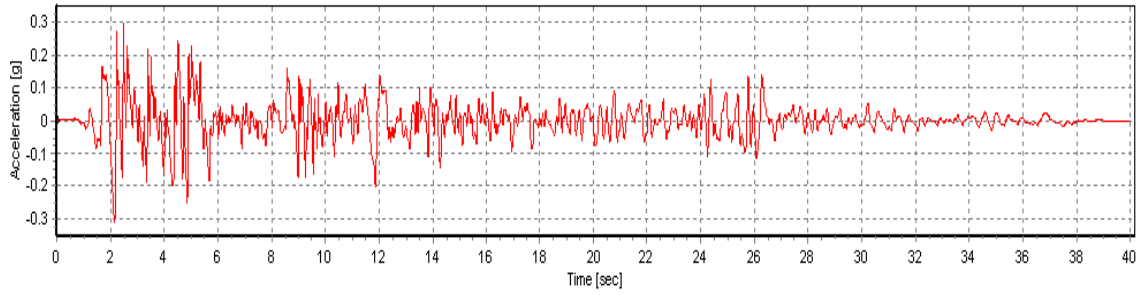


Figure 6-4 NS Ground Record from the 1940 El Centro earthquake at Imperial Valley. Station 117 El Centro Array #9117

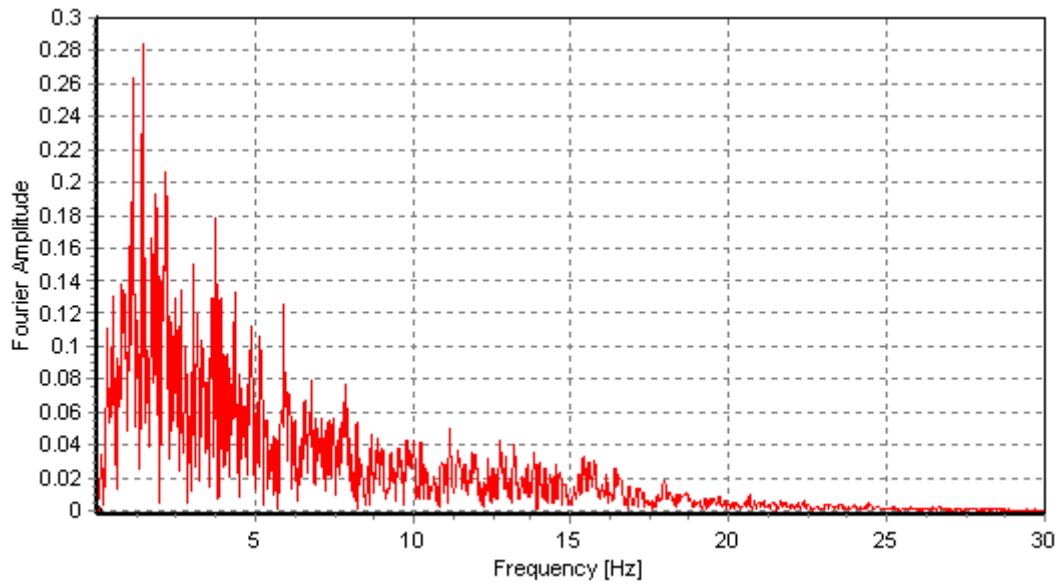


Figure 6-5 Fourier Spectrum for El Centro earthquake

The response acceleration spectrum for 5% damping for this ground motion is presented in Figure 6-3.

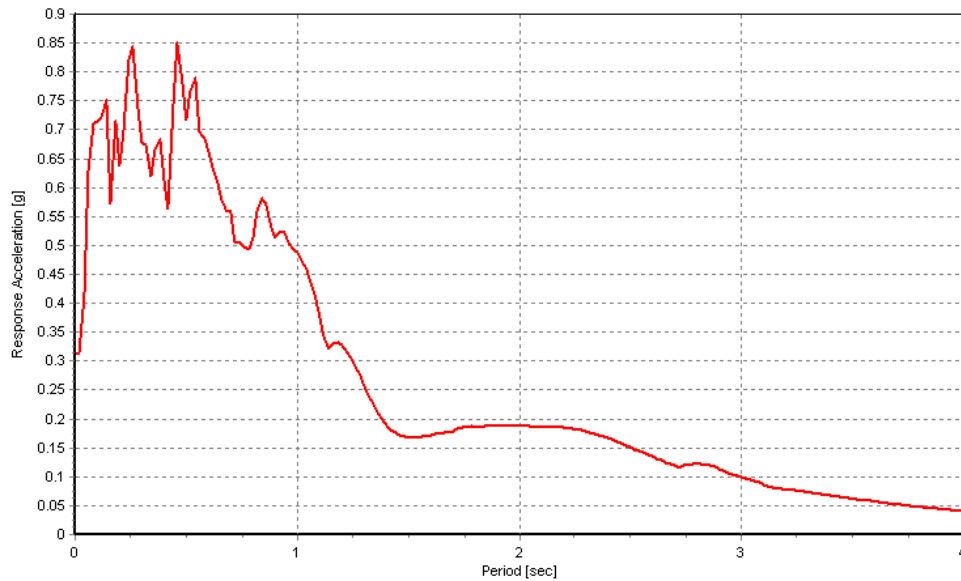


Figure 6-6 Response Acceleration Spectra for 5% of damping from El Centro Earthquake

6.2.3 MEXICO ACCELERATION RECORD

The EW acceleration versus time history from the SCT Station of the 1985 Mexico earthquake is shown in Figure 6-7. Even though the duration of the record was 180 seconds, the duration of the strong motion was around of 32 seconds. The peak ground acceleration (PGA) was only 0.16 g and occurred at 9.74 seconds. Figure 6-8 shows the Fourier spectrum for the ground motion. It can be appreciated that the dominant frequency was 0.5 Hertz (2 seconds). The acceleration response spectrum for 5% damping for this ground motion is presented in Figure 6-9.

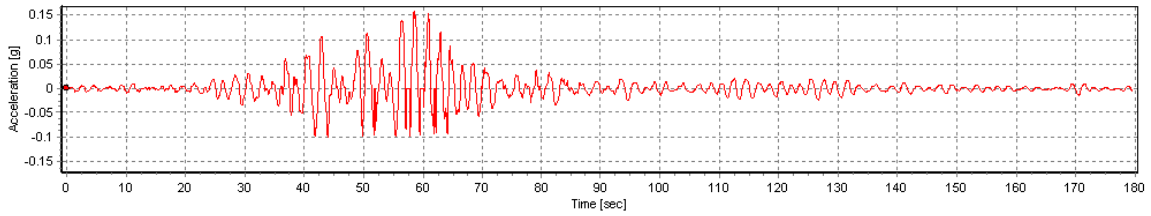


Figure 6-7 Ground record for the Mexico earthquake (1985)

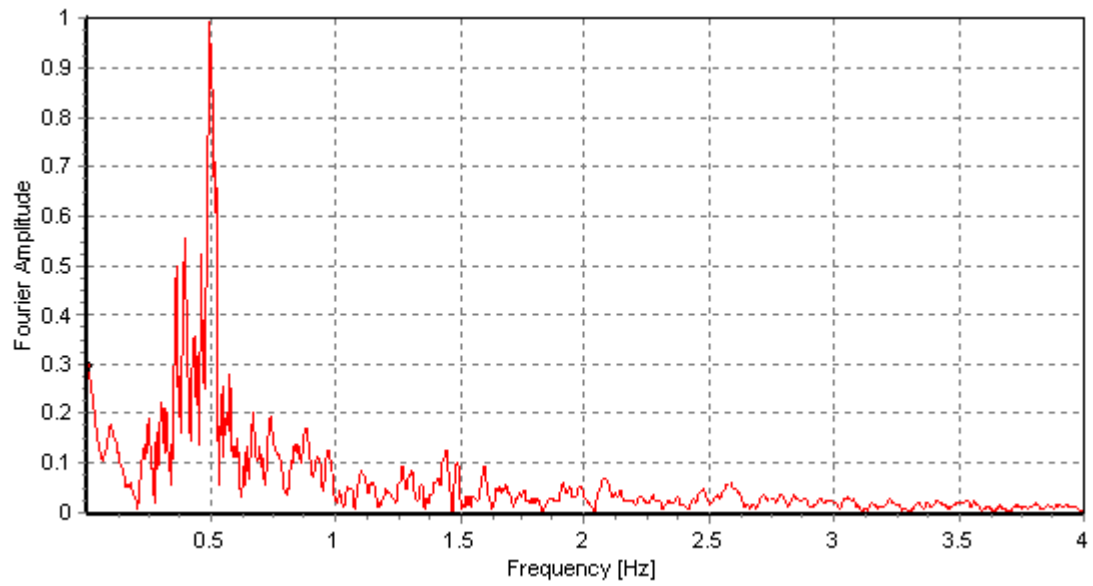


Figure 6-8 Fourier Spectrum for the Mexico earthquake (1985)

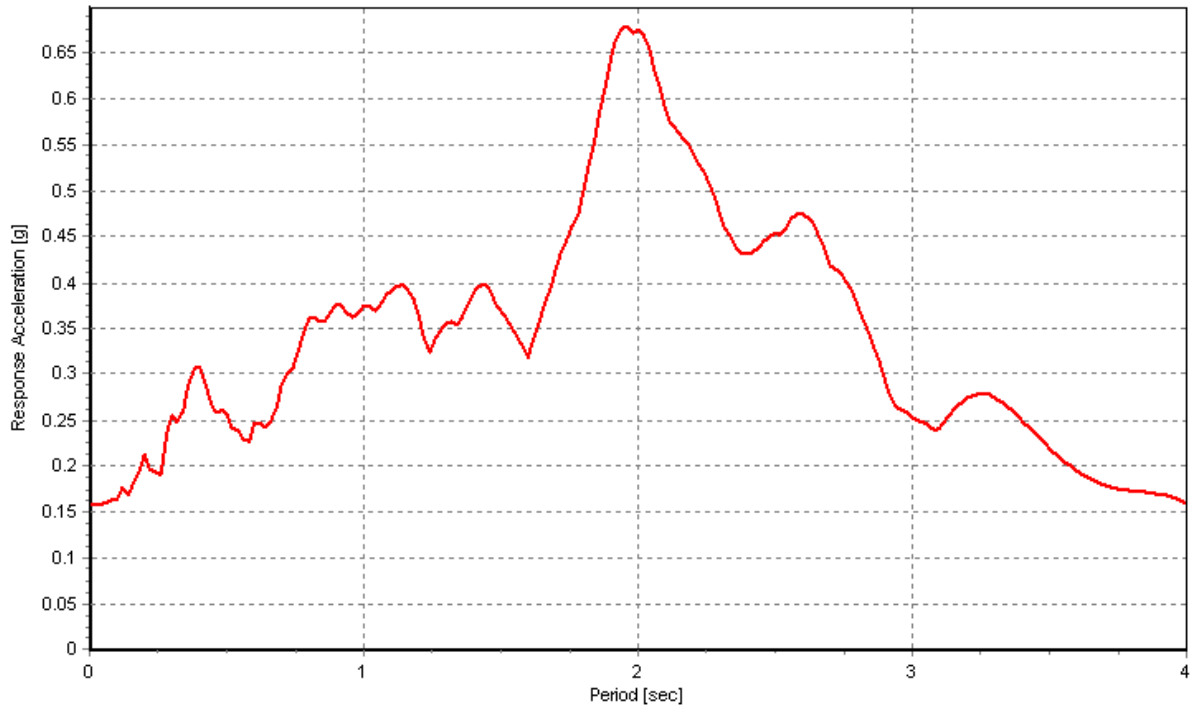


Figure 6-9 Response Acceleration Spectrum for 5% of damping for the Mexico 1985 earthquake

7 ANALYSIS OF SCHOOL BUILDINGS

7.1 INTRODUCTION

Rojas (2005) compiled a brief data base of schools building plans of typical construction in Puerto Rico in which the year of design ranged from 1972 to 1988. An example of a typical two story school frame building is shown in Figure 7-1. The main lateral resisting mechanism of the school buildings is the moment resisting frame. Most of these schools were designed according to the Puerto Rico building code of 1968.



Figure 7-1 Typical two story school building in Puerto Rico; a) Front view and b) Lateral view

Since the Puerto Rico building code of 1968 does not have any ductility provision it is expected that deficiencies such as lack of confining transverse reinforcement in columns, beams and within the joint core and insufficient anchorage length to footing or joints are present in school buildings designed with the 1968 code, exterior joints of a two and three story building typical of school in Puerto Rico are modeled with the proposed exterior joint

model. This chapter presents the static and dynamic analysis of the two and three story exterior frames.

7.2 DESCRIPTION OF THE FRAMES

The typical dimensions of the selected frames to be analyzed as well as the beam and column section used in the analysis are shown in Figure 7-2. The lack of confinement within the joint core was the only deficiency taken into account in the analysis.

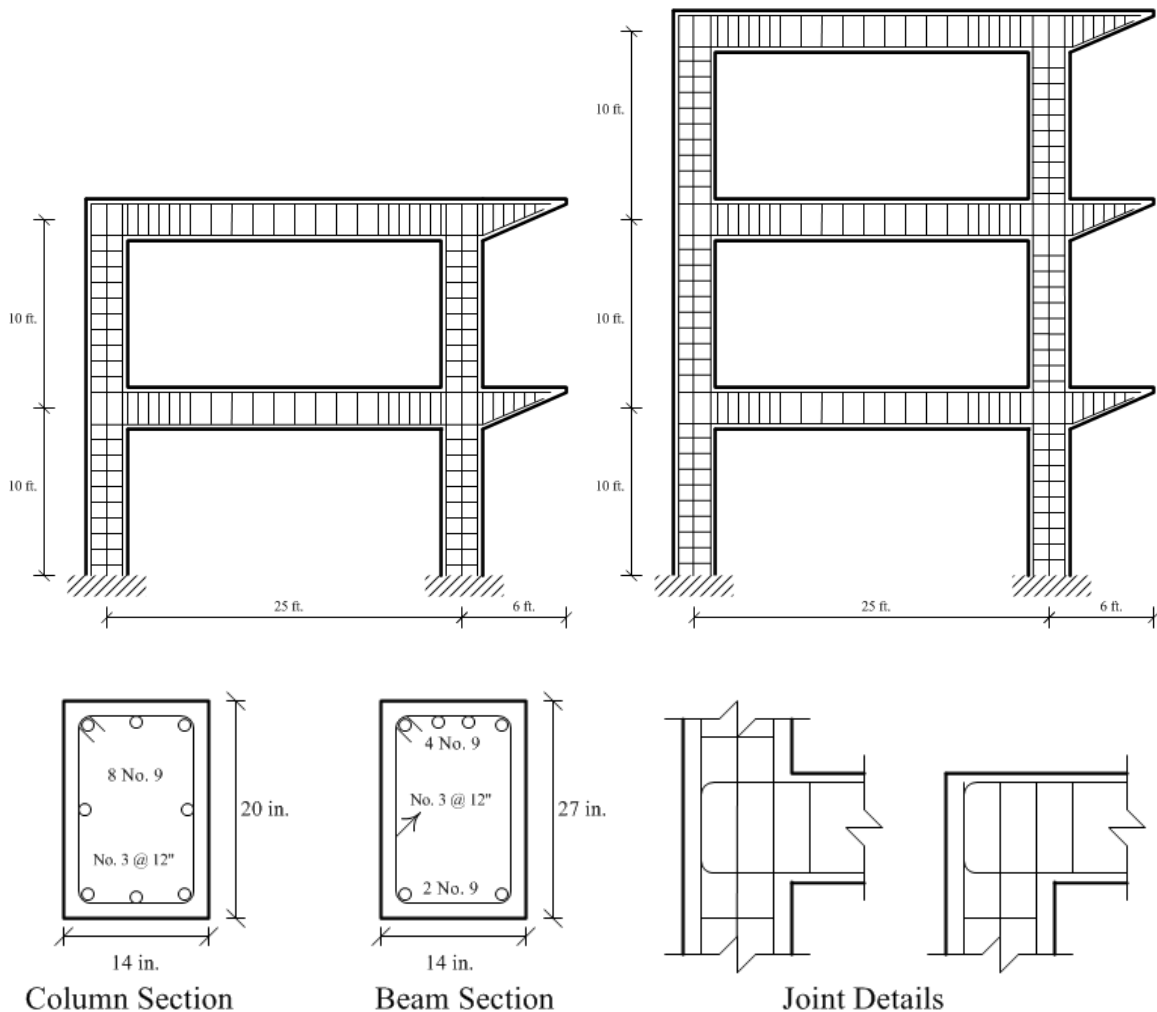


Figure 7-2 Details of the two and three level school frame building

The beam length and column height are 25 ft and 10 ft respectively. The beam and column cross sections as well as its reinforcing details are also shown in Figure 7-2. These dimensions were selected from the database constructed by Rojas (2005). From tributary area, the service load for the roof and floor beams was 1.3 kip/ft and 1.7 kip/ft respectively. For all columns, the service load was of 0.3 kip/ft. Regarding the material properties, the concrete and the steel yield strength was selected to be $f'_c = 4,000$ psi and $f_y = 60,000$ psi respectively, since these were typical values from the database.

7.3 MODEL OF THE FRAME

In order to establish the difference in behavior in modeling the frame with and without the joint element, two models were created. One of the models was constructed considering rigid joints, and assuming that there are not any deficiencies in the structure. The other model was constructed using the proposed joint model (flexible joints assumption).

It can be appreciated in Figure 7-2 that both frames have cantilever beams. However since these beams cannot provide any stiffness to the exterior joint, the effect of these beams were modeled as external moments, produced by the service load as shown in Figure 7-3. Even though Figure 7-3 only shows the two story frame, the same concept applies to the three story frame. The value of the moment produced by the cantilever beams for the roof level M_2 was computed as 11.7 kip-ft. The value of the external moment for the floor levels M_1 was computed as 19.5 kip-ft.

As in the case of the model of the beam column subassemblies, the frame was modeled in Opensees (McKenna and Fenves 2000). Since the capabilities of the program and the detail of the material and element models were explained in Chapter 4, here only the elements and material models used in the frame model will be given.

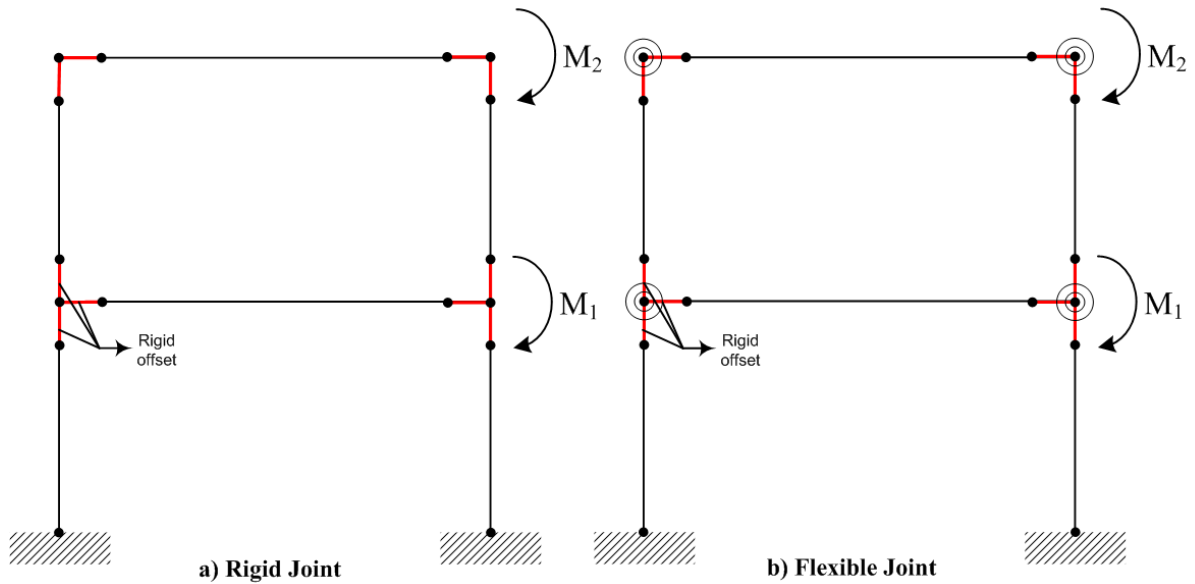


Figure 7-3 Two story frame model

Beam and column elements were modeled with the beam with hinges element in which the beam and column hinge length were taken as one half the beam and column section height respectively. The hinge behavior was modeled using the fiber approach. The beam and column elements were assumed as cracked. Beam and column moment of inertia were multiplied by 0.35 and 0.7 respectively. In the dynamic analysis, the used damping ratio was 2%. Steel reinforcement was modeled using the Steel01 uniaxial material. The concrete was modeled using the Concrete01 material for both, the confined concrete (inside the stirrups) and for the unconfined concrete (outside the stirrups) in which the values of the concrete parameters were computed using the Kent and Park modified model. It is important to

mention that even though the beams and columns are modeled from center to center node, a rigid offset was set to specify that the beam and column forces are computed at the face of beam and columns respectively. For the case of the flexible joint frame, each joint was modeled using the Pinching04 material, as explained in Chapter 4 in which the break points of the envelope were set using the procedure described in Chapter 3. Finally, Table 7-1 summarizes the natural period for the two and three story frame for the rigid and flexible joint assumption respectively.

Table 7-1 Natural Period of the School Buildings Frames

No. Story	Natural Period (seconds)	
	Rigid Joints	Flexible Joints
2	0.23	0.25
3	0.36	0.40

7.4 STATIC PUSHOVER ANALYSIS

The two and three story frames were subjected to a displacement controlled static pushover analysis. The analysis was set in two parts considering the P-Delta effect in columns. In the first part the frame is analyzed only for the gravitational loads that are applied in beams and columns. After that, the frame was pushed laterally up to attain certain value of displacement that was specified in the analysis. In this study, this limit was set at 5% of drift since it is

believed that at this drift the structure will suffer extensive damage. Using higher values of drift can cause convergence problems that can stop the analysis.

7.4.1 RESULTS FOR THE TWO STORY FRAME

The results of the pushover analysis for the two story frame buildings are summarized in Figure 7-4, which shows the Load versus Drift curves for the rigid and flexible joints assumptions, respectively and in Figure 7.5 which shows the sequence of plastic hinges formation for different drift levels, corresponding to the two cases considered.

For the rigid joint assumption, the curve shows that the structure remains elastic up to a drift of around 0.5%, where the first stiffness change occurs. This change is attributed to the formation of plastic hinges in the bottom of the first story columns (Figure 7-5 (a)). From this point up to a drift of around 1.5% the curve shows gradual stiffness degradation, which corresponds to the formation of plastic hinges in the following sequence (Figure 7-5 (a) and (b)): first story beam at both ends (events 2 and 3); at the top of the second story right column (event 4); at the beginning of the second story beam (event 5) and at the top end of the first story right column (event 6). At a drift of 4.9%, the curve appears become horizontal. This can be related to the formation of a collapse mechanism (Figure 7-5 (c)) since both columns of first floor have plastic hinges at both ends (event 8). The maximum attained load considering rigid joint was 150 kips.

Load versus Drift Graph for the Two Story Frame

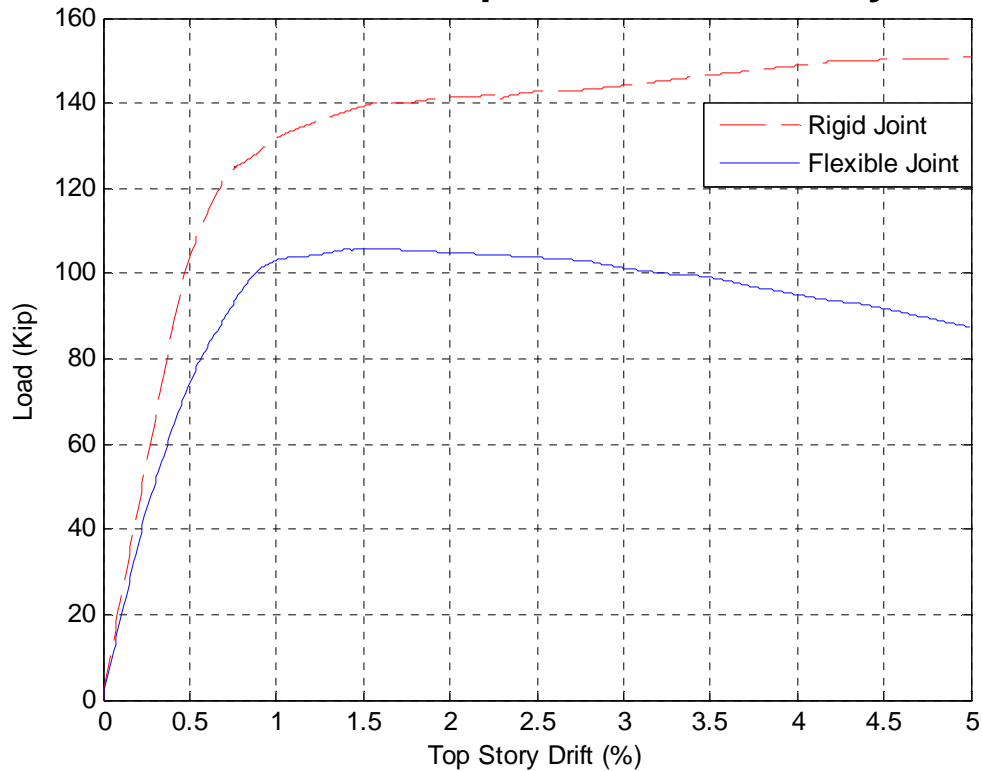


Figure 7-4 Pushover analysis results for the two story frame

For the flexible joint assumption, the curve shows that the structure remains elastic up to a drift of around 0.3%, where the first stiffness change occurs. This change is related to the cracking of the first story right joint (Figure 7-5 (d)). The second noticeable stiffness change occurs at a drift of around 0.5%, which is associated to the cracking of the second story right joint. The third appreciable stiffness degradation occurs at around of 0.87% of drift. This is related to the cracking of the first story left joint. It is important to note that even though between the second and third change of stiffness, a plastic hinge was formed at both columns of the first story, this event was inappreciable in the pushover curve. The fourth change of stiffness occurs at a drift of about 1% and is attributed to the fact that the first story right joint

reached its peak strength and to the cracking of the second story left joint almost simultaneously.

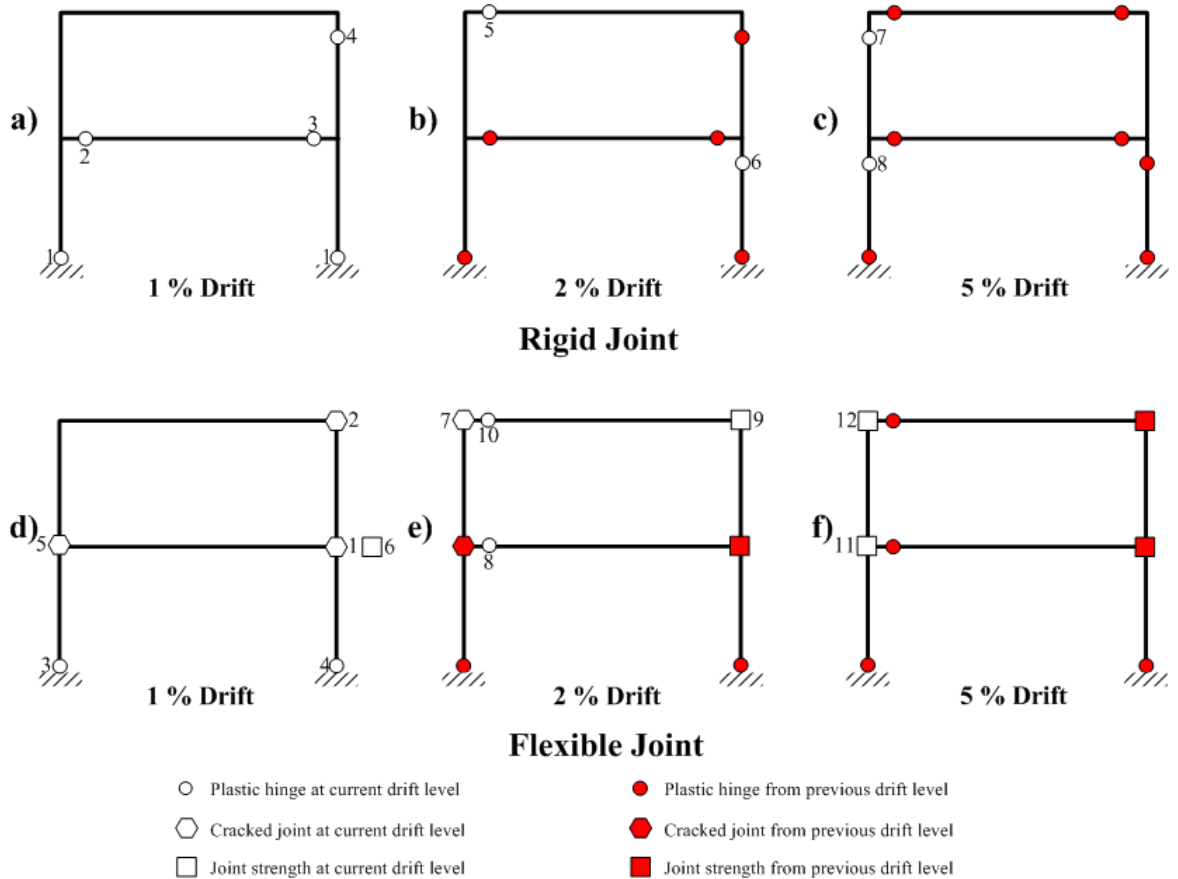


Figure 7-5 Sequence of plastic hinges events for the two story frame

For a drift of about 1.5%, the curve shows a plateau, attaining the maximum load of 106 kips. At this point, the second story right joint reaches its peak strength. At higher drifts, the curve shows a gradually strength degradation (negative slope). This is due to the fact that the local behavior of the right joints of both stories are controlling the global behavior of the frame, since they attained their peak strength first. Figure 7-6 shows the local behavior of each one of the joint of the frame in terms of their moment –rotation relationship. It can be seen that

the global behavior is controlled mainly by the local behavior of the right joint at both stories.

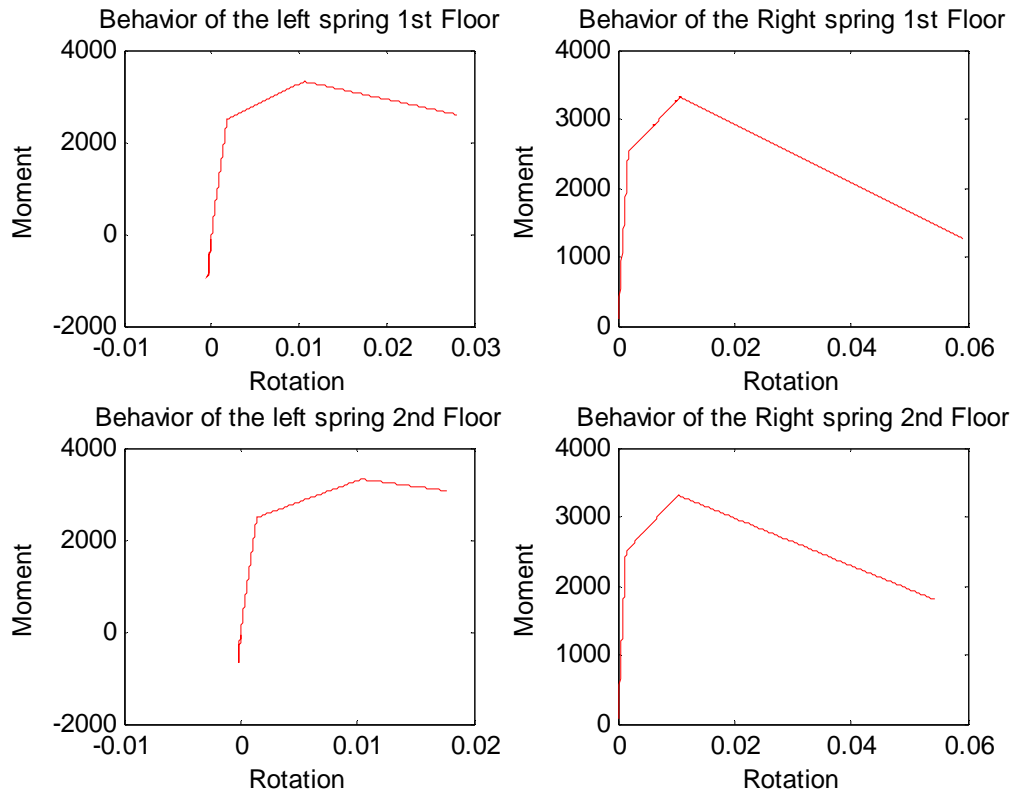


Figure 7-6 Local behavior of the joints for the two story frame pushover analysis.

7.4.2 DISCUSSION OF RESULTS

When analyzing the results obtained from the pushover analysis for the two story frame, it was shown that the observed behavior differs substantially when comparing the rigid and flexible joint assumptions. The first difference in the behavior of the two curves was in the fundamental periods, which was 0.23 and 0.25 seconds for the rigid and flexible cases, correspondingly. This slight difference between the periods is attributed to the presence of

the spring element in the joint in the flexible joint case. This is the main reason why the two graphs do not have the same initial slope. Another discrepancy occurred at the elastic limit. Figure 7-4 shows that the structure remained elastic up to a drift of 0.5% for the case of rigid joint and 0.27% for the flexible joint. The lateral loads related to these drift were 100 and 50 kip respectively. This represents a reduction of 50% in the lateral load attributed to the cracking of the left joint of the first floor and the right joints of both stories. Another noticeable disparity occurs in the maximum attained lateral load. For the case of rigid joint it was of 150 kip and occurred at a 5% of drift. However, in the case of flexible joint it was 106 kip and occurred around a drift of 1.5%. This represents a reduction of 30% in the maximum lateral load.

A noticeable difference also occurs in the sequence of plastic hinges for different drift levels as shown in Figure 7-5. At 1% of drift for the rigid joint case 5 plastic hinges were formed. These were located at the base of both first story columns, at both ends of first story beam and at the top of the right column of the second story (Figure 7-5(a)). However at this same drift for the case of flexible joint only two plastic hinges were formed at the base of both columns of the first story (Figure 7-5 (d)). The damage instead of appearing in form of plastic hinges is now concentrated at the first story joints and at the right joint of the second story, since these joints were cracked. Also the right joint of the first floor attained its maximum strength. At 2% of drift for the rigid joint case two new plastic hinges were formed. These were located at the left end of the second story beam and at the top end of the first story right column (Figure 7-5(b)). At this same drift for the case of flexible joint also

two new plastic hinges were formed at the left end of both story beams (Figure 7-5 (e)). The damage was increased in the right joint of second floor since it attained its maximum strength. The left joint of the same floor also suffered damage since it was cracked. Finally at 5% of drift, Figure 7-5(c) shows that two new plastic hinges formed at the top ends of the first and second story left columns. The appearance of a plastic hinge at the top end of the first floor left column forms a collapse mechanism since both columns at both ends have plastic hinges. For the case of flexible joints, no new plastic hinges appeared. However, the damage in the left joints of both story increased since these joints attained their maximum strength (Figure 7-5(f)).

Finally, as shown in Figure 7-6, all joints experimented strength degradation since all joints are in the descending branch of their moment-rotation behavior. The right joints of both floor suffered the largest amount of damage.

7.4.3 RESULTS FOR THE THREE STORY FRAME

The results of the pushover analysis for the three story frame are summarized in Figure 7-7 which shows the Load versus Drift curves for the rigid and flexible joints assumptions, respectively. Figure 7-8 shows the sequence of plastic hinges formation for different drift levels, corresponding to the two cases considered.

For the rigid joint assumption, the curve shows that the structure remains elastic up to a drift of around 0.5%, where the first stiffness change occurs. This change is attributed to the

formation of plastic hinges in both ends of the first story beam and at the bottom of first floor columns (Figure 7-8 (a)) that occurs almost simultaneously.

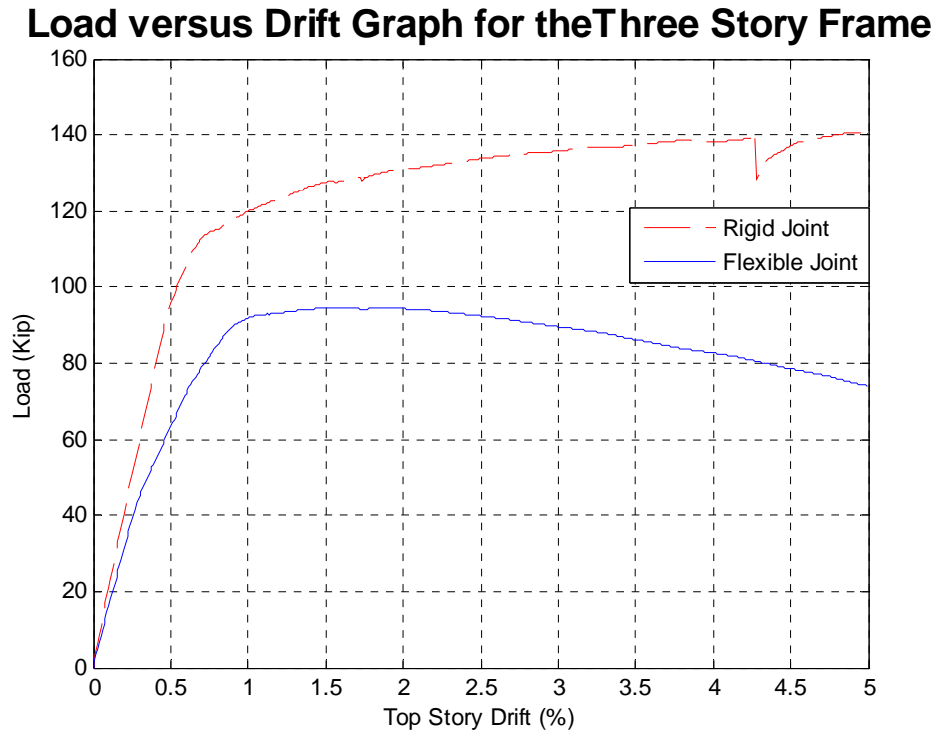


Figure 7-7 Pushover analysis results for the three story frame

The second and third stiffness changes occurs around 0.7% and 1% of drift respectively, and are due to the formation of plastic hinges at both ends of the second story beam. Between 1 and 2% of drift the curve shows gradual stiffness degradation, which corresponds to the formation of plastic hinges in the following sequence (Figure 7-8(a) and (b)): top end of the second story column ends; at the bottom end of the second story left column; at the top end of the third and first story right column, respectively and at the left end of the third story beam. From this point up to the drift of 5%, the curve practically remains with the same

stiffness. The discontinuity that occurs at around 4.3% of drift is apparently due to convergence problems. The maximum load was 140 kips.

For the case of flexible joint assumption, the first stiffness change occurs due to the cracking of the right joint of the first and second story (around 0.3% of drift). The second stiffness change occurs around 0.62% of drift, due to the cracking of the right joint of the third story. The formation of plastic hinges at the bottom end of the two columns of the first story reflects only a slight change in the stiffness (at around 0.7 % of drift). However, the cracking of the left joints of the first and second story and the reaching of the joint strength in the right joint of the second story reflects in an abrupt change of the stiffness (at between 0.9 and 1 % of drift). Once the left joint of the third story is cracked (at 1.5% drift) and the right joint of the same story attains its strength (at 2% of drift) the curve shows a plateau. At this point the frame reaches its maximum load of 95 kip. From this point up to the end of the analysis, the curve starts to present gradually strength degradation. This is due to the fact that the local behavior of the right joints of the frame are controlling the global behavior of the frame, which can be appreciated in Figure 7-9.

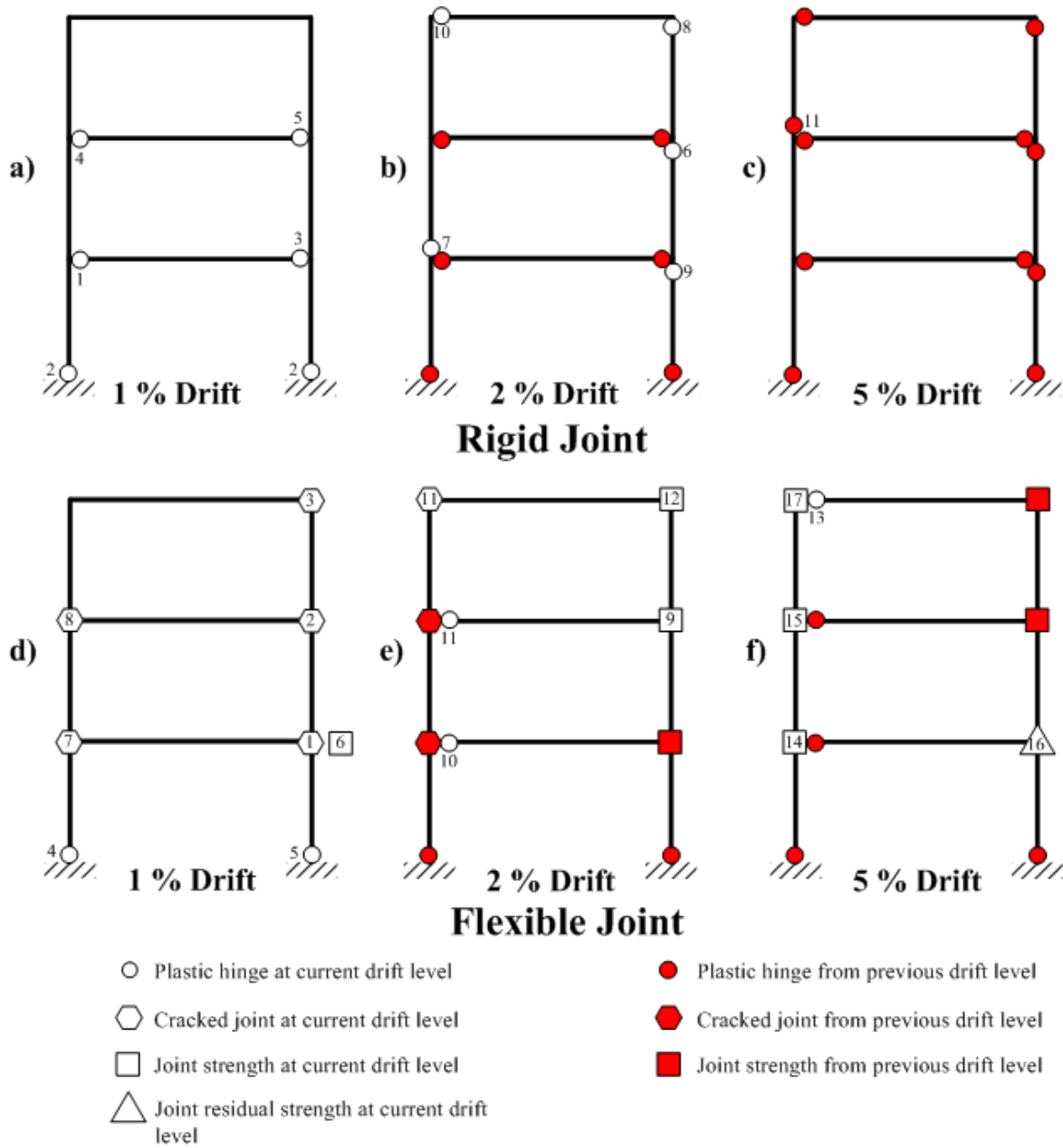


Figure 7-8 Sequence of plastic hinges events for the three story frame

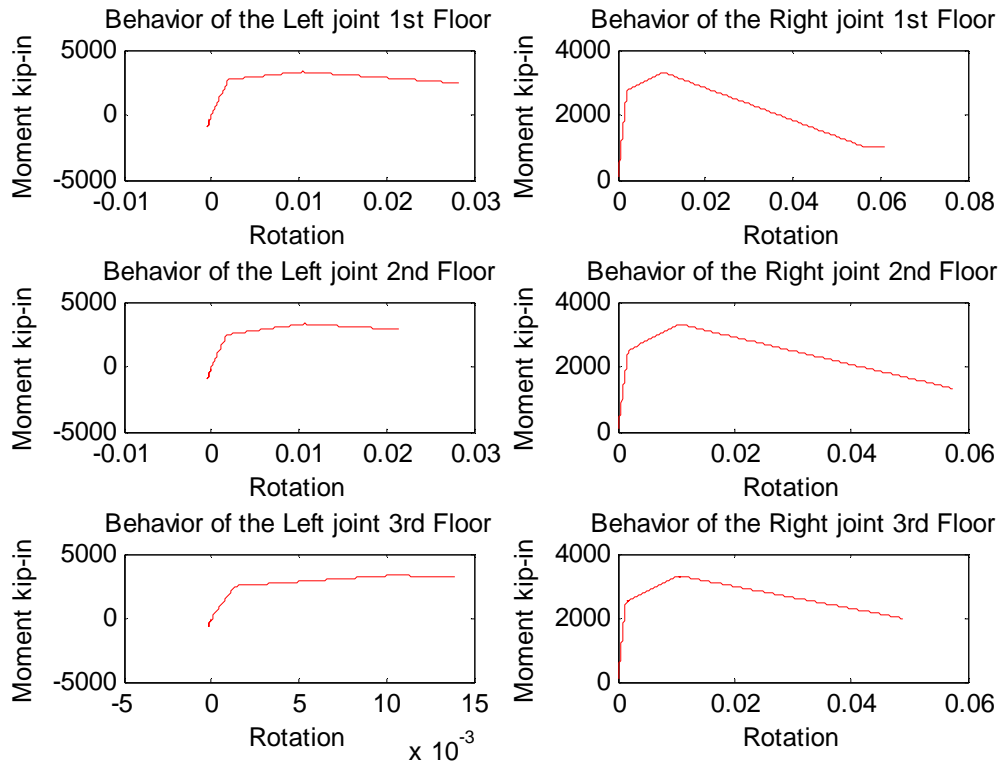


Figure 7-9 Local behavior of the joints for the three story frame pushover analysis

7.4.4 DISCUSSION OF RESULTS

When analyzing the results obtained from the pushover analysis for the three story frame, it can be appreciated that the observed behavior differs substantially when comparing the rigid and flexible joint assumptions. The first difference in the behavior of the two curves was in the fundamental periods, which was 0.36 and 0.40 seconds for the rigid and flexible cases, correspondingly. Figure 7-7 shows the difference in the elastic limit that exists between the two cases considered. As in the case of the two stories frame the elastic limit was calculated at a drift of 0.5% for the case of rigid joints and at 0.3% for the flexible joints. The lateral loads related to these drifts were 93 and 37 kip respectively. This represents a reduction of

60% in the lateral load that is attributed mainly to the cracking of the left joint of first and second story and to the right joints of all stories. Another noticeable disparity occurs in the maximum attained lateral load. For the case of rigid joints it was 140 kip and occurred at a 5% drift. However, in the case of flexible joints it was 95 kip and occurred around a drift of 2%. This represents a reduction of 32% in the maximum lateral load.

A noticeable difference also occurs in the sequence of plastic hinges for different drift levels as shown in Figure 7-8. At 1% of drift for the rigid joints case, six plastic hinges were formed. These were located at the base of both first story columns and at both ends of first and second story beams (Figure 7-8 (a)). However at this same drift for the case of flexible joints only two plastic hinges were formed at the base of both columns of the first story (Figure 7-8(d)). The damage instead appeared in the form of plastic hinges and it is now concentrated at the first and second story joints and at the right joint of the third story, since these joints were cracked. Also the right joint of the first floor attained its maximum strength. At 2% of drift for the rigid joints case, 5 new plastic hinges were formed. These were located at the left end of the third story beam, at the top end of the first, second and third story right column and at the bottom end of the second story left column (Figure 7-8(b)). At this same drift for the case of flexible joint also two new plastic hinges were formed at the left end of the first and second story beams (Figure 7-8(e)). The damage was increased in the right joints of the second and third floor since they attained their maximum strength. The left joint of the third floor also suffered damage since it was cracked. Finally, at 5% of drift Figure 7-8(c) shows that one new plastic hinge formed at the bottom end of the third story left column. For

the case of flexible joints, one new plastic hinges appeared in the left end of the third story beam. The damage in the joints increased since the left joints of all stories attained their maximum strength and the first story right joint attained its residual strength (Figure 7-8 (f)).

7.5 DYNAMIC ANALYSIS

The two and three story buildings were subjected to El Centro and to the artificial earthquake developed for the cities of Mayagüez and Ponce. The El Centro earthquake was selected since it is an historical earthquake that has been widely used by researchers. The Mayagüez earthquake was selected because it is an earthquake developed for the seismic characteristics of Puerto Rico. The results of these analyses, is presented in the following sections. Finally, in section 7.6 the maximum attained values of base shear and drift from the dynamic analysis are compared with the static pushover analysis curve for the two and three story school buildings and for the rigid and flexible joint assumption.

7.5.1 RESULTS FOR THE TWO STORY FRAME

7.5.1.1 RESULTS FOR THE EL CENTRO EARTHQUAKE

The comparison of the top story drift history for the El Centro earthquake for the two cases considered is shown in Figure 7-10. The sequence of plastic hinges is presented in Figure 7-11. In this figure, the value between parentheses indicates the time in seconds at which the event occurred. The local behavior of all joints of the frame is presented in Figure 7-12. Finally, the maximum drifts to the right and left for the two story frame are shown in Figure 7-13. A discussion of the above figures cited before is presented next.

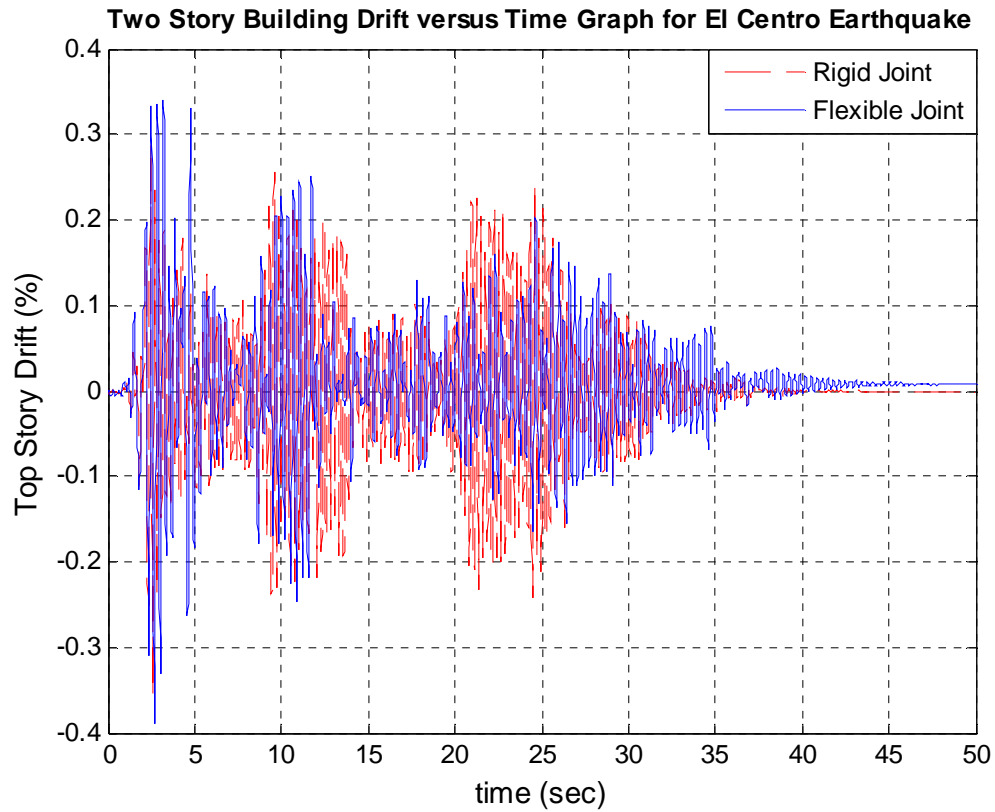


Figure 7-10 Top Story Drift versus time for the El Centro earthquake for the two story frame

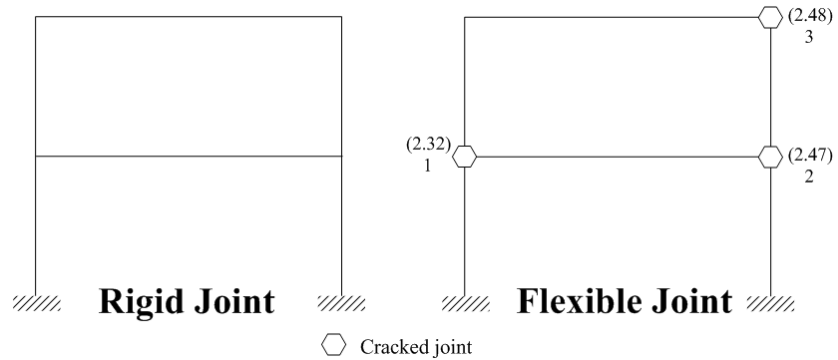


Figure 7-11 Sequence of plastic hinges for the two story frame for the El Centro earthquake (values in parentheses are in seconds)

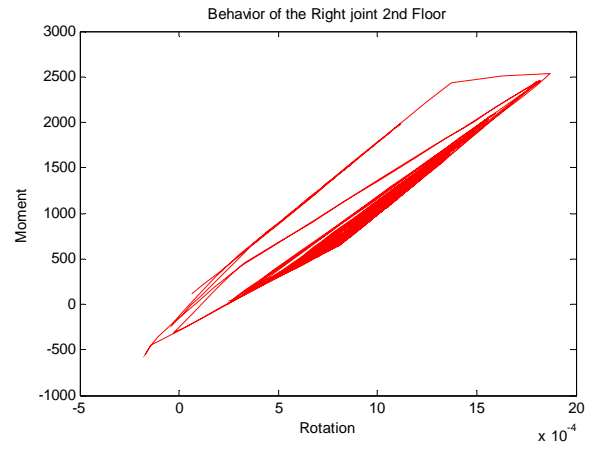
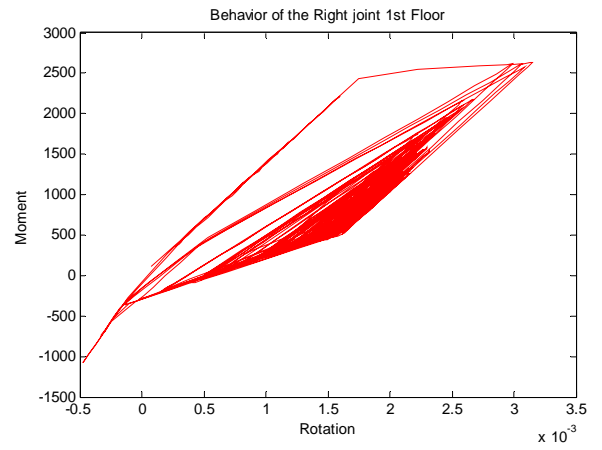
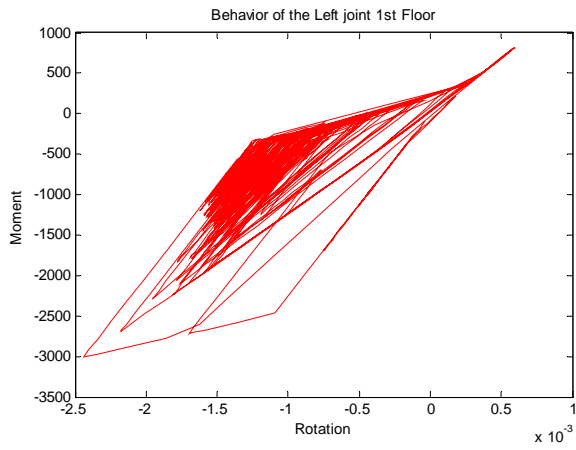


Figure 7-12 Local behavior of the joints for the two story frame for the El Centro earthquake

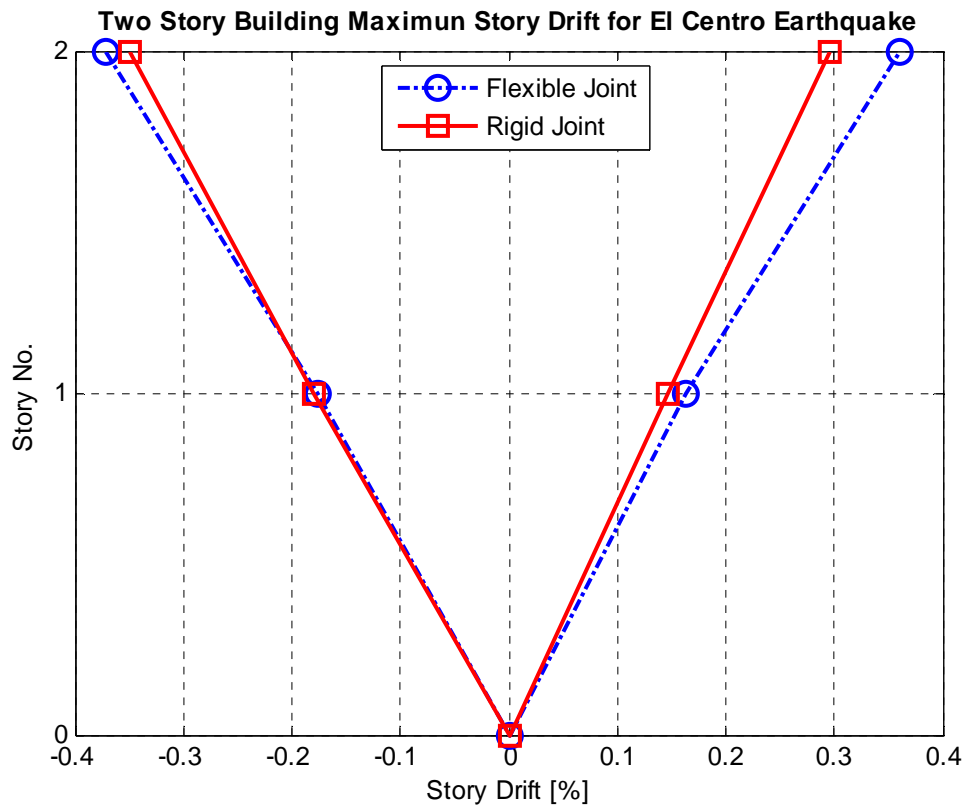


Figure 7-13 Maximum story displacement for the El Centro earthquake

The comparison of the top story drift history for the two cases considered is shown in Figure 7-10. The maximum drifts to the right and left for the case of rigid joints were 0.29% (at 2.46 seconds) and -0.36% (at 2.58 seconds) respectively. For the case of flexible joints these values were 0.34% (at 3.21 seconds) and -0.39% (at 2.69 seconds) correspondingly. Figure 7-11 shows that the rigid joints frame remained elastic since no plastic hinge formed during the earthquake. However, for the flexible joints frame three of the four joints were cracked. In Figure 7-11, the value in parentheses indicates the time at which the joints suffered damage, in this case when they were cracked. From Figure 7-12 it can be appreciated that during the earthquake the cracked joints were loaded beyond their cracked point. The

maximum attained load by the joints occurred at 2.69 seconds for the first story left joint, and at 3.21 seconds for the second story right joint, which coincides with the time when the maximum drifts to the right and left were obtained. Thus, the difference in the drift for both cases is associated to the fact that the flexible joint case became more flexible since 75% of its joints were cracked during the earthquake. This fact is also observed at the end of the earthquake, since the top story of the flexible joints case is not oscillating around zero drift, indicating that a permanent damage is present in the frame. Finally, Figure 7-13 clearly shows that the local behavior of the two joints of the first floor are governing the drift in the frame.

7.5.1.2 RESULTS FOR THE MAYAGÜEZ EARTHQUAKE

The comparison of the top story drift history for the Mayagüez earthquake for the two cases considered is shown in Figure 7-14. The sequence of plastic hinges is presented in Figure 7-15. In this figure, the value within parentheses indicates the time in seconds at which the event occurred. The local behavior of all joints of the frame is presented in Figure 7-16. Finally the maximum drifts to the right and left for the two story frame are shown in Figure 7-17. A discussion of these figures is presented in the next section.

7.5.1.2.1 DISCUSSION OF THE RESULTS

The top story drift history for the Mayagüez earthquake (Figure 7-14) shows that for the rigid joints case the maximum drifts to the right and left drifts were 0.63% (at 6.7 seconds) and -

0.59% (at 6.7 seconds) respectively. For the case of flexible joint these values were 0.71% (at 8.84 seconds) and -0.78% (at 8.62 seconds) respectively. Figure 7-15 shows that the rigid joints frame presents plastic hinges in both columns of the first floor at the base.

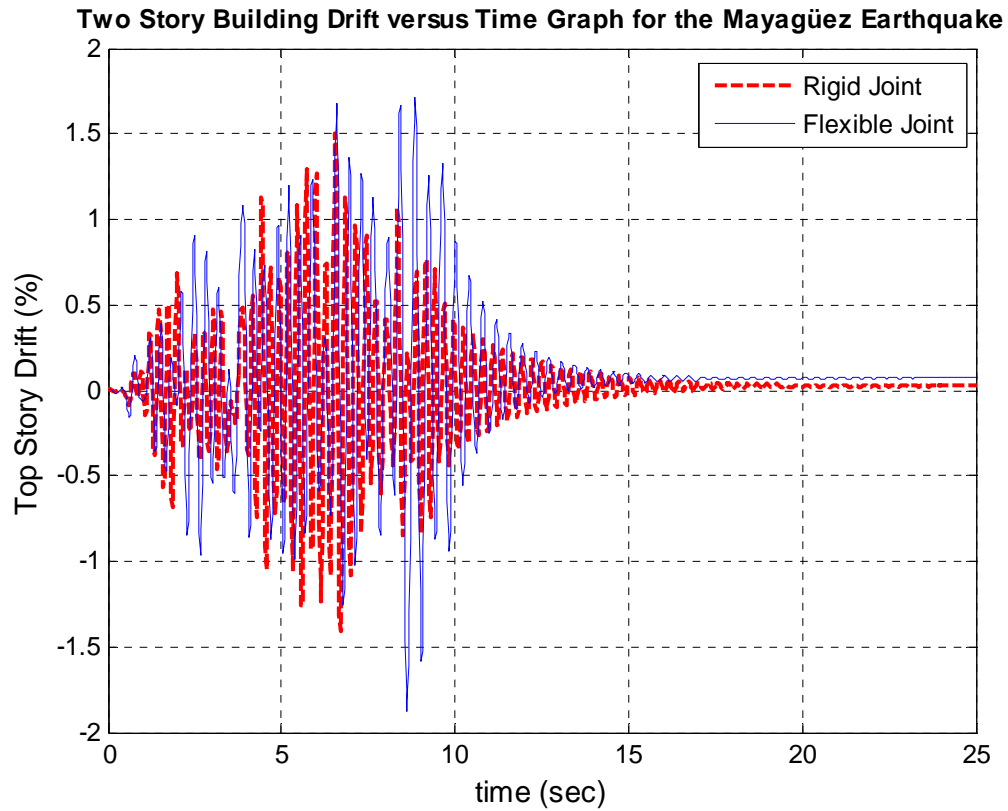


Figure 7-14 Top Story Drift versus time for the Mayagüez earthquake for the two story frame

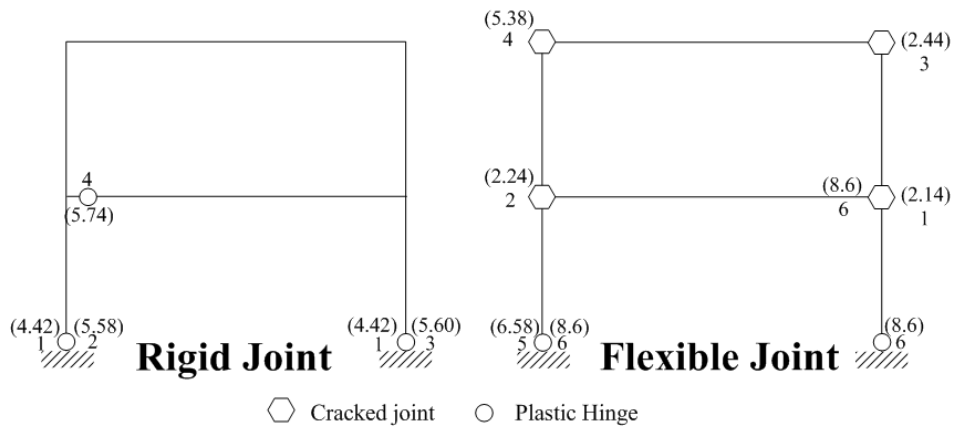


Figure 7-15 Sequence of plastic hinges for the two story frame for the Mayagüez earthquake (values in parentheses are in seconds)

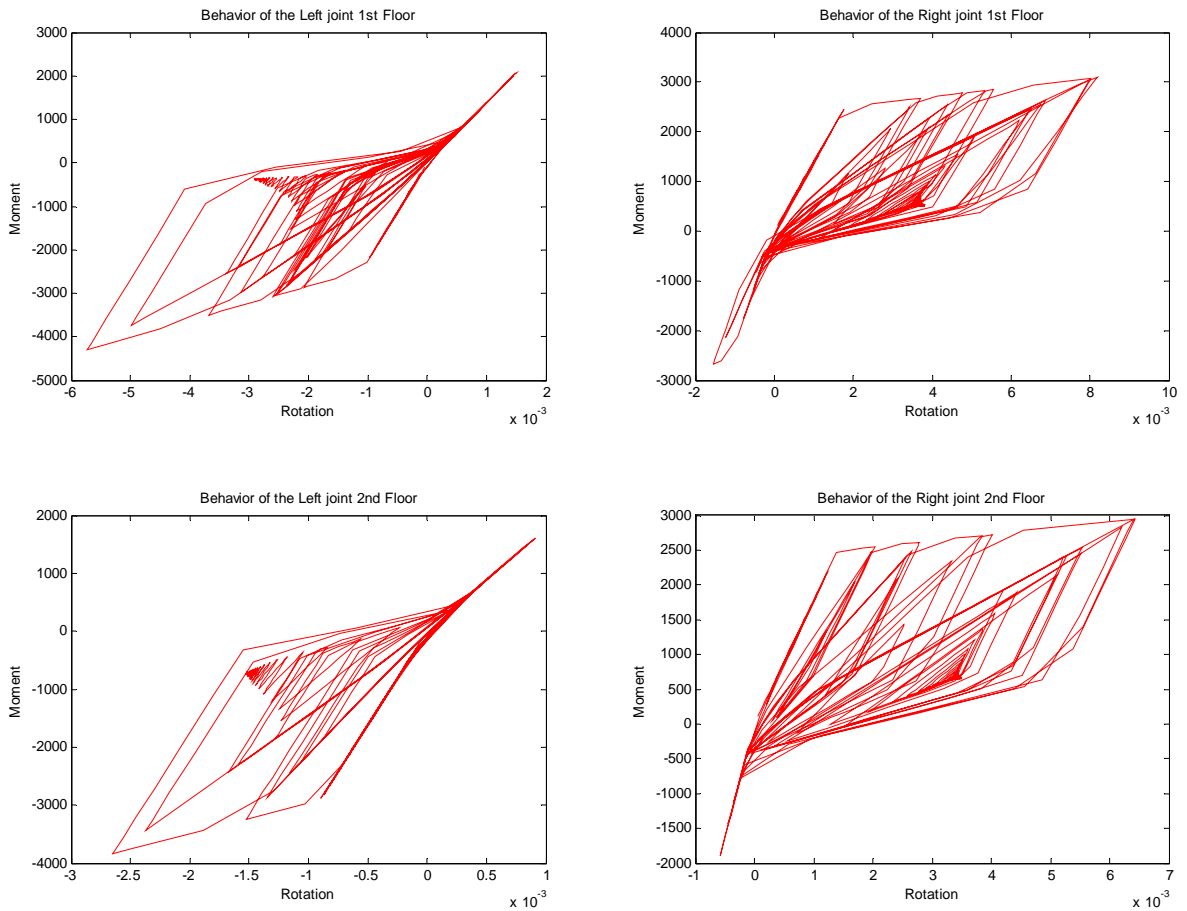


Figure 7-16 Local behavior of the joints for the two story frame for the Mayagüez earthquake

The number to the left indicates that the plastic hinges were formed in the leftmost steel at the bottom of the column, while the number to the right indicates that the plastic hinges were formed in the rightmost steel at the bottom of the column. Plastic hinges were formed simultaneously at 4.42 seconds at the leftmost steel of both columns of first floor at the base and almost at the same time (around 5.6 seconds) at the rightmost steel of both columns at the base. At 5.74 seconds, a plastic hinges also were formed at the left beam of the first floor. The presence of these plastic hinges is corroborated since the graph is not oscillating around the zero drift, indicating that the structure is not remaining in the elastic range.

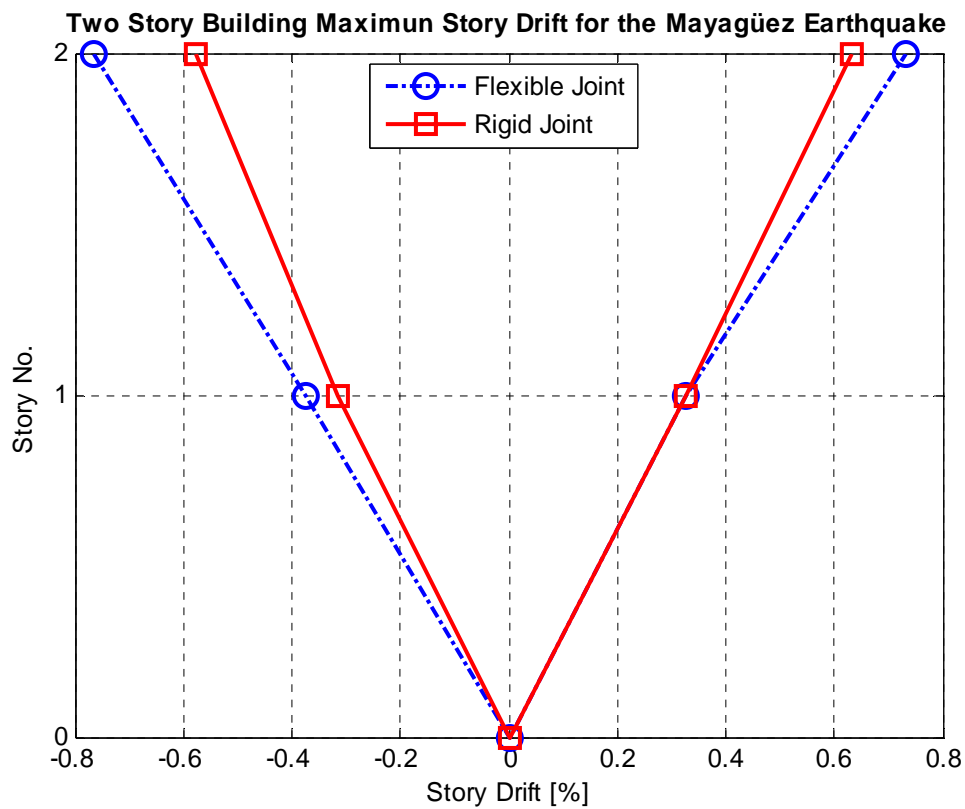


Figure 7-17 Maximum story displacement for the Mayaguez earthquake

In the other hand, for the flexible joints frame all joints were cracked in the sequence shown in Figure 7-15. The right joint of the first floor, was cracked in both direction. In addition, plastic hinges were formed at the base of both columns at the first floor. The first plastic hinges were formed at 6.58 second, at the base of the left column of the first floor. The other plastic hinges occurred simultaneously at the right column of the first floor at the base to the 8.6 seconds of the earthquake. In Figure 7-15, the value in parentheses indicates the time at which the joints suffered damage, in this case when they were cracked, but in Figure 7-16 it can be appreciated that during the earthquake, the cracked joints were loaded beyond of their cracked point. Even though both cases had plastic hinges at both columns of the first floor, the difference in the drift for both cases is associated to the fact that the flexible joints case became more flexible since all joints were cracked during the earthquake. This fact is also observed at the end of the earthquake, since flexible joints case is more shifted than the rigid joint case. This is an indication of a permanent damage produced by the cracked joint. Finally, from Figure 7-17 it can be interpreted that the local behavior of the joints are governing the drift in the frame since the maximum values of drifts to the right and left of the frame occurred in the flexible joints case.

7.5.2 RESULTS FOR THE THREE STORY BUILDING

7.5.2.1 RESULTS FOR THE EL CENTRO EARTHQUAKE

The comparison of the top story drift history for the El Centro earthquake for the two cases considered is shown in Figure 7-18. The sequence of plastic hinges is presented in Figure 7-19. In this figure, the value between parentheses indicates the time in seconds at which the

event occurred. The local behavior of all joints of the frame is presented in Figure 7-20. Finally the maximum drifts to the right and left for the three story frame is shown in Figure 7-21. A discussion of the above figures is presented in the next section.

7.5.2.1.1 DISCUSSION OF RESULTS

Since the drift history shown in Figure 7-18, for the case of rigid joints indicate that the frame was oscillating around the origin (zero drift) at the end of the earthquake, it is interpreted that this frame had no damage and thus remained elastic. This observation is confirmed in Figure 7-19 given that no plastic hinges were formed in the frame. For the case of flexible joint, the first event is related to the crack, simultaneously (at 2.07 seconds) of the right joint of the first and second story. This is reflected in the first peak of around 0.4% of drift that the frame reaches. To the 2.34 seconds, the left joints of the first and second story also were cracked. This caused the first peak of around -0.44% of drift. Around the 4.9 seconds, the right joint of the third story cracks almost simultaneously with the formation of a plastic hinge of the top steel of the first story left column at the base.

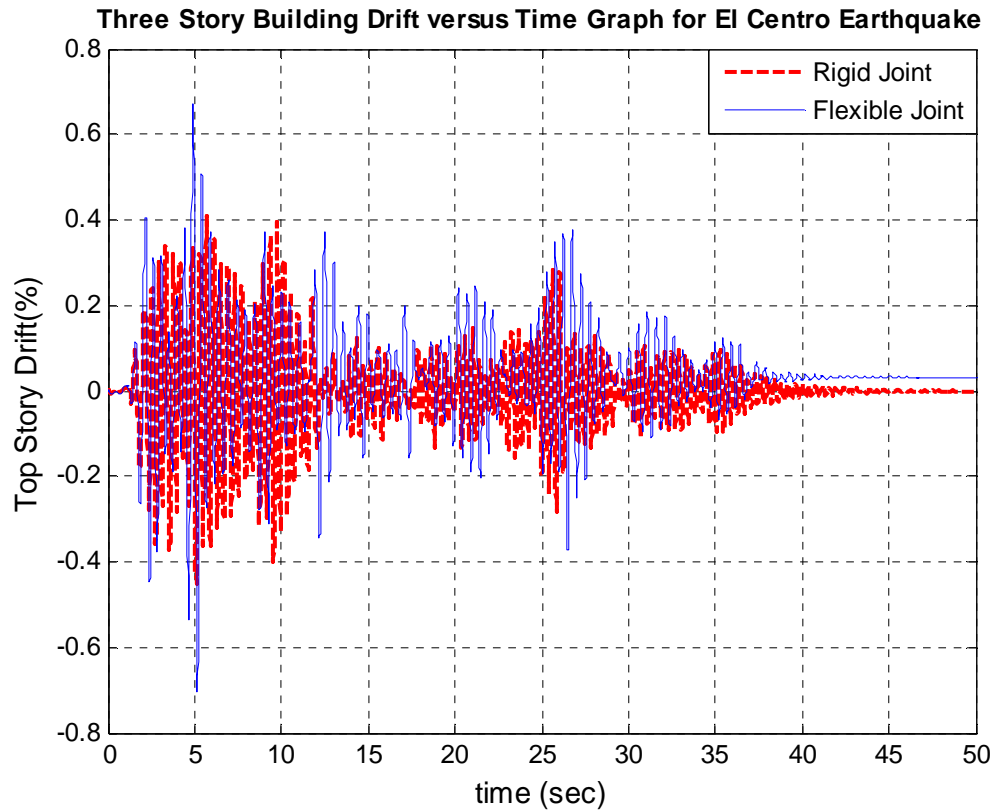


Figure 7-18 Top Story Drift versus time for the El Centro earthquake for the three story frame

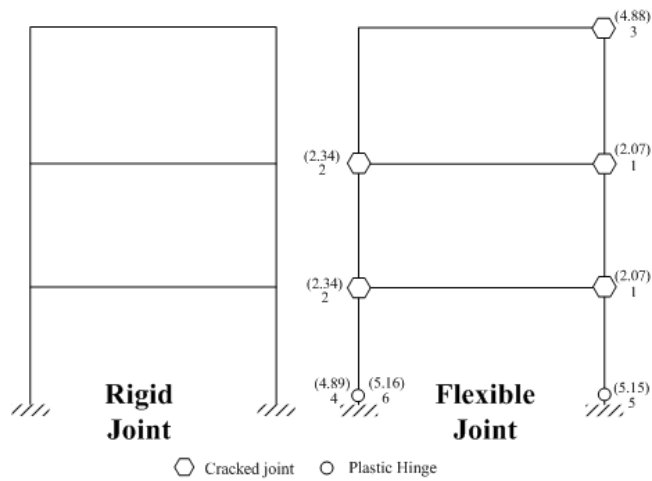


Figure 7-19 Sequence of plastic hinges for the El Centro earthquake for the three story frame

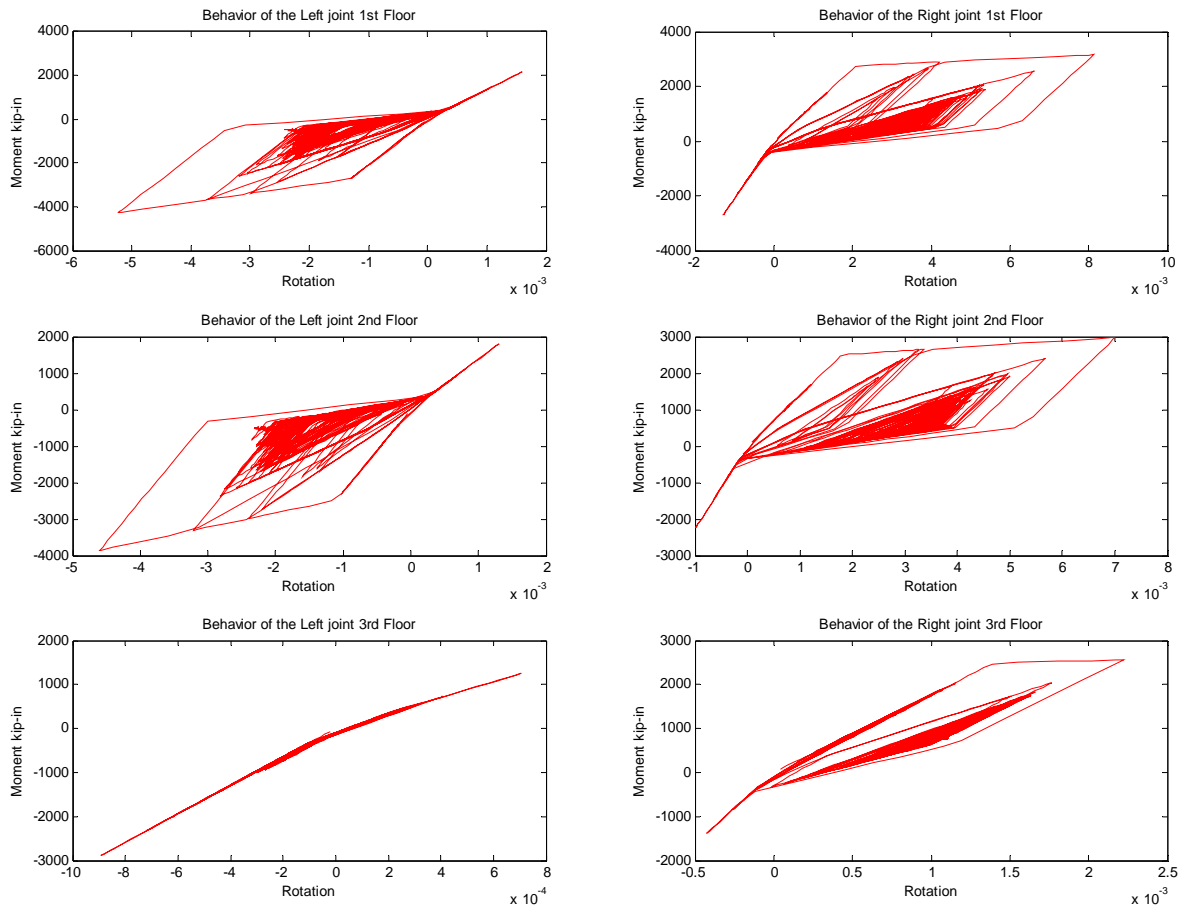


Figure 7-20 Local behavior of joints for the El Centro earthquake for the three story frame

This event originates the peak drift of 0.67%. In that same order, at around 5.15 seconds and almost at the same time, plastic hinges were formed at the rightmost steel of the first story both column causing the peak at a drift of -0.69%. The cracking of the five of the six joint along with the formation of plastic hinges at the base of the column of the first story caused permanent deformations to the structure that can be appreciated at the end of the earthquake in Figure 7-18. The local behavior of all joints (Figure 7-20) also confirmed the damage of the joint at the end of the earthquake.

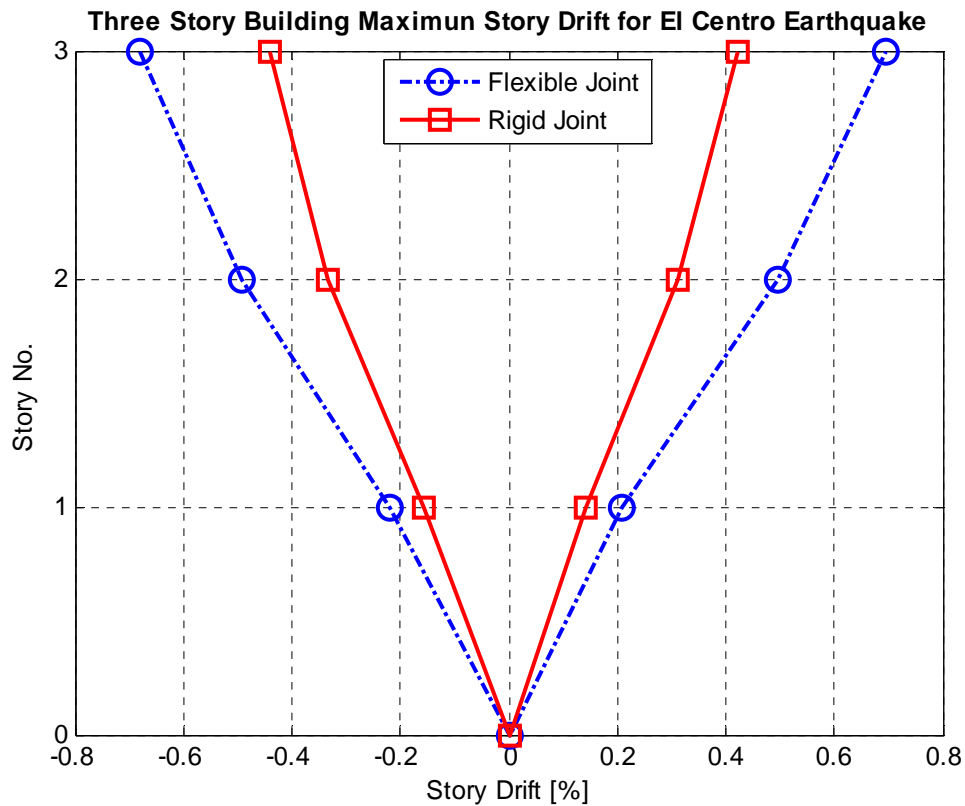


Figure 7-21 Maximum story displacement for the El Centro earthquake for the three story frame

Finally, Figure 7-21 summarizes the maximum drifts to the right and left at each story, attained during the El Centro earthquake. It can be appreciated that the fact that the joints were cracked, increased the drift at both sides of the frame.

7.5.2.2 RESULTS FOR THE MAYAGUEZ EARTHQUAKE

The comparison of the top story drift history for the Mayagüez earthquake for the two cases considered is shown in Figure 7-22. The sequence of plastic hinges is presented in Figure 7-23. In this figure, the value between parentheses indicates the time in seconds at which

occurred the event. The local behavior of all joints of the frame is presented in Figure 7-24. Finally the maximum drifts to the right and left for the three story frame is shown in Figure 7-25. A discussion of the above figures is presented in the next section.

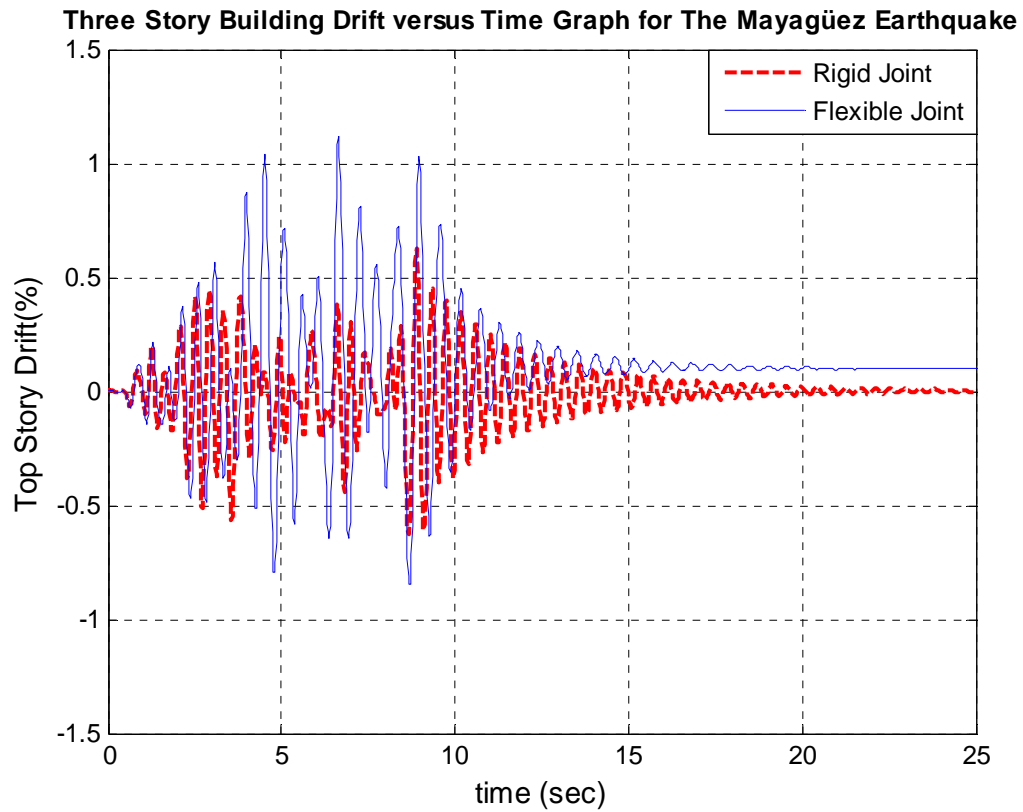


Figure 7-22 Top Story Drift versus time for the Mayagüez earthquake for the three story frame

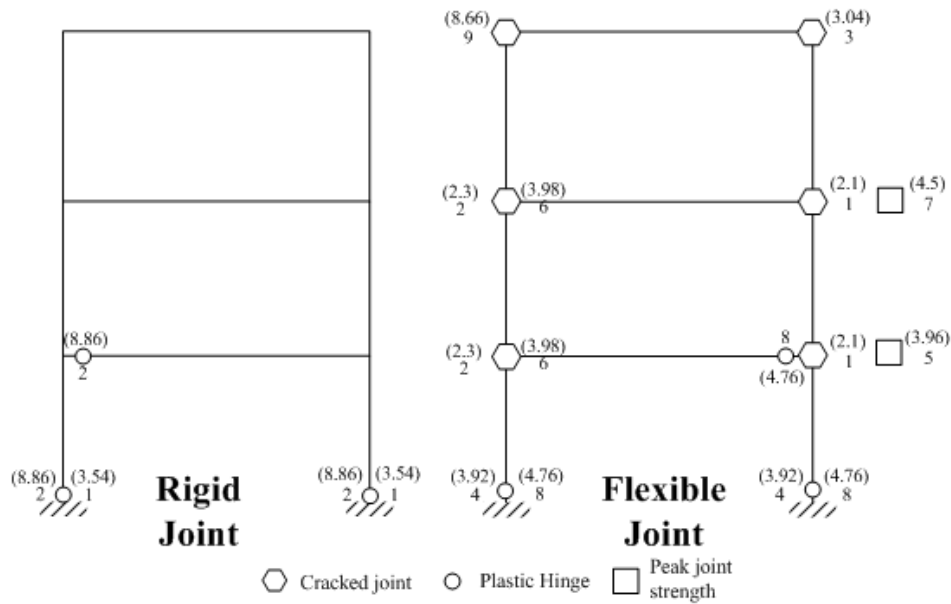


Figure 7-23 Sequence of plastic hinges for the Mayagüez earthquake

7.5.2.2.1 DISCUSSION OF RESULTS

When comparing the drift history for the Mayagüez earthquake (Figure 7-22) for both cases considered in can be appreciated that there is a significance difference among them. For the rigid joints frame, at the end of the history, the structure ventured in the nonlinear behavior since plastic hinges were formed at both faces at the base of the first story column and in the left end of the first story beams (Figure 7-23). At around 3.6 seconds, a peak of -0.57% of drift occurred and it is attributed to the formation of the plastic hinges in the rightmost steel of the first story columns at the base. For the case of the flexible joints at the 2.1 seconds the left joints of the first and second story were cracked simultaneously, inducing the peak in the graph at around 0.38% of drift. At the 2.3 seconds, the right joint of the first and second story also simultaneously were cracked, causing the peak at around -0.47% of drift.

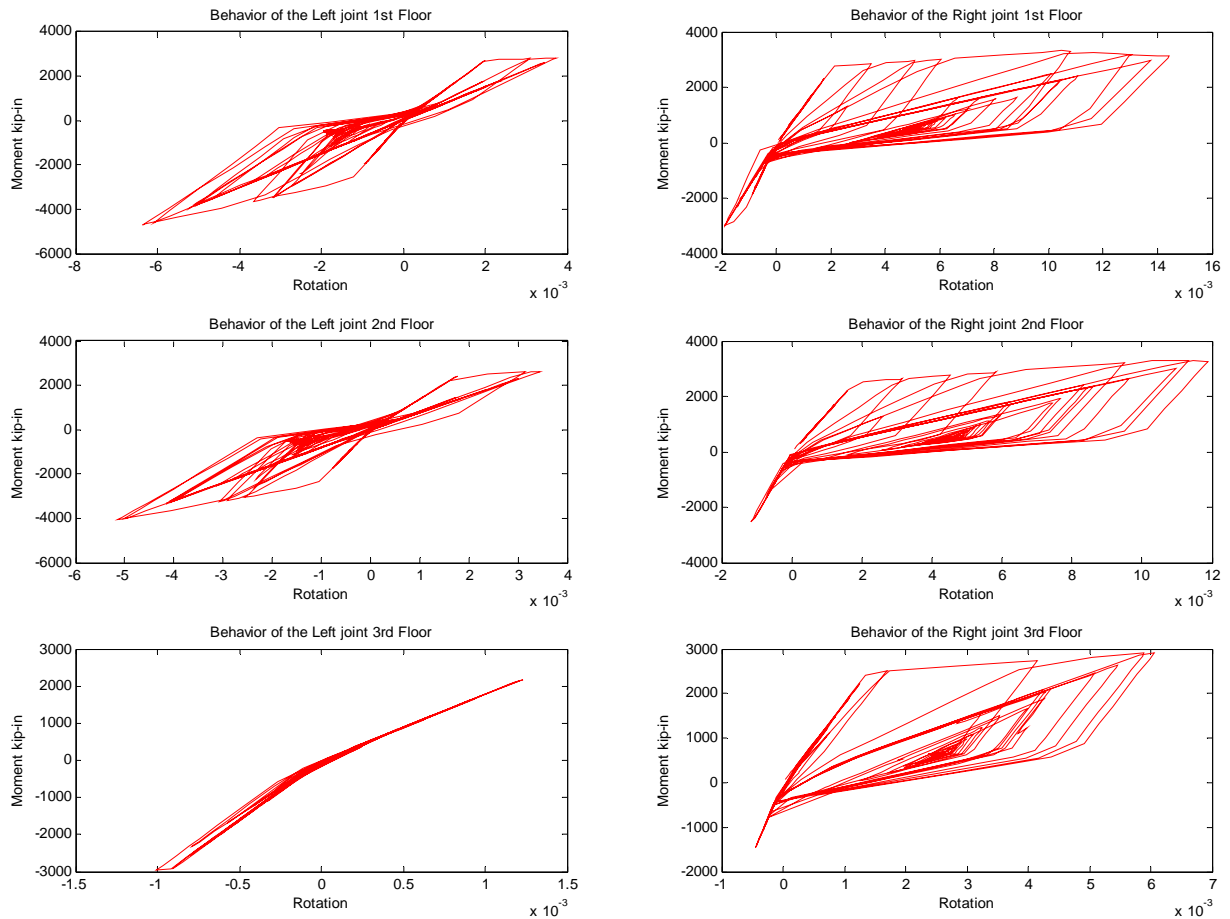


Figure 7-24 Local behavior of joints for the Mayagüez earthquake for the three story frame

At the 3.04 seconds the left joint of the third floor was cracked, being the reason of the peak at around 0.56% of drift. The simultaneous formation of plastic hinges at the leftmost steel of the first story column (3.92 seconds) along with the fact that the right joint of the first story attained its peak strength (3.96 seconds) and that the left joint of the first and second story joint simultaneously were cracked in the positive direction (3.98 seconds), caused a peak at around 0.85% of drift. At the 4.5 seconds, the right joint of the second story reaches its maximum strength, inducing the peak at around 1.04% of drift.

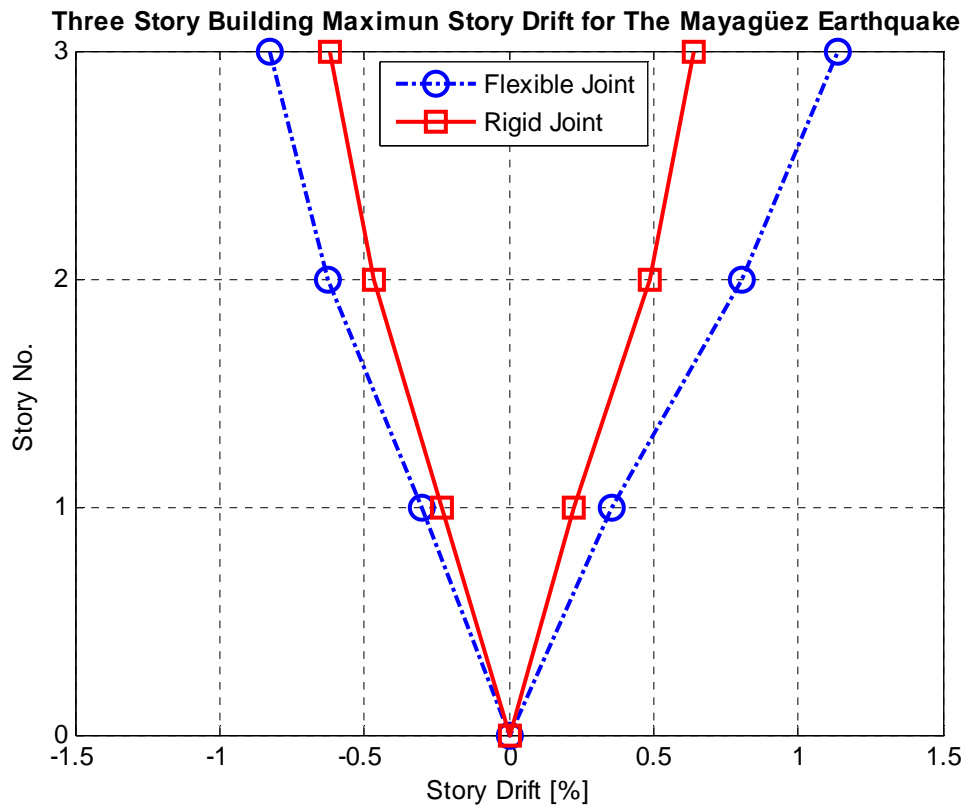


Figure 7-25 Maximum story displacement for the Mayagüez earthquake for the three story frame

The formation of plastic hinges at the same time at the rightmost steel of the first column at the base (4.76 seconds) induced the peak of -0.8% of drift. Finally the peak at -0.85% of drift was caused by the cracking of the left joint of the third floor. At the final of the drift history, the frame remains with a permanent drift of around 0.1%, as consequence of the suffered damages, mainly in the joints (Figure 7-24). Figure 7-25 summarizes the maximum drifts to the right and left at each story, attained during the Mayagüez earthquake. It can be noticed that the difference between the drifts, when comparing the two cases, is higher for the case of the maximum drift to the right. This is because the first and second right joint attained its peak strength and at the final of the analysis were the more damaged joints.

7.6 COMPARISON OF THE RESPONSE FROM THE STATIC AND DYNAMIC ANALYSIS

In order to identify the state of damage suffered by the two and three story frames, the maximum values of the total base shear and the drift obtained from the dynamic analysis, as shown in Table 7-2, were plotted against the pushover curve for both the rigid and the flexible joints assumption.

Table 7-2 Summary of maximum response from the dynamic analyses

Building	Earthquake	Drift (%)		Base Shear (Kip)	
		Rigid	Flexible	Rigid	Flexible
2 Story	El Centro	0.36	0.39	81	64
	Mayagüez	0.63	0.78	120	110
3 Story	El Centro	0.45	0.7	93	96
	Mayagüez	0.63	1.12	112	106

It is important to mention that these values do not necessary occurred at the same time. For the two story frame, Figures 7.26 and 7.27 show the comparison of the results from the static and the dynamic analysis for the rigid and the flexible joints assumption respectively. The comparison of the responses from the static and dynamic analysis for the three story frame are shown in Figures 7-28 and 7-29 for the rigid and flexible joints assumptions respectively. From this comparison, it can be appreciated that the state of damage in the frames coincides in both the static and dynamic analysis. When the maximum drift from the dynamic analysis falls below the elastic limit drift (0.5% for the rigid joints assumption for both buildings) the structures remained elastic, as occurred in the rigid joints frames for the El Centro earthquake (see Figures 7-19 and 7-23). Also, when the maximum drift was beyond the elastic limit drift, the damage in the frames at such drift was very similar to that observed in the static pushover

analysis. That means, the same sequence of plastic hinges were observed in both the static and dynamic analysis.

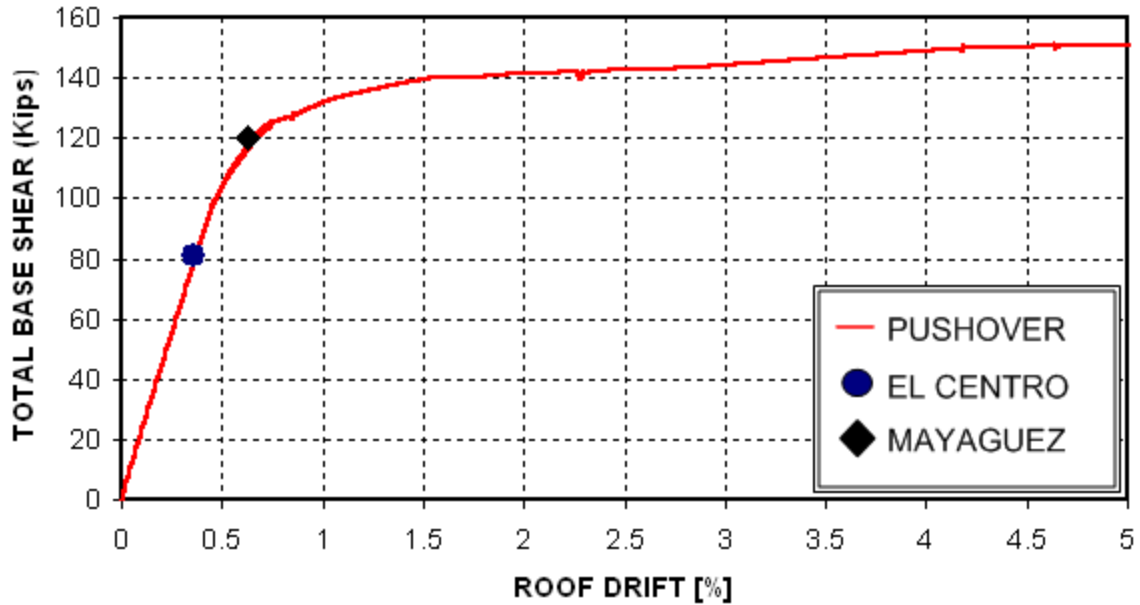


Figure 7-26 Static versus dynamic response for the two story building with rigid joints

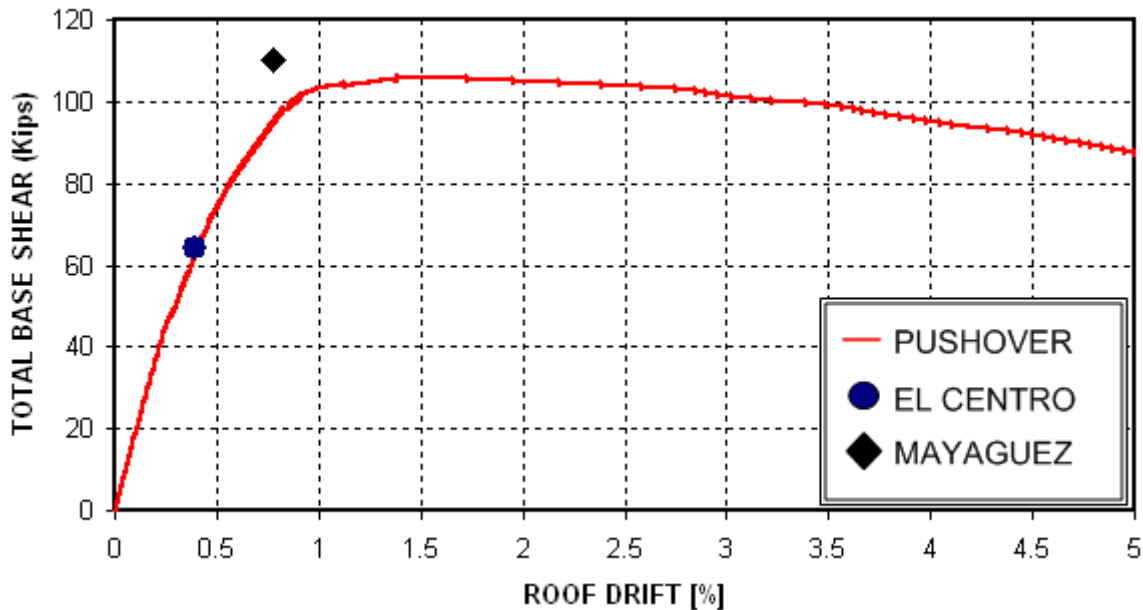


Figure 7-27 Static versus dynamic response for the two story building with flexible joints

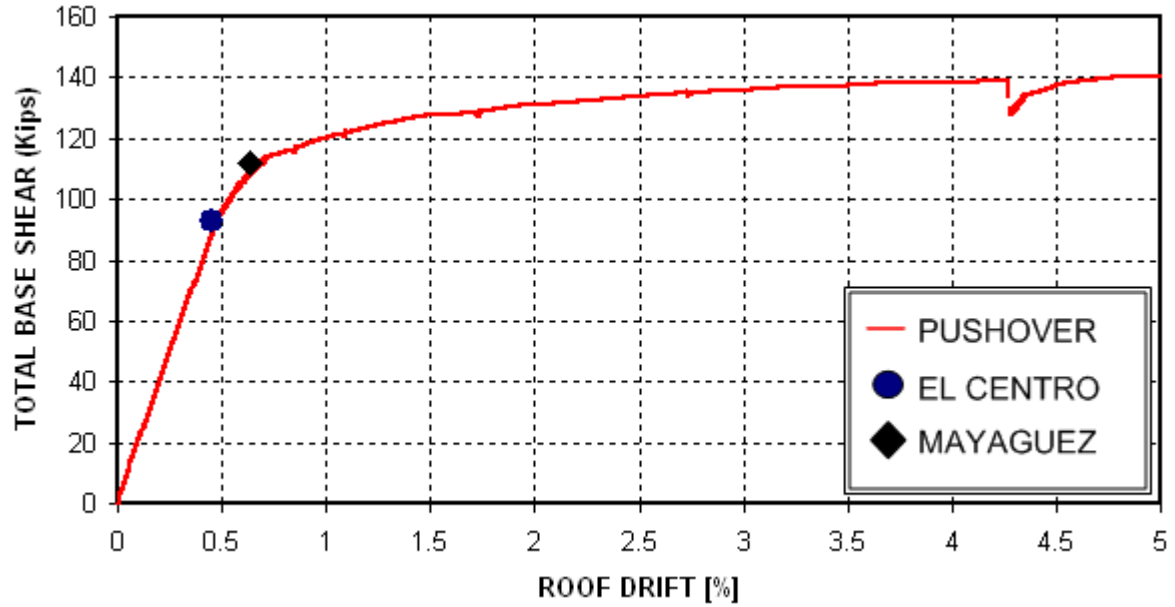


Figure 7-28 Static versus dynamic response for the three story building with rigid joints

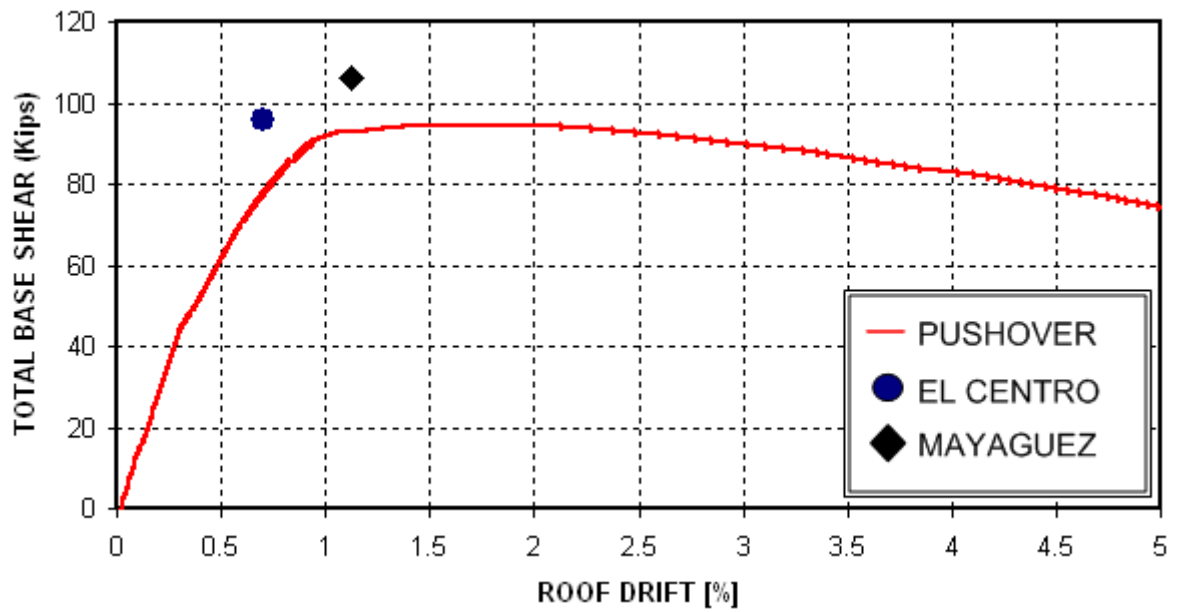


Figure 7-29 Static versus dynamic response for the three story building with flexible joints

7.7 CONCLUSIONS

In this chapter a two and three story frame with all joints being exterior joints, typical of school buildings in Puerto Rico were investigated using the proposed joint model. Pushover static analysis and dynamic analyses were carried out. In order to establish the difference in behavior two models were created, named the rigid joint case and the flexible joint case. The rigid joint assumption which neglects any deficiencies in the joint and the flexible joint assumption which takes into account that the frame has unreinforced joints. Even though the difference in the initial fundamental period among the two cases was small, the observed behavior in both the static and dynamic analysis was quite different mainly due to the local behavior of the joints.

The main observations from the static and dynamic analysis can be listed as follows:

- For the case of the static pushover analysis (see Figure 7-4 and Figure 7-7) the curves for the two and three story flexible joint frame were much seemed. When comparing with the rigid joint case, the first change in stiffness occurred at a relative low drift (around 0.3% for both flexible cases) and is associated to the cracking of some of the joints. Also the curve shows that once the frame attained the maximum load (coincidentally at a drift of around 1.5 % for the two and three story frame) its experimented gradual strength degradation. This performance is strongly related to the local joint behavior (see Figure 7-6 and Figure 7-9) and thus it can be interpreted that the strength of the global frame behavior is highly influenced by the local joint behavior.

- The joint elements are working as a fuse in both frames since their presence reduced and/or delayed the formation of plastic hinges mainly in the beams, because the damage instead of forming as plastic hinge in beams and columns is concentrated directly in the joint.
- The presence of the joint model reduced in 30% and 32% for the two and three story frame respectively, the maximum attained lateral load in the pushover analysis.
- In the dynamic analysis, the presence of the joint model increases the story drift. This increase ranged from around 8 to 24% for the two story frame and from 56 to 78% for the three story frame.
- The sequence of plastic hinges at the same drift in both the static and dynamic analysis was very similar.

8 ANALYSIS OF MULTISTORY BUILDINGS

8.1 INTRODUCTION

In the previous chapter two exterior frames of two and three stories typical of schools building in Puerto Rico, were analyzed with the proposed exterior joint model. These frames have in common that they were a one bay frame, thus all joints of the frames were exterior joints. In order to establish how the local behavior of exterior joints influence the global behavior of frames with more than one bay, three multistory three bays buildings are selected to be analyzed with the exterior joint model. A static pushover analysis and a dynamic analysis were carried out for each building. As in the case of the schools building frame, two cases also were considered. The first one assumes that the frame was designed with a more current code, thus any deficiencies are present. The second ones assume that the exterior joints lacks of transverse reinforcement. This chapter presents the results of the pushover static analysis and the dynamic analysis for the chosen frames. The assumptions made for the school building in previous chapter also applies for this chapter.

8.2 DESCRIPTION OF THE FRAMES

Daza Duarte (1996) designed three multistory building of 5, 10 and 15 stories following the provisions of the 1968 Puerto Rico Building Code (ARPE 1968). Structures designed with this code result in members with poor reinforcement details. That means that the poor confinement specifically in the exterior joints does not lead to a ductile response of the structure, promoting the shear failure which is undesirable in the current earthquake design

philosophy. Even though there is not available and inventory of multistory building constructed before 1970 in Puerto Rico, it is clear that many of these structures exist and are still in use in the Island. Thus it is important to study the behavior of these structures under earthquake loadings. In this study three typical multistory buildings in Puerto Rico designed by Daza Duarte (1996) were selected to be analyzed. The typical layout of these buildings is shown in Figure 8-1.

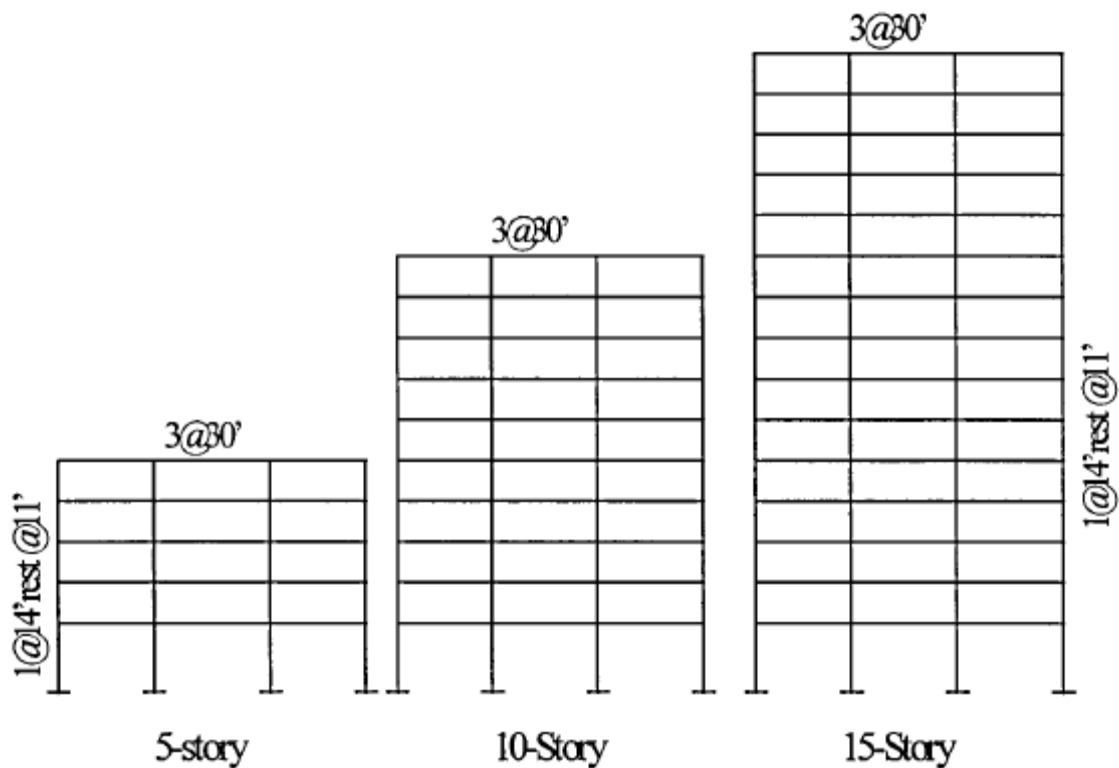


Figure 8-1 Layout of 5, 10 and 15 Story Building Frame (Daza Duarte 1996)

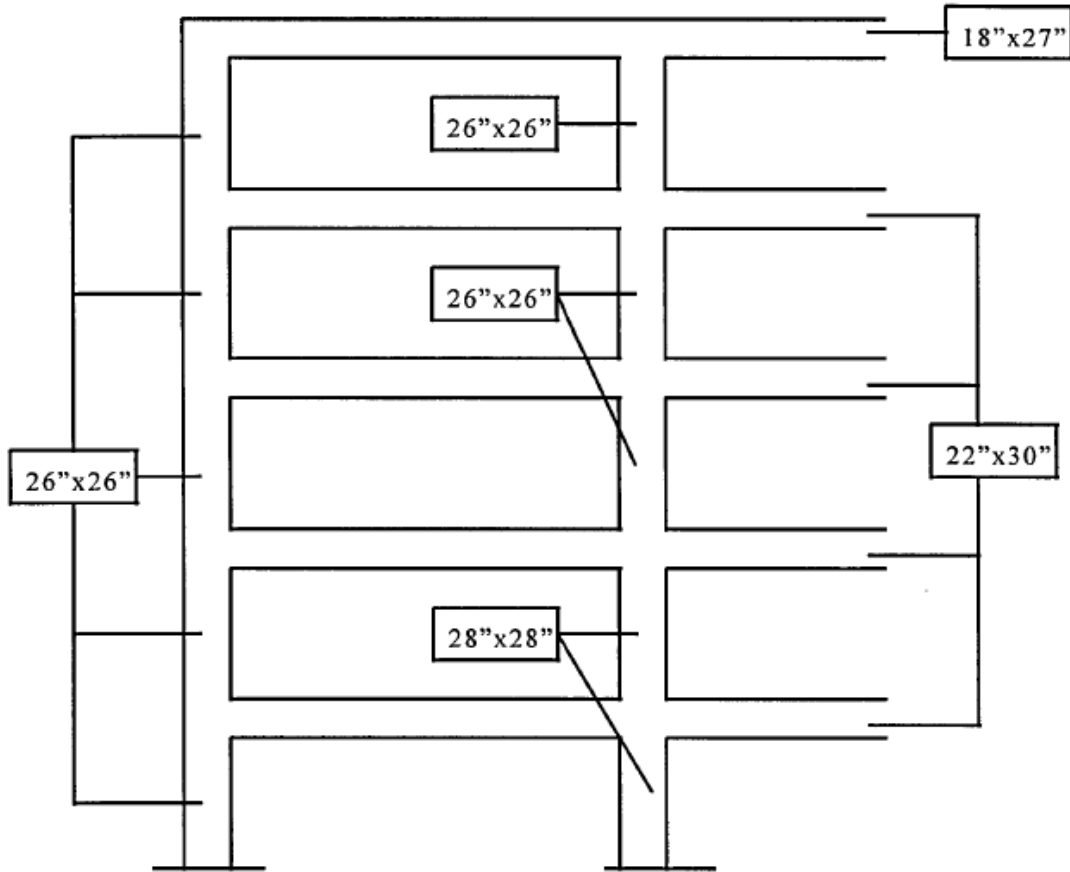
The frames have three spans of length 30 ft. (center to center). In all the frames, the height of the first story is 14 ft. while the height of the rest of the stories is 11 ft. Daza Duarte (1996) indicates that the approximated weight per story and per frame is 348 kips for the five story building; 350 kips for the 10 story building and 360 kips for the 15 story building. These

weights were distributed along beam and column of the frame, assuming a 90% goes to the beams and 10% goes to the columns of each story. The 90% that goes to the beams was divided by the total length of the beam in the floor (90 ft.) to obtain the distributed weight along the beams. In the same way, the 10% that goes to the columns was divided by the total length of columns of the floor (56 ft. for the first story column and 44 ft. for the rest of the story columns). The distributed weight along beams and columns for each building used in the analysis are summarized in Table 8-1. In the dynamic analysis, the used damping ratio was 2%

Table 8-1 Distributed weight along members used in the analysis

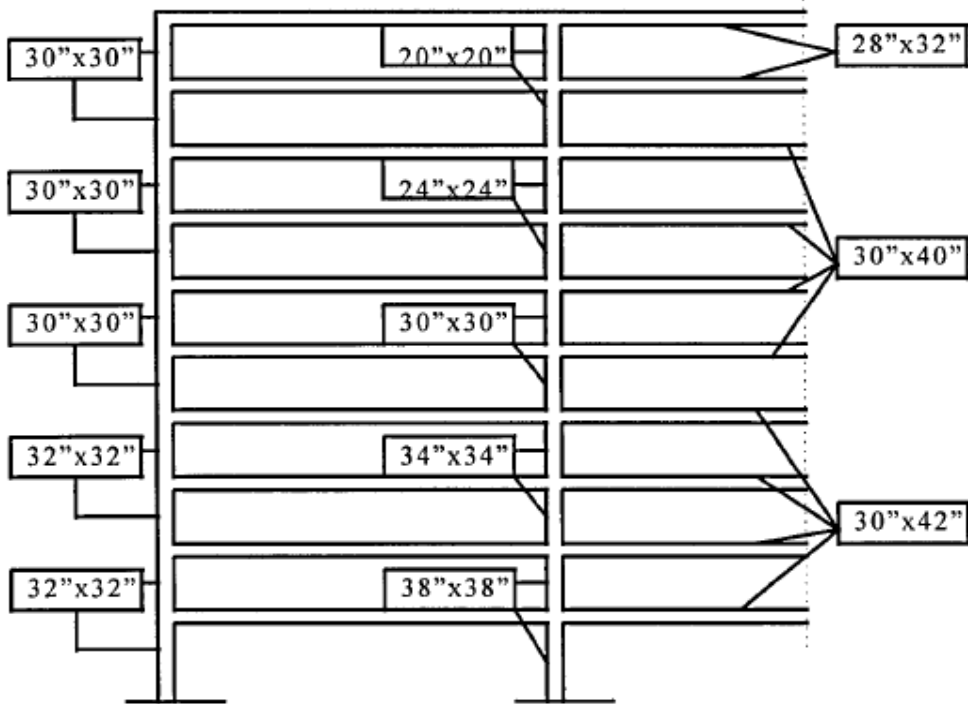
Building	Distributed load in kip/ft.		
	Beams	1 st Story Columns	Rest of Columns
5 Story	3.48	0.62	0.79
10 Story	3.50	0.63	0.80
15 Story	3.60	0.64	0.81

Regarding the material properties, the concrete and the steel yield strength were assumed to be $f'_c = 4,000$ psi and $f_y = 60,000$ psi respectively. Finally, the cross sectional sizes and the main reinforcement at members ends are presented in Figure 8-2 through 8-4.



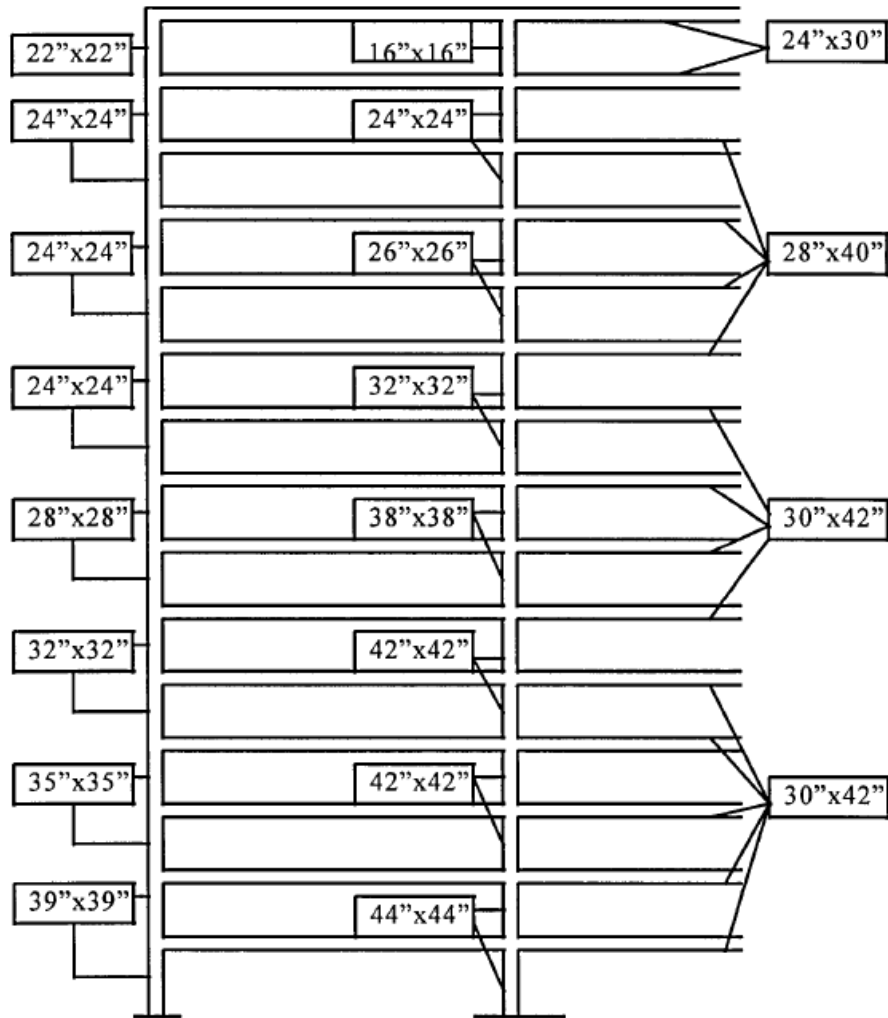
<p>LEVELS 1-4</p>  <p>5 in² 2.36 in²</p>	<p>ROOF</p>  <p>3.95 in² 1.76 in²</p>	BEAMS
<p>LEVELS 1-2</p>  <p>6 in² 6 in²</p>	<p>LEVELS 3-5</p>  <p>4 in² 4 in²</p>	
<p>LEVELS 1-2</p>  <p>3.54 in² 3.54 in²</p>	<p>LEVELS 3-5</p>  <p>2.36 in² 2.36 in²</p>	INTERIOR COLUMNS

Figure 8-2 Cross sectional sizes and reinforcement details at member ends of the 5 Story frame (Daza Duarte 1996)



<p>10.16 in² 2.95 in² LEVELS 1-4</p>	<p>10.16 in² 2.95 in² LEVELS 5-9</p>	<p>7.62 in² 2.4 in² ROOF</p>	BEAMS	
<p>8 in² 8 in² LEVELS 1-2</p>	<p>7 in² 7 in² LEVELS 3-4</p>	<p>6 in² 6 in² LEVELS 5-10</p>	EXTERIOR COLUMNS	
<p>10.92 in² 10.92 in²</p>	<p>7.8 in² 7.8 in²</p>	<p>5.08 in² 5.08 in²</p>	<p>4 in² 4 in²</p>	INTERIOR COLUMNS

Figure 8-3 Cross sectional sizes and reinforcement details at member ends of the 10 Story frame (Daza Duarte 1996)



<div style="display: flex; justify-content: space-around;"> <div style="border: 1px solid black; padding: 5px; text-align: center;"> 10.92 in² 3.16 in² </div> <div style="border: 1px solid black; padding: 5px; text-align: center;"> 9.36 in² 3.16 in² </div> <div style="border: 1px solid black; padding: 5px; text-align: center;"> 6.24 in² 2.37 in² </div> </div> <p style="text-align: center;">LEVELS 1-10 LEVELS 11-14 LEVEL 15</p>	BEAMS
<div style="display: flex; justify-content: space-between;"> <div style="border: 1px solid black; padding: 5px; text-align: center;"> 14.04 in² 14.04 in² </div> <div style="border: 1px solid black; padding: 5px; text-align: center;"> 14.04 in² 14.04 in² </div> <div style="border: 1px solid black; padding: 5px; text-align: center;"> 10.92 in² 10.92 in² </div> <div style="border: 1px solid black; padding: 5px; text-align: center;"> 9.36 in² 9.36 in² </div> <div style="border: 1px solid black; padding: 5px; text-align: center;"> 9.36 in² 9.36 in² </div> <div style="border: 1px solid black; padding: 5px; text-align: center;"> 7.8 in² 7.8 in² </div> <div style="border: 1px solid black; padding: 5px; text-align: center;"> 7.8 in² 7.8 in² </div> </div> <p style="text-align: center;">LEVELS 1-2 LEVELS 3-4 LEVELS 5-6 LEVELS 7-8 LEVELS 9-12 LEVELS 13-14 LEVEL 15</p>	EXTERIOR COLUMNS
<div style="display: flex; justify-content: space-between;"> <div style="border: 1px solid black; padding: 5px; text-align: center;"> 29.64 in² 29.64 in² </div> <div style="border: 1px solid black; padding: 5px; text-align: center;"> 24.96 in² 24.96 in² </div> <div style="border: 1px solid black; padding: 5px; text-align: center;"> 14.04 in² 14.04 in² </div> <div style="border: 1px solid black; padding: 5px; text-align: center;"> 14.04 in² 14.04 in² </div> <div style="border: 1px solid black; padding: 5px; text-align: center;"> 9.36 in² 9.36 in² </div> <div style="border: 1px solid black; padding: 5px; text-align: center;"> 6.24 in² 6.24 in² </div> <div style="border: 1px solid black; padding: 5px; text-align: center;"> 3.12 in² 3.12 in² </div> </div> <p style="text-align: center;">LEVELS 1-2 LEVELS 3-6 LEVELS 7-8 LEVELS 9-10 LEVELS 11-12 LEVELS 13-14 LEVEL 15</p>	INTERIOR COLUMNS

Figure 8-4 Cross sectional sizes and reinforcement details at member ends of the 15 Story frame (Daza Duarte 1996)

8.3 MODEL OF THE FRAMES

The element, material and section models from Opensees described in Chapter 7 are also used to model the multistory frames in this chapter. Regarding the interior joints, the results of the experimental test performed by Walker (2001) demonstrated that the behavior of interior joints without any reinforcement is similar to the exterior joints since the force versus drift curve from the specimens show strength and stiffness degradation and pinched behavior. However the behavior of the exterior joints in past earthquakes has shown to be more critical than the interior ones probably because interior joints are better confined by the adjacent beams. As the purpose of this chapter is to investigate how the local behavior of exterior joints influence the global behavior of the frame, the interior joints were modeled as rigid. Finally, Table 8-2 summarizes the natural period for the two and three story frame for the rigid and flexible joint assumption respectively.

Table 8-2 Natural period of the multistory frames

No. Story	Natural Period (seconds)	
	Rigid Joints	Flexible Joints
5	0.88	0.91
10	1.24	1.27
15	1.73	1.79

8.4 STATIC PUSHOVER ANALYSIS

The results of the static pushover analysis are discussed separated for each one of the buildings in the next subsections. In all cases, only the flexible joints model will be discussed.

8.4.1 RESULTS FOR THE FIVE STORY FRAME

The results of the pushover analysis for the five story frame are summarized in Figure 8-5 which shows the Load versus Drift curves for the rigid and flexible joints assumptions, respectively. Figure 8-6 shows a comparison of the sequence of plastic hinges formation for different drift levels.

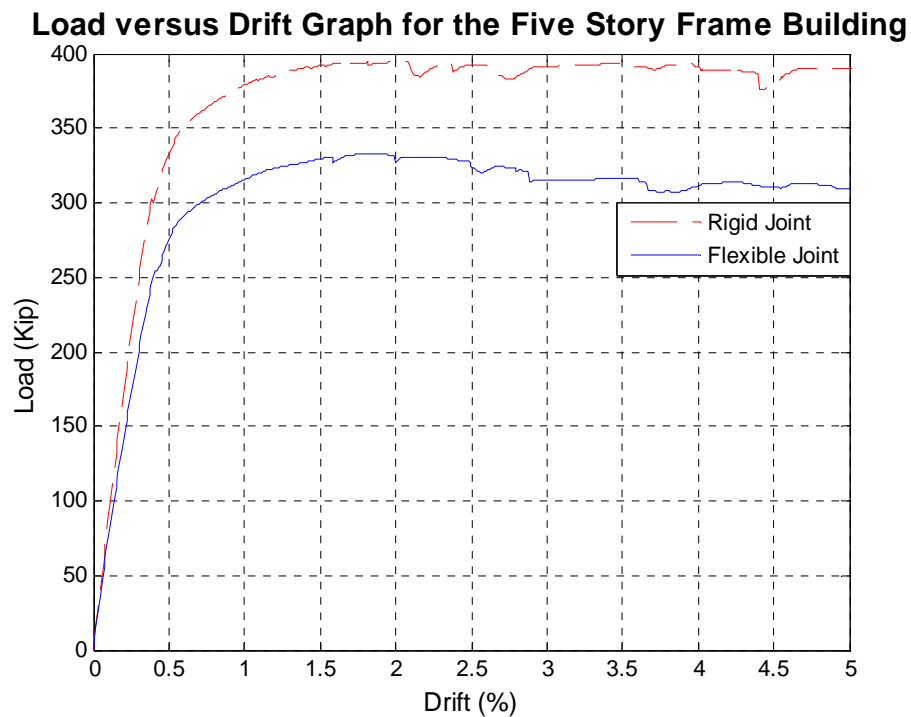


Figure 8-5 Pushover analysis results for the five story frame

For the flexible joints assumption, the pushovers curve shows that the structure remains elastic up to a drift of around 0.07%, where the first stiffness change occurs. This change is

due to the almost simultaneously cracking of all joints of the first two stories of the frame (events 1 through 3, as shown in Figure 8-6). At a drift of 0.41%, the second stiffness change occurs. Between the first and second stiffness change, events 4 through 7 (Figure 8-6) take place which include the formation of plastic hinges in the first two beams of the first and second story. At a drift of 0.55%, the third change of stiffness occurred, associated to events 8 to 13, that include that exterior right joints of the first and second floor reaching their peak strength and the formation of plastic hinges at the bottom of the first, second and fourth column of the first floor, as well as the formation of plastic hinges in two beams of the third floor.

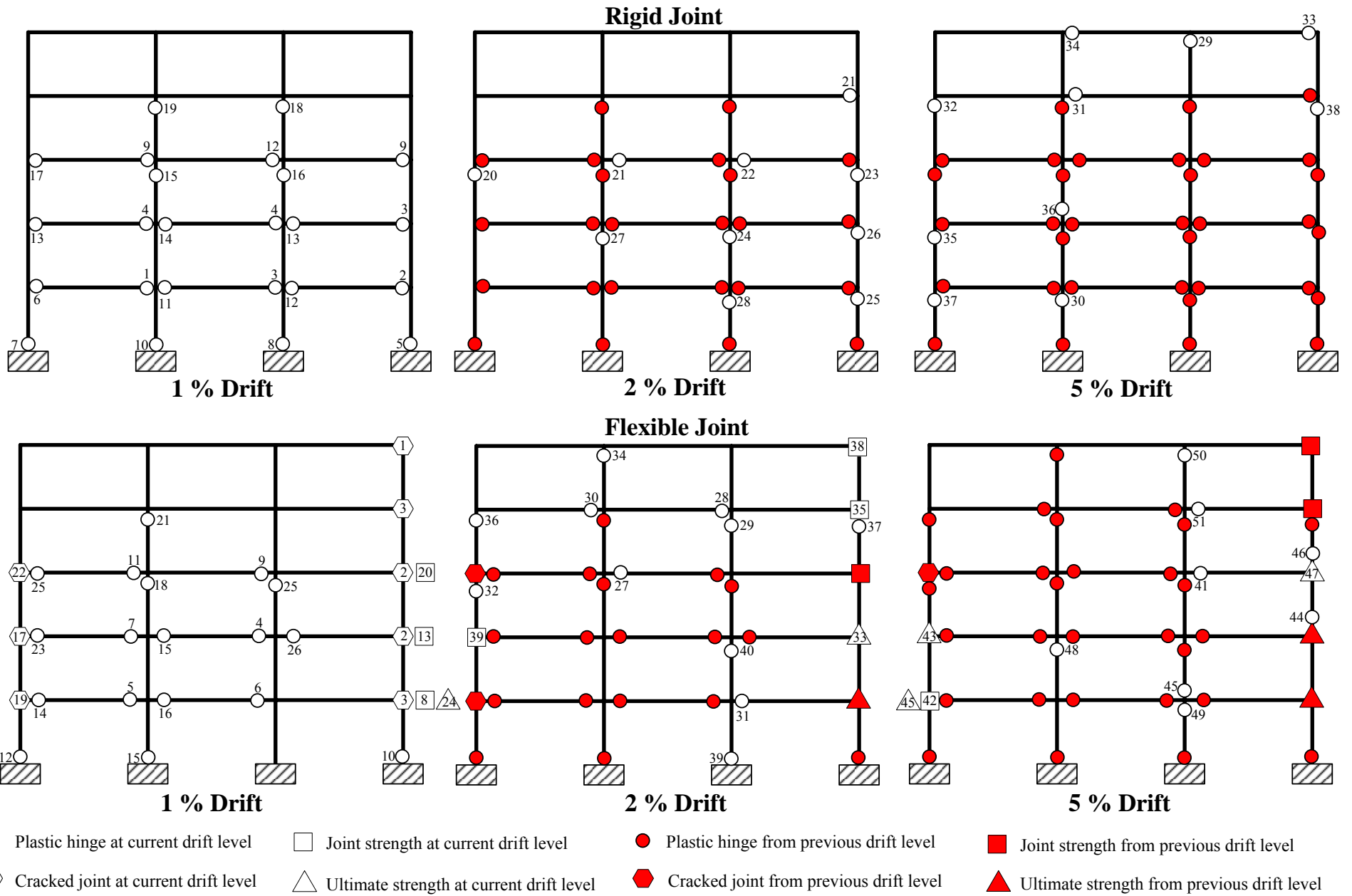


Figure 8-6 Sequence of plastic hinges events for the five story frame

At a drift of 0.85%, the fourth change of stiffness occurred. Between the third and fourth stiffness change, events 14 to 22 occurred (Figure 8-6), which includes cracking of the left joints of the first, second and third floor and the right joint of the third floor reaching their peak strength. The fifth stiffness change occurred at around 1.24% of drift. Between the fourth and fifth stiffness change, events 23 to 32 occurred; they include the right joint of the first floor reaching its residual strength (event 24). The curve attains its maximum lateral load (333 kip) at a drift around 1.8%. At that point, the right exterior joint of the second floor reached its residual strength (event 33). Also the left exterior joint of the second floor (event 39) and the right joint of the fourth and fifth floor (events 35 and 38) reached their peak strength. At this drift, the right exterior joints of the first and second floor have reached their residual strength, and the right joints of the remaining floors have reached their peak strength. This indicates that from this instant their local behavior will show strength degradation (negative slope). This behavior is clearly reflected in the global behavior of the structure since the pushover curve shows a reduction in the lateral load between a drift of 1.8 and 2.9%. At the end of the analysis, Figure 8-6 shows that plastic hinges formed at the left external beams at both the rigid and flexible joint assumptions. However, at the right external beams, there were no plastic hinges in the flexible joints model, since all the damage was concentrated at the joints. Finally, the maximum lateral load reached in both model was 395 and 333 kip for the rigid and flexible joints assumption respectively. This represents a reduction in capacity of 16% when flexible joints are considered.

8.4.2 RESULTS FOR THE TEN STORY FRAME

The results of the pushover analysis for the ten story frame are summarized in Figure 8-7 which shows the Load versus Drift curves for the rigid and flexible joints assumptions, respectively, and Figure 8-8 to 8-10 which show a comparison of the sequence of plastic hinges formation at different drift levels.

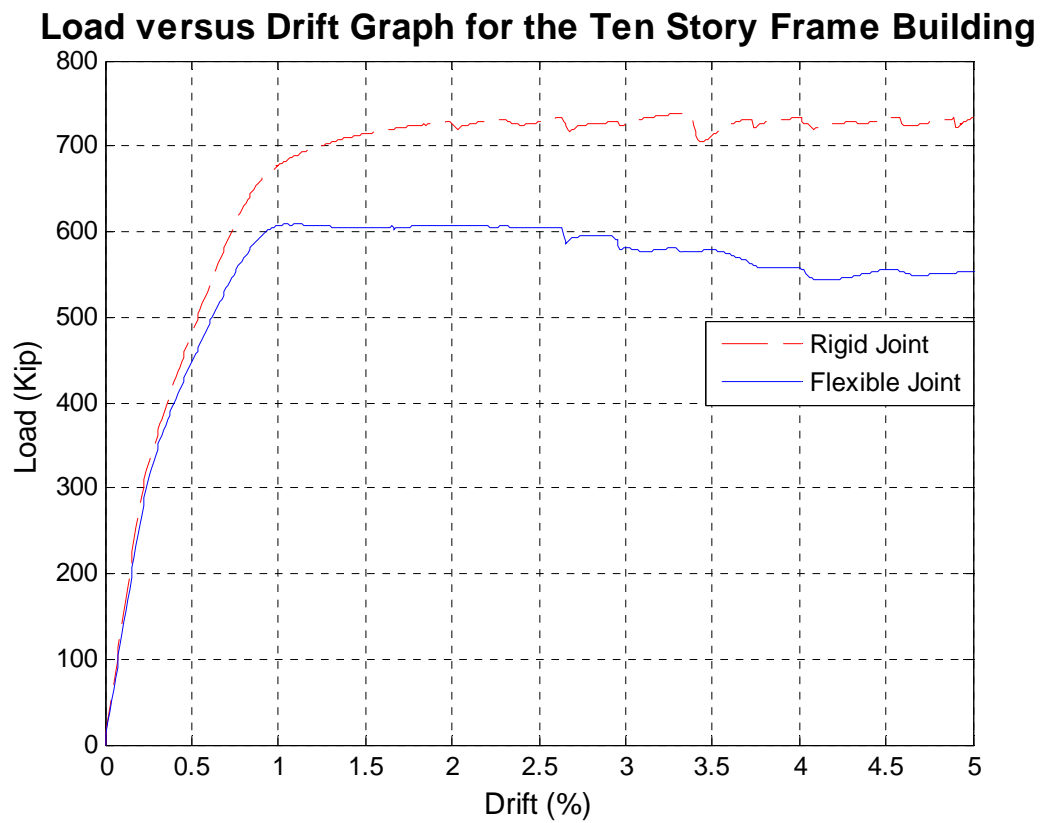


Figure 8-7 Pushover analysis results for the ten story frame

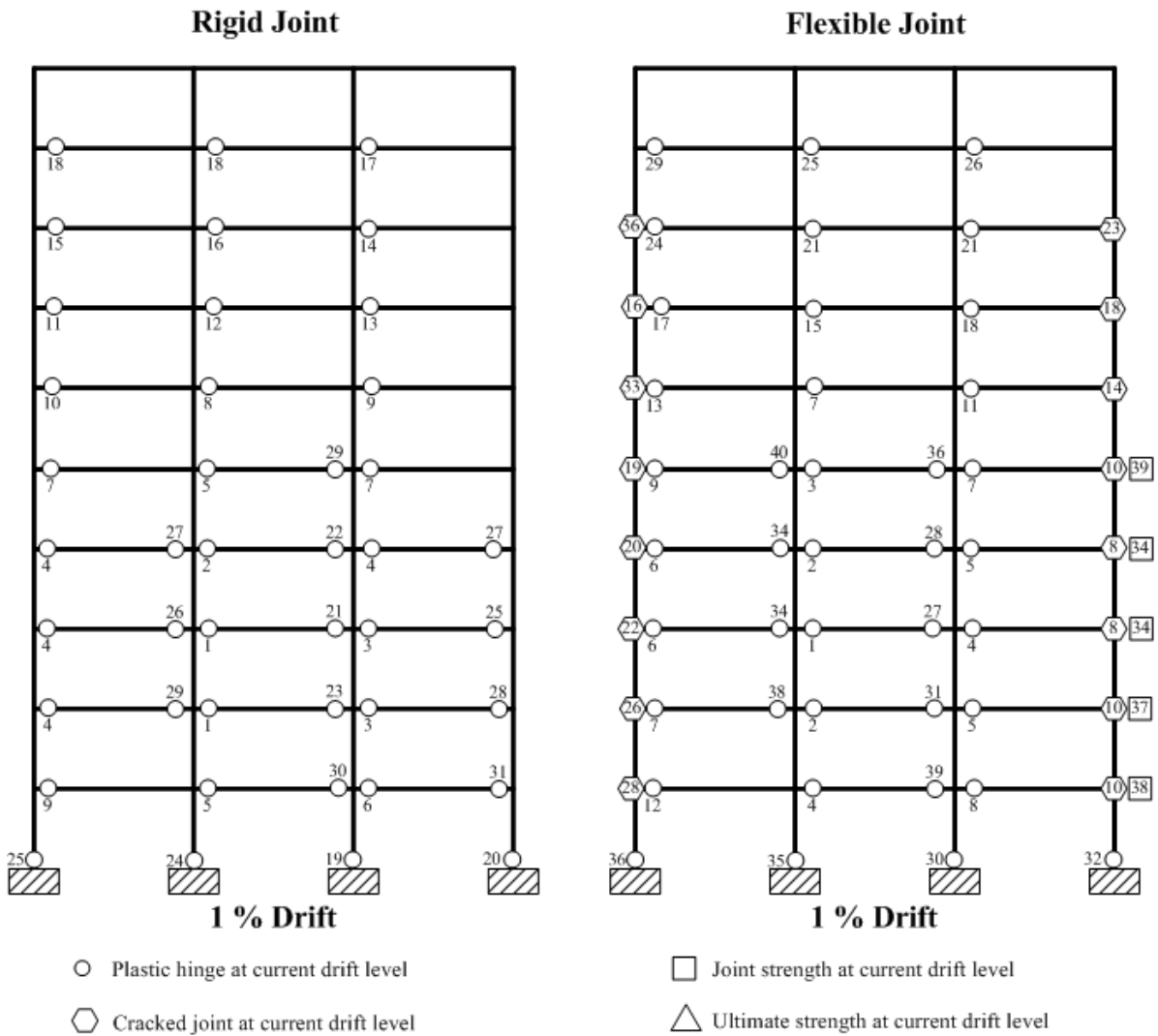


Figure 8-8 Sequence of plastic hinges events at 1% drift for the ten story frame

For the flexible joints assumption, the curve shows that the structure remains elastic up to a drift of around 0.20%, where the first noticeable stiffness change occurs. This change is related to the formation of plastic hinges in some beams of the first to fifth floor (events 1 to 4 as shown in Figure 8-8).

The almost simultaneously cracking of the right joints of the first five floors (events 8 to 10), induces the second change of stiffness at a drift of around 0.3%.

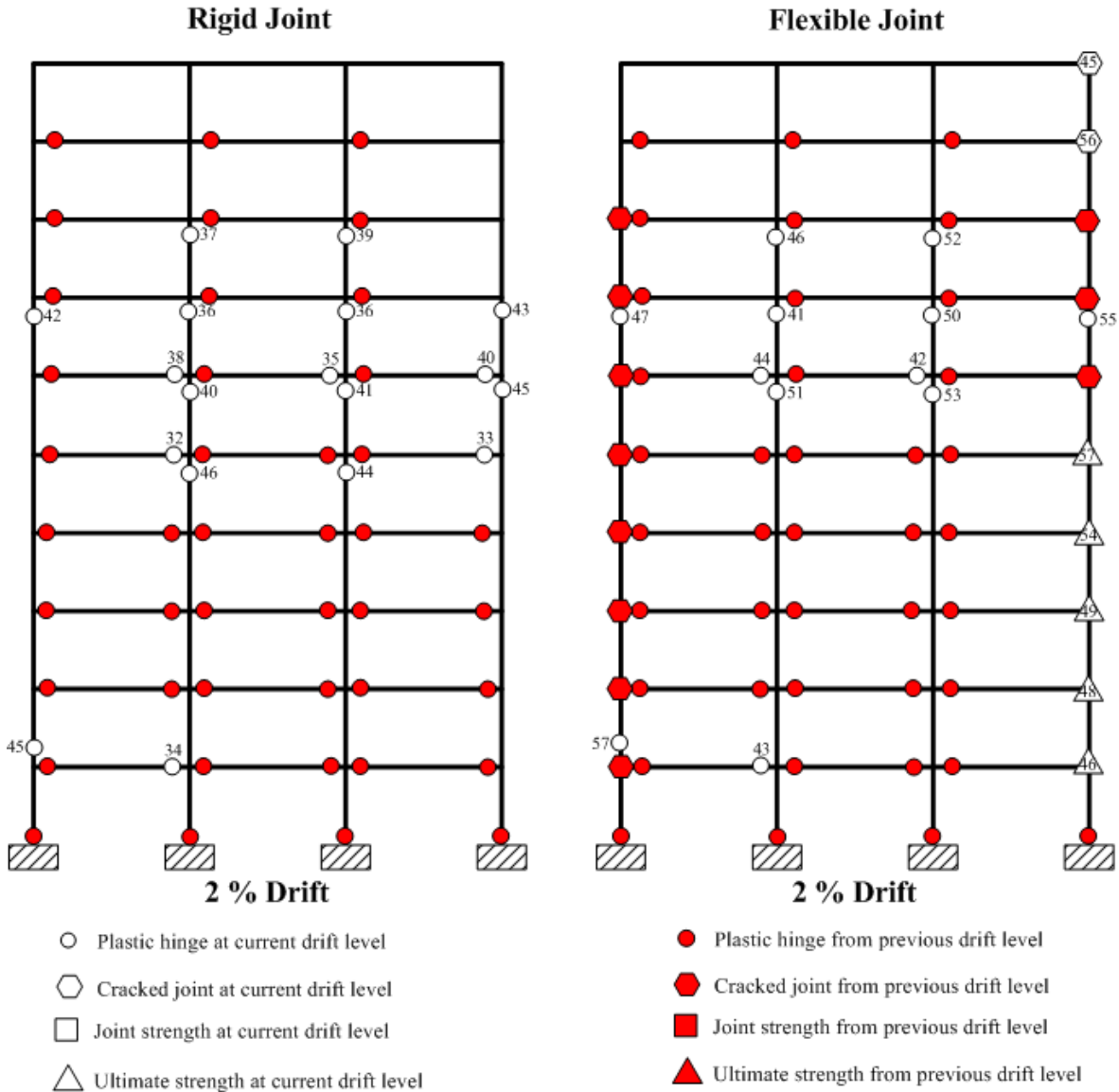


Figure 8-9 Sequence of plastic hinges events at 2% drift for the ten story frame

The third change of stiffness occurs at a drift of 0.7%. This change is associated with the occurrence of the events 11 to 26, which includes the cracking of eight joints. At this drift a total of 13 joints have reached their cracking point. At a drift of 0.85% occurs the fourth

change of stiffness. Between the third and fourth stiffness changes takes place the events 27 to 34, which include the cracking of two new joints that increases to 15 the number of cracked joints. This represents 75% of the frame exterior joints, in which two of these (right joints of the third and fourth floor) reached their peak strength. Figure 8-7 shows that at 1% of drift the structure reached its maximum lateral load (609 kip).

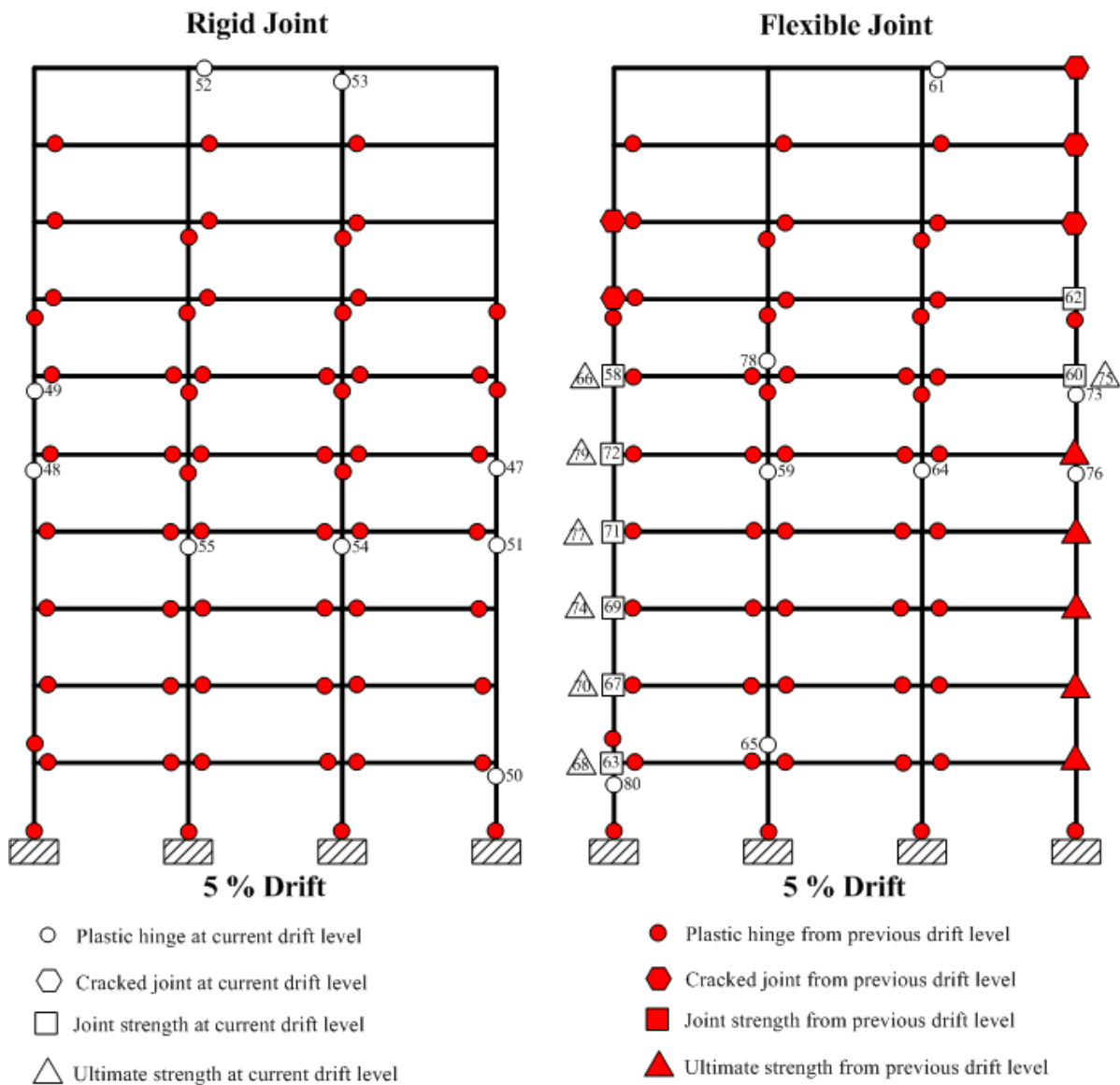


Figure 8-10 Sequence of plastic hinges events at 5% drift for the ten story frame

From this point up to a drift of 1.4% (events 34 to 46) the lateral load presents a slightly decrease. This reduction can be explained by the fact that the right joints of the first, second and fifth floor reached their residual strength and thus lost their stiffness. From this point, the global behavior of the structure is governed by the local behavior of the exterior joints.

Between a drift of 1.4 and 2.6% (events 44 to 60) the lateral load versus drift curve becomes horizontal. This is mainly due to the fact that the right joints of the second to fifth floors also reached their residual strength. At this instant the right joints of the first five floors have reached their residual strength, which implies that these joints are not contributing to the global stiffness of the frame. From this point, the curve does not show a defined slope. This could be associated with numerical convergence problems. However it is important to mention that the trend indicates that the system is losing strength and therefore it can be said that the local behavior of the exterior joints is strongly governing the behavior of the entire frame.

At higher drifts, Figure 8-10 shows that due to the use of joints model the formation of plastic hinges at the right external beams, do not appear since all the damage was concentrated at the joints. However, the same amount of plastic hinges was kept at the left external beams even though the left external joints also suffered damage. Finally, the maximum lateral load reached in both models was 738 and 609 kip for the rigid and flexible joint assumption respectively. This represents a reduction in capacity of 18% when flexible joints are considered.

8.4.3 RESULTS FOR THE 15 STORY FRAME

The results of the pushover analysis for the fifteen story frame are displayed in Figure 8-11 which shows the Load versus Drift curves for the rigid and flexible joints assumptions, respectively. Figures 8-12 through 8-14 show a comparison of the sequence of plastic hinges formation for different drift levels.

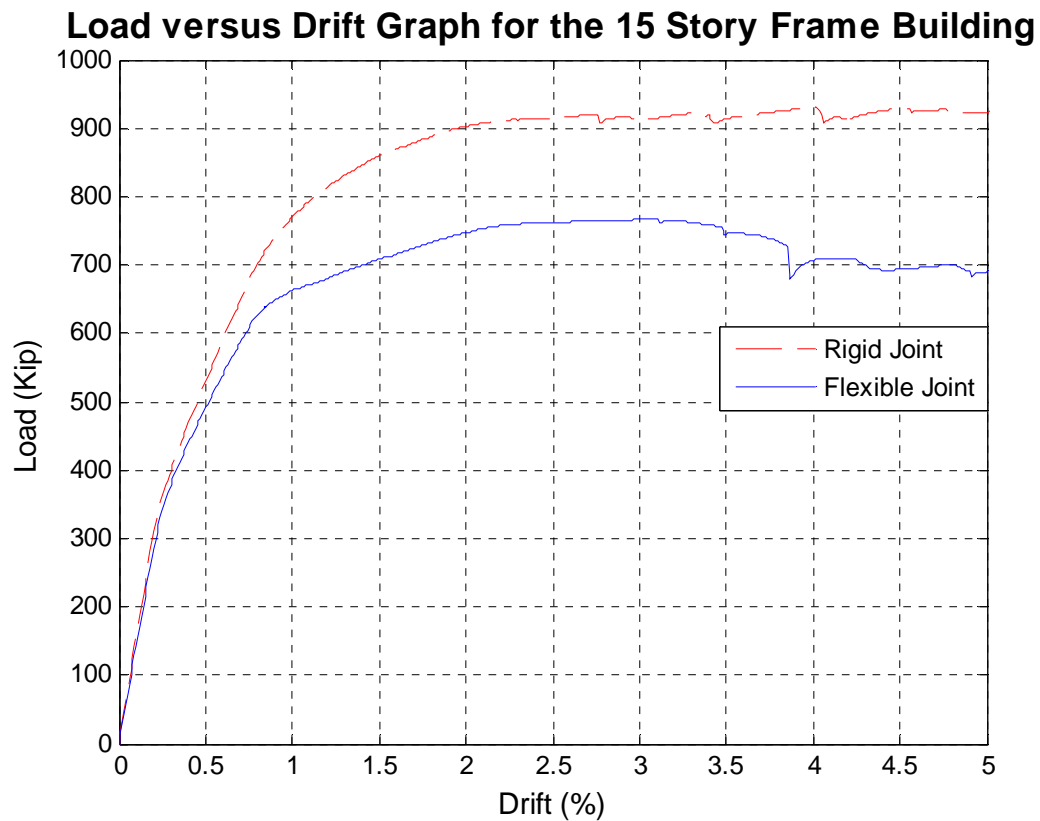


Figure 8-11 Pushover analysis results for the 15 story frame

For the flexible joint assumption, the curve shows that the structure remains elastic up to a drift of around 0.26%, where the first noticeable stiffness change occurs. This change is related to events 1 to 7 (Figure 8-12) which corresponds to the formation of plastic hinges in beams and to the cracking of the right joints of the third, fourth and fifth floor.

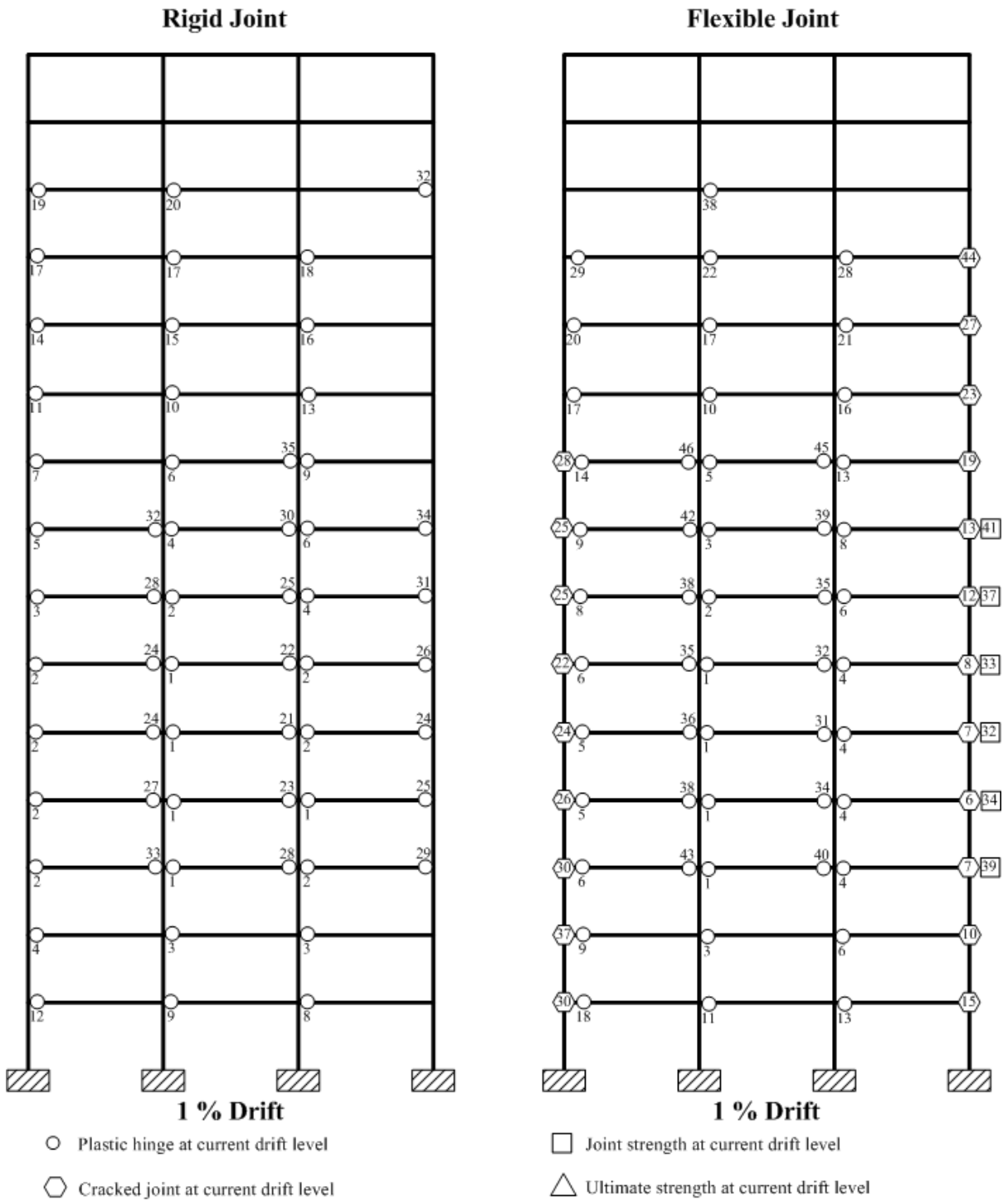


Figure 8-12 Sequence of plastic hinges events at 1% drift for the 15 story frame

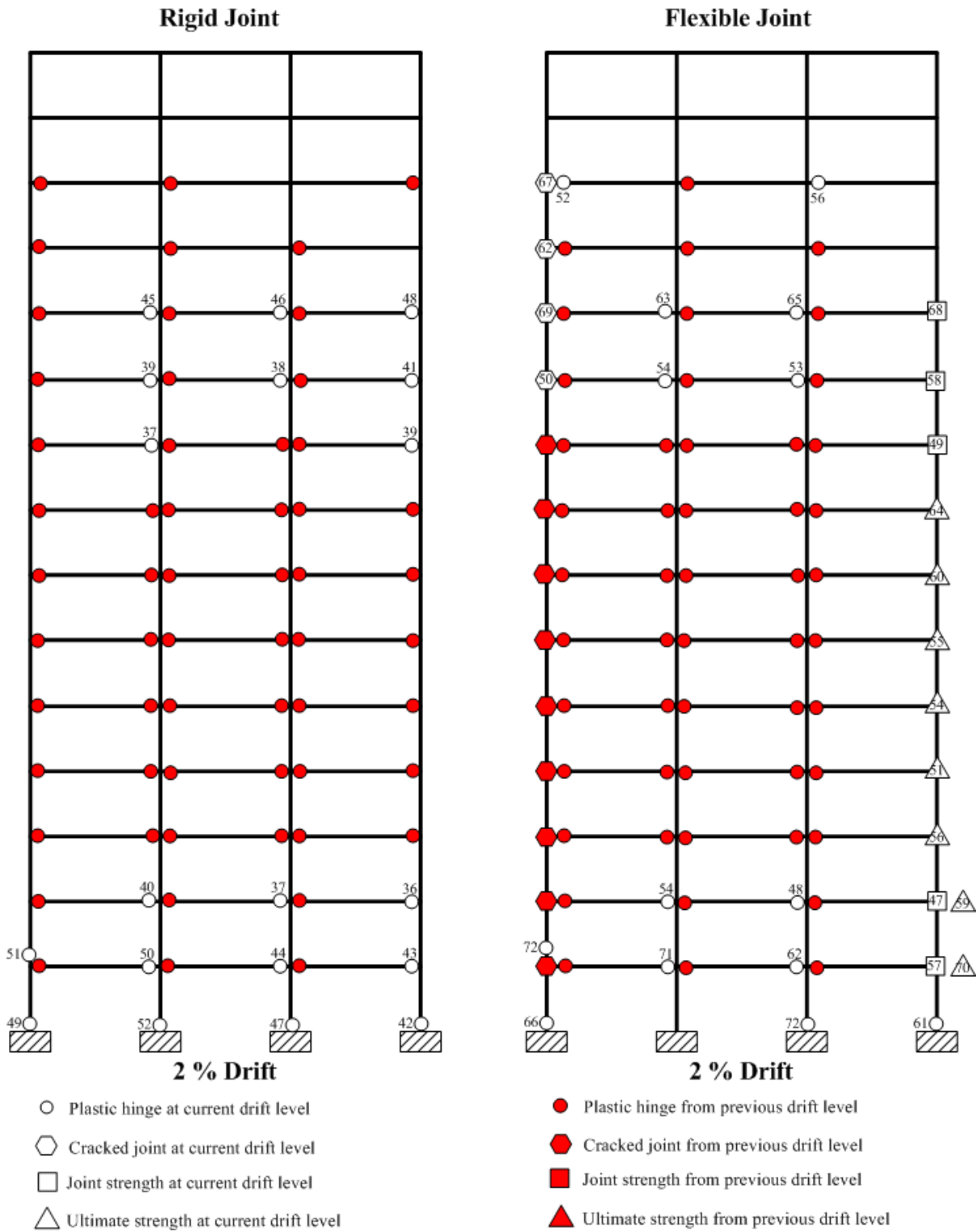


Figure 8-13 Sequence of plastic hinges events at 2% drift for the 15 story frame

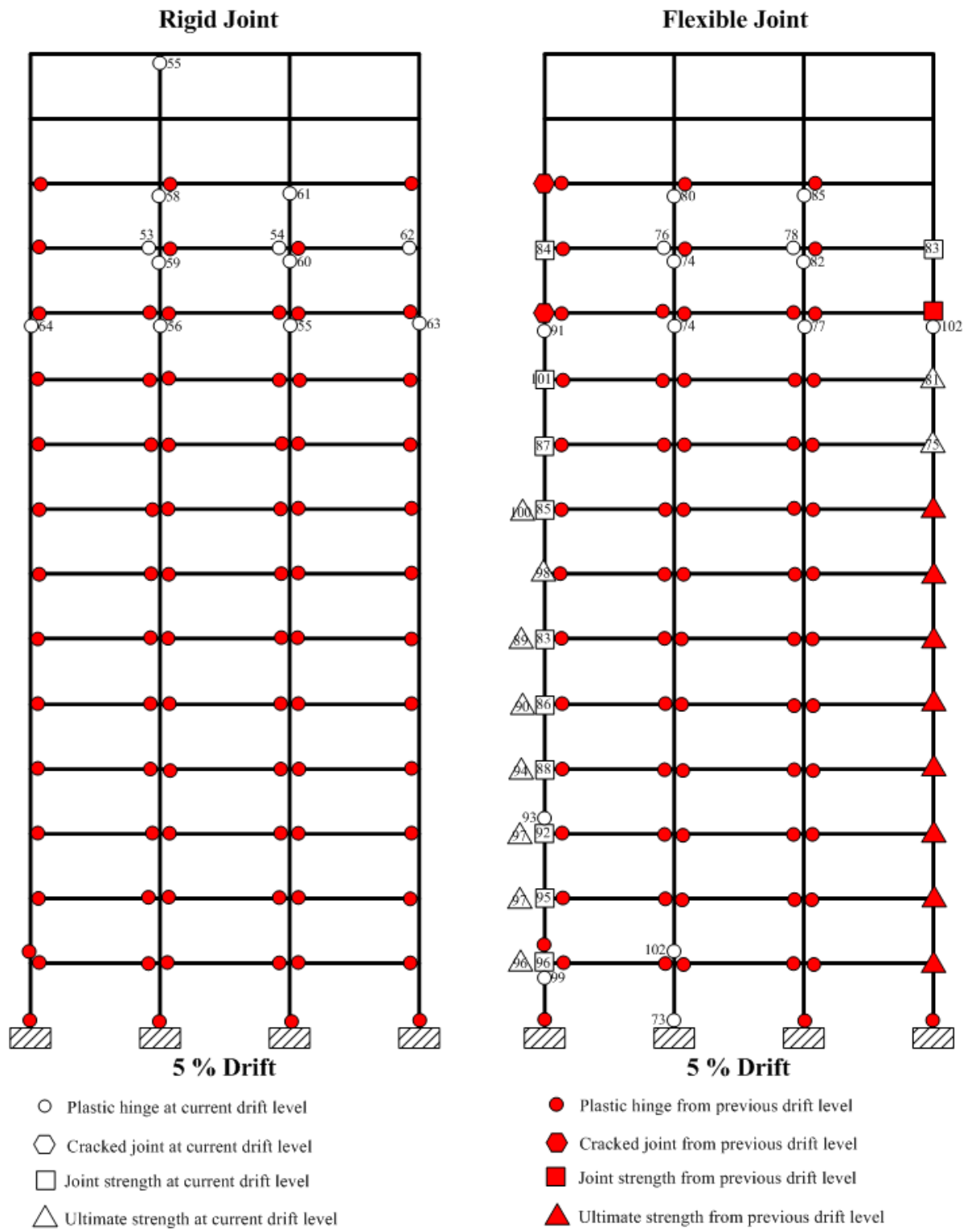


Figure 8-14 Sequence of plastic hinges events at 5% drift for the 15 story frame

At a drift of 0.4% the second change of stiffness occurs, which is related to the occurrence of the events 8 to 19. At this point 9 joints have been cracked; however it appears that the joints are not governing the global behavior. At a drift of 0.8% the third change of stiffness occurs, associated to the events 20 to 35, which include the cracking of several joints. This increases to 19 the number of cracked joints, of which 3 have reached their maximum strength. Between a drift of 0.8 and 1%, it can be noted that there is a continuous change in the stiffness of the frame. Events 35 to 49 have occurred in this interval. At this point, the number of cracked joints increased to 20, and eight of them reached their peak strength. It is, that once a joint attains its maximum strength, it starts to lose strength and stiffness, which could be the main reason of the rapid decrease of the system stiffness. At around 2.2% of drift, another stiffness change takes place. Between the previous and this stiffness change occurs the events 50 to 75, which includes that the right joints of the first nine floors have reached their residual strength. At a drift of 2.5% the curve shows small stiffness. However at a drift of 3.1%, the curve became horizontal, reaching its maximum lateral load of 767 kips. At this point the right joint of the first 10 floors of the frame have reached their residual strength and the curve shows that the system is losing lateral strength. This is an indicator that local behavior of the exterior joints is controlling the global behavior of the frame. From this point up to the end of the analysis, a continuous decrease of the strength of the system can be observed. Also convergence problems appeared to be the reason of the instability in the negative slope shown.

At the end of the analysis, Figure 8-14 shows that presence of the joint model disable the formation of plastic hinges at the right external beams, since all the damage was concentrated at the joints. However, the same amount of plastic hinges was kept at the left external beams even though the left external joints also suffered damage. Finally, the maximum lateral load reached was 930 and 767 kips for the rigid and flexible joint assumption respectively. This represents a reduction in capacity of 18% when flexible joints are considered.

8.5 DYNAMIC ANALYSIS

As for the case of school buildings of the previous chapter, the multistory buildings were subjected to the historical earthquake of El Centro of 1940 and to the artificial earthquake developed for the cities of Mayagüez and Ponce. In addition, the structures were subjected to the Mexico earthquake of 1985. Even though the peak ground acceleration (PGA) for this earthquake was relatively low (0.16g), due to the duration of the earthquake and the soil characteristics of the Mexico city, multistory buildings between 10 and 15 story were severely damaged during this earthquake. Since the structures being studied fall in this range, this earthquake was also included to examine the performance of these structures. The results of the dynamic analysis is presented and discussed in the following sections. In section 8.6 the maximum attained values of base shear and drift from the dynamic analysis are compared with the static pushover analysis curve for the three buildings and for the rigid and flexible joints assumption.

8.5.1 RESULTS FOR THE FIVE STORY FRAME

8.5.1.1 RESULTS FOR EL CENTRO EARTHQUAKE

The comparison of the top story drift history for El Centro earthquake for the two cases considered is shown in Figure 8-15. The sequence of plastic hinges is presented in Figure 8-16. In this figure, the value within parentheses indicates the time in seconds at which the event occurred. The maximum drifts to the right and left for the five story frame are shown in Figure 8-17. Finally the local behavior of the first story joint is presented in Figure 8-18. A discussion of the figures is presented in the next section.

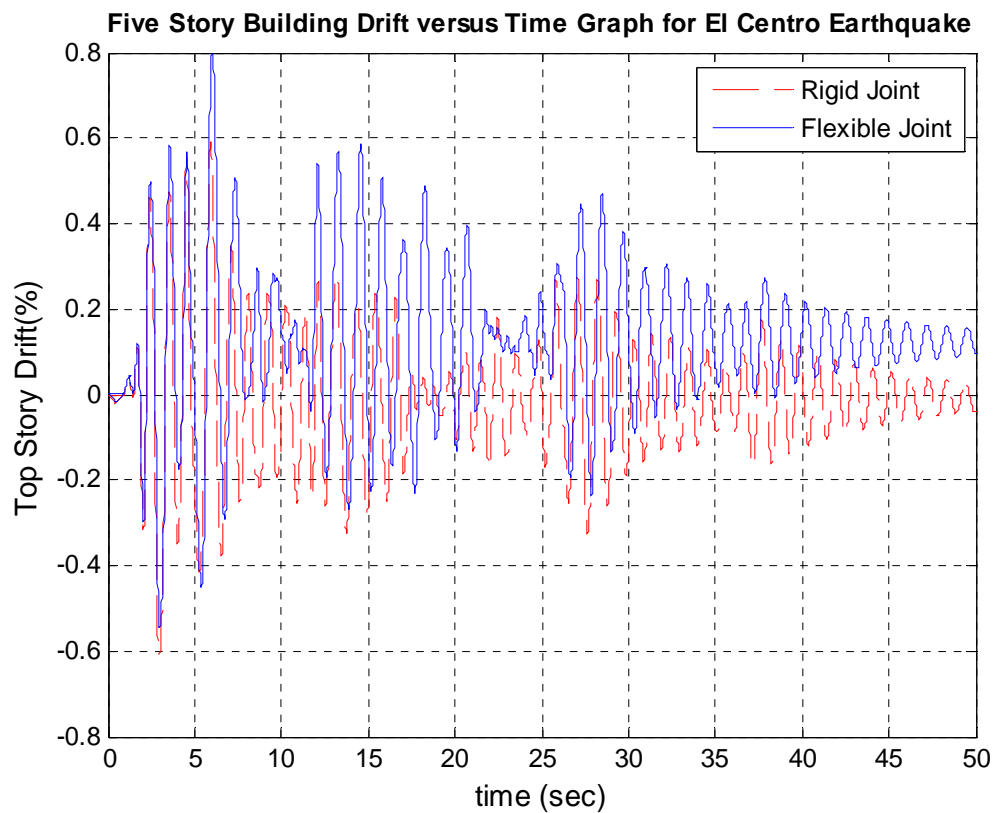


Figure 8-15 Top Story Drift versus time for El Centro earthquake for the five story frame

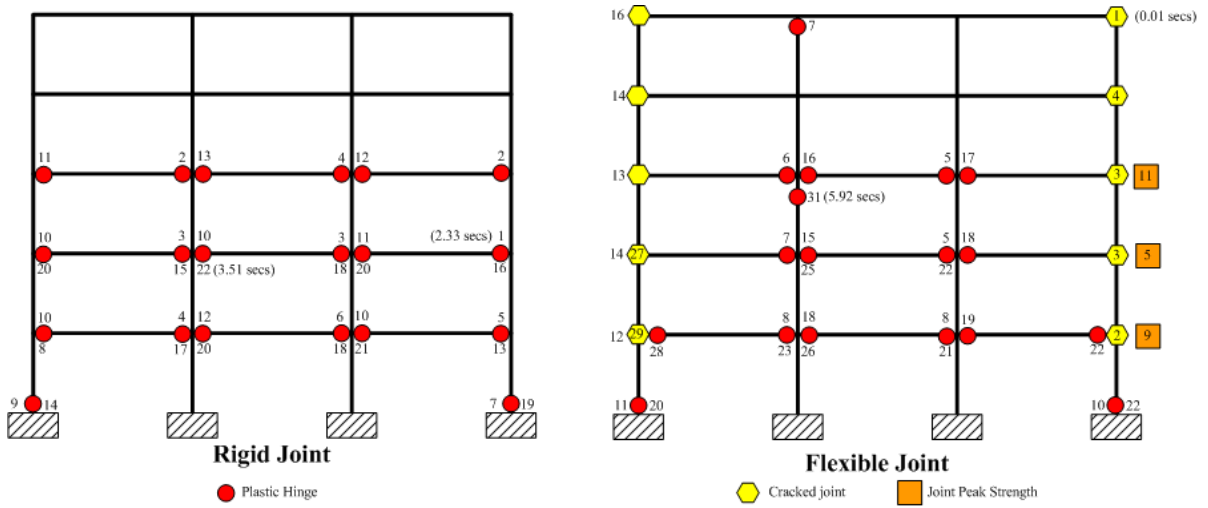


Figure 8-16 Sequence of plastic hinges for the five story frame for El Centro earthquake

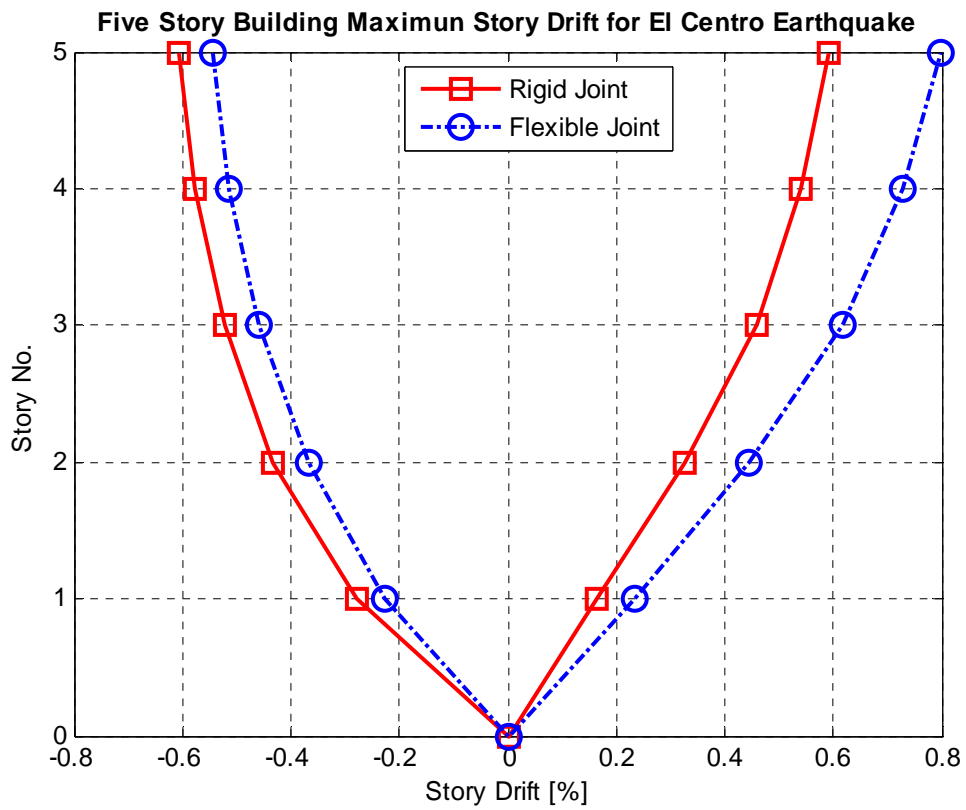


Figure 8-17 Maximum story drift for El Centro earthquake

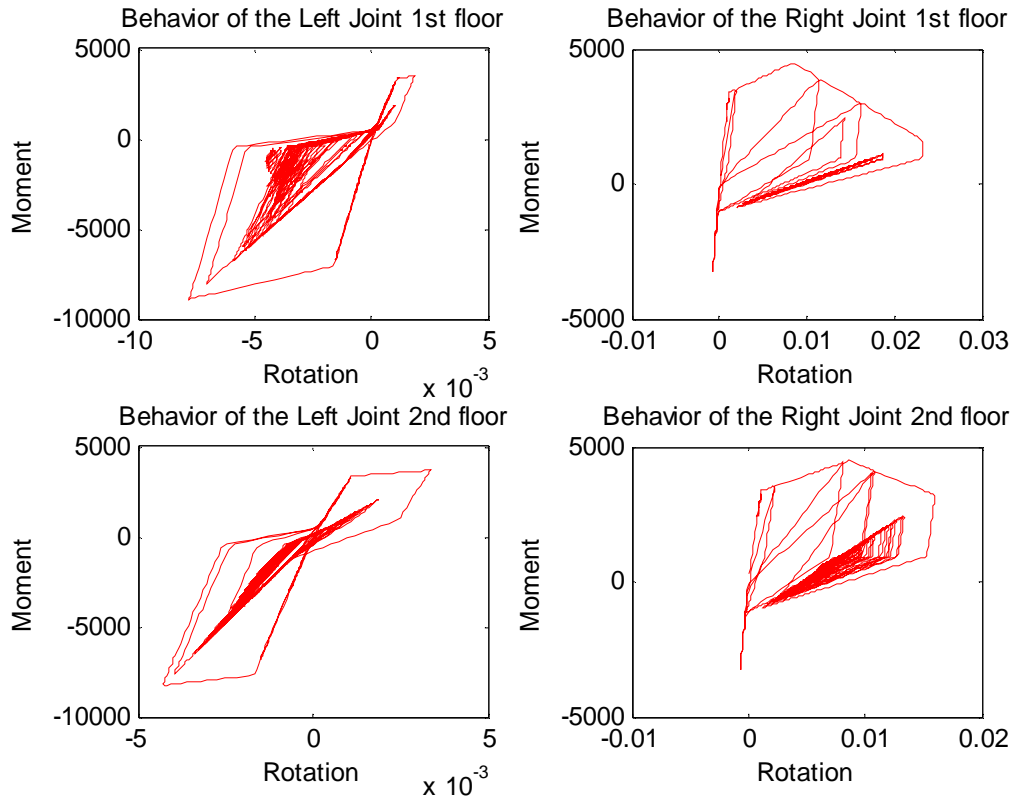


Figure 8-18 Local behavior of first story joints for El Centro earthquake

The comparison of the top story drift history for the two cases considered is shown in Figure 8-15. The maximum drifts to the right and left for the case of rigid joints were 0.59% (at 5.92 seconds) and -0.61% (at 2.96 seconds) respectively. For the case of flexible joints these values were 0.80% (at 6.02 seconds) and -0.54% (at 2.99 seconds) respectively. At around 6 seconds, when the maximum right drift for the flexible joints case occurred, all exterior right joints and the left joints of the first and second floor were cracked in their positive direction. In addition the right joint of the first, second and third floor reached their peak strength. It can be appreciated from Figure 8-18 that the right joint of the first floor was close to reaching the residual strength. At around 3 seconds, when the maximum left drift for the flexible joint

case occurred all left exterior joints were cracked in the negative direction. From these observations one can conclude that the peak values of the drift for the case of the flexible joints are mainly related to the inclusion of the flexible joints in the model, since at the time that these values took place the amount of plastic hinges formed in the beams and columns in both cases was very similar. This is also confirmed in Figure 8-17, which shows the comparison of the maximum drifts to the right and left per story for the two cases considered. At the end of the time history analyses it can be seen that both frames present permanent deformation since both drift traces were somewhat shifted from the origin.

8.5.1.2 RESULTS FOR THE MAYAGÜEZ EARTHQUAKE

The comparison of the top story drift history for the Mayagüez earthquake for the two cases considered is shown in Figure 8-19. The sequence of plastic hinges is presented in Figure 8-20. In this figure, the value within parentheses indicates the time in seconds at which the event occurred. The maximum drifts to the right and left for the five story frame are shown in Figure 8-21. Finally the local behavior of the first story joint is presented in Figure 8-22. A discussion of the above figures is presented next.

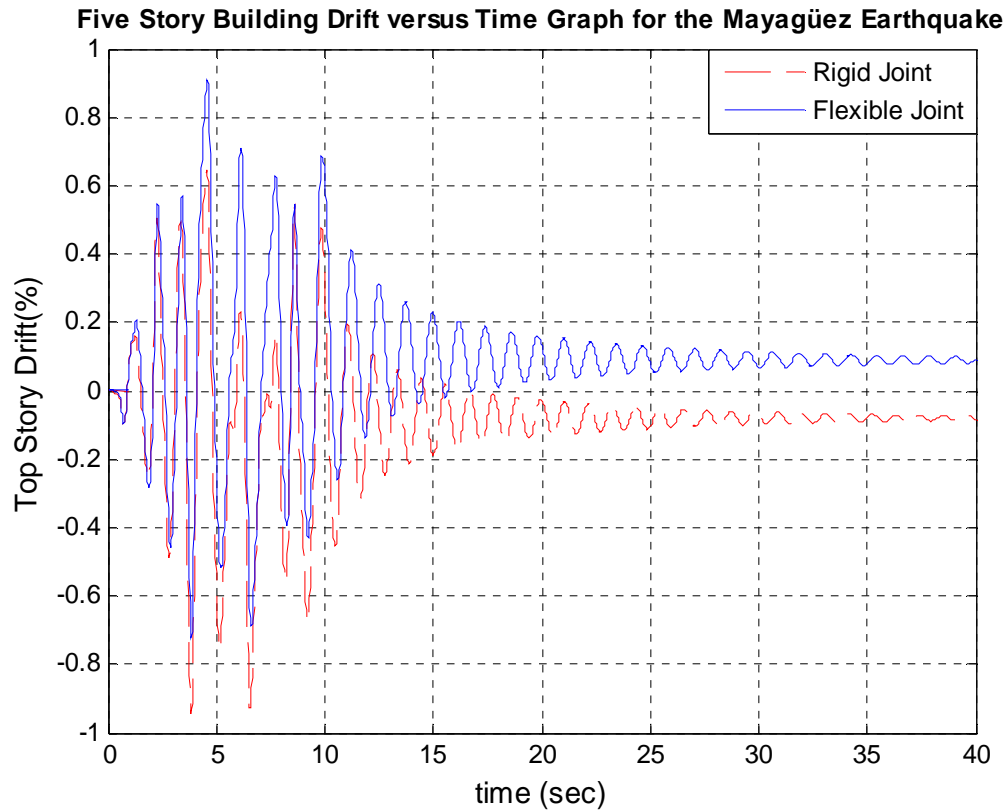


Figure 8-19 Top Story Drift versus time for the Mayagüez earthquake for the five story frame

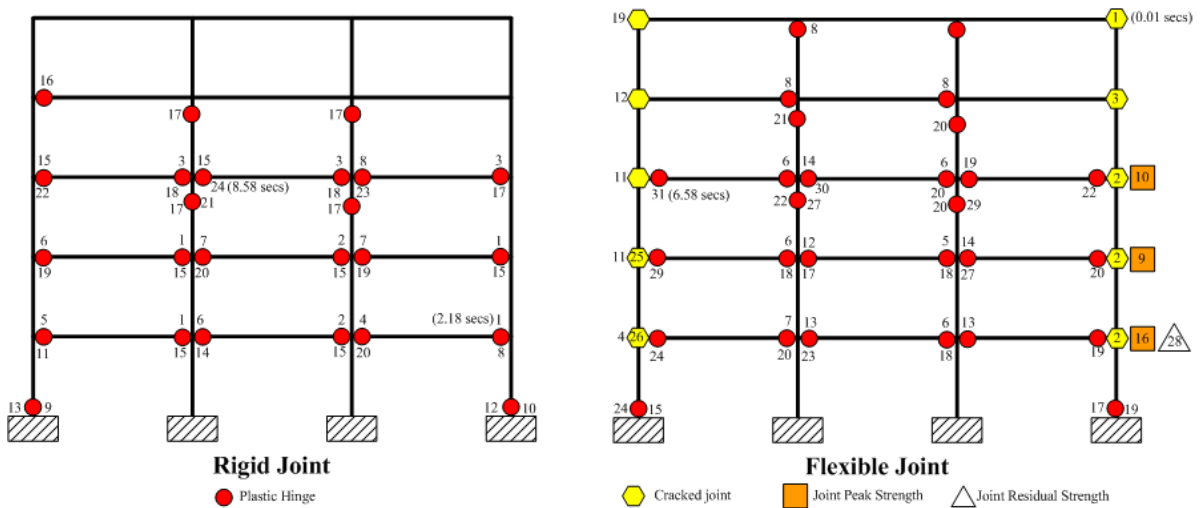


Figure 8-20 Sequence of plastic hinges for the five story frame for the Mayagüez earthquake

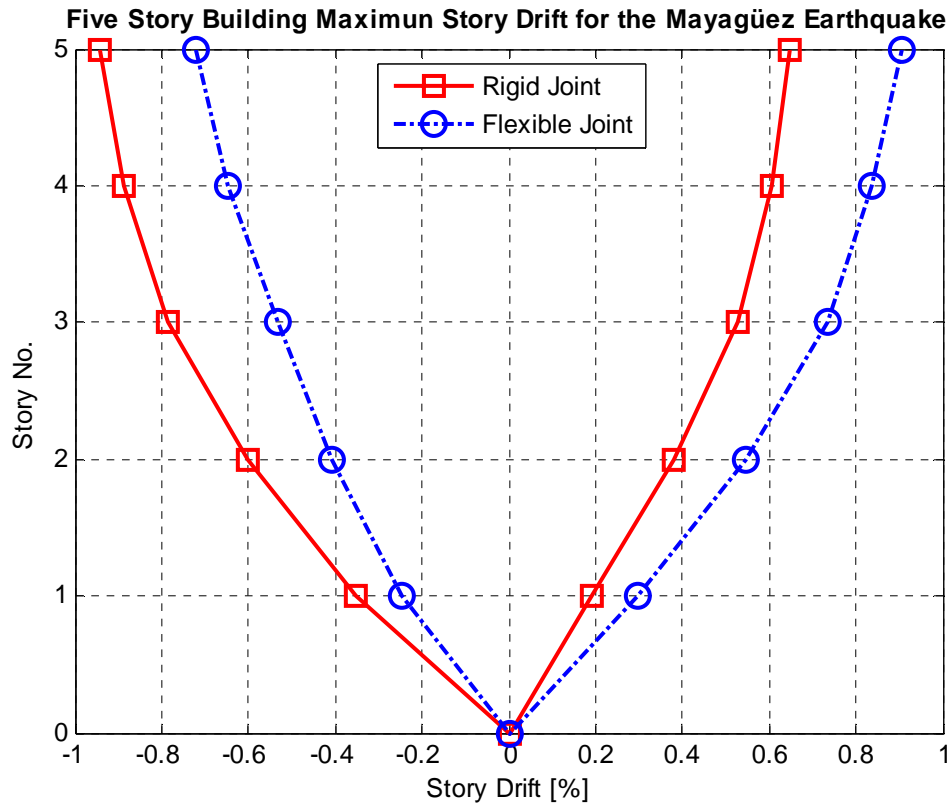


Figure 8-21 Maximum story drift for the Mayagüez earthquake

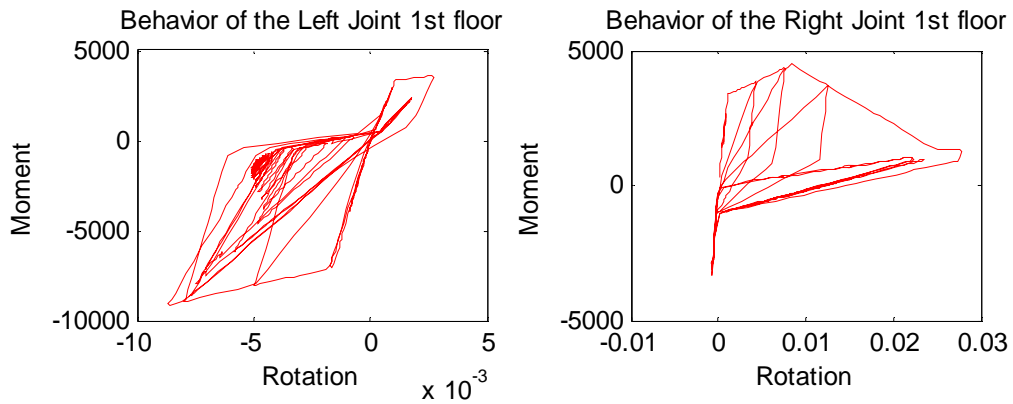


Figure 8-22 Local behavior of first story joints for the Mayagüez earthquake

The comparison of the top story drift history for the two cases considered is shown in Figure 8-19. The maximum drifts to the right and left for the case of rigid joints were 0.65% (at 4.56 seconds) and -0.94% (at 3.86 seconds) respectively. For the case of flexible joints these values were 0.91% (at 4.6 seconds) and -0.72% (at 3.86 seconds) respectively. It can be appreciated from this figure that the two curves are very similar in the first 3 seconds of the earthquake, since all peaks of both curves coincide. At about 4.6 seconds, when the maximum drift for the flexible joints case occurred, the first floor right joint reached its residual strength, the second and third floor right joints reached their peak strength and the remaining two joints of the right were cracked and thus this drift can be attributed directly to the damage suffered by right joints of the frame. This can be appreciated clearly in Figure 8-22 which shows the local behavior of the first story joints. At around 3.9 seconds, when the minimum drift for the flexible joint case occurred all left exterior joints were cracked in the negative direction. From these observations one can conclude that peak values of the drift for the case of the flexible joint are mainly related to the damage of the joints, since at the time that these values took place the amount of plastic hinges formed in beams and columns in both cases were similar. Finally, at the end of the analysis it can be appreciated that both cases present permanent deformation since both curves were shifted from the origin, however the flexible joint case curve is most shifted to the positive side since the damage in the right joint were larger than the damage in the joint of the left side.

8.5.1.3 RESULTS FOR THE MEXICO EARTHQUAKE

The comparison of the top story drift history for the Mexico earthquake for the two cases considered is shown in Figure 8-23. The sequence of plastic hinges is presented in Figure

8-24. The maximum drifts to the right and left for the five story frame are shown in Figure 8-25. Finally the local behavior of the first story joint is presented in Figure 8-26. A discussion of these figures is presented next.

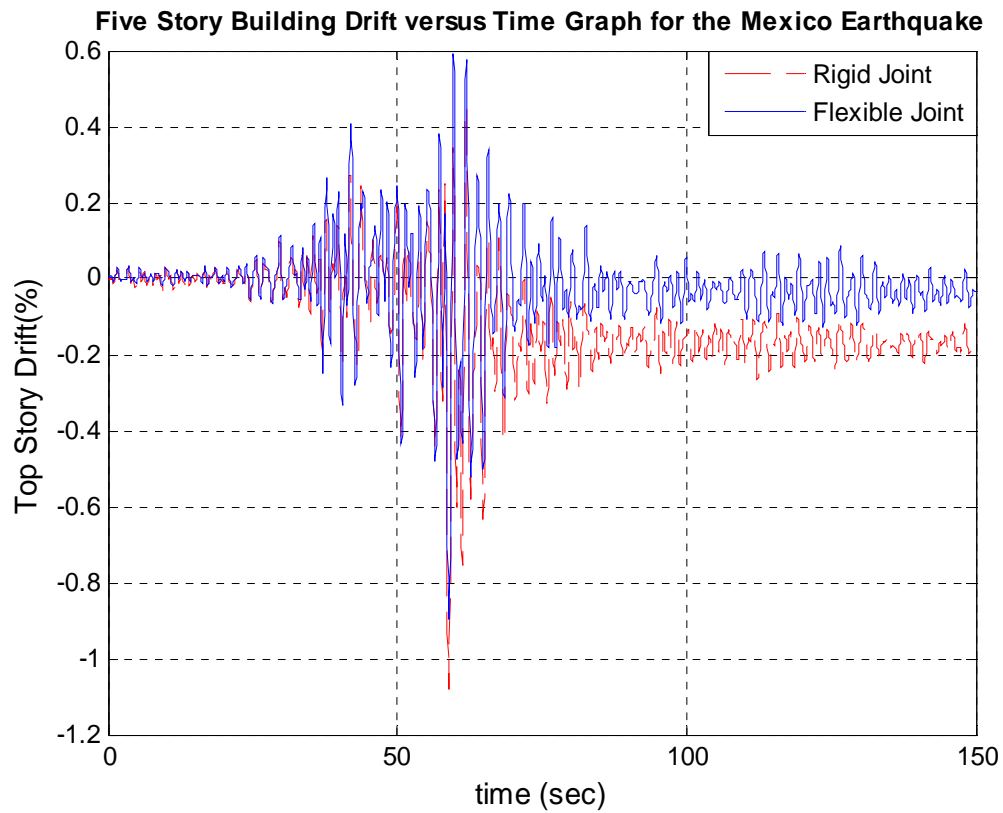


Figure 8-23 Top Story Drift versus time for the Mexico earthquake for the five story frame

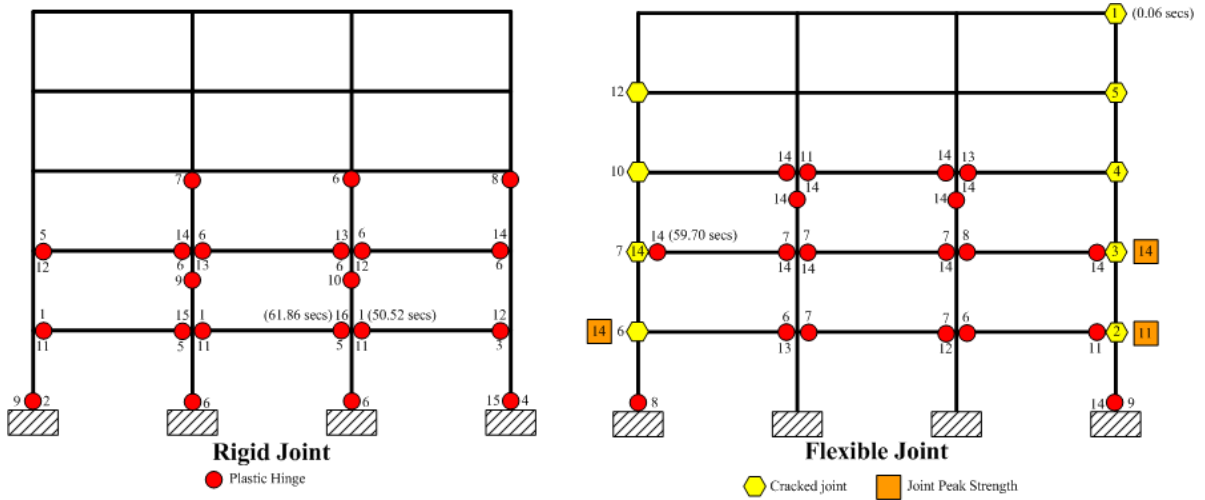


Figure 8-24 Sequence of plastic hinges for the five story frame for the Mexico earthquake

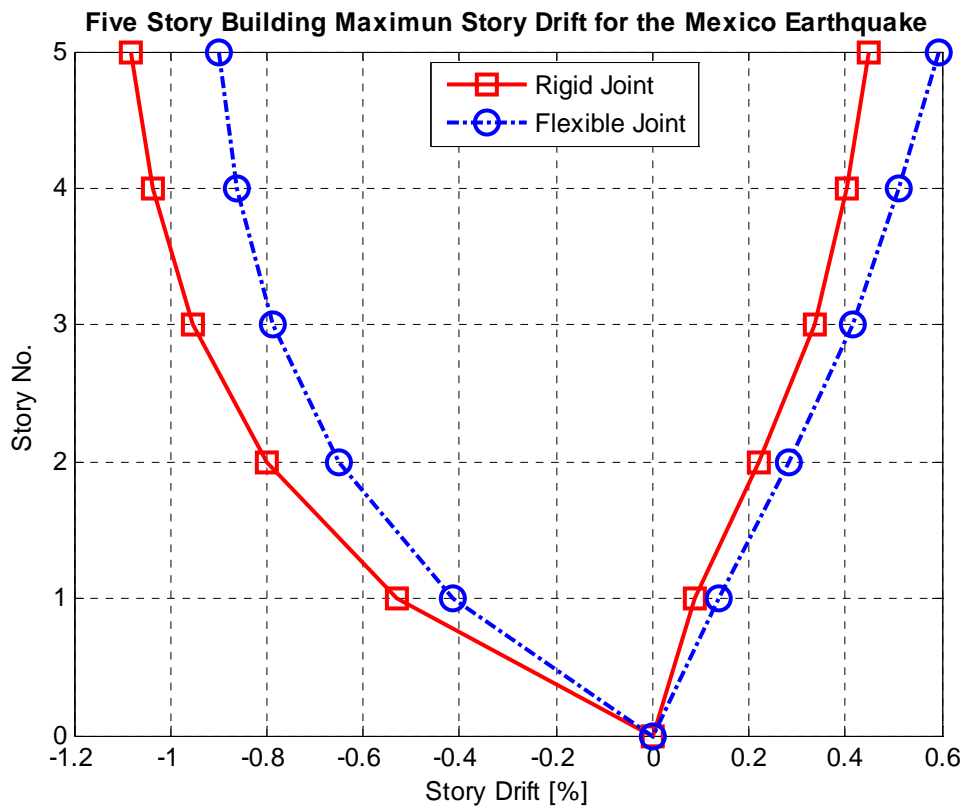


Figure 8-25 Maximum story drift for the Mexico earthquake

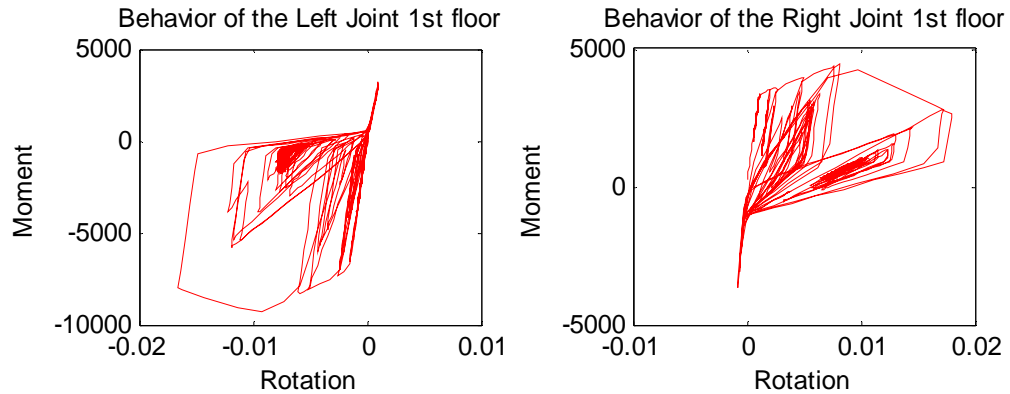


Figure 8-26 Local behavior of first story joints for the Mexico earthquake

The comparison of the top story drift history for the two cases considered is shown in Figure 8-23. The maximum drifts to the right and left for the case of rigid joints were 0.48% (at 61.92 seconds) and -1.09% (at 58.92 seconds) respectively. For the case of flexible joints these values were 0.59% (at 59.76 seconds) and -0.89% (at 59.04 seconds) respectively. Figure 8-23 also shows that the two curves were very similar, up to a time of 68 seconds approximately. For the maximum drift to the right, the frame with flexible joints has higher drift than the obtained for the rigid joint assumption, even though the plastic hinges formed are similar. The reason for this observation could be the fact that all exterior right joints were cracked in the positive direction, including that the joints of the first and second floor reached their peak strength. However for the maximum drift to the left, the frame with rigid joints has drift higher than the attained with the frame with flexible joints. This can be attributed to the fact that plastic hinges were formed in all columns of the first floor for the rigid joints assumption. This appears to be influenced more the drift since even though almost all joints of the left were cracked in the negative direction, including that the first story left joint reached its peak strength.

8.5.2 RESULTS FOR THE TEN STORY FRAME

8.5.2.1 RESULTS FOR EL CENTRO EARTHQUAKE

The comparison of the top story drift history for El Centro earthquake for the two cases considered is shown in Figure 8-27. The sequence of plastic hinges is presented in Figure 8-28. In this figure, the value between parentheses indicates the time in seconds in which the event occurred. Finally the maximum drifts to the right and left for the ten story frame are shown in Figure 8-29. A discussion of the above figures is presented next.

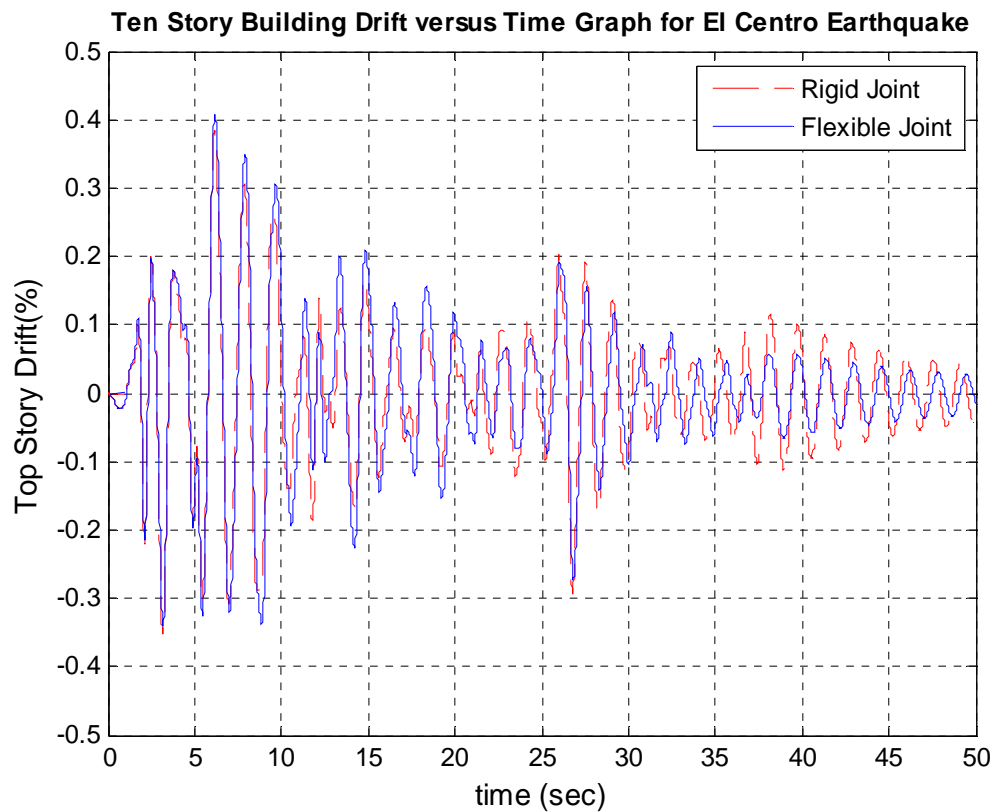


Figure 8-27 Top Story Drift versus time for El Centro earthquake for the ten story frame

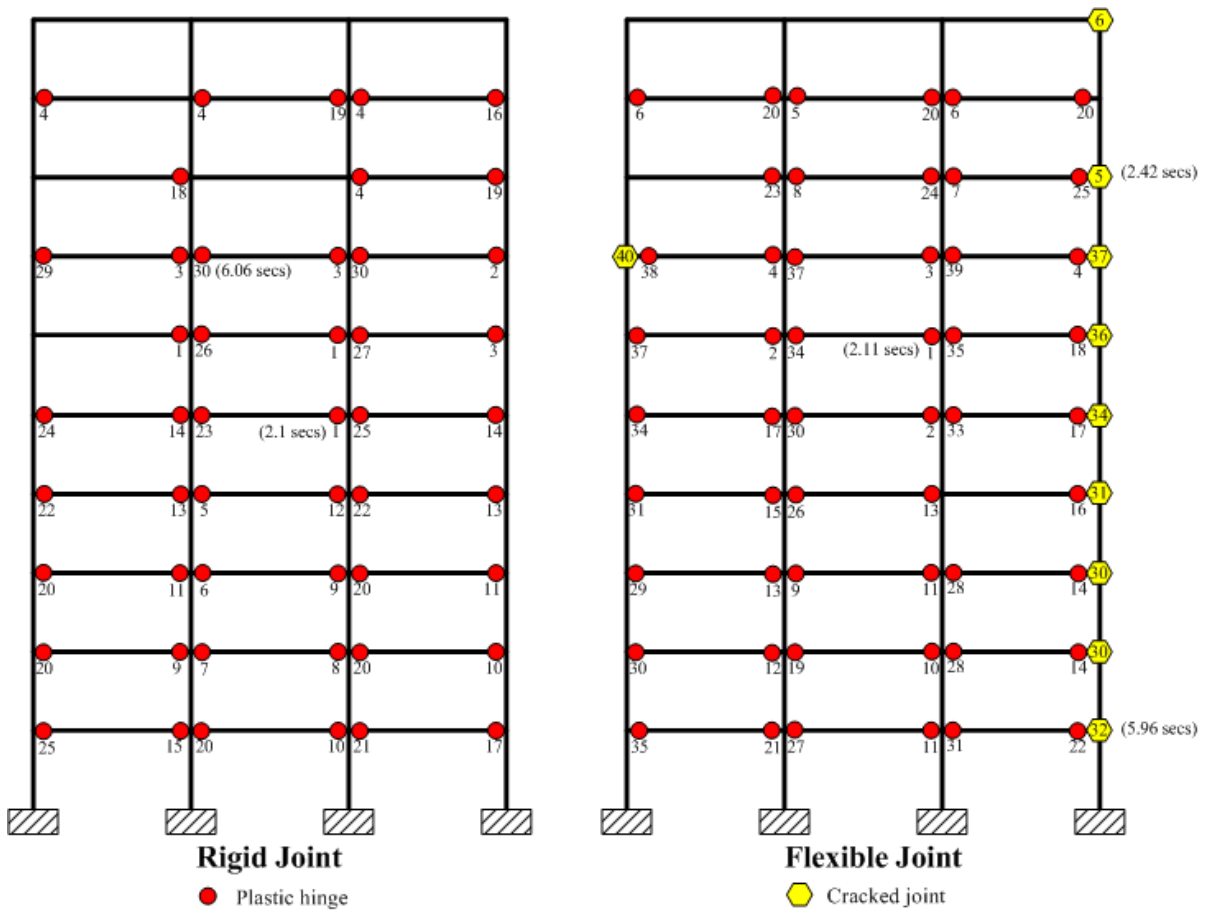


Figure 8-28 Sequence of plastic hinges for the ten story frame for El Centro earthquake

The comparison of the top story drift history for the two cases considered is shown in Figure 8-27. The maximum drifts to the right and left for the case of rigid joints were 0.38% (at 6.14 seconds) and -0.35% (at 3.17 seconds) respectively. For the case of flexible joints these values were 0.41% (at 6.17 seconds) and -0.34% (at 3.18 seconds) correspondingly. The last event for the rigid joint frame and for the flexible joint cases occurred at 6.06 and 6.15 seconds respectively. It can be appreciated from this figure that the two curves are very similar, since almost all peaks of both curve coincides during the first 35 seconds of the

quake. This coincidence is also observed in the number of plastic hinges (Figure 8-28) formed at the end of the analysis.

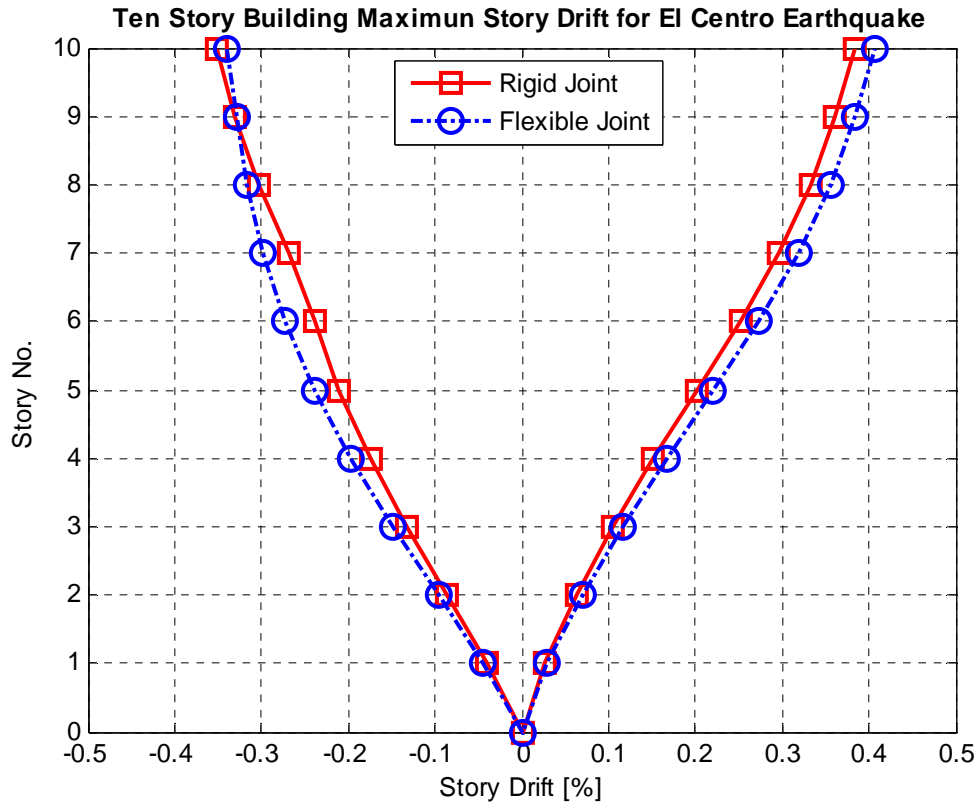


Figure 8-29 Maximum story drift for El Centro earthquake

The maximum drift to the right at each story for the flexible joints frame (Figure 8-29) are slightly higher than for the rigid joints frame even though the number of plastic hinges is almost the same for both cases. This can be attributed mainly to the presence of the joints, since 10 of them were cracked in the positive direction. The maximum drift to the left at each story for the flexible joints frame is also slightly higher for the first eight floors of the frame. This fact also is attributed to the presence of the joints model, even though none of the joints of the frame is cracked in the negative direction, since the elastic stiffness of the flexible joints is lower than the rigid joints.

8.5.2.2 RESULTS FOR THE MAYAGÜEZ EARTHQUAKE

The comparison of the top story drift history for the Mayagüez earthquake for the two cases considered is shown in Figure 8-30. The sequence of plastic hinges is presented in Figure 8-31. In this figure, the value within parentheses indicates the time in seconds at which the event occurred. Finally the maximum drifts to the right and left for the ten story frame are shown in Figure 8-32. A discussion of the above figures is presented in the next section.

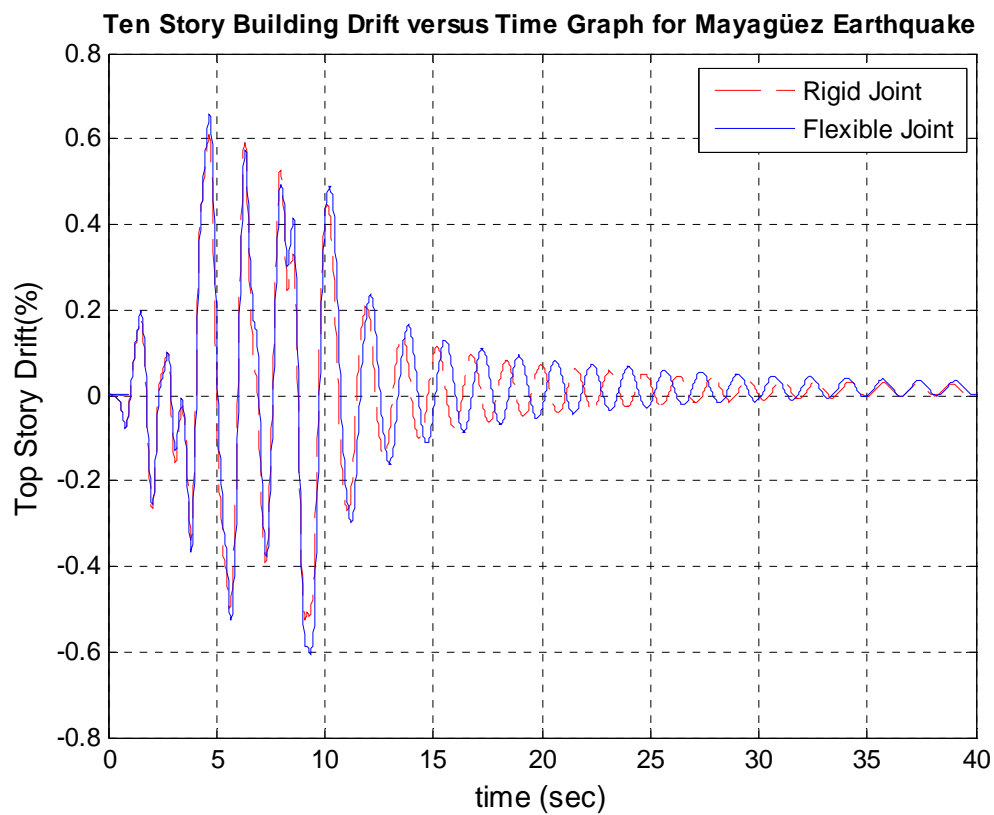


Figure 8-30 Top Story Drift versus time for the Mayagüez earthquake for the ten story frame

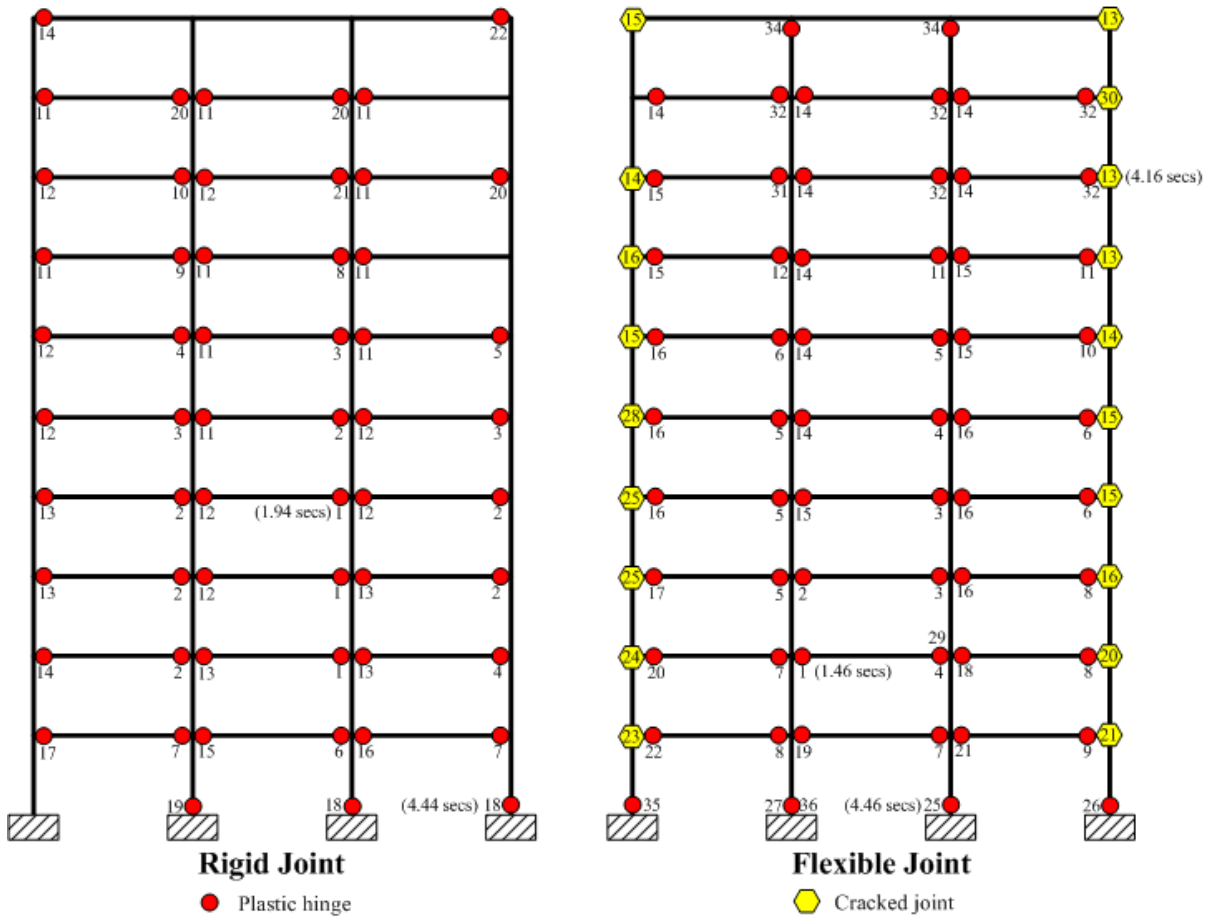


Figure 8-31 Sequence of plastic hinges for the ten story frame for the Mayagüez earthquake

The comparison of the top story drift history for the two cases considered is shown in Figure 8-30. The maximum drifts to the right and left for the case of rigid joints were 0.61% (at 4.78 seconds) and -0.53% (at 9.08 seconds) respectively. For the case of flexible joints these values were 0.66% (at 4.68 seconds) and -0.60% (at 9.32 seconds) correspondingly. The last event for the rigid joints frame and for the flexible joints cases occurred at 9.02 and 9.24 seconds respectively. It can be appreciated from this figure that the two curves are very similar, since almost all peaks of both curve coincides during the first 10 seconds of the

quake. This coincidence is also observed in the number of plastic hinges (Figure 8-31) formed at the end of the analysis.

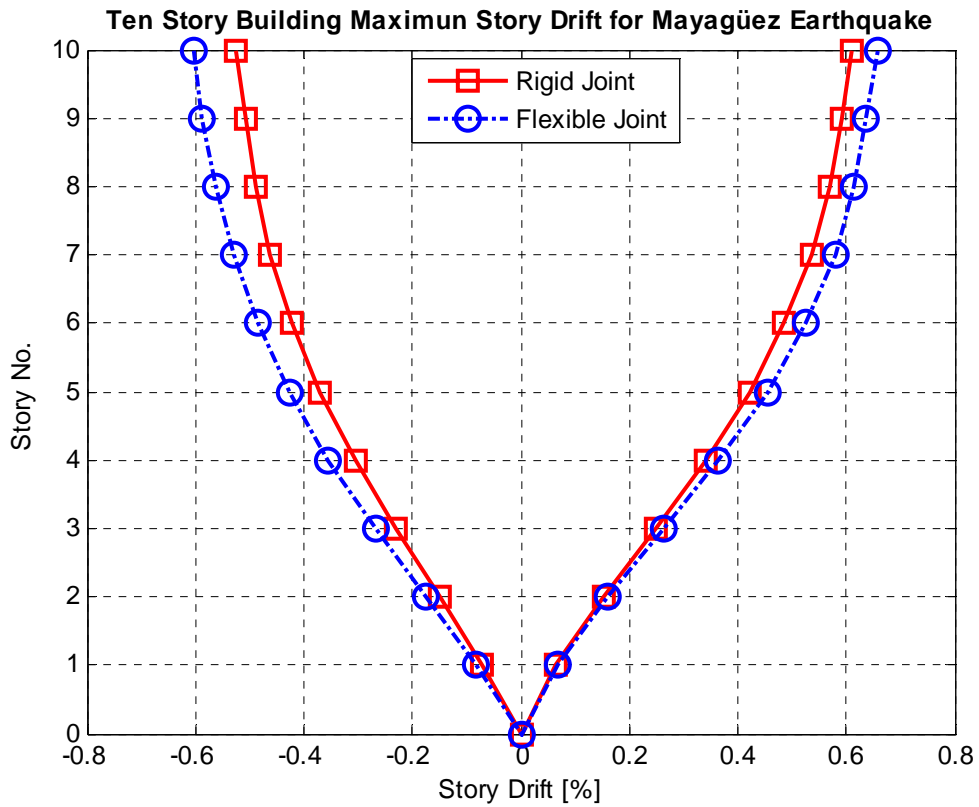


Figure 8-32 Maximum story drift for the Mayagüez earthquake

The maximum drift to the right and left at each story of the frame (Figure 8-31) is higher for the flexible joint case, since at the end of the analysis 95% of the exterior joints of the frame were cracked.

8.5.2.3 RESULTS FOR THE MEXICO EARTHQUAKE

The comparison of the top story drift history for the Mexico earthquake for the two cases considered is shown in Figure 8-33. The sequence of plastic hinges is presented in Figure 8-34. Finally the maximum drift to the right and left for the ten story frame are shown in Figure 8-35. A discussion of the above figures is presented in the next section.

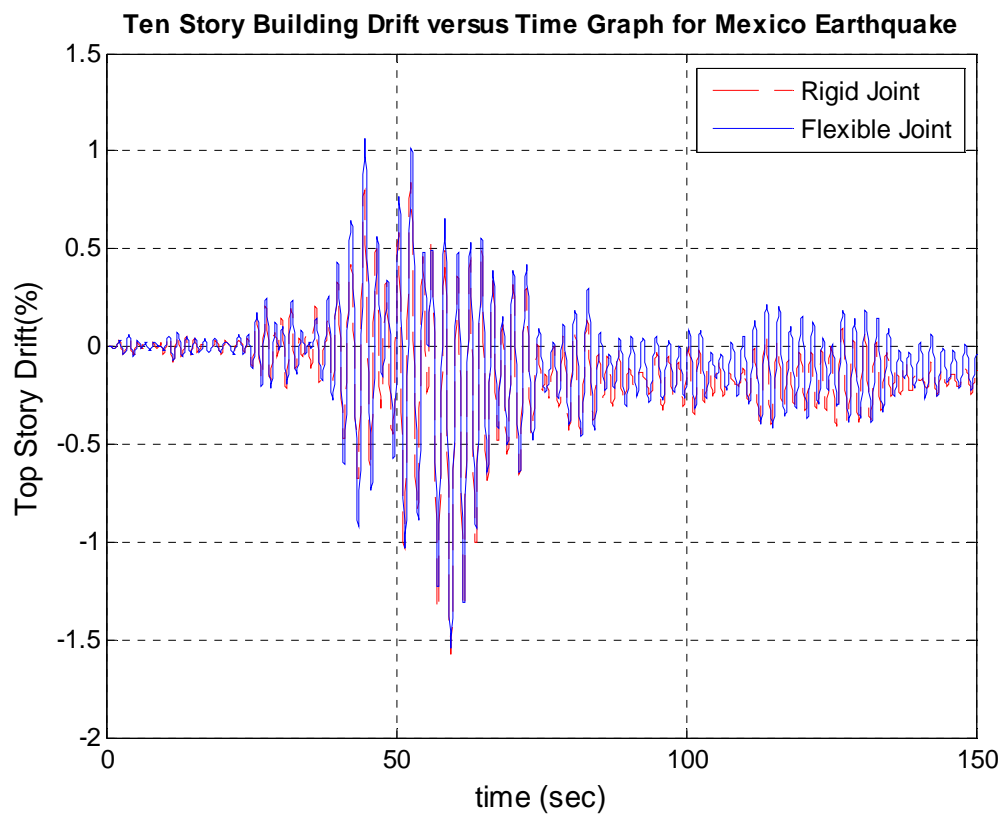


Figure 8-33 Top Story Drift versus time for the Mexico earthquake for the ten story frame

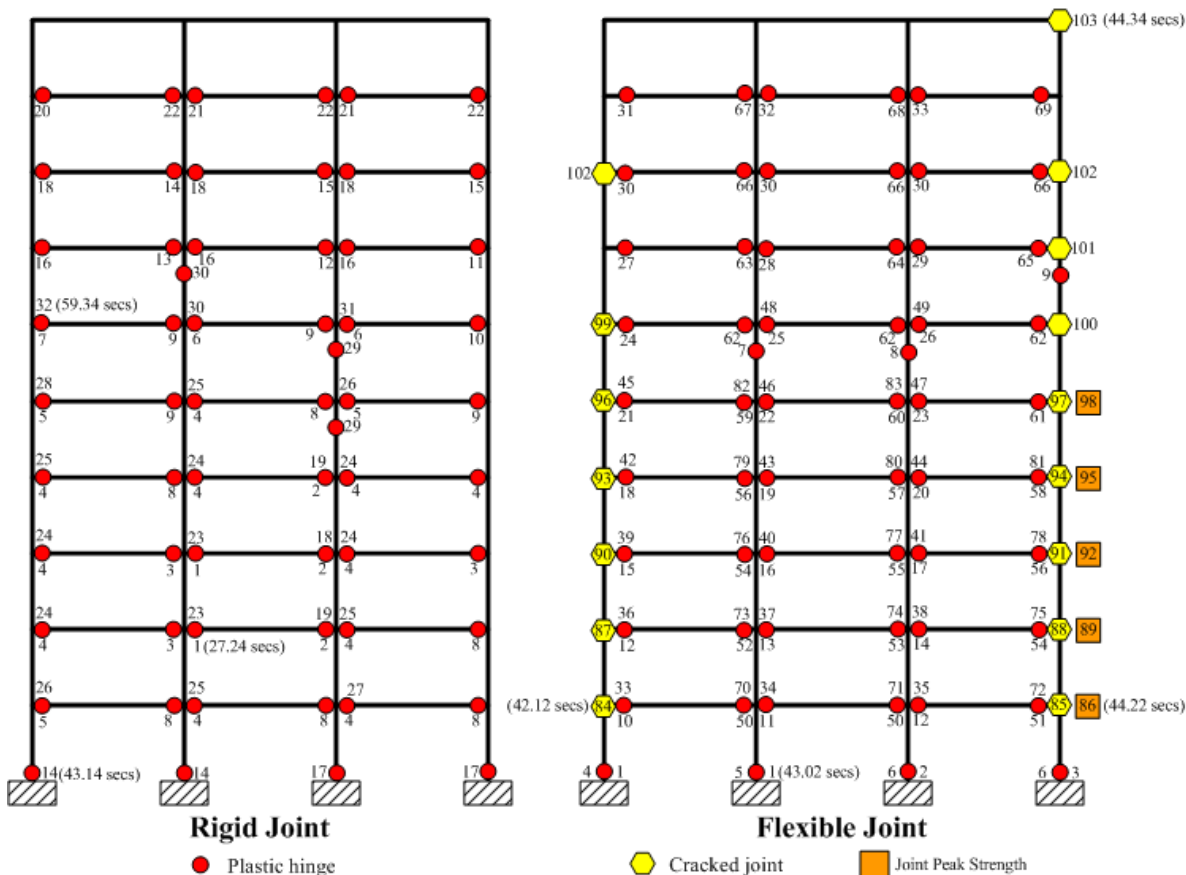


Figure 8-34 Sequence of plastic hinges for the ten story frame for the Mexico earthquake

The comparison of the top story drift history for the two cases considered is shown in Figure 8-33. The maximum drifts to the right and left for the case of rigid joints were 0.80% (at 44.34 seconds) and -1.60% (at 59.28 seconds) respectively. For the case of flexible joints these values were 1.06% (at 59.28 seconds) and -1.54% (at 59.28 seconds) correspondingly. The last event for both cases occurred at 59.34 seconds. It can be appreciated from this figure that the two curves are very similar, since almost all peaks of both curves coincide during the first 83 seconds of the quake. This coincidence is also observed in the number of plastic hinges (Figure 8-34) formed at the end of the analysis.

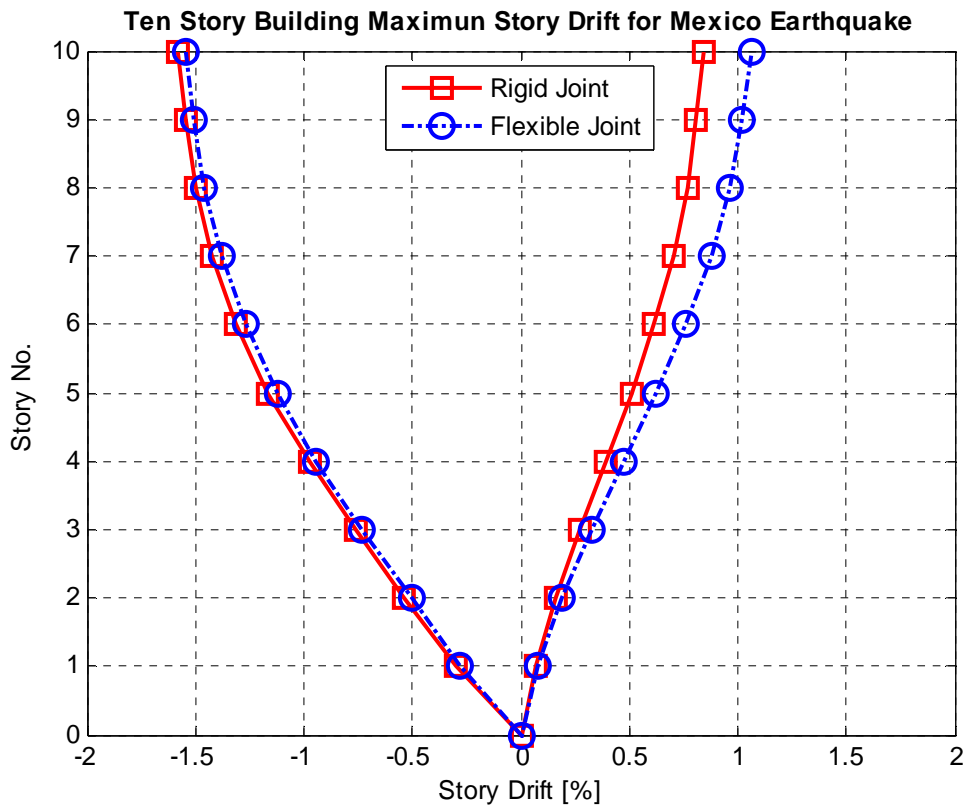


Figure 8-35 Maximum story drift for the Mexico earthquake

The maximum drifts to the right at each story for the flexible joints frame (Figure 8-35) are higher than for the rigid joints frame even though the number of plastic hinges is almost the same for both cases. This can be attributed mainly to the presence of the joints, since 16 of them (80%) were cracked in the positive direction, including that five of them attained their peak strength. The maximum drift to the left at each story for both frames is almost the same in all floor of the frame.

8.5.3 RESULTS FOR THE 15 STORY FRAME

8.5.3.1 RESULTS FOR EL CENTRO EARTHQUAKE

The comparison of the top story drift history for El Centro earthquake for the two cases considered is shown in Figure 8-36. The sequence of plastic hinges is presented in Figure 8-37. In this figure, the value within parentheses indicates the time in seconds at which the event occurred. Finally the maximum drifts to the right and left for the two story frame are shown in Figure 8-38. A discussion of these figures is presented next.

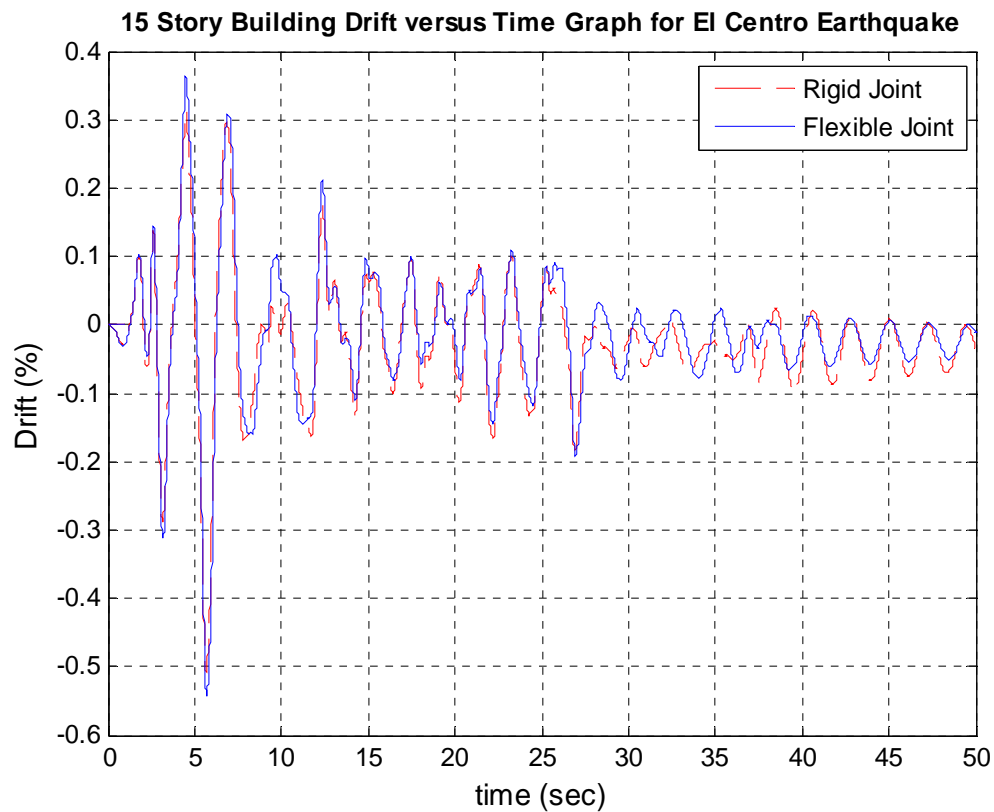
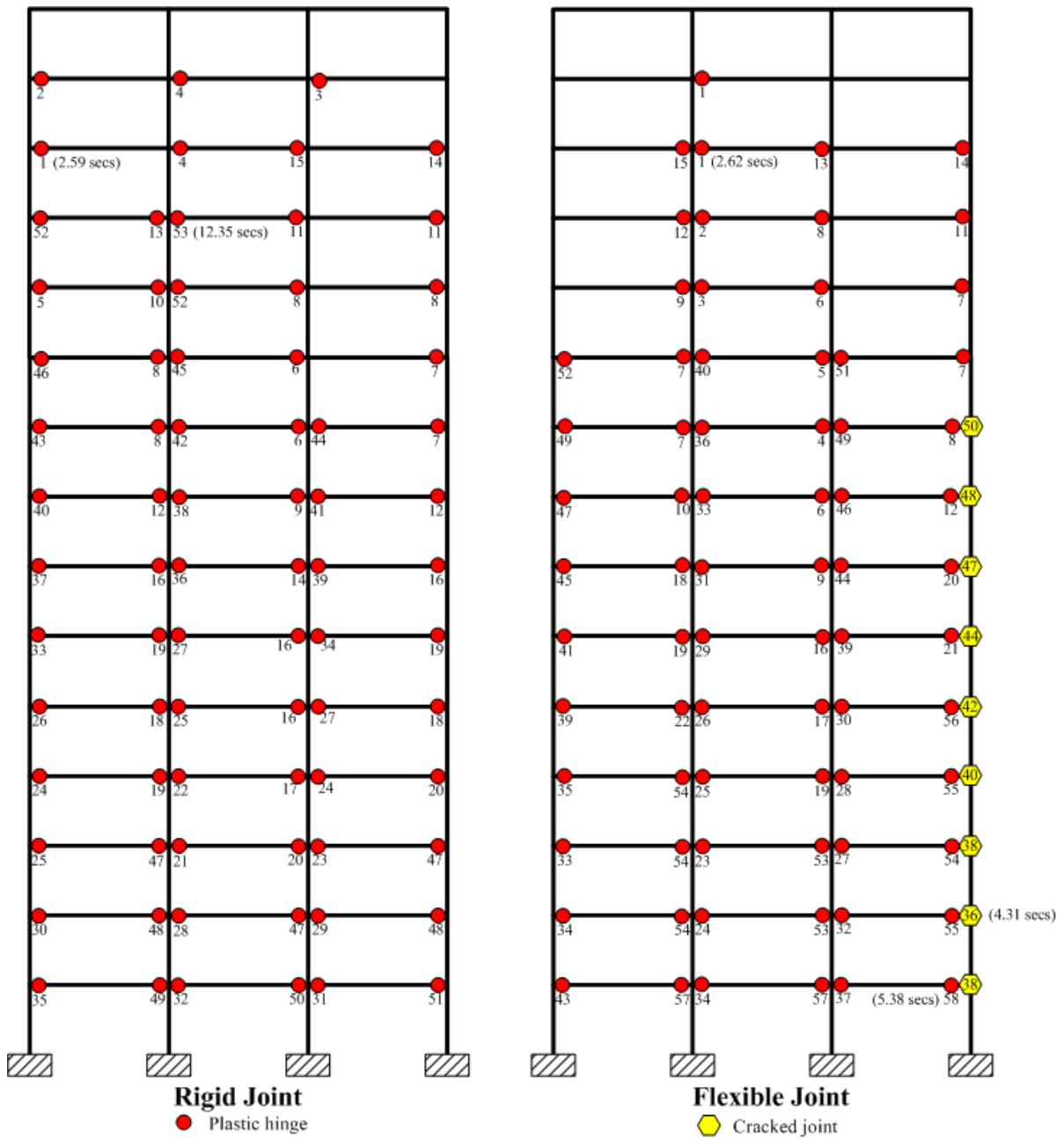


Figure 8-36 Top Story Drift versus time for El Centro earthquake for the 15 story frame



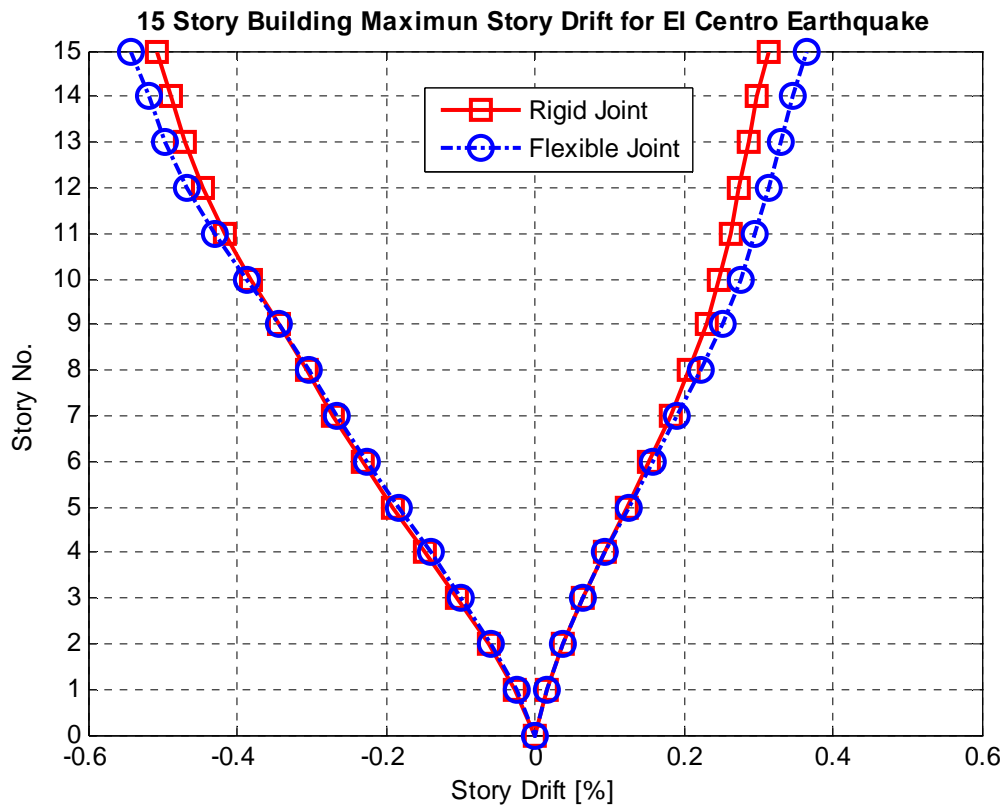


Figure 8-38 Maximum story drift for the El Centro earthquake

The comparison of the top story drift history for the two cases considered is shown in Figure 8-36. The maximum drifts to the right and left for the case of rigid joints were 0.31% (at 4.64 seconds) and -0.51% (at 5.68 seconds) respectively. For the case of flexible joints these values were 0.36% (at 4.51 seconds) and -0.54% (at 5.67 seconds) respectively. The last event for the rigid joints frame and for the flexible joints cases occurred at 12.35 and 5.38 seconds respectively. It can be observed from Figure 8-36 that the two curves are very similar, since almost all peaks of both curve coincides during the first 27 seconds of the quake. The number of plastic hinges (Figure 8-37) formed at the end of the analysis was also very similar. As it can be seen in Figure 8-38, the maximum drift to the right at each story is

almost the same for the two cases, up to the seventh floor. From this floor up to the last floor the drift was gradual increasing. For the case of the maximum drift to the left, somewhat seemed also occurred since up to the tenth floor the drift was almost the same for both cases. It then increases gradually up to the last floor and it is higher for the flexible joints frame. In both cases, this behavior is related to the presence of the joint even though only 9 of them (30%) were cracked during the analysis.

8.5.3.2 RESULTS FOR THE MAYAGÜEZ EARTHQUAKE

The comparison of the top story drift history for El Centro earthquake for the two cases considered is shown in Figure 8-39. The sequence of plastic hinges is presented in Figure 8-40. In this figure, the value within parentheses indicates the time in seconds at which the event occurred. Finally the maximum drifts to the right and left for the two story frame are shown in Figure 8-41. A discussion of the figures is presented in the next paragraphs.

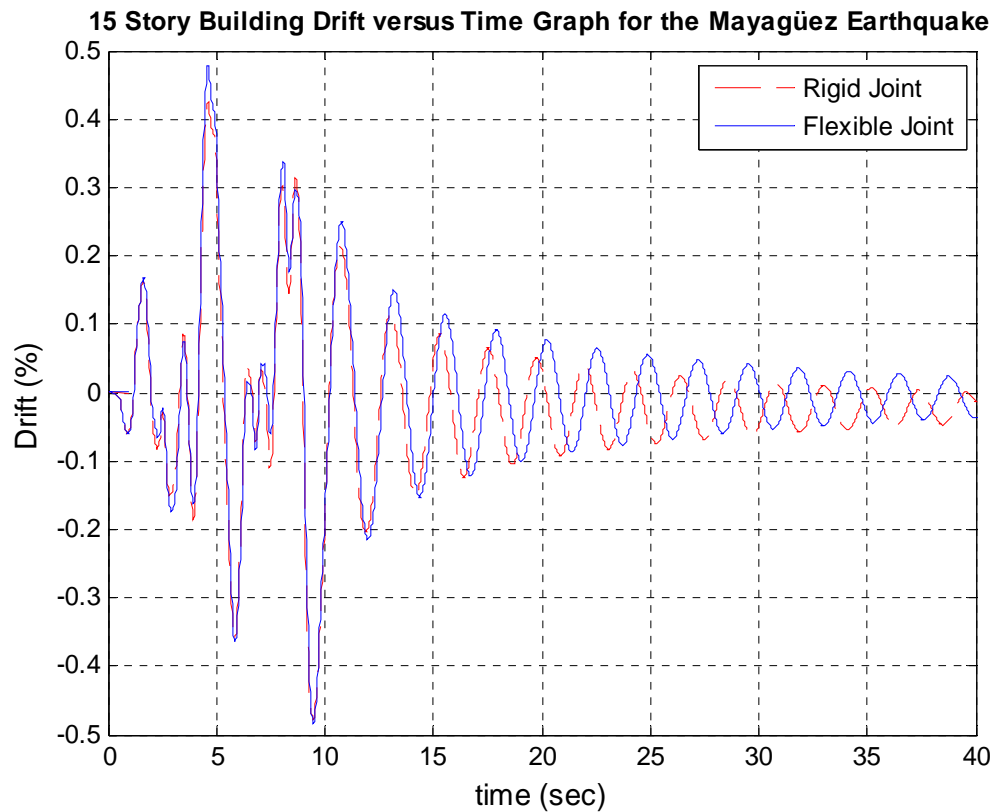


Figure 8-39 Top Story Drift versus time for the Mayagüez earthquake for the 15 story frame

The comparison of the top story drift history for the two cases considered is shown in Figure 8-39. The maximum drifts to the right and left for the case of rigid joints were 0.42% (at 4.66 seconds) and -0.48% (at 9.48 seconds) respectively. For the case of flexible joints these values were 0.48% (at 4.62 seconds) and -0.49% (at 9.48 seconds) respectively. The last event for the rigid joints frame and for the flexible joints cases occurred at 9.2 and 8.88 seconds respectively. Figure 8-41 shows that the two curves are very similar, since almost all peaks of both curve coincides during the first 11 seconds of the quake.

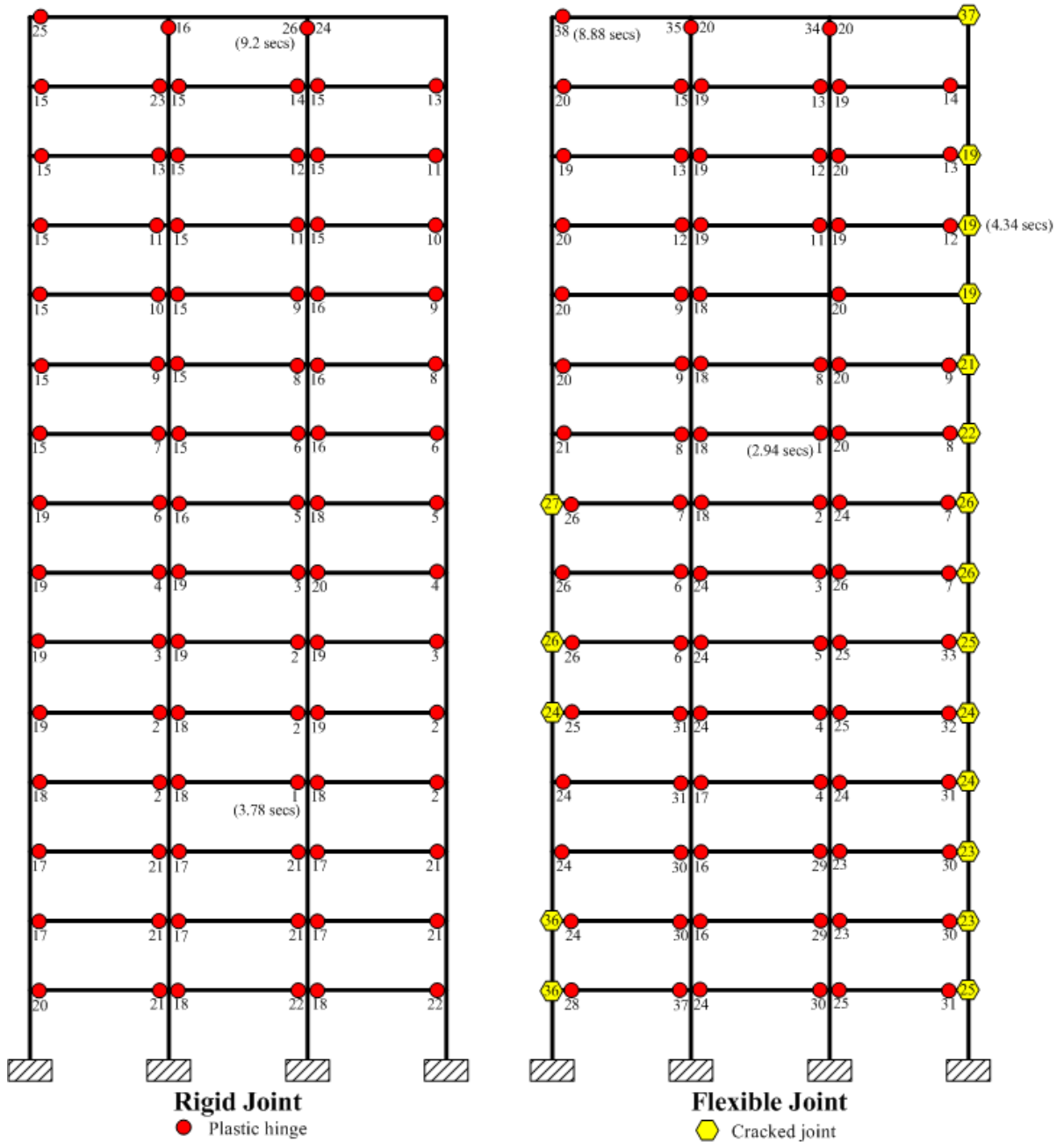


Figure 8-40 Sequence of plastic hinges for the 15 story frame for the Mayagüez earthquake

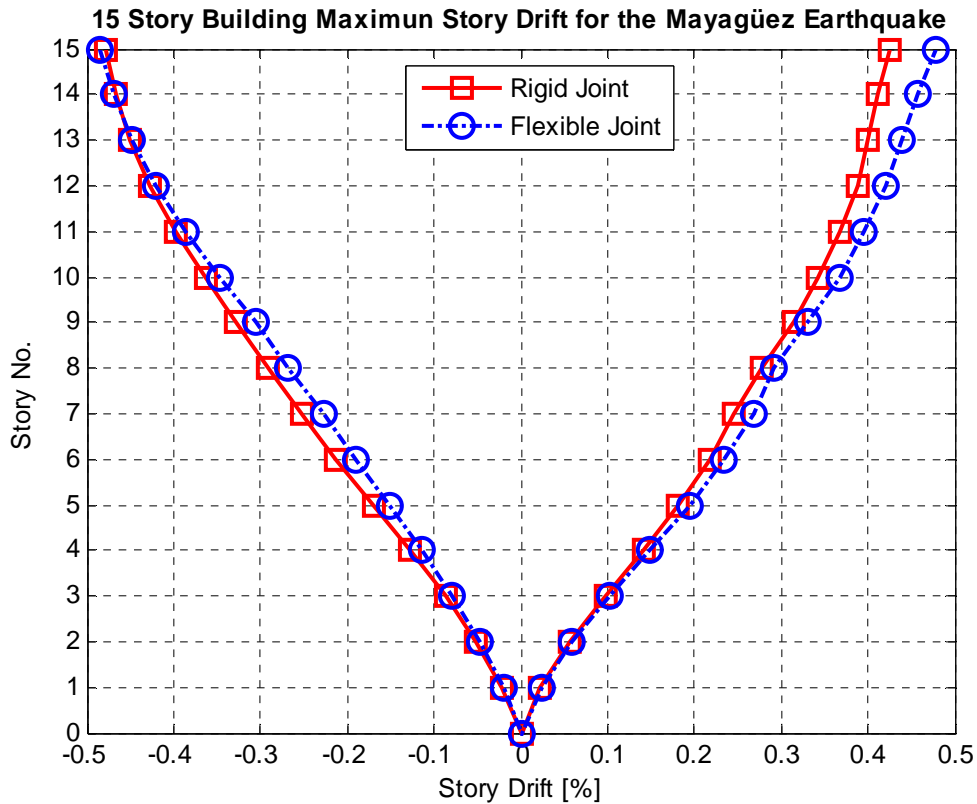


Figure 8-41 Maximum story drift for the Mayagüez earthquake

The number of plastic hinges (Figure 8-40) formed at the end of the analysis was the same for both cases. As it can be appreciated from Figure 8-41, the maximum drift to the right at each story for the flexible joints case was greater than for the rigid joints case. Even though the number of plastic hinges is the same for both case, it is evident that this difference in drift is due to the presence of the joint model, since 19 (63%) of the joints were cracked at the end of the analysis.

8.5.3.3 RESULTS FOR THE MEXICO EARTHQUAKE

The comparison of the top story drift history for El Centro earthquake for the two cases considered is shown in Figure 8-42. The sequence of plastic hinges is presented in Figure 8-43. In this figure, the values within parentheses indicate the time in seconds at which the event occurred. Finally the maximum drifts to the right and left for the fifteen story frame is shown in Figure 8-44. A discussion of the figures is presented in the next section

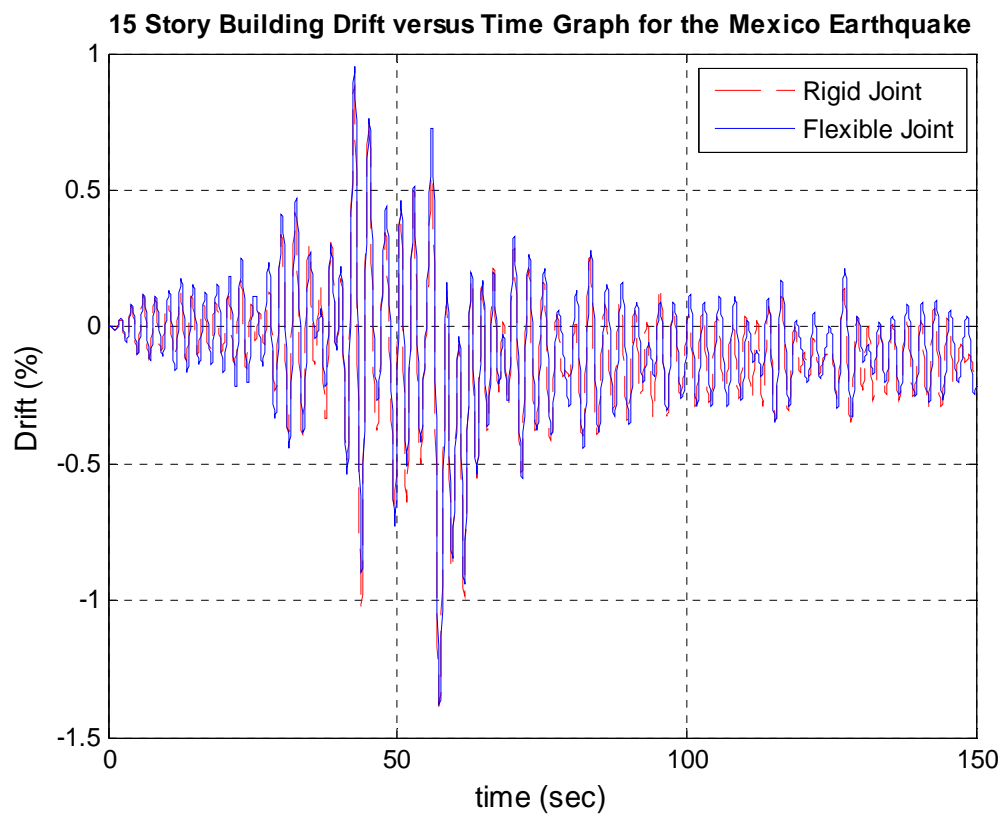


Figure 8-42 Top Story Drift versus time for the Mexico earthquake for the 15 story frame

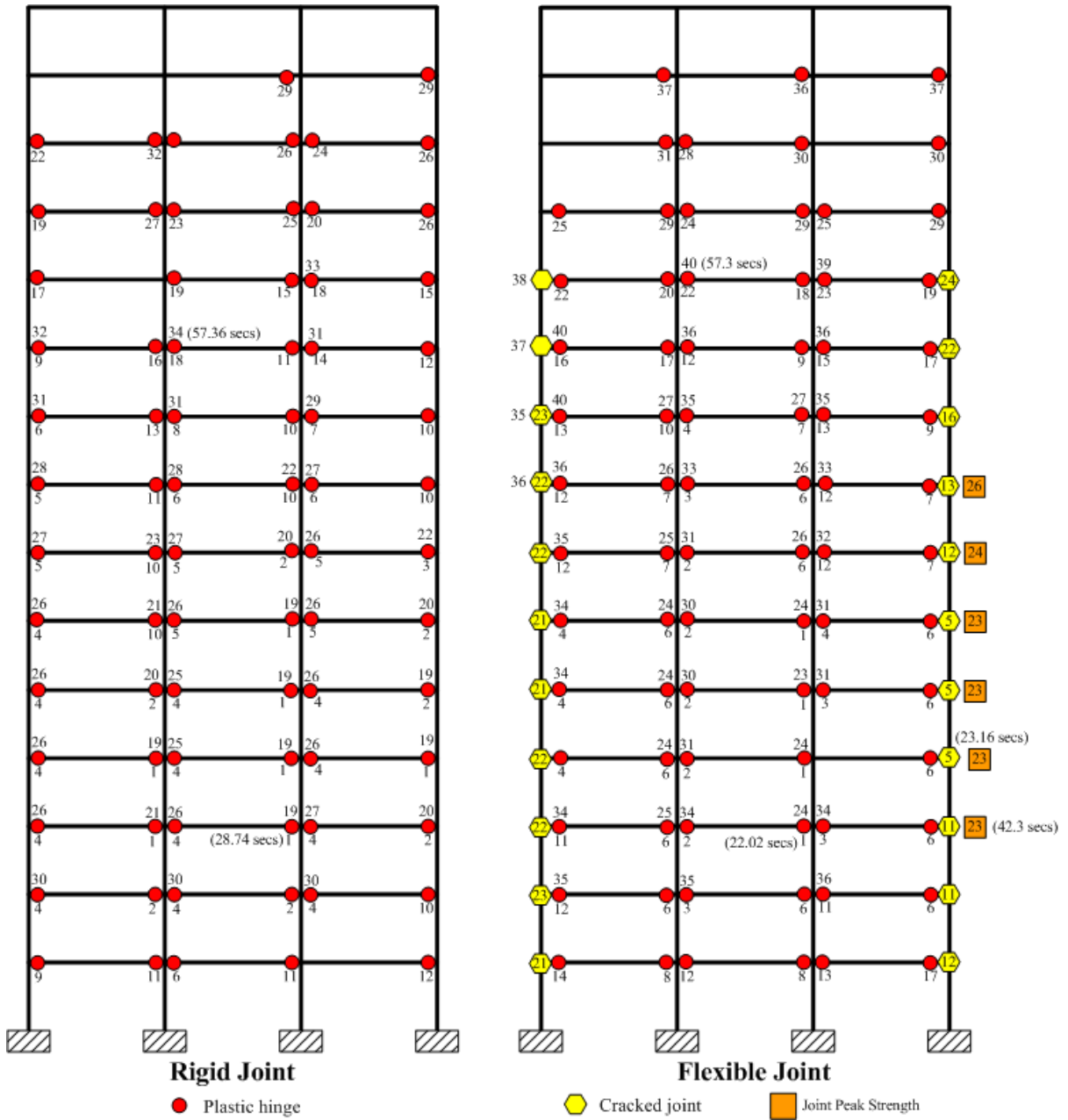


Figure 8-43 Sequence of plastic hinges for the 15 story frame for the Mexico earthquake

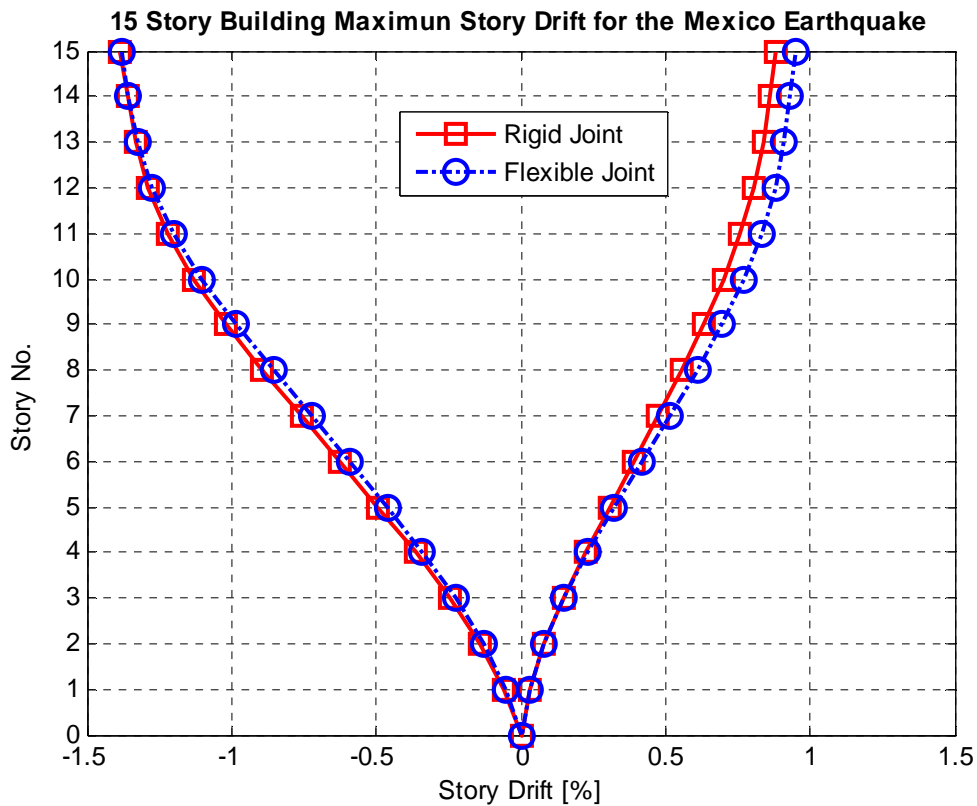


Figure 8-44 Maximum story drift for the Mexico earthquake

The comparison of the top story drift history for the two cases considered is shown in Figure 8-42. The maximum drifts to the right and left for the case of rigid joints were 0.88% (at 42.6 seconds) and -1.39% (at 57.3 seconds) respectively. For the case of flexible joints these values were 0.95% (at 42.66 seconds) and -1.38% (at 57.36 seconds) correspondingly. The last event for both cases occurred at 57.36 seconds. It can be appreciated from this figure that the two curves are very similar, since all peaks of both curve occurs at almost the same time during the analysis. The maximum drift to the right at each story for the flexible joints frame (Figure 8-44) are slightly higher than for the rigid joints frame even though the number of plastic hinges is almost the same for both cases. This can be attributed mainly to the presence of the flexible joints, since 22 of them (73%) were cracked in the positive direction,

including that six of them attained their peak strength. The maximum drift to the left at each story for both frames is almost the same in all floor of the frame

8.6 COMPARISON OF THE RESPONSE FROM THE STATIC AND DYNAMIC ANALYSES

The maximum values of the total base shear and the drift obtained from the dynamic analysis for the five, ten and fifteen story frames, for the rigid and flexible joint assumption are summarized in Table 8-3. It is important to mention that these values do not necessarily occurred at the same time in the dynamic analyses.

Table 8-3 Summary of maximum response from the dynamic analysis

Building	Earthquake	Drift (%)		Base Shear (Kips)	
		Rigid	Flexible	Rigid	Flexible
5 Story	El Centro	0.61	0.8	403	373
	Mayaguez	0.94	0.91	400	354
	Mexico	1.08	0.9	420	400
10 Story	El Centro	0.38	0.41	445	454
	Mayaguez	0.61	0.66	711	659
	Mexico	1.58	1.54	741	726
15 Story	El Centro	0.51	0.54	567	534
	Mayaguez	0.48	0.49	758	709
	Mexico	1.39	1.38	834	802

In order to have an idea of how damaged are the frames, the values of the maximum response from Table 8-3 were plotted against the original pushover curves for both the rigid and flexible assumptions, for the five, ten and fifteen story building frames. They are shown in Figures 8-45 through 8-50.

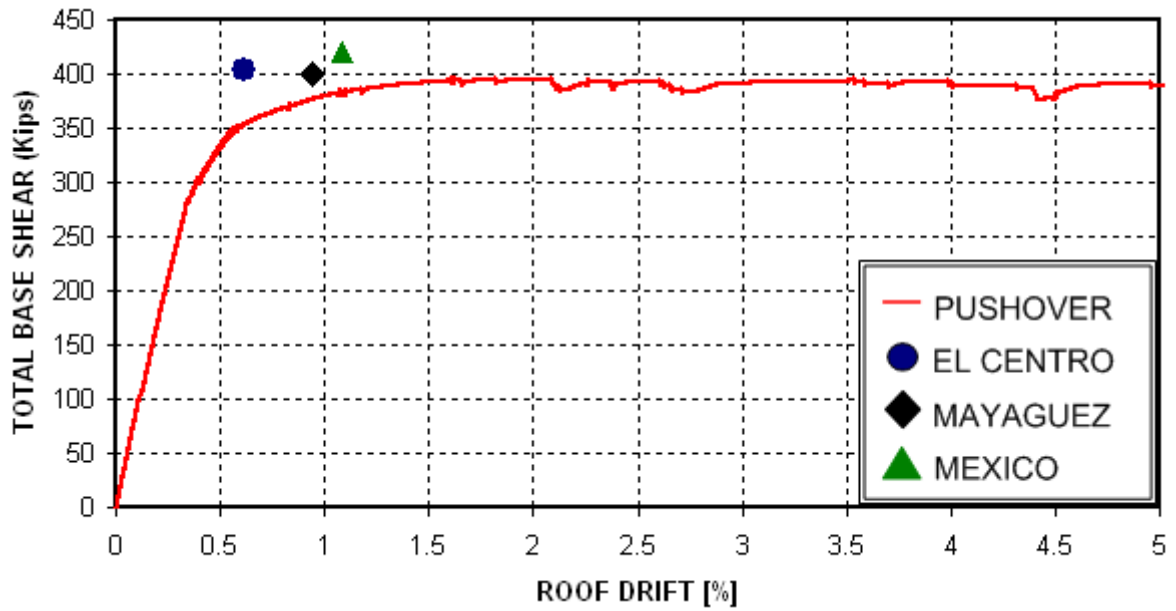


Figure 8-45 Static versus dynamic response for the five story building with rigid joints

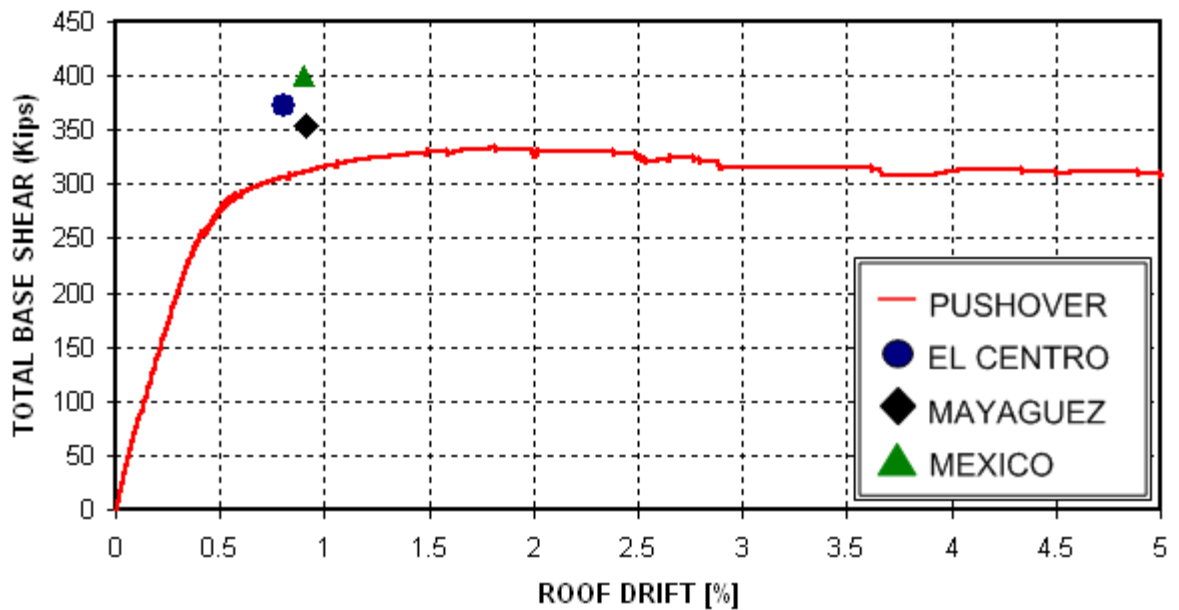


Figure 8-46 Static versus dynamic response for the five story building with flexible joints

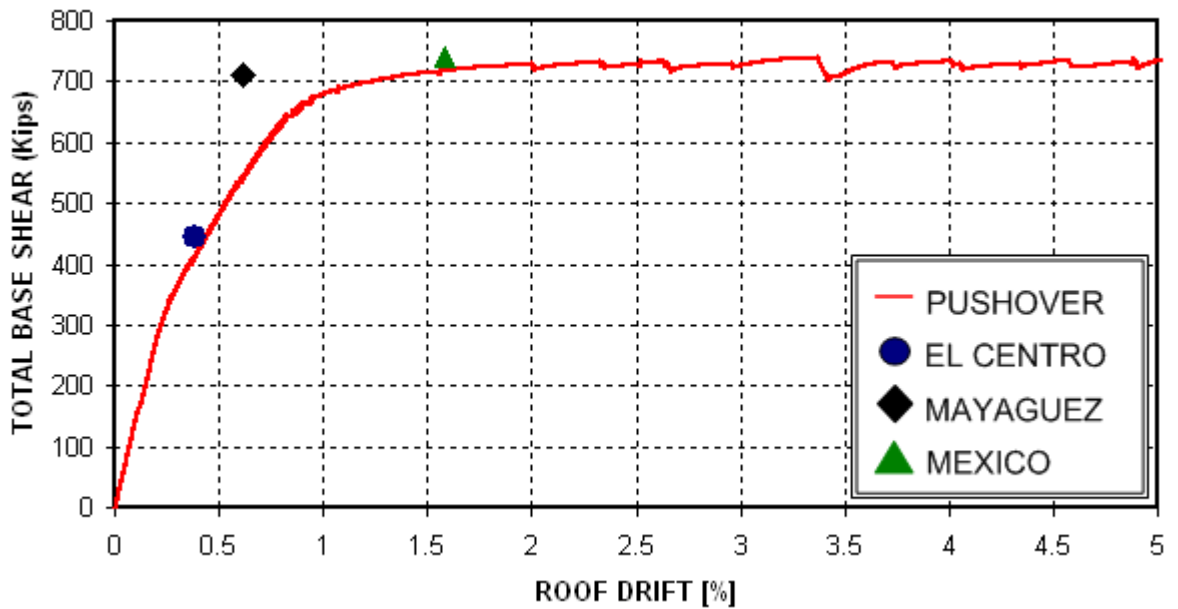


Figure 8-47 Static versus dynamic response for the ten story building with rigid joints

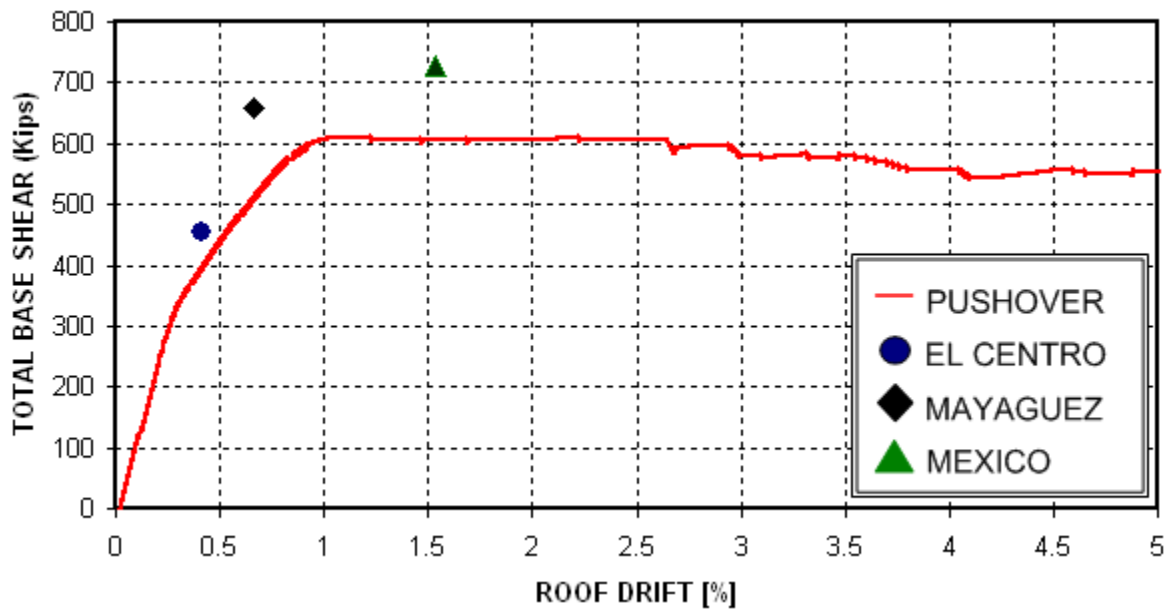


Figure 8-48 Static versus dynamic response for the ten story building with flexible joints

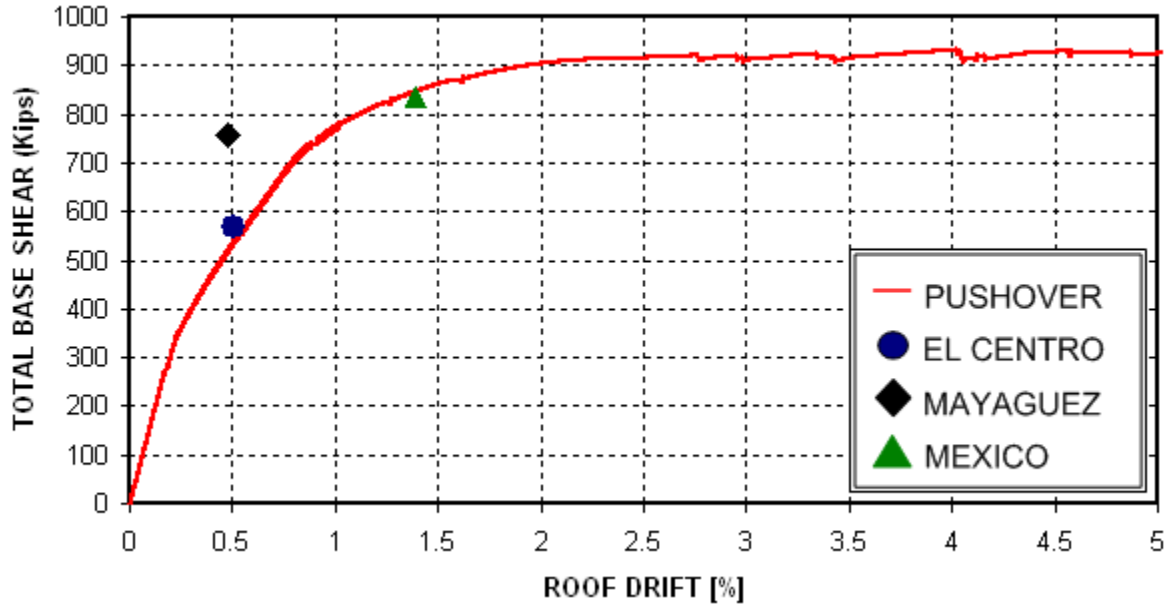


Figure 8-49 Static versus dynamic response for the fifteen story building with rigid joints

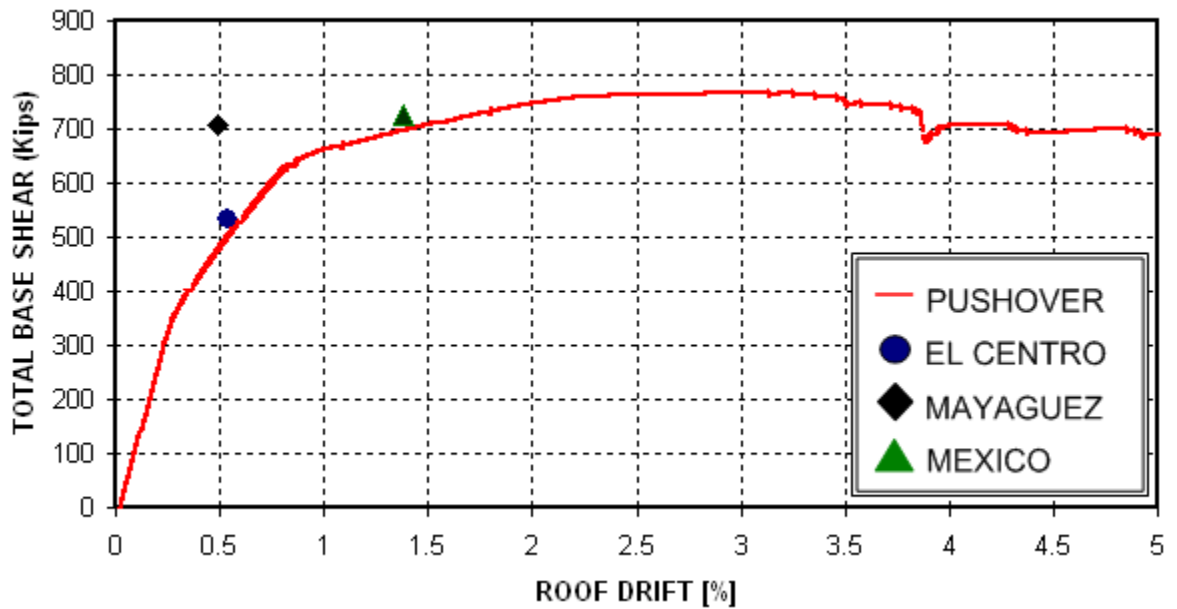


Figure 8-50 Static versus dynamic response for the fifteen story building with flexible joints

8.7 CONCLUSIONS

In this chapter three multistory three spans frames of 5, 10 and 15 stories were investigated. The exterior joints were modeled with the proposed joint model, while the interior joints were assumed as rigid since these joint have not shown to be as critical as the exterior joints. Pushover static analysis and dynamic analyses were carried out. As for the case of the previous chapter, two cases of each multistory frame were considered (with rigid joints and flexible joints). The main observations for the static and dynamic analyses are summarized next:

- The behavior of the flexible joints frame in the pushover analysis was characterized for reaching the peak lateral load at certain level of drift (1% for the five and ten story and 3% for the 15 story frame) and from that points the lateral load decreases. This behavior is typical of the local joint behavior and thus the exterior joints are strongly affecting the global behavior of the frame.
- When comparing the maximum lateral load of the two cases considered, a reduction in the lateral load was observed. This reduction was of 16% for the five story frame and 18% for the ten and fifteen frame.
- The behavior of the rigid and flexible joint frames in the dynamic analysis was very similar up to attaining peak displacements. However, it was observed that after these points the curves start to detach, meaning that a change of stiffness is occurring. This change was related to the behavior of the exterior joints since the amount in plastic hinges were almost the same for both cases (rigid and flexible) in all multistory frame.

- The maximum top story drift for the case of the five story frame was below of 1% for the three earthquakes considered. For the ten and 15 story frame this value was around 1.5% only when such structures were subjected to the Mexico earthquake.
- The maximum drifts did not correspond to any of the two models consistently.
- The static pushover analysis gave a good approximation of the expected dynamic behavior of the frames.

9 CONCLUSIONS AND FUTURE WORK

9.1 SUMMARY

In the initial part of this thesis, the risk that represents reinforced concrete structures designed before 1970 was presented, since the seismic provisions of design codes at that time were not as strict as they are in modern design codes. Structures were designed mainly for gravity loads and thus the use of frames with unreinforced joints was common. Also, past earthquakes have demonstrated that unreinforced exterior joints are more prone to failure than unreinforced interior joints, in some cases initiating the collapse of structures. This situation motivated the main objective of this research which was the development of a model for exterior unreinforced concrete joints with the purpose of studying the seismic vulnerability of reinforced concrete frame structures designed before or during the early 70's. The scope, specific objectives and the methodology employed in this research was presented in Chapter 1. Previous experimental and analytical work done in reinforced concrete joints as well as important background information was presented in Chapter 2. The detailed methodology for the development of the proposed model was presented in Chapter 3. Such model consisted in an envelope curve which defined three states of the local behavior of exterior joints, named the cracking point, the maximum joint strength point and the residual moment point of the joint. Once the model was defined, it was implemented in the nonlinear analysis structural program Opensees, whose main characteristics were summarized in Chapter 4. In order to validate the proposed model, 19 experimental tests from the literature were numerically simulated in Chapter 5. It was found that the proposed model compares

with reasonable accuracy the response of such test. With the purpose of evaluating structures designed before 1970 several concrete frames were analyzed using pushover static analysis and dynamic analysis. For the dynamic analysis, three earthquakes were used which main characteristics were presented in Chapter 6. Five concrete frames designed with the Puerto Rico code of 1968 were selected. In order to compare the response of the frames with and without the flexible joints, two cases were created named rigid joints and flexible joints. In Chapter 7, the analysis of two and three story one bay frames typical of school buildings in Puerto Rico was presented. Finally Chapter 8 presents the analysis of three multistory, three bay frames of five, ten and fifteen stories. In these frames the interior joints were modeled as rigid.

9.2 CONCLUSIONS

The main conclusions that can be drawn from this research are:

- 1.** The proposed exterior joint model is adequate for the modeling of unreinforced concrete exterior joints since it reproduced with reasonable accuracy the response of 19 two dimensional tests reported in the literature and for its simplicity it can be easily implemented in Opensees for the analysis of concrete frame.
- 2.** The proposed model identified three points of the local behavior of the joints, each of them associated with a state of damage of the joint, which made it useful in the vulnerability assessment of frames with unreinforced exterior joints.

3. The pushover curves for all studied frames showed that these curves are strongly influenced by the local behavior of the exterior joints since once a curve attains its maximum loads it starts to lose strength which is typical of the behavior of unreinforced concrete joints.
4. The presence of the exterior joint model translated into a reduction of the lateral load capacity of frames since the flexible joints frames experienced a drop in their lateral load for all frames studied compared with those with rigid joints frames. This drop was of 30% for the two story school building frame, 32% for the three story school building frame 16% for the five story frame and 18% for the 10 and 15 story building frames.
5. The dynamic analysis indicated that maximum top drift for the two and three story school building frames was strongly related to the joint damage. For the case of the two stories frame under the two earthquakes, which only experiences cracked joints, this increase was 19% and 25 % for El Centro and Mayagüez earthquakes respectively. For the case of the three story frame this increase was 40% for El Centro record which caused cracking at 83% of the joints. The increase was 45% for the Mayagüez earthquake which caused that two joints reached their peak strength.
6. For the case of the multistory multi span frames in which interior joints were modeled as rigid, the maximum drift to the right was greater in the flexible joint cases when

compared with the rigid joint cases. However, the opposite occurred at the maximum drift to the left, since in almost all cases rigid joint frames had drift greater than the flexible joint cases. This phenomenon is attributed to the fact that when exterior joints reached their cracking or peak point, the frame gets permanent deformations in the right direction.

9.3 RECOMENDATIONS FOR FUTURE WORK

It is important to compile an inventory of multistory buildings in Puerto Rico that can serve as a base to extend the analysis and assess their vulnerability. This database can serve to construct fragility curves for these types of buildings.

Since this investigation was mainly focused on the effects of unreinforced concrete joints in frames designed before 1970, it would be interesting to include in a future analysis a model for the interior joints.

It is recommended to include in the proposed model, a maximum rotation.

Since the proposed model can identify three stages of the local behavior of joints, it would be interesting to make analysis that includes the removal of the joints and the columns that are connected through the joints once the joints attain their maximum rotation. One can then study how the forces are redistributed among the remaining elements of the frame.

Since the proposed model was developed only for two dimensions, it is recommended to extend the model to take into account the tridimensional effects.

REFERENCES

Alath S, and Kunnath, S.K. (1965), "Modeling inelastic shear deformation in RC beam-column joints." Engineering Mechanics: Proceeding of Tenth Conference, University of Colorado at Boulder, ASCE, Vol. 2, pp. 822 – 825.

Administración de Reglamentos y Permisos, ARPE (1968). Reglamento de Edificación de Puerto Rico, Santurce, Puerto Rico.

Anderson, M., Lehman, D. and Stanton, John. (2008). "A cyclic shear stress-strain model for joints without transverse reinforcement." Engineering Structures 30, 941- 954.

Antonopoulos, C. P. and Triantafillou, T. C., (2003) "Experimental Investigation of FRP-Strengthened RC Beam-Column Joints," ACSE Journal of Composites for Construction, Vol. 7, No. 1, Feb. 2003, pp 39-49.

Beres, A., Pessiki, S. P., White, R. N. and Gergely P. (1996). "Implications of experiments on the seismic behavior of gravity load designed RC beam-to-column connections." Earthquake Spectra, 12(2), pp. 185-198.

Celik, O.C., and Ellingwood, B.R., (2008) "Modeling beam-column joints in fragility assessment of gravity load designed reinforced concrete frames." Journal of Earthquake Engineering, V. 12, No. 3, pp. 357-381.

Clyde, C., Pantelides, C. P. and Reaveley, L. D. (2000). "Performance-based evaluation of exterior reinforced concrete building joints for seismic excitation." Pacific Earthquake Engineering Research Center, College of Engineering, University of California, Berkeley, PEER Report 2000/05, 50 pp.

Daza Duarte, L.G. (1996): "Methodology to evaluate existing reinforced concrete frames under earthquake loads", PhD. thesis, Department of Civil Engineering, University of Puerto Rico, Mayagüez Campus.

Ehsani, M. R. and Wight, J. K. (1985). "Exterior reinforced concrete beam-to-column connections subjected to earthquake-type loading." ACI Structural Journal, 83(4), pp. 492-499.

El-Metawally, S. E. and Chen, W. F. (1988). "Moment-rotation modeling of reinforced concrete beam-column connections." ACI Structural Journal, 85(36), pp. 384-394.

Fujii S. and Morita, S. (1991). "Comparison between interior and exterior RC beam-column joint behavior." *Design of Beam-Column Joints for Seismic Resistance*, ACI Special Publication SP-123-6, pp. 145 – 165.

Ghobarah, A. and Biddah, A. (1999). "Dynamic analysis of reinforced concrete frames including joint shear deformation." *Engineering Structures*, V. 21, pp. 971 – 987.

Ghobarah, A. and Youssef, M. (1999). "Modeling of reinforced concrete structural walls." *Journal of Structural Engineering*, 21(10), pp. 912-923.

Ghobarah, A. and Said, A (2001)., " Seismic Rehabilitation of Beam-Column Joints using FRP laminates," *Journal of Earthquake Engineering*, V. 5, No. 1, pp. 113-129.

Hanson, N. W. and Connor, H. W. (1967). "Seismic resistance of reinforced concrete beam-column joints." *Journal of the Structural Division Proceedings of the American Society of Civil Engineers*, pp. 533 – 560.

Hassan, W.M., Park, S., Lopez, R., Mosalam, K.M. and Moehle, J.P. (2010), "Seismic response of older type reinforced concrete corner joints", *Proceedings of the 9th U.S. National and 10th Canadian Conference on Earthquake Engineering*, July 25-29, Toronto, Ontario, Canada, Paper No. 1616.

Hwang, S. J., and Lee, H. J. (1999). "Analytical model for predicting shear strengths of exterior reinforced concrete beam-column joints for seismic resistance." *ACI Structural Journal*, 96(5), pp. 846–857.

Hwang, S. J., and Lee, H. J. (2000). "Analytical model for predicting shear strengths of interior reinforced concrete beam-column joints for seismic resistance." *ACI Structural Journal*, 97(1), pp. 35–44.

Hacuto, S., Park, R. and Tanaka, H. (2000). "Seismic load tests on interior and exterior beam-column joints with substandard reinforcing details." *ACI Structural Journal*, 97(1), pp. 35-44.

Hwang, S. J., Lee, H. J., Liao, T. F., Wang, K. C. and Tsai, H. H. (2005). "Role of hoops on shear strength of reinforced concrete beam-column joint." *ACI Structural Journal*, 102(3), pp. 445-453.

Irizarry, J. (1999). "Design Earthquakes and Design Spectra for Puerto Rico's Main Cities Based on Worldwide Strong Motion Records", M.Sc. thesis, Department of Civil Engineering, University of Puerto Rico, Mayagüez Campus.

Kaku, T. and Asakusa, H. (1991). "Ductility estimation of exterior beam-column subassemblages in reinforced concrete frames." Design of Beam-Column Joints for Seismic Resistance, ACI Special Publication SP-123-7, pp. 167- 185.

Karsan, I. D., and Jirsa, J. O. (1969). "Behavior of concrete under compressive loading." Journal of Structural Division ASCE, 95(ST12).

Karayannis, C. G., Chalioris, C. E., and Sirkelis, G. M., (2008) "Local Retrofit of Exterior RC Beam-Column Joints Using Thin RC Jackets- An Experimental Study," Earthquake Engineering and Structural Dynamics, V. 37, pp. 727-746.

Kim, J. and LaFave, J. M (2007), "Key Influence Parameters for the Joint Shear Behavior of RC Beam-Column Connections," Engineering Structures, No. 29, pp. 2523-2539.

Jirsa, J. O.(1981): "Beam-Column Joints: Irrational Solutions to a Rational Problem", ACI SP 72, pp. 177-198.

Lehman, D.E., and Moehle, J.P. (2000), "Seismic Performance of Well-Confined Concrete Bridge Columns," PEER Report 1998/01, University of California, Berkeley, Dec. 2000.

Lowes, L. N. and Altoontash, A. (2003). "Modeling reinforced-concrete beam-column joints subjected to cyclic loading." Journal of Structural Engineering, 129(2), pp. 1686-1697.

Lowes, L.N., Mitra, N., and Altoontash, A., "A Beam-Column Joint Model for Simulating the Earthquake Response of Reinforced Concrete Frames," PEER Report 2003/10, 2004.

Megget, L. M. (1974). "Cyclic behaviour of reinforced concrete beam-column joints." Bulletin of the New Zealand National Society for Earthquake Engineering 7 (1).

Maison, B. F. (1992). "PC-ANSR A computer program for nonlinear structural analysis." University of California, Berkeley, California.

Mazzoni Silvia, McKenna Frank, Scott H. Michael, Fenves L Gregory., et al. (2007), "OpenSees Command Language Manual", <http://opensees.berkeley.edu/OpenSees/manuals/usermanual/OpenSeesCommandLanguageManual.pdf>

Montejo, L. (2004). "Generation and Analysis of Spectrum-Compatible Earthquake Time Histories using Wavelets", M.Sc. thesis, Department of Civil Engineering, University of Puerto Rico, Mayagüez Campus.

McKenna, F., (2005). "OpenSees: Open system for earthquake engineering simulation." (<http://opensees.berkeley.edu>), University of California, Berkeley.

Moacyr, G., Alva, S., Homce de Cresce, A. L. and El Debs M. K. (2007). "An experimental study on cyclic behaviour of reinforced concrete connections." *Canadian Journal of Civil Engineering*, Vol. 34, 2007.

Mitra, N. and Lowes, L. N. (2007). "Evaluation, calibration, and verification of a reinforced concrete beam-column joint model." *Journal of Structural Engineering*, V. 133(1).

Moehle, J. (2007). "Mitigation of collapse risk in vulnerable buildings." Project Proposal.

National Academy of Science (1971), "The San Fernando earthquake of February 9, 1971: Lessons from a moderate earthquake on the Fringe of a Densely Populated Region"

Ortiz, I.R. (1993) "Strut and tie modeling of reinforced concrete short beams and beam-column joints", PhD thesis, University of Westminster.

Park, R. and Paulay, T. (1975). "Reinforced concrete structures", John Wiley, New York.

Park, R., Priestley, M. J. N., and Gill, W. D. (1982). "Ductility of square confined concrete columns." *Journal of Structural Division, ASCE*, 108(4), pp. 929-950.

Parker, D. E. and Bullman, P. J. M.,(1997) "Shear Strength within RC Beam-Column Joints," *The Structural Engineer*, V. 75, No. 4, Feb. 1997, pp. 53-57.

Pinkham, C.W. et al. (1997). "Recommendations for design of beam-column joints in monolithic reinforced concrete structures". American Concrete Institute, Committee 352.

Priestley, M. and Hart, G. (1994). "Seismic behavior of "as-built" and "as-designed" corner joints." SEQAD Report to Hart Consultant Group, Report #94-09, 93 pp. plus appendices.

Park, R. et al. (1995). "The Hyogo-ken Nanbu earthquake (the great Hanshin earthquake) of 17 January 1995: report of the NZNSEE Reconnaissance Team." *Bulletin of the New Zealand National Society for Earthquake Engineering*, 28(1), pp. 1-98.

Pampanin, S., Calvi, G. M. and Moratti, M. (2002). "Seismic behavior of RC beam-column joints designed for gravity loads." 12th European Conference on Earthquake Engineering Paper reference 726.

Pantelides, J. C., Hansen, J., Nadauld, J. and Reaveley, L.D. (2002). "Assessment of reinforced concrete building exterior joints with substandard details." Report 2002/18 Pacific Earthquake Engineering Research Center, College of Engineering, University of California, Berkeley May 2002.

Pantazopoulou, S., and Bonacci, J., (1992), "Consideration of Questions about beam-column joints", *ACI Structural Journal*, V.89, No.1, pp. 27-37.

Pampanin S, Magenes G. and Carr A. (2003). "Modelling of shear hinge mechanism in poorly detailed RC beam-column joints". Proceedings of the FIB 2003 Symposium, May 6-8, Athens, Greece, Technical Chamber of Greece, CD-ROM.

Pampanin,S., Akguzel, U. and Attanasi, G. (2007). "Seismic upgrading of 3-D exterior R.C. beam column joints subjected to bidirectional cyclic loading using GRFP Composites." FRPRCS-8, University of Patras, Patras, Greece, July 16-18.

Park, R. (2002). "A summary of results of simulated seismic load test on reinforced concrete beam-column joints, beam and columns with substandard reinforcing details." *Journal of Earthquake Engineering*, 6(2), pp. 147-174.

Park, S. and Mosalam, K.M. (2009), "Shear strength models of exterior beam-column joints without transverse reinforcement", Pacific Earthquake Engineering Research Center, Report No. PEER 2009/106, November 2009.

Paulay, T. and Scarpas A.(1981): "The behaviour of exterior beam-column joints", *Bulletin of the New Zealand National Society for earthquake engineering*, Vol. 14, No. 3.

Rojas Mercedes, Norberto J (2005), "Consideration of the short column effect in the seismic vulnerability of the structures", MS thesis, University of Puerto Rico at Mayagüez.

Sarsam, K.F. and Phipps, M.E., (1985) "The shear design of in-situ reinforced beam-column joints subjected to monotonic loading", *Magazine of concrete research*, V. 37, No. 130, pp. 16-28.

Seckin, M. and Uzumeri, S. M. (1980). "Exterior beam-column joints in reinforced concrete frames." *Proceeding of Seventh World Conference on Earthquake Engineering, Structural Aspects*, Turkey.

Scott, R. H., Feltham I. and Whittle, R. T. (1994): "Reinforced concrete beam-column connections and BS 8110", *The Structural Engineer*, Volume 72, No. 4, 1994, pp. 55-60.

Scott, R.H., and Hamil, S.J.,(1998) "Connection Zone Strain in the Reinforced Concrete Beam Column Connections," *Proceedings of the 11th International Conference on Experimental Mechanics*, Oxford, UK, pp. 65-69.

Shin, M. and LaFave, J. M. (2004) "Testing and modeling for cyclic joint shear deformations in rc beam-column connections," *Proceedings of the Thirteenth World Conference on Earthquake Engineering*, August 1–6, 2004, Vancouver, B.C., Canada, Paper No. 0301.

Tsonos, A.G. (2007), "Cyclic load behavior of RC beam-column subassemblages of modern structures", *ACI Structural Journal*, V. 104, No.4, pp. 468-478.

Uzumeri, S.M. (1977). "Strength and ductility of cast-in-place beam-column joints." *ACI Publication SP 52-12: Reinforced Concrete Structures in Seismic Zones*, 293-350.

Vollum, R.L. (2008), "Design and analysis of exterior beam column connections", PhD thesis, Imperial College of Science Technology and Medicine-University of London.

Walker, S.G., (2001), "Seismic Performance of Existing RC Beam–Column Joints," MSCE thesis, University of Washington.

Wong, H. F. (2005). "Shear strength and seismic performance of non-seismically designed reinforced concrete beam-column joints." Ph.D. Dissertation, The Hong Kong University of Science and Technology, Hong Kong, China.

Youssef, M. and Ghobarah, A. (2001). "Modelling of RC beam-column joints and structural walls." *J. of Earthquake Engineering*, 5(1), 93 – 111. Aydin, K. and C. Tang, "Millimeter wave radar scattering from model ice crystal distributions," *IEEE Trans. Geosci. Remote Sens.*, vol. 35, pp. 140-146, 1997 a.

Zhang, L., and Jirsa, J.O. (1982), "A study of shear behavior of RC beam-column joints", PMFSEL Report No. 82-1, University of Texas at Austin.